AUBURN UNIVERSITY

THERMAL CONDUCTIVITY OF HETEROGENEOUS MIXTURES

AND

LUNAR SOILS

Final Report

Contract NAS8-26579

R. I. Vachon, A. G. Prakouras,
R. Crane, and M. S. Khader

School of Engineering
Department of Mechanical Engineering
Thermoscience Group

Under Contract With

George C. Marshall Space Flight Center
National Aeronautics & Space Administration

Administered Through

ENGINEERING EXPERIMENT STATION

AUBURN UNIVERSITY
AUBURN, ALABAMA 36830

October, 1973

AUBURN UNIVERSITY

THERMAL CONDUCTIVITY OF HETEROGENEOUS MIXTURES

AND

LUNAR SOILS

Final Report

Contract NAS8-26579

by

R. I. Vachon, A. G. Prakouras,
R. Crane, and M. S. Khader

School of Engineering
Department of Mechanical Engineering
Thermoscience Group

Under Contract With

George C. Marshall Space Flight Center
National Aeronautics & Space Administration

Administered Through

ENGINEERING EXPERIMENT STATION
Auburn University
Auburn, Alabama 36830

October, 1973

TABLE OF CONTENTS

TABLE OF CONTENTS (Continued)

LIST OF ILLUSTRATIONS

LIST OF ILLUSTRATIONS (Continued)

LIST OF ILLUSTRATIONS (Continued)

LIST OF ILLUSTRATIONS (Continued)

LIST OF ILLUSTRATIONS (Concluded)

LIST OF TABLES

LIST OF TABLES (continued)

FOREWORD

This document is the final report for Contract NAS8-26579, "Thermal Conductivity of Heterogeneous Mixtures and Lunar Soils." The work was performed by R. I. Vachon, A. G. Prakouras, R. A. Crane and M. S. Khader of Auburn University, Department of Mechanical Engineering, for the National Aeronautics and Space Administration, George C. Marshall Space Flight Center. The period of performance of this study was from October 1970 to October 1973.

ABSTRACT

The heat transport properties of the lunar soil are important in determining the thermal response of the lunar surface. This information leads toward a wider understanding of the nature of the moon and ultimately of the universe itself. The study to be described in this report concerns itself only with one aspect of the greater problem; the theoretical evaluation of the effective thermal conductivity of granular materials. The basic approarch has been entirely analytical as others have previously undertaken direct heat transfer measurements. This work supplements the experimental results of the thermal probe on the Apollo 17 mission as well as the experiments performed on lunar samples which have been returned from previous Apollo missions. Moreover the results are intended as an aid in future evaluation of the extensive scientific data from both the manned and unmanned exploratory probes. The basic formulation is intended to be as general as possible; this allows application of the final results not only to terrestial bodies which are yet to be explored but also to a wide range of non-space related technological applications. These include such diverse engineering applications as nuclear power generation, petroleum production, food processing, chemical production, underground energy transmission and thermal insulation design. In addition

analogous diffusion type problems are met in work concerning magnetism, electricity and hydrodynamics.

NOMENCLATURE

A. Roman Alphabet

Symbol		Dimensional Units
A	Cross-sectional area	m^2
$\bar{a}(T)$	Rosseland mean absorption coefficient	m^{-1}
B	$\left[k_d/C(k_c - k_d)\right]$	
C	Geometrical constant	
d	Particle diameter	m
D	One dimensional solid fraction	m
D_a	Lower truncation point of granules	m
D_b	Upper truncation point of granules	m
D_p	Effective pore size	m
$(D_p)_c$	Effective pore size for conduction	m
$(D_p)_h$	Hydraulic diameter	m
e	Emissivity	
E	Young's modulus	N/m^2
F	Ratio of constituent temperature gradients	
F_1	Force between particles	N
F_o	k_e/k_o	

F_w	$(k_e - k_\infty) / (k_o - k_\infty)$	
F_∞	k_e/k_∞	
f	Frequency function	
f_i	Depolarization factor	
g	Gravitational acceleration	m/sec^2
g^*	Temperature jump distance	m
h_r	Coefficient associated with surface microroughness	
k	Wiener's constant	
k_c	Conductivity of continuous phase	kcal/m-hr-^oK
k_{c_r}	Contact conductivity	kcal/m-hr-^oK
k_d	Conductivity of discontinuous phase	kcal/m-hr-^oK
k_e	Effective conductivity	kcal/m-hr-^oK
k_g	Conductivity of gaseous phase	kcal/m-hr-^oK
k_g^*	Conductivity of gaseous phase at reduced pressures	kcal/m-hr-^oK
k_k	Coefficient associated with microgaps at contact areas	
k_r	Radiant conductivity	kcal/m-hr-^oK
k_s	Conductivity of solid phase	kcal/m-hr-^oK
k_{c_o}	Effective conductivity for uniform heat flux	kcal/m-hr-^oK
k_{e_p}	Wiener's parallel phase effective conductivity	kcal/m-hr-^oK

k_{e_s}	Wiener's series phase effective conductivity	kcal/m-hr-^{o}K
k_{c_∞}	Effective conductivity for parallel isotherms	kcal/m-hr-^{o}K
Kn	Knudsen number	
m	Hamilton's shape factor	
M	Measure of sample size	
n	Coordination number	
N	Grid Size	
N_c	Number of contact points per unit volume	
p	Pressure	N/m^2
pij	Pressure tensor	N/m^2
p_b	Breakaway pressure	N/m^2
P	Volume fraction of continuous phase (porosity)	
P_1	One dimensional solid fraction	
Pr	Prandtl number	
Q	Total heat transfer	kcal/hr
q_r	Radiation heat flux	kcal/hr-ft^2
r	Sphere radius	m
r_c	Contact area radius	m
R_c	Contact resistance	hr-^{o}K/kcal
$\overline{R}_c$	Total conduction thermal resistance	hr-^{o}K/kcal
R_e	Effective bulk resistance	hr-^{o}K/kcal

R_i	Effective element resistance	hr-°K/kcal
R_L	Resistance to heat flow due to contraction of heat flow lines	hr-°K/kcal
R_o	Resistance due to oxidizing film	hr-°K/kcal
R_s	Resistance of solid sphere with two contact areas	hr-°K/kcal
R_{s_p}	Resistance due to microroughness of solid particles	hr-°K/kcal
R_1	Solid particle thermal resistance	hr-°K/kcal
s	Molecular diameter	m
S	Two-dimensional solid fraction	
T	Temperature	
w	Overrelaxation factor	
x	Sample dimension	m
x_o	Radius of deformed particle	m
V_h	Mean void equivalent hole volume	m^3
z	Depth below the surface	m

B. Greek Alphabet

α	Thermal accommodation coefficient	
δ_{ij}	Kronecker delta	
ϵ	Local solid fraction	
$\bar{\epsilon}$	Bulk solid fraction	
λ	Molecular mean free path	m
$\bar{\lambda}$	Effective molecular mean free path	m
μ	Mode of solid or void fraction	
μ_1	Mode of one-dimensional solid fraction	

ν	Poisson's ratio	
ρ	Density	kgr/m^3
ρ_∞	Solid material density	kgr/m^3
ρ_o	Surface material density	kgr/m^3
σ	Standard deviation of solid or void fraction	
σ_1	Standard deviation of one-dimensional solid fraction	
σ_b	Stefan-Boltzman constant	$kcal/m^2\text{-}^\circ K^4$
ϕ	Local solid fraction	

I. INTRODUCTION AND OUTLINE OF REPORT

Considerable effort has been expended over the past sixty years to find means of calculating the effective thermal conductivity of heterogeneous mixtures from the conductivities of the individual components [1-128].* Interests in developing techniques for such calculations have been motivated by the widespread applications of heterogeneous mixtures in such diverse fields as nuclear power generation [21], food processing [76], chemical industry [75], process equipment design [37], geology [23], petroleum production [36], thermal insulation design [26], cryogenics [60] and foundary work [58].

About three years ago researchers at the Marshall Space Flight Center in Huntsville were working on the development of a thermophysical model of the lunar surface. During the course of this development it was found that a method of predicting the effective thermal conductivity of the lunar soil was required. A review of the available literature indicated that application of the proposed correlations to the case of lunar soils resulted in considerable error between analytical and experimental values. As a result, a study was undertaken at Auburn University to determine the causes of failure and develop new correlations. The scope of this study is to extend or develop analytical

*Numbers in brackets refer to references cited.

techniques of predicting the constant thermal conductivity of heterogeneous mixtures and include methods for the prediction of variable thermal conductivity. The techniques developed in this report are as generally applicable as possible, but specific enough for the analytical results to be compared with experimental data for many classes of heterogeneous mixtures, and in particular with the experimental results on basalt powders under vacuum conditions.

The term heterogeneous mixtures encompasses a large number of single-phase, two-phase or multi-phase physical systems, an excellent classification of which is given in [70]. The common characteristics of all these systems, with respect to the conduction of heat, is the thermal conductivity and volume fraction of each individual phase. Apart from these characteristics, the conduction of heat in heterogeneous mixtures in general depends on the following parameters.

1. Particle shape and size distribution;
2. Pore shape and size distribution;
3. Coordination number;
4. Contact resistance.

Obviously, all parameters do not enter the problem for each class of heterogeneous mixtures. For example, in the determination of the effective thermal conductivity of emulsions and suspensions the last three parameters are not relevant. The relevant parameters in each case can be determined by considering the modes in which heat is transferred through the mixture. It has been generally agreed by the investigators that the transfer of energy occurs by three mechanisms [29, 30, 32].

1. Through the voids by conduction, convection and radiation;
2. Through a series path consisting of an effective solid-path length and void-path length;
3. Through the solid phase, the energy flowing from one particle to the next through the area of contact.

The extent to which each mechanism influences the overall heat transfer process depends on the geometry of the system under consideration, together with the environment the heterogeneous mixture is subjected to, as defined by temperature, pressure, and mechanical loading conditions.

The effective thermal conductivity of a heterogeneous mixture may be defined as the ratio of the overall heat flux to the overall temperature gradient. This approach requires that the material be treated as a continuous single phase so that the temperature distribution predicted by such a model coincides with that of the physical system only "in the large" [4]. This concept has proven to be a very effective tool in predicting the transfer of heat through heterogeneous systems, the dimensions of which are much larger than the dimensions of the individual components.

Construction of a model that represents reasonably well heterogeneous materials has proved to be a difficult problem. Calculation of the effective conductivity of this model has proved to be equally complex. The difficulty does not arise from ignorance of the fundamental laws involved but from complications in applying them [20]. A detailed solution of the conduction problem would require knowledge of the shape, size, location and conductivity of each particle in the system, together with the interactions between particles. Furthermore, a complicated numerical method of solution would be required.

To overcome these difficulties, investigators have generally followed two methods of approach.

1. A basic repeated structural unit that represents reasonably well the heterogeneous mixture has been isolated, and equations have been derived from special geometries of this unit cell based on the assumption that heat flows in straight lines, normal to parallel isothermal planes.

2. Based on the assumption of a regular or random distribution of spherical particles in such small concentrations that there is no field interaction, the temperature distribution in the system is determined. Subsequently, the effective thermal conductivity of the system is evaluated from the Fourier-Biot law.

In this study both methods have been analyzed and refined, so that they can be applied to many classes of heterogeneous mixtures, over a wide range of pressures and temperatures. In the proposed developments, consideration will be primarily directed to two-phase granular systems and powders for which the following assumptions are valid.

1. The thermal properties of the constituents are both homogeneous and isotropic;

2. All samples are large in comparison with individual particle size;

3. All samples contain a sufficient number of particles so that they can be considered typical of the selected packing;

4. The convective component of heat transfer is sufficiently small to be neglected.

The first three assumptions are consistent with the concept of the effective thermal conductivity of granular materials, and permit one to extend the results obtained from the analysis of a unit cube of the material to the packing as a whole. The fourth assumption is based on the studies of Waddams [6] and Wilhelm et al [37] who concluded that natural convection is negligible for pressures below 10 atmospheres, and

particle diameters less than 3 to 6 mm. Consequently for most granular materials and powders the transfer of heat by natural convection is negligibly small.

In Chapter 2 of this report the background information, consisting of prominent models proposed in the literature, is presented. The available heat transfer models for heterogeneous systems are classified as being either flux law models or Ohm's law models. The Ohm's law models are further classified according to the heat flow assumptions as being either uniform heat flux models or parallel isotherms models.

In Chapter 3 several representative models have been applied to 172 granular materials, and the calculated values have been compared to experimental results. The comparisons are presented in a graphical form. A careful analysis of Figures 3-1 through 3-17 indicates that the discrepancy between the analytical models and the physical granular systems can be attributed to one of the following causes.

1. Failure to account for finite particle contact area;
2. Failure to utilize a realistic geometry, or a realistic distribution of the two phases;
3. Idealized heat flow assumptions.

As a result of this analysis, the aim of this study has been focused on an attempt to develop models in which the above three sources of error are partially or totally eliminated.

The effect of the uniform heat flux and parallel isotherms assumptions on the predicted thermal conductivity of randomly packed granular systems has been investigated in Chapter 4. Special attention has been

directed to the idealized heat flow assumptions, because the possibility of utilizing either one simplifies considerably the problem. However, application of the uniform heat flux assumption to a physically realistic probabilistic model results in calculated effective conductivities that are too low, whereas application of the parallel isotherms assumption results in calculated effective conductivities that are too high. The reason for such behavior is that infinite and zero conductivities in the normal to the heat flow direction are associated with the parallel isotherms and uniform heat flux assumptions respectively.

In Chapter 5 a parallel isotherms probabilistic model has been developed. This model is based upon an extension of concepts originally proposed by Tsao [8], on the basis of which the effective thermal conductivity can be expressed in terms of the mode, μ, and the standard deviation, σ, of the one dimensional porosity as introduced by Tsao. The mode, μ, has been approximated by the bulk porosity of the granular system, and the standard deviation, σ, has been correlated to the solid volume fraction only, on the basis of experimental evidence. The resulting equation has been used to determine the effective thermal conductivity of packed beds with solid fractions between 0.30 and 0.70.

The same basic concepts have been applied in the development of the stochastic model of Chapter 6. Noting that the effective conductivity tends to reach a fixed value for σ sufficiently large, limiting expressions have been developed for the effective thermal conductivity utilizing both the parallel isotherms and the uniform heat flux assumptions.

Then, rather than assuming both an unrealistic heat flow model and a distorted distribution, an experimentally derived correlation factor has been obtained for each of the limiting expressions. In addition, an experimentally derived weighting factor has been obtained relating both limiting expressions to experimental data.

In Chapter 7, the packing characteristics of random heterogeneous mixtures have been utilized to define the phase distribution in a unit cube of a granular material, by extending the digital simulation technique originally proposed by Baxley and Couper [20]. The temperature distribution in the unit cube was then determined assuming both three-dimensional heat transfer, potential field interaction, and contact resistance between particles. Finally, the effective thermal conductivity of the material was determined by summing heat flows in the direction of the mean heat flow only.

All models discussed up to this point are generally applicable to granular materials at interstitial gas pressures ranging from atmospheric to vacuum. In particular, for a vacuum environment, the basic modes of heat transfer are conduction through the granules and contact areas, and radiation. This situation is analyzed in Chapter 8 on the basis of a parallel isotherms model consisting of an array of spheres. The effect of changes in bulk density and mechanical loading with depth are included, and compared to experimental data on lunar fines.

In Chapters 9 and 10 the results obtained by all models are compared and evaluated with respect to the simplifying assumptions introduced in each model. Moreover, recommendations are made concerning

the extent of the applicability of each model and the areas where more work is required in order to improve the dependability of the predicted effective thermal conductivity values.

The dependence of the effective thermal conductivity on pressure and temperature, at reduced interstitial gas pressures, has been generally recognized and treated extensively in the literature. Reduction of pressure to extremely low values decreases the effective thermal conductivity of the system by one or more orders of magnitude [62]. This has been attributed to the decrease of the apparent gas conductivity when the mean free path of the gas molecules is of the same order of magnitude or larger than the effective pore size, as indicated in Appendix A. Also, at very low pressures, experimental evidence shows that the effective thermal conductivity of the system is very sensitive to temperature changes [3], indicating that radiative heat transfer between particle surfaces is a controlling factor. The aspects of radiation heat transfer are treated in Appendix B.

In the case of heat flow in granular systems "in vacuo", the convergence of the heat flux lines to the contact areas between particles is characterized by the contact resistance, as indicated in Appendix C.

It is evident that for the development of an accurate model for the prediction of the conductivity of granular systems, the geometry of the model should rely heavily on the characteristics of packed beds. A short review of the advances in packing theory is presented in Appendix F. Two of the characteristics of packed beds are of particular

importance to the heat transfer problem. These are the effective pore size and the coordination number, and are treated separately in Appendices D and E respectively.

In summary, the content and results of this report are as follows:

1. A critical review and classification of previously published models is presented together with a review of the parameters associated with the flow of heat through granular systems;

2. Previously published models have been compared to a large number of experimental data, the results have been evaluated with respect to the basic assumptions introduced in the development of each model, and the causes of failure have been summarized;

3. A theoretical development is presented about the effect that the assumptions of uniform heat flux and parallel isotherms have on the calculated effective thermal conductivity, and the theory has been substantiated by experimental evidence;

4. Four new models based on recent results of packing theory have been developed, and have been successfully applied to granular materials for a pressure range from atmospheric to vacuum;

5. The sources of error for all models have been analyzed and related to the geometry and modes of heat transfer;

6. Detailed recommendations with respect to the geometric parameters required for the description of a generalized physically realistic model have been presented;

7. The results of all models have been utilized in the construction of a recommended physically realistic model, which cannot be analyzed

at present due to lack of experimental data required for the determination of a number of the parameters.

II. BACKGROUND

Because of the broad occurence of systems involving heat transfer in granular materials, considerable attention has been given to the formulation of a model to allow the prediction of the effective thermal conductivity. Unfortunately, the complexity of the mechanisms contributing toward heat flow is such that no truly satisfactory model has been obtained. The continued proliferation of alternate models attests to these difficulties. Nevertheless progress has been made in developing a representative model and it is now possible to determine the effective thermal conductivity of systems whose constituent conductivities are of similar magnitudes.

Available heat transfer models for heterogeneous systems are generally classified as being either flux-law models or Ohm's law models. The flux law model appears to have received the earliest attention and will be discussed first here.

Flux Law Models

Flux-law models are characterized by their general approach to the determination of the effective thermal conductivity. First a solution is found to the equation describing the temperature field. The heat flow and temperature gradient are also sought. The Fourier-Biot law of heat conduction is then applied to determine the effective

thermal conductivity. The principal advantage of this approach lies in the fact that the actual curvature of heat flux lines and isotherms may be taken into account. Most of the methods applicable to heat transfer in heterogeneous materials were originally developed for use in electrical theory, magnetism or hydrodynamics. However each case is applicable to heat transfer in heterogeneous systems in that the same mathematical equations apply.

In considering a cube of heterogeneous material containing a single particle, the fundamental heat conduction equation may be written separately in each of the two phases. It is stipulated that the boundary conditions require a continuous temperature distribution and a continuous heat flux within the field. If each phase is itself isotropic and homogeneous the equations reduce to the form of Laplace's equation. Solutions of this equation are well known.

Maxwell [9] used this technique in finding an expression for the effective conductivity of a suspension of spheres

$$\frac{k_e}{k_c} = \frac{k_d+2k_c-2\bar{\varepsilon}(k_c-k_d)}{k_d+2k_c+\bar{\varepsilon}(k_c-k_d)} \qquad (2\text{-}1)$$

In the derivation of this equation, it was assumed that the spheres were at sufficient distances from one another that the disturbance of the flux lines around each particle did not extend to neighboring particles. It follows that the geometry of the array of particles does not influence the effective thermal conductivity wherever Equation (2-1) applies.

Several authors have worked to extend the model for dilute suspensions to include solids of alternate geometries. Burgers [10]

and Fricke [11] developed equations for disperse suspensions with ellipsoidal solid particles. Many particle shapes, including flakes, spheres and needles, may be approximated by ellipsoids by properly selecting the relative size of the semi-principal axes. Burgers' equation was

$$k_e = \frac{(1-\bar{\varepsilon})k_c + \bar{\varepsilon}Fk_d}{(1-\bar{\varepsilon}) + \bar{\varepsilon}F} \qquad (2\text{-}2)$$

In this relation F represents the ratio of the overall average temperature gradient in the discontinuous phase to that in the continuous phase. This ratio was found to be given by

$$F = \frac{1}{3} \sum_{i=1}^{3} \left[1 + \left(\frac{k_d}{k_c} - 1\right) f_i\right]^{-1}$$

The factor, f_i, referred to as the depolarization factor, depends on the length of the semi-principal axes of the ellipsoid. These factors have been normalized such that $\sum_{i=i}^{3} f_i = 1$. If the three semi-principal axes are equal the particles become spheres and Equation (2-2) reduces to Equation (2-1).

DeVries [12] applied Equation (2-2) to granular materials in calculating the thermal conductivity of soils. He found that if $0 \leq k_d/k_c \leq 10$ then the error obtained from Burgers' equation would be less than 10%. Obviously if the conductivities of the constituent phases are sufficiently close there will be very little disturbance in the flux lines around the particles. Thus the restriction stated by Maxwell is satisfied even though the particles are in close proximity.

Hamilton and Crosser [13] extended Burgers' development to include particles of arbitrary shape. The particle shape was defined in terms of sphericitity, ψ, that is in terms of the ratio of the surface area of a sphere compared to that of a particle having the same volume [66]. An empirical relation was developed giving the ratio of the average temperature gradients, F, as a function of the sphericity and the constituent conductivities. The modified Maxwell equation used by Hamilton and Crosser is

$$\frac{k_e}{k_c} = \frac{k_d + (m-1)k_c - (m-1)\,\bar{\varepsilon}\,(k_c - k_d)}{k_d + (m-1)k_c + \bar{\varepsilon}\,(k_c - k_d)} \qquad (2\text{-}3)$$

where $m = 3/\psi$. It was found that whenever $0 \leq k_d/k_c \leq 100$ the shape of the solid particles had little influence on the overall conductivity of disperse systems. For spherical particles ($\psi = 1$) Equation (2-3) reduces to Maxwell's equation.

Lord Rayleigh [14] considered the case in which the interaction between particles could no longer be neglected. In essence Laplace's equation was solved to find the potential field in and about a single spherical particle. Noting that the Laplace equation is linear it was then possible to utilize the principle of superposition to determine the equivalent field for a given particle distribution. Using a cubic array Lord Rayleigh, with a slight correction given by Runge [15], obtained

$$\frac{k_e}{k_c} = \frac{\left(\frac{2k_c+k_d}{k_c-k_d}\right) - 2\bar{\varepsilon} - 0.525\left(\frac{3k_c-3k_d}{4k_c+3k_d}\right)\bar{\varepsilon}^{10/3}}{\left(\frac{2k_c+k_d}{k_c-k_d}\right) + \bar{\varepsilon} - 0.525\left(\frac{3k_c-3k_d}{4k_c+3k_d}\right)\bar{\varepsilon}^{10/3}} \qquad (2\text{-}4)$$

It should be noted that this equation reduces to Maxwell's equation whenever $\bar{\varepsilon}$ is sufficiently small that the last term in the numerator and denominator may be neglected. Meredith and Tobias [16] have followed Lord Rayleigh's development including a larger number of terms from the infinite series defining the temperature field. The equation is

$$\frac{k_e}{k_c} = \frac{\frac{2k_c+k_d}{k_c-k_d} - 2\bar{\varepsilon} + 0.409\left(\frac{6k_c+3k_d}{4k_c+3k_d}\right)\bar{\varepsilon}^{\frac{7}{3}} - 2.133\left(\frac{3k_c-3k_d}{4k_c+3k_d}\right)\bar{\varepsilon}^{\frac{10}{3}}}{\frac{2k_c+k_d}{k_c-k_d} + \bar{\varepsilon} + 0.409\left(\frac{6k_c+3k_d}{4k_c+3k_d}\right)\bar{\varepsilon}^{\frac{7}{3}} - 0.906\left(\frac{3k_c-3k_d}{4k_c+3k_d}\right)\bar{\varepsilon}^{\frac{10}{3}}} \qquad (2\text{-}5)$$

Both equations compare closely with available experimental results obtained for spheres packed in a cubic geometry. However these equations do not appear applicable to systems with widely differing constituent conductivities [16]. Moreover, results do not compare favorably with those obtained for random packing of spheres. The explanation for this descrepancy is offered by Laubitz [17] that although the mathematics is exact the model is so artificial that it radically departs from real powders.

Bruggeman [18] allowed both for particle size variation and arbitrary particle orientation, by assuming that various elements of the same type have in their neighborhood all possible distributions

of elements of all possible types, in the same frequency in which the different types are encountered in the two-phase mixture. He applied Maxwell's equation to find the effective conductivity of an arbitrary two-phase system, and then using this value as the conductivity of the continuous phase he applied Maxwell's equation again to find the effective conductivity when one more particle is added to the system. If this process is repeated indefinitely, for an infinite particle size range, the effective conductivity approaches a limit given by

$$1 - \bar{\varepsilon} = \frac{k_e - k_d}{k_c - k_d} \left(\frac{k_c}{k_e}\right)^{1/3} \tag{2-6}$$

Using the same basic approach but accounting for only two additions of the solid particles, Meredith and Tobias [19] obtained a second relation

$$\frac{k_e}{k_c} = \left[\frac{4k_c + 2k_d - 2\bar{\varepsilon}(k_c - k_d)}{4k_c + 2k_d + \bar{\varepsilon}(k_c - k_d)}\right]\left[\frac{4k_c + 2k_d - \bar{\varepsilon}(4k_c - k_d)}{4k_c + 2k_d - \bar{\varepsilon}(k_c - 2k_d)}\right] \tag{2-7}$$

Baxley and Cooper [20] utilized a digital simulation technique to describe heat transfer in heterogeneous materials. The model incorporated a random placement technique to arrange solid cubes in a square array. The Laplace equation was then written for the entire two phase region and was solved utilizing a numerical relaxation technique. Once having obtained the proper temperature distribution

for the system, the effective conductivity was obtained by applying the Fourier-Biot law. The resulting equations were given in terms of a computer code. Calculational results obtained from the model appear to correlate data for suspensions with good accuracy. The authors note that solid particles of any shape could be considered by constructing such particles from sufficiently small cubes. The success of this technique has motivated the construction and analysis of a similar model for powders and granular materials, which is one of the subjects of this study.

Summarizing the flux law models it is found that they may be generally categorized as extensions of the Maxwell model or as finite difference models. The models derived from Maxwell's formulation may suffer from one or more of a series of shortcomings as applied to granular systems. Maxwell's original equation failed to account for the interaction of the flux lines around particles. Other equations are restricted to a regular and quite unrealistic array. Each breaks down when applied to systems in which the conductivity of the discontinuous phase is several orders of magnitude larger than that of the continuous phase. Ideally, for systems in which the solid particles touch, k_e/k_c should approach infinity as k_d/k_c approaches infinity; however, this condition is not met in these equations [16]. The reason for this discrepancy appears to be explained by Meredith and Tobias. They suggest that it is due to the neglection of higher order terms in the equation defining the temperature distribution. Thus,

these equations do not appear applicable to the case of granular systems in a medium of extremely low conductivity.

Ohm's Law Models

The mathematical complexity of the formulation and solution of the flux law model has precluded consideration of anything but the simplest shaped particles and arrangements. Since these formulations have not proved satisfactory in describing most physical systems of randomly packed powders, attention has more recently centered around alternate approaches. Here the Ohm's law model has been used extensively. This model bypasses the determination of the temperature field and seeks instead to evaluate the equivalent thermal resistance for a given array.

Wiener [7] was among the first to apply the electrical analogy to the problem of heat transfer in heterogeneous systems. While he did not obtain an expression for the effective thermal conductivity, it was shown that the value would lie between those predicted by the following formulas:

$$k_{es} = \frac{k_d k_c}{\bar{\varepsilon} k_c + (1-\bar{\varepsilon}) k_d} \tag{2-8}$$

$$k_{ep} = \bar{\varepsilon} k_d + (1-\bar{\varepsilon}) k_c \tag{2-9}$$

These two equations, referred to as Wiener's bounding formulas (Wiernerschen Grenzformeln), represent the cases in which the component resistances are arranged respectively in series, Figure (2-2a), and in parallel, Figure (2-1a) while Equations (7-8) and (2-9) establish

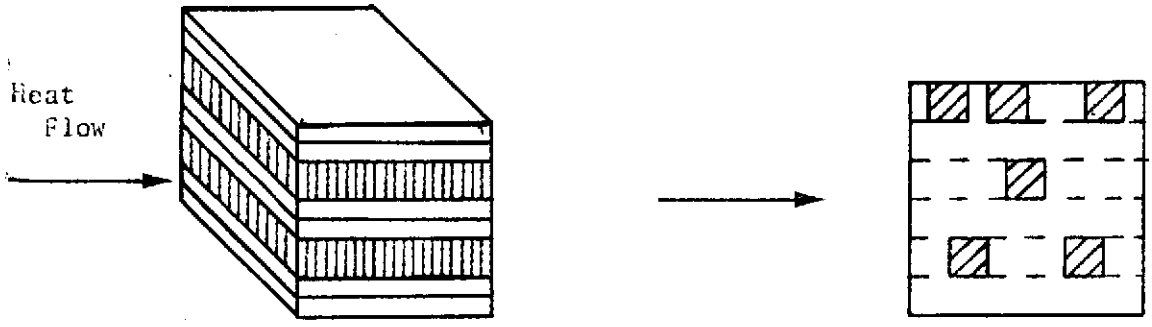

(a) Parallel Model (b) Loeb's Model

FIGURE 2-1. UNIFORM HEAT FLUX MODELS

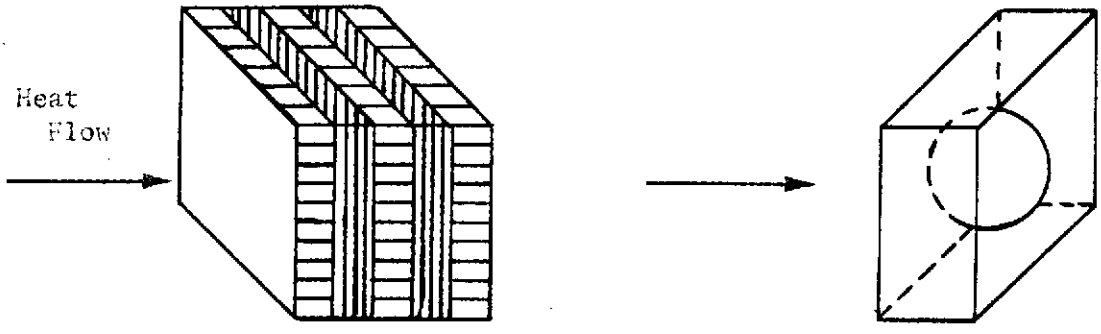

(a) Series Model (b) Jefferson's Model

FIGURE 2-2. PARALLEL ISOTHERMS MODELS

upper and lower bounds on the effective conductivity they are not intended to be used to calculate the actual value. This is because the effective conductivity of the system is strongly influenced by the constituent's arrangement [21]. Since neither case corresponds to the actual geometrical arrangement neither formula is satisfactory for such cases.

Several applications have been made of Wiener's results. Note that Equation (2-9) represents the effective thermal conductivity as the weighted arithmetic mean of the constituent conductivities; Equation (2-8) represents the thermal conductivity as the weighted harmonic mean. Lichteneker [22] proposed an equation in which the effective conductivity corresponded to the weighted geometric mean

$$k_e = k_c^{(1-\bar{\varepsilon})} k_d^{\bar{\varepsilon}} \tag{2-10}$$

Woodside and Messmer [23] report that this equation is generally valid for the range $0 < k_d/k_c < 20$. Whenever k_d/k_c exceeds 20 the Lichteneker equation overestimates the effective conductivity.

Bruggeman [18] states that Equation (2-10) allows for random orientation of particles in two directions only. For a truly three-dimensional random dispersion he generalized the Lichteneker equation to obtain

$$k_e = k_c^{[(1-\bar{\varepsilon})\ (1-k\bar{\varepsilon})]}\ k_d^{\bar{\varepsilon}[1+k(1-\bar{\varepsilon})]} \tag{2-11}$$

where

$$k = \frac{3}{2} \frac{k_d - k_c}{(2\sqrt{k_d} + \sqrt{k_c})(2\sqrt{k_c} + \sqrt{k_d})}$$

Another method of generalizing Wiener's results involves geometrically rearranging the physical system. It would seem reasonable that, since the parallel and series arrangements represent the limiting cases, an equivalent system composed of elements acting partly in parallel and partly in series could be used to represent the physical system.

Several authors have approximated a granular system by representing the solid particles as cubes arranged in a cubic lattice. The uniform spacing between particles is maintained such that the idealized system retains the proper volume fractions. A typical unit cell of this model is represented in Figure (2-3a). It is assumed that the effective thermal conductivity may be determined by considering the equivalent electrical resistances in parallel and in series and by applying Ohm's law.

In taking such an approach, certain additional simplifying assumptions are generally required. The assumption of straight and parallel heat flux lines yields the equivalent electrical network for the cubic array shown in Figure (2-3b). An alternate assumption of straight and parallel isotherms leads to a different equivalent network as shown in Figure (2-3c).

The two networks result in different effective conductivities both of which are approximations to the exact solution. In fact, these two cases represent two bounding solutions to the simplified model. The exact solution will yield an effective conductivity between those given

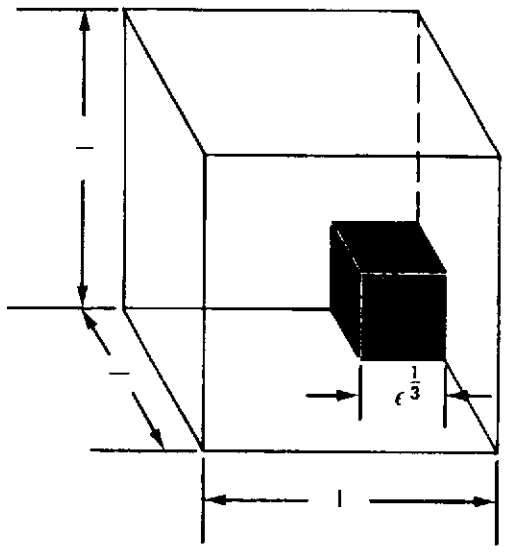

(a)

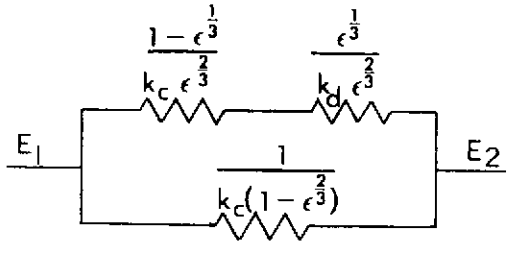

(b)

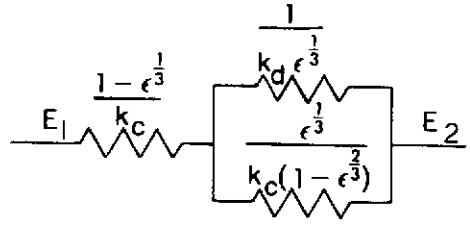

(c)

FIGURE 2-3. CUBIC LATTICE REPRESENTATION OF GRANULAR MATERIAL

by the two electrical networks. This is more clearly seen when one considers a nodal point representation of the temperature field in the proposed system. If the resistances normal to the direction of heat flow are assumed to be very large, the heat flow will remain uniform in the direction of the temperature gradient. Conversely, if the lateral resistances are taken as zero the potential will be equal in each lateral plane. Therefore, the assumption of linear and parallel heat flux lines is equivalent to the assumption of infinite lateral resistance; the assumption of parallel isotherms is equivalent to that of zero lateral resistance. The actual laterial resistance will, of course, fall somewhere between zero and infinity so that these two cases form the bounding conditions. Whether the two solutions represent the bounding conditions for the physical system depends upon the suitability of the proposed model.

It is generally assumed that either one or the other bounding condition represents a close approximation to the flow of energy in the proposed model. The suitability of this assumption will be discussed after the respective models have been considered. In compensation for this approximation it has been found possible to consider much more complex geometries than those which are possible using the flux-law model.

Uniform Heat Flux

Lichteneker [24] and son Frey [25] developed the uniform heat-flux model shown in Figure (2-3b). The effective thermal conductivity is then given as

$$\frac{k_e}{k_c} = \frac{(1 - \bar{\varepsilon}^{\frac{1}{3}} + \bar{\varepsilon}) + \frac{k_c}{k_d}(\bar{\varepsilon}^{\frac{1}{3}} - \bar{\varepsilon})}{(1 - \bar{\varepsilon}^{\frac{1}{3}}) + \frac{k_c}{k_d}\bar{\varepsilon}^{\frac{1}{3}}} \qquad (2\text{-}12)$$

It should be noted that this geometry results in a definite gap between particles and a complete absence of solid to solid contact. While such a model is suitable for dilute suspensions it is doubtful if it could adequately represent granular materials. In cases where the gas conductivity is much less than the solid conductivity, solid to solid heat conduction may, in fact, be the major mode of heat transfer. In such cases it might be anticipated that the proposed model would yield consistently low results, especially in light of the fact that the assumption of linear heat flux lines should lead to low results.

A number of investigators have continued to develop a similar model using various schemes to overcome the problem of the relatively large gap between particles. One such technique is to distort the solid cube, elongating it in the direction of heat flow. Woodside and Messmer [23], Schotte [26], Smith [27] and Willhite, Kunii and Smith [31] developed models assuming such an arrangement. Woodside and Messmer obtained

$$\frac{k_e}{k_c} = \frac{(\bar{\varepsilon} + 0.03)^2 k_d}{0.03k_d + \bar{\varepsilon}k_c} + 0.97 - \bar{\varepsilon} \qquad (2\text{-}13)$$

The equation of Willhite, Kunii and Smith is

$$\frac{k_e}{k_c} = 1 + \bar{\varepsilon}\left(1 - \frac{k_c}{k_d}\right) + \frac{\gamma}{\alpha}\left(1 - \frac{k_c}{k_d}\right)^2 \bar{\varepsilon} \qquad (2\text{-}14)$$

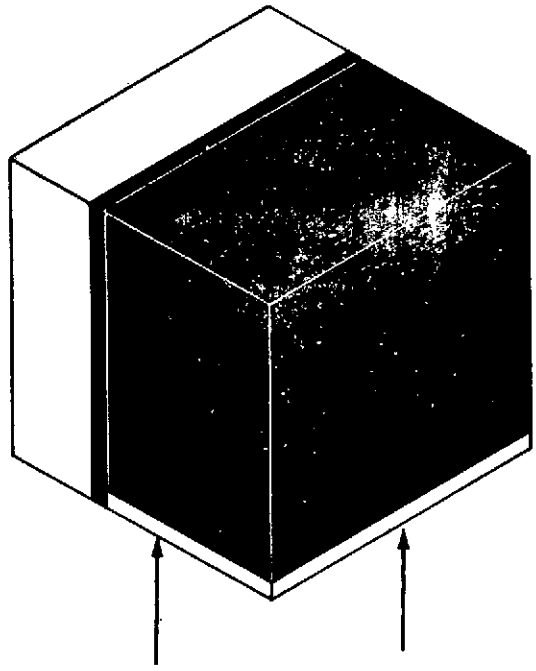

FIGURE 2-4. PARALLELOPIPED REPRESENTATION OF GRANULAR MATERIAL

where

$$\alpha = \frac{\sin^2\theta}{2} \frac{\left(\frac{k_d-k_c}{k_d}\right)^2 \sin^2\theta}{\ln\left[\frac{k_d}{k_c} - \left(\frac{k_d}{k_c} - 1\right)\cos\theta\right] - \frac{k_d-k_c}{k_d}(1-\cos\theta)}$$

$$\theta = \sin^{-1}\sqrt{\frac{2}{n}}$$

In this relation n is the average number of contact points on the particle. The experimentally derived parameter, γ, represents the ratio of the effective length of the solid particle to the diameter of the physical particle. The authors state that a value $\gamma = 2/3$ correlates a wide range of data.

A number of investigators have continued to develop similar models using various schemes to overcome the problem of the relatively large gap between particles. Bernstein [44] effectively utilized this approach in arranging rectangular particles in a staggered two dimensional array. For high porosity ($\varepsilon \geq 0.5$) systems the solid cube was distorted by lengthening its dimension in the direction of heat flux while decreasing its lateral dimensions to maintain the proper volume fractions. For low porosity systems ($\varepsilon \leq 0.5$) Bernstein interchanged the solid and void regions of the unit cube so that the effective thermal conductivity is given by the equations

$$\frac{k_e}{k_c} = \frac{4\bar{\varepsilon}}{\left(1 + \frac{k_c}{k_d}\right)} + \frac{k_d}{k_c}(1 - 2\bar{\varepsilon}) \qquad (2\text{-}15a)$$

$$\bar{\varepsilon} \leq .50$$

$$\frac{k_e}{k_c} = \frac{4(1-\bar{\varepsilon})}{\left(1 + \frac{k_c}{k_d}\right)} + 2\bar{\varepsilon} - 1 \qquad (2\text{-}15b)$$

$$\bar{\varepsilon} \geq .50$$

A second scheme of reducing the gap between particles considers a portion of the solid phase to pass entirely through the unit cube. This accounts for the residual conductivity of the system in a pure vacuum. A typical element of this type is shown in Figure (2-4). Several authors [28-34] have used this technique to include contact between particles. However, most of these developments have required the inclusion of one or more parameters which must be experimentally obtained for each sample. Generally this information is not available.

Using the same basic assumption of linear heat flux lines Schumann and Voss [35] developed a model using a somewhat different geometry. It was assumed that a unit cell of the material could be replaced by an equivalent geometry in which the two phases are divided by a rectangular hyperbola. Thus the solid phase appears as a somewhat distorted "cylinder" arranged in a square array oriented normal to the direction of heat flux. The varying fraction of the solid phase seems much more representative of the physical system. The effective thermal conductivity obtained by Schumann and Voss is:

$$\frac{k_e}{k_c} = (1-\bar{\varepsilon})^3 + \frac{1 - (1-\bar{\varepsilon})^3}{\left(\frac{k_c}{k_d} + p\,\frac{k_c}{k_d} - 1\right)}\left\{1 + \frac{p(1+p)(k_c-k_d)}{k_c+p(k_c-k_d)} \ln\left[\frac{k_c}{k_d}\,\frac{(1+p)}{p}\right]\right\} \qquad (2\text{-}16)$$

where p is implicitly defined by the relation:

$$1 - \bar{\varepsilon} = p(p+1) \ln \frac{1+p}{p} - p$$

The inclusion of an implicit relation makes the equation somewhat difficult to solve analytically although a graphical tabulation has been given.

In comparison to the Lichteneker and son Frey model, the model of Schumann and Voss is much more realistic in representing granular systems in that the finite gap between particles has been eliminated. Nevertheless the effective thermal conductivity obtained from this equation still tends to fall below experimentally obtained values. This tendency was noted separately by Preston [36] and Wilhelm [37]. Both authors presented correction terms to the Schumann and Voss equation to bring the calculated value closer to the experimental data. Wilhelm's correlation has been widely used, and its predictions are in good agreement with many experimental data for granular materials since it was constructed from these data. This equation is

$$\log(\Delta \times 10^5) = m + n \left(\frac{k_d}{1-\bar{\varepsilon}} \right) \qquad (2\text{-}17)$$

where Δ in cal/cm-sec-$^\circ$K is an error term to be added to calculated conductivities according to Schumann and Voss, and the "least squares" values of the constants are

$$m = 0.859 \pm 0.051$$

$$n = 3.12 \pm 0.29 \ (\text{cal/cm-sec-}^\circ\text{K})^{-1}$$

Gorring and Churchill [4] used a development somewhat analogous to Schumann and Voss' for three dimensional particles. In this case, an equivalent geometry was assumed in which the two phases were separated by a parabola of revolution. The solid particles then appear as distorted "spheres" arranged in a square array. For this geometry the effective conductivity is given by

$$\frac{k_e}{k_c} = \frac{\pi}{6\left(1-\frac{k_c}{k_d}\right)CB}\left\{\ln\left(\frac{\sqrt{B^2-Bx_o+x_o^2}}{B+x_o}\right)+\sqrt{3}\tan^{-1}\left(\frac{2x_o-B}{\sqrt{3}B}\right)\right.$$

$$\left.-\sqrt{3}\tan^{-1}\left(\frac{1}{\sqrt{3}}\right)\right\}+\left\{1-\frac{\pi x_o^2}{4}\right\} \qquad (2\text{-}18)$$

where: $$B = \left[\frac{k_c}{C(k_d-k_c)}\right]^{\frac{1}{3}}$$

for $\bar{\varepsilon} \leq \frac{\pi}{10}$, $x_o = 1.0$

$$C = \frac{10\bar{\varepsilon}}{\pi}$$

for $\bar{\varepsilon} \geq \frac{\pi}{10}$, $x_o = \frac{1.0}{C^{\frac{1}{3}}}$ $\qquad C = \left[\frac{3\pi}{5\pi-20\bar{\varepsilon}}\right]^{\frac{3}{2}}$

Systems of spherical particles arranged in a square array were studied by Hengst [38] and later by Lyalikov [39] and Kaganer [40]. Kaganer's expression for the effective conductivity of granular systems assumes the form

$$\frac{k_e}{k_c} = \frac{n\bar{\varepsilon}k_d}{2(k_d-k_c)}\left[\frac{k_d}{k_d-k_c}\ln\left(\frac{k_d}{k_c}\right)-1\right] \qquad (2\text{-}19)$$

In this expression n is taken as the average number of contacts for each particle. Note that the geometry utilized in this model is precisely the same as that assumed by Lord Rayleigh in the case of touching spheres ($\bar{\epsilon} = 0.524$). Equation (2-18) is suggested for use with packing fractions greater than 0.524. Physically this is difficult to visualize as denser packings are not possible with the prescribed geometry.

Deissler and Eian [41] accounted for variations in packing fractions in a different manner. Two separate models were developed to account for such variations. One model considered spheres in a cubic array with point contact; the second used cylinders in a square array with line contact. Including the cases in which the material is composed of all solid or all gas, the relation between k_e/k_c and k_d/k_c is then known for four values of $\bar{\epsilon}$. For any other packing fraction the effective conductivity could be found by interpolation. Krupiczka [42] used the same approach but introduced solutions for the spherical and cylindrical arrays based on flux-law models. Krupiczka then curve fitted his solutions together with certain experimental data to obtain

$$\frac{k_e}{k_c} = \left(\frac{k_d}{k_c}\right)^{[0.280 - 0.757 \ln (1-\bar{\epsilon}) - 0.057 \ln (k_d/k_c)]} \qquad (2\text{-}20)$$

Loeb [69] was one of the first to deviate from an assumed rigid geometry and account for the distribution of the two phases. His basic assumption is that if a unit cube of the two-phase material is subdivided into parallel to the heat flow tubes, the dispersed phase may be arranged to lie completely within a set of tubes (Figure 2-1b). An electrical analogy is then written for each tube, and the conduc-

tance of the unit cube is expressed as the sum of the tube conductances. The final expression for the effective thermal conductivity is

$$k_e = k_c \left[(1-P_c) + \frac{P_c}{P_L \frac{k_c}{k_d} + (1-P_L)} \right] \qquad (2\text{-}21)$$

where: P_c = fraction of cross-sectional area occupied by the tubes

P_L = fraction of tube length occupied by discontinuous phase.

Parallel Isotherms

As previously noted, the development of an Ohm's law model requires first the selection of an equivalent geometry. Then either the assumption of uniform heat flux or parallel isotherms may be used. It is not surprising, then, that frequently models of each type have been developed starting from the same basic configuration.

Russell [43] selected the same cubic array of cubical particles as Lichteneker and son Frey. Assuming parallel isotherms, Russell obtained

$$\frac{k_e}{k_c} = \frac{\bar{\varepsilon}^{\frac{2}{3}} + \frac{k_c}{k_d}(1-\bar{\varepsilon}^{\frac{2}{3}})}{\bar{\varepsilon}^{\frac{2}{3}} - \bar{\varepsilon} + \frac{k_c}{k_d}(1 - \bar{\varepsilon}^{\frac{2}{3}} + \bar{\varepsilon})} \qquad (2\text{-}22)$$

Here again, the model does not consider solid to solid contact so that it might be anticipated that results would tend to fall below experimental values. Laubitz [17] reported that Russell's equation typically gave results which were low by about a factor of two.

Jefferson [78] derived an expression for spherical particles, each enclosed in a unit cube of the continuous phase. His derivation

is based on one-half such unit (Figure 2-2b), and the resulting equations are

$$k_e = k_c \left[1 - \frac{\pi}{4(1+2n)^2} \right] + \frac{\pi}{4(1+2n)^2} \left[\frac{(0.5+n)\, k_a\, k_c}{0.5\, k_c + n\, k_a} \right]$$

$$k_a = k_c \cdot k_d \left[\frac{2k_d}{(k_d - k_c)^2} \ln \left(\frac{k_d}{k_c}\right) - \frac{2}{k_d - k_c} \right] \qquad (2\text{-}23)$$

$$n = 0.403 \left(\bar{\varepsilon} \right)^{-1/3} \approx 0.5$$

Baxley and Couper [20] report that for suspensions and emulsions the average error of Equation (2-22) is 21%.

Godbee and Ziegler [45] developed a parallel isotherm model analogous to that proposed by Woodside and Messmer. The solid particles in a heterogeneous system were replaced by a pore free parallelopiped within the representative material cube. The authors have obtained an expression relating the dimensions of the solid region to the material volume fractions and the particle size distribution so that the effective thermal conductivity is given by the relation

$$\frac{k_e}{k_c} = \left\{ \frac{1}{\dfrac{D/x}{\left(1 - \dfrac{S}{x^2}\right) + \dfrac{k_d}{k_c}\left(\dfrac{S}{x^2}\right)} + \left(1 + \dfrac{D}{x}\right)} \right\} \qquad (2\text{-}24)$$

where

$$S = \frac{D^2}{2} \int_{D_a}^{D_b} e^{-u^2/2}\, du$$

$$x = \left(\frac{SD}{1-\bar{\epsilon}}\right)^{1/3}$$

Topper [46], Webb [47] and Woodside [48] proposed models incorporating spherical particles arranged in a cubic lattice similar to that of Hengst. The introduction of spherical particles will tend to reduce the gap between particles. Unfortunately the method is restricted by the requirement that the spheres do not overlap, i.e. the solid fraction must be less than 0.524. Most granular materials tend to pack to a higher density so that this model is of restricted application. The formula developed by Woodside is

$$\frac{k_e}{k_c} = \frac{1}{1 - \left[\frac{6\bar{\varepsilon}}{\pi}\right]^{\frac{1}{3}} \left[1 - \left(\frac{a^2-1}{a}\right) \ln\left(\frac{a+1}{a-1}\right)\right]} \qquad (2\text{-}25)$$

where:

$$a = \left[1 + \frac{4}{\pi\left(\frac{k_d}{k_c} - 1\right)\left(\frac{6\bar{\varepsilon}}{\pi}\right)^{\frac{2}{3}}}\right]^{\frac{1}{2}}$$

$$0 \leq \bar{\varepsilon} \leq 0.524$$

Tsao [8] was able to overcome the problem of introducing solid to solid contact while simultaneously introducing a truly randomly packed array. The development of the stochastic model is indicated in Figure (2-5a). Considering a typical unit cube, the heterogeneous material was divided into a large number of laminae oriented normal to the direction of heat flow. By taking the laminae sufficiently thin the area of each phase will remain essentially constant across the element. Thus the two phases may be viewed as acting in parallel across the laminae. The arrangement of the parallel resistances do not affect the overall resistance so that the element may be replaced by one in which the two phases have been segregated as shown in Figure (2-5b). Similarly since each of the laminae may be viewed as a resistance acting in series the order of the laminae may be arbitrarily changed. For simplicity Tsao arranged the elements in order of decreasing solid fraction. This final arrangement is shown in Figure (3c). Probability theory was then used to develop an expression for the shape of the distribution curve. The final expression is given in terms of the experimentally obtained solid distribution parameters μ_1 and σ_1

$$k_e = \frac{1}{\int_0^1 \frac{dP_1}{k_c + \frac{(k_d - k_c)}{\sigma_1\sqrt{2\pi}} \int_{P_1}^{1} e^{-1/2\left[\frac{x-u_1}{\sigma_1}\right]^2} dx}} \qquad (2\text{-}26)$$

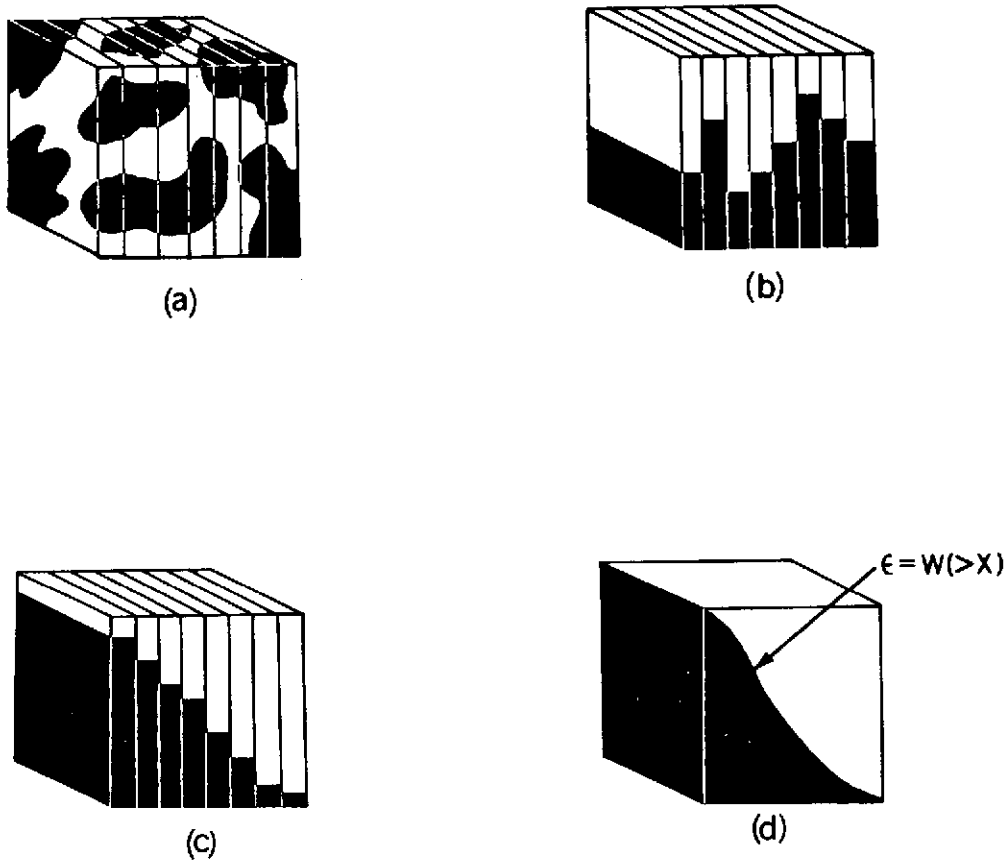

FIGURE 2-5. EQUIVALENT GEOMETRIES FOR LINEAR ISOTHERMS

Here μ_1 represents the mean solid fraction and σ_1 represents the standard deviation of the solid fraction in the horizontal laminae of the redistributed element shown in Figure (2-5d); these laminae are chosen parallel to the direction of heat flow as opposed to the vertical laminae used in the redistribution. A considerable amount of theoretical and experimental work has been done on material distributions in packed beds [49-51]. These studies show that the mean solid-area fraction is equal to the bulk solid fraction but thus far no data is given to evaluate the standard deviation in solid area fraction of these redistributed elements. Furthermore, it does not appear possible to evaluate this parameter directly.

Warren and Messmer [52] noted that Tsao failed to normalize the frequency distribution used in Equation (2-26). This is not a serious fault provided that μ_1 is sufficiently small. Under the conditions $3\sigma_1 < \bar{\epsilon}$ and $3\sigma_1 < (1-\bar{\epsilon})$ the normalized distribution reduces to that used in Tsao's correlation.

One important contribution by Tsao was to show how random distributions could be analyzed without resorting to the regular arrays assumed by each of the previous investigations. Furthermore, this correlation is applicable to granules of any shape and size distribution. Thus Tsao's correlation is one of the most general equations presented thus far.

Summarizing the Ohm's law models, it is found that they are characterized by unrealistic assumptions regarding the lateral conductivity of the mixture. Frequently these models retain the same

unrealistic geometries common to the flux law models. However, more realistic geometries can and have been used with this type of analysis.

Equations have been developed to predict the thermal conductivity for special cases. Very dilute suspensions and emulsions are represented quite adequately by the Maxwell equation. However, each of the proposed models retains one or more approximations which greatly limits their utility and accuracy when applied to granular materials. The purpose of this study is to derive a general set of equations which will predict the effective thermal conductivity of a two phase granular system while overcoming these specific objections.

III. COMPARISON OF PUBLISHED MODELS AND CRITIQUE

Before an attempt can be made to develop models that improve the predicted effective thermal conductivity values, an investigation of when and why already published models fail should be made. To accomplish this, a number of the models presented in Chapter 2 have been applied to the granular systems listed in Table 6-I. The models chosen are those which are most widely used in the current literature and in present engineering practice. In cases where the development of two models is only slightly different, one of the two is chosen.

The results are presented in Figures (3-1) through (3-18) and summarized in Table 3-I. The figures are classified according to the categories mentioned in Chapter 2 as follows:

1. Figures (3-1) through (3-4) present flux law models;
2. Figures (3-5) through (3-13) present Ohm's Law, uniform heat flux models;
3. Figures (3-13) through (3-16) present Ohm's Law, parallel isotherms models;
4. Figures (3-17) and (3-18) present Lichtenecker's weighted equations.

Figures 3-1 through 3-4 indicate that the flux law models are in good agreement with experimental measurements at low constituent

conductivity ratios, but predict considerably lower values at high constituent conductivity ratios. There is a number of reasons to explain this behavior. First, the heat flow path from particle to particle is neglected due to the absence of a finite particle contact area. Thus an important mode of heat transfer at high conductivity ratios is not taken into account. Second, the idealized particle shape and geometry utilized in the models do not provide a sufficiently close approximation to the geometry of most granular materials. Finally, with the exception of Bruggeman's equation, the flux law models have been extrapolated beyond the porosity range for which they are theoretically applicable ($\frac{\pi}{6} \leq P \leq 1$).

It should be noted that whereas the conductivities predicted by Lord Rayleigh's and Meredith and Tobias' equations are comparable, Bruggeman's equation represents a considerable improvement of the calculated values. This is probably an indication that the geometry of any future flux law model should not radically depart from the geometry of real granular systems.

Figures 3-5 through 3-13 indicate that in general uniform heat flux models predict low effective thermal conductivities and the discrepancy increases with the ratio of constituent conductivities. As it will be discussed in detail in Chapter 4, the uniform heat flux assumption necessitates that the conductivity of the constituents in the normal to the heat flow direction be zero. Consequently, the low predicted thermal conductivities are an expected result of the linear

heat flow assumption. However, the equation of Woodside and Messmer predicts high values at low constituent conductivity ratios, but when k_d/k_c increases beyond a certain limit the calculated values become low. The explanation of this behavior lies on the geometry assumptions introduced in the model. In the Woodside and Messmer model the solid phase is elongated in the direction of heat flow, thus rendering the calculated effective conductivity high at low values of k_d/k_c. However, when k_d/k_c increases, the absence of finite contact areas between particles and the linear heat flow assumption come into effect, and as a result the calculated effective conductivities are low.

It is seen that the equations of Preston, Wilhelm et al, and Krupiczka, which include correlation terms, are in very good agreement with the experimental data for granular materials and powders at atmospheric pressures.

Figures 3-14 through 3-16 indicate that parallel isotherms models generally predict high values for the effective thermal conductivity. Again, this is due to the introduction of infinite conductivity in the normal to the heat flow direction, necessitated by the heat flow assumption. Russell's model is an exception to this conclusion, since it predicts low values at high ratios of constituent conductivities. This is probably due to the simplified geometry of the model, and to the relatively large gaps between particles. It appears that the influence of the simplified geometry and the absence of contact areas between particles dominate over the influence of the heat flow assumption.

In Figures (3-17) and (3-18) Lichtenecker's weighted equations are compared to experimental data. Evidently the values predicted by these equations are in error, indicating that any such future attempt should rely heavily on experimental evidence.

Summarizing the comparison of published models, it is found that the major sources of error can be attributed to the following causes.

1. Distorted or idealized geometry;
2. Idealized heat flow;
3. Absence of finite particle contact area.

Not all sources of error are applicable to each one of the models discussed. Typically, one or more are applicable in each case. However, it is difficult to isolate a prior source of error for a particular model. It appears that the discrepancy between calculated and experimental values is due to an interaction of all sources, each source dominating over a particular range of k_d/k_c depending on the geometry and heat flow assumptions. Consequently, in any more refined model the influence of each of the above sources of error should be minimized, especially if it is expected that the model should be applicable to granular materials having large ratios of constituent conductivities. Such an attempt has been undertaken in the models that will be described in the rest of this study. First, however, the effects of the uniform heat flux and parallel isotherms assumptions will be investigated, because if it were possible to utilize either

assumption, the problem of finding the effective thermal conductivity of granular materials would be simplified considerably.

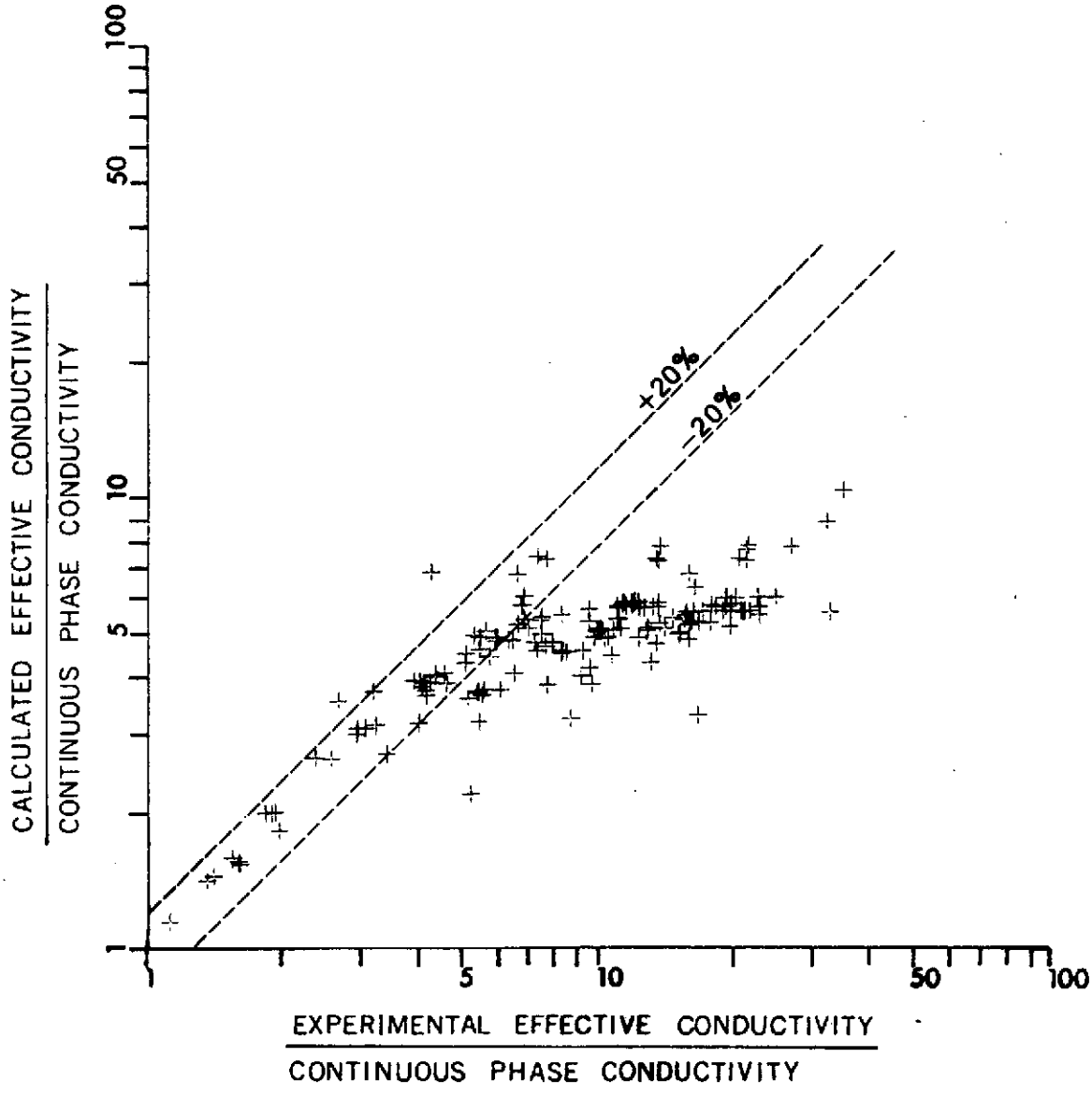

FIGURE 3-1. COMPARISON OF EXPERIMENTAL RESULTS WITH CALCULATED CONDUCTIVITY FOR THE MAXWELL EQUATION.

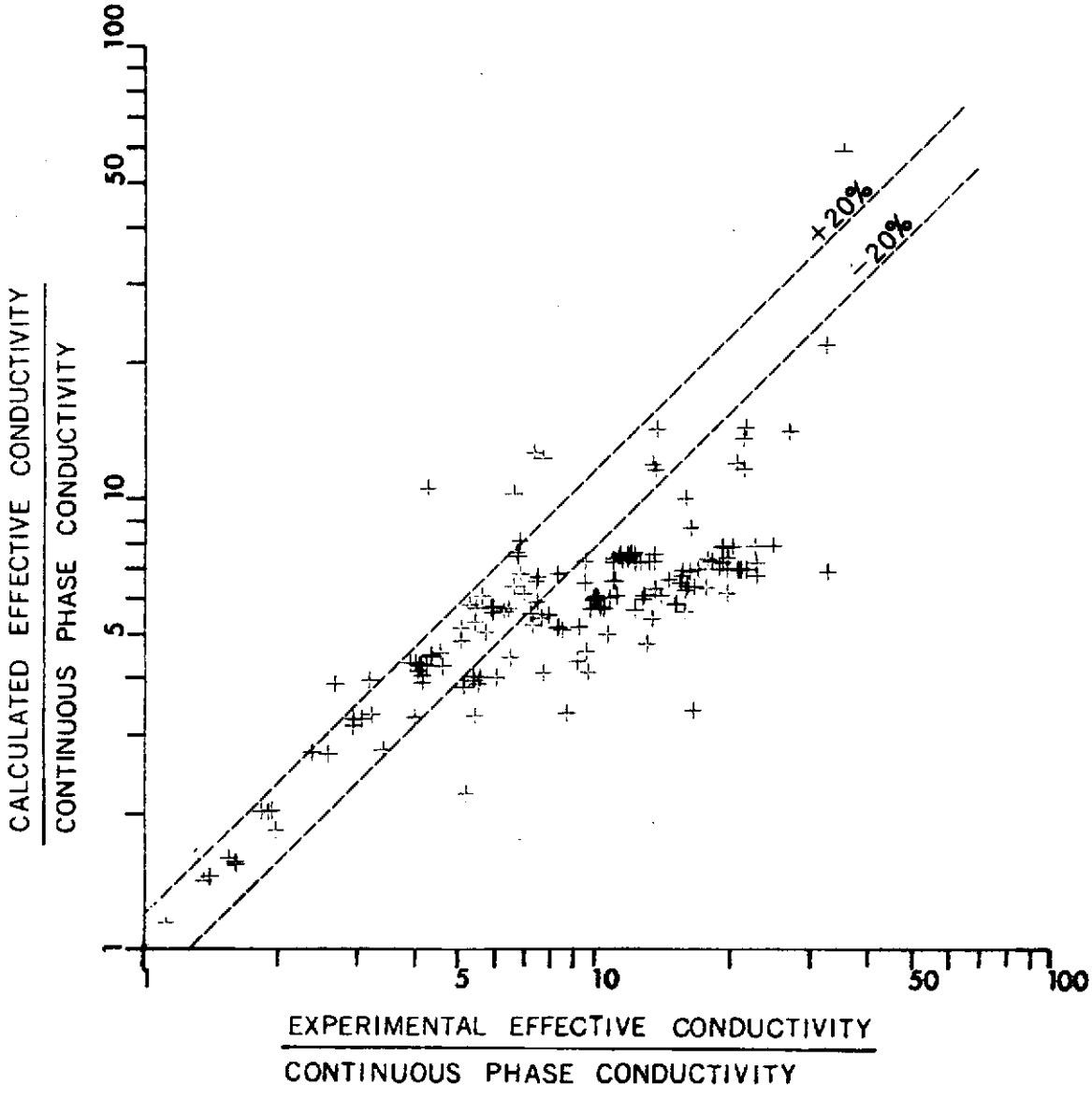

FIGURE 3-2. COMPARISON OF EXPERIMENTAL RESULTS WITH CALCULATED CONDUCTIVITY FOR THE LORD RAYLEIGH EQUATION.

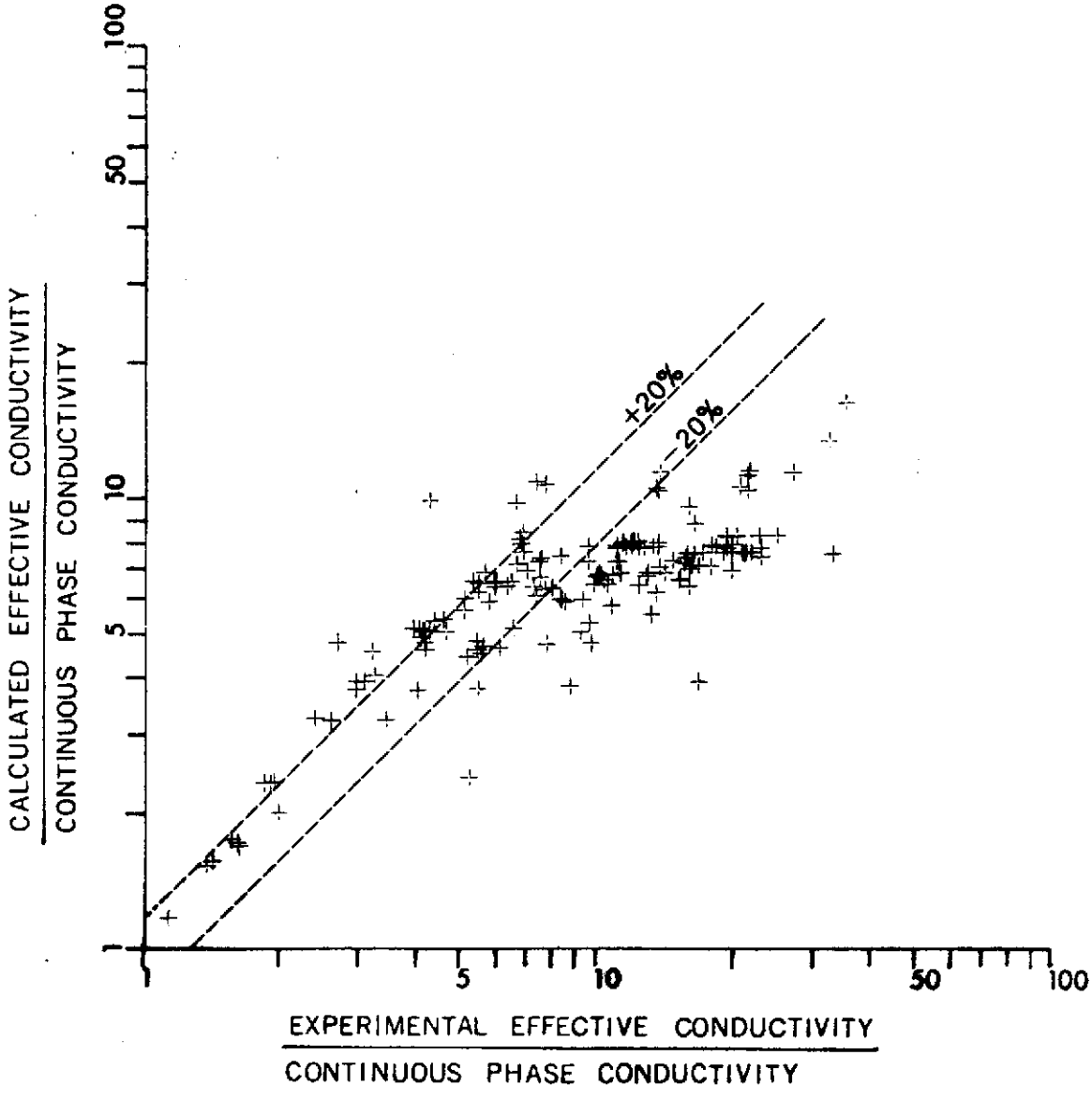

FIGURE 3-3. COMPARISON OF EXPERIMENTAL RESULTS WITH CALCULATED CONDUCTIVITY FOR THE MEREDITH AND TOBIAS EQUATION.

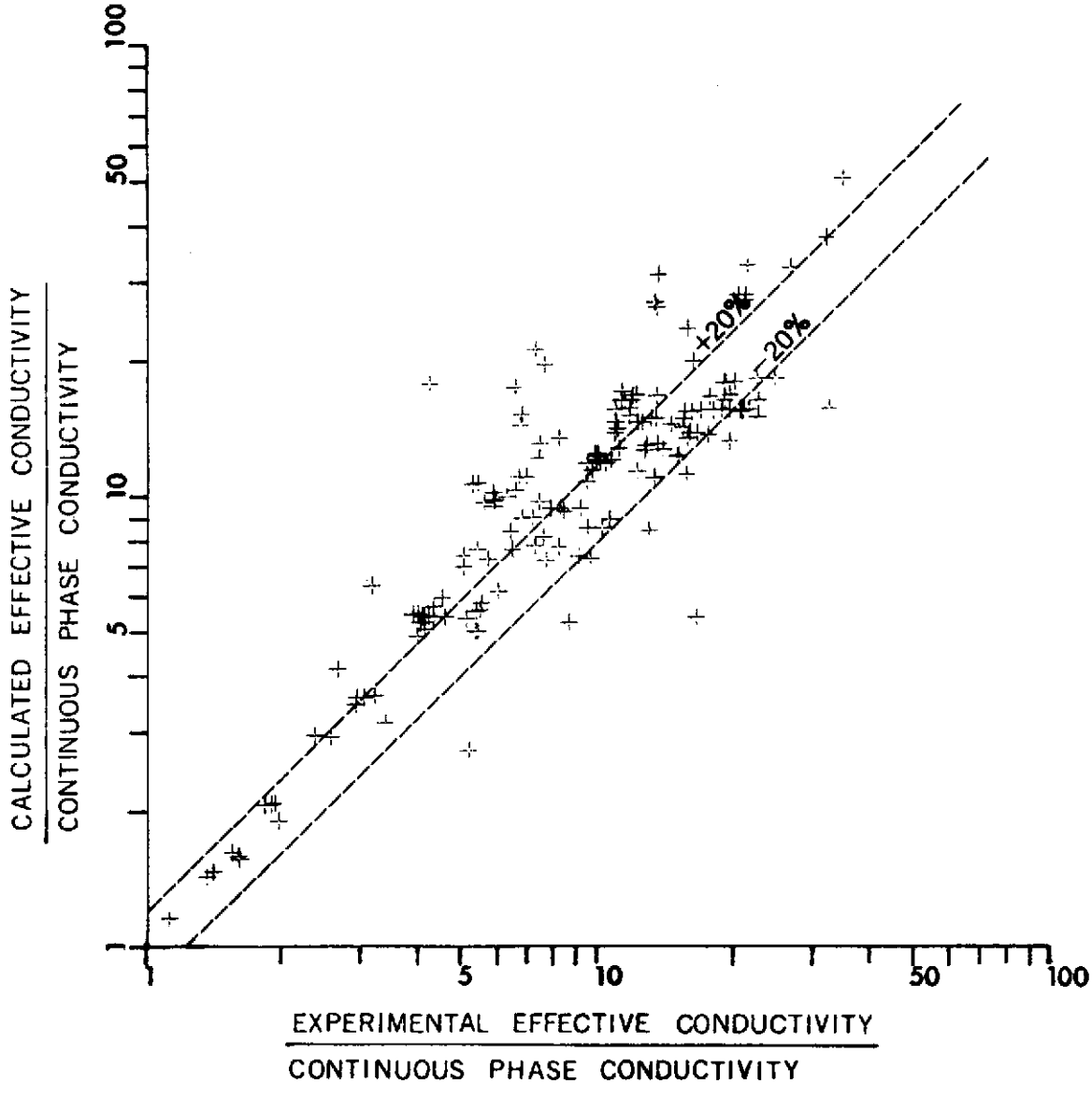

FIGURE 3-4. COMPARISON OF EXPERIMENTAL RESULTS WITH CALCULATED CONDUCTIVITY FOR THE BRUGGEMAN EQUATION.

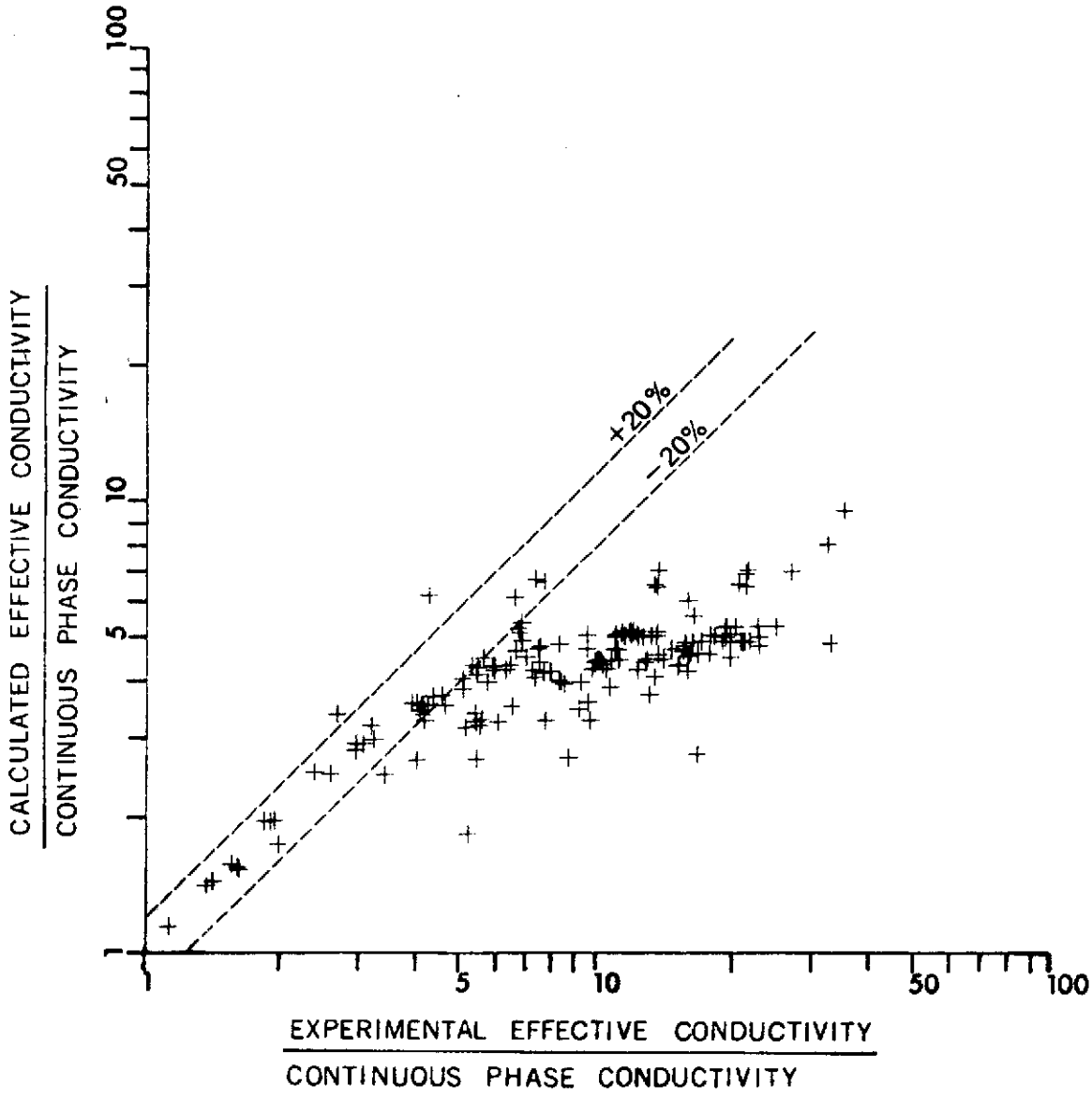

FIGURE 3-5. COMPARISON OF EXPERIMENTAL RESULTS WITH CALCULATED CONDUCTIVITY FOR THE SON FREY EQUATION.

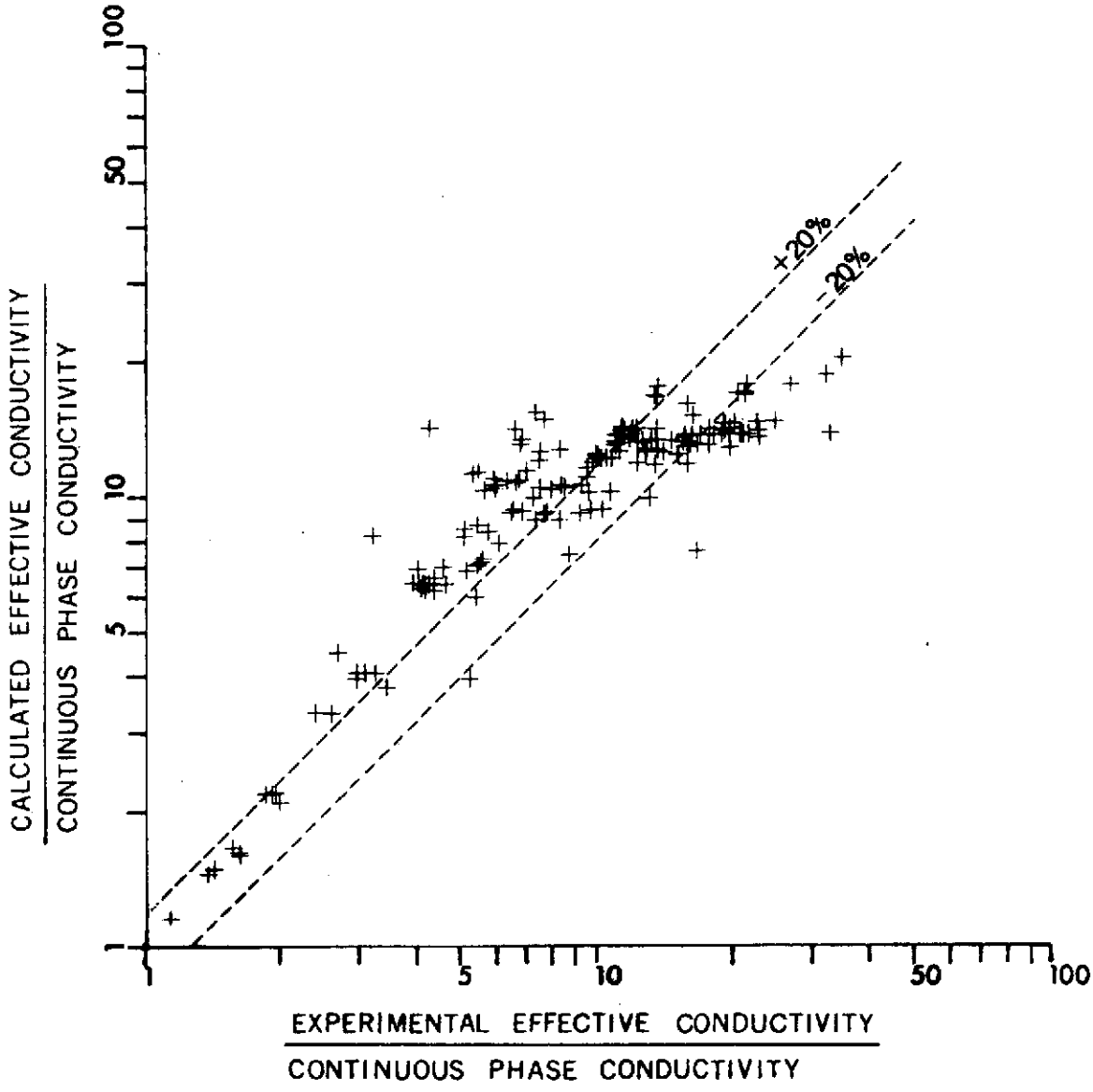

FIGURE 3-6. COMPARISON OF EXPERIMENTAL RESULTS WITH CALCULATED CONDUCTIVITY FOR THE WOODSIDE AND MESSMER EQUATION.

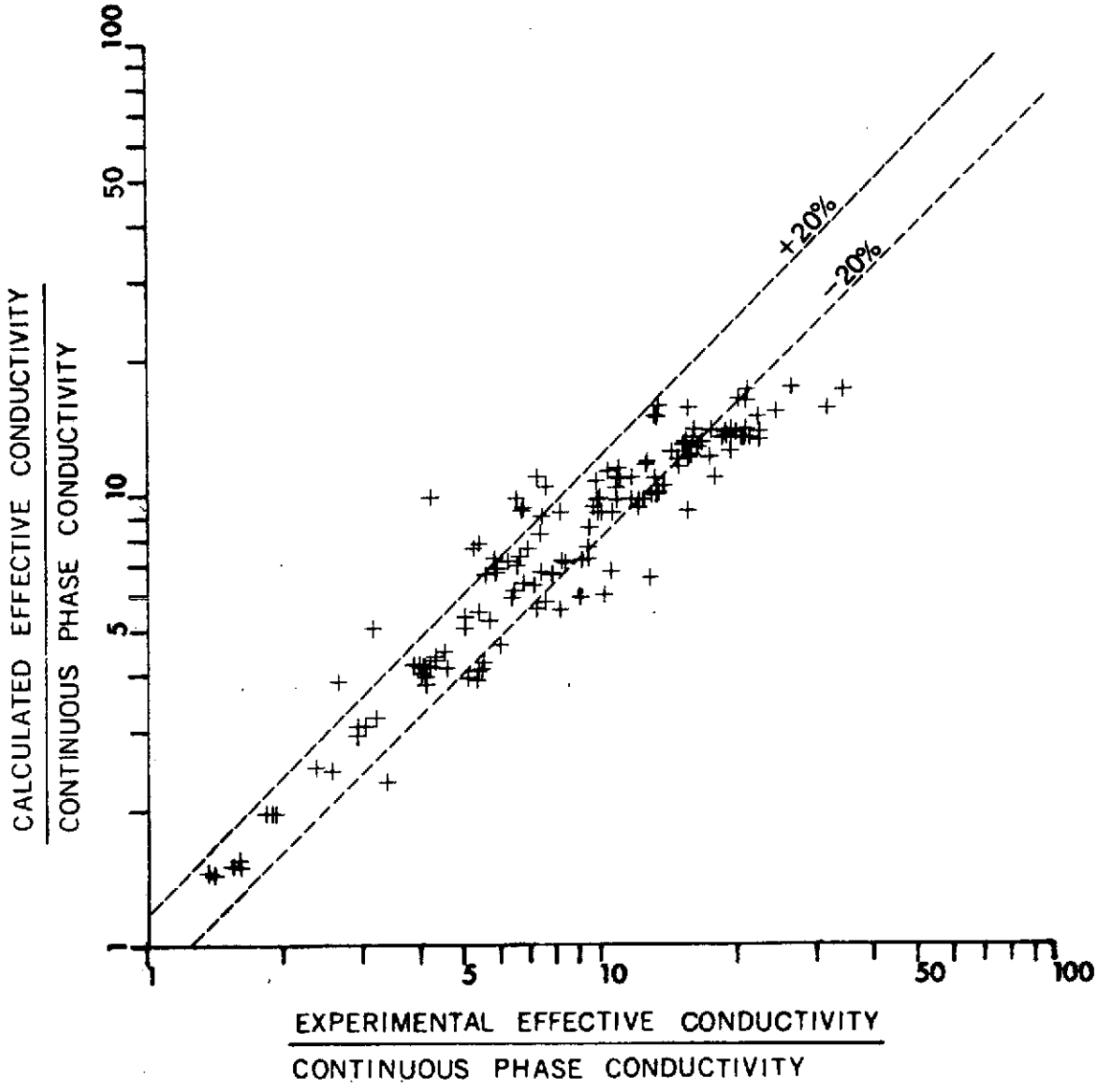

FIGURE 3-7. COMPARISON OF EXPERIMENTAL RESULTS WITH CALCULATED CONDUCTIVITY FOR THE KANAGER EQUATION.

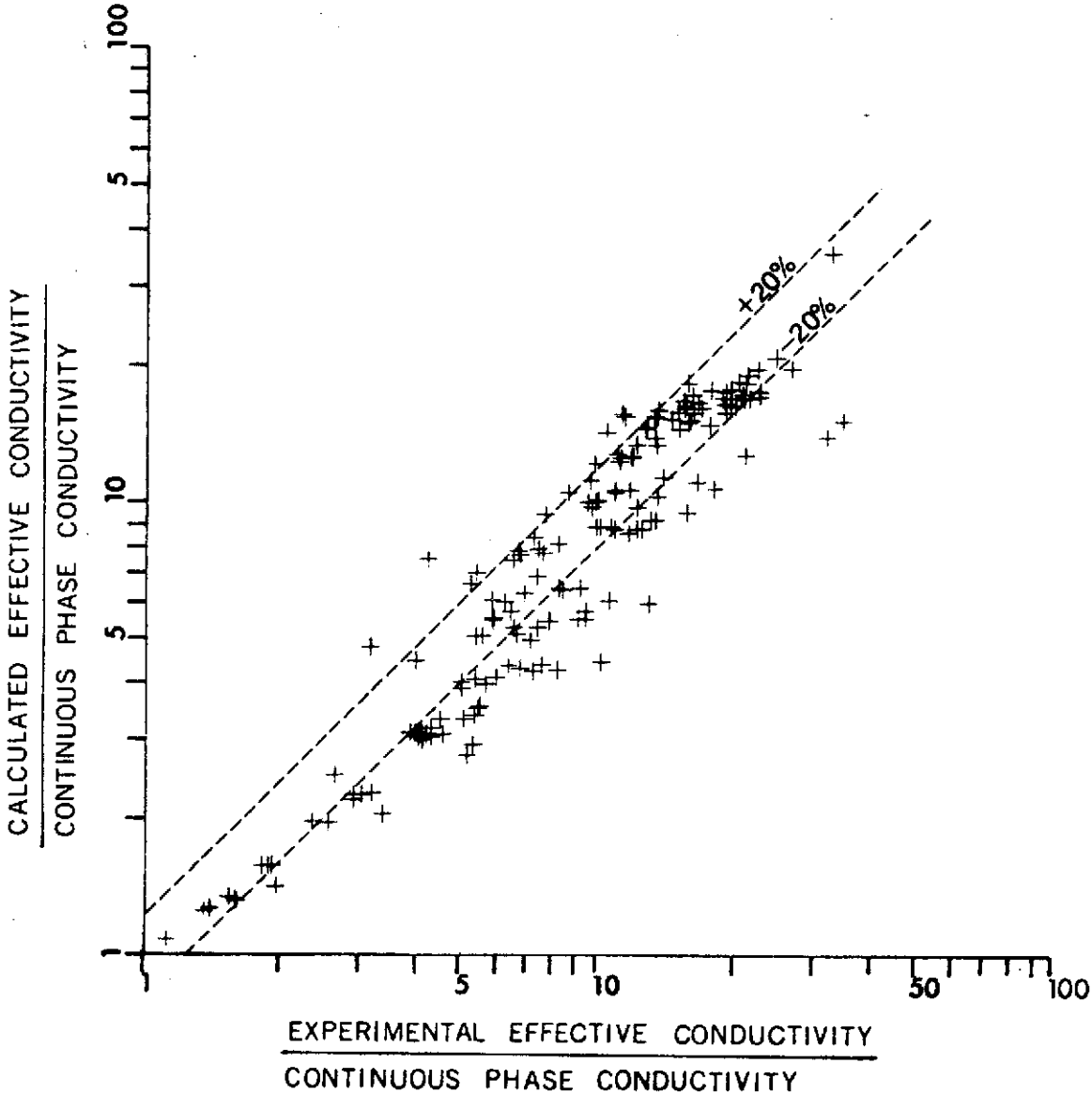

FIGURE 3-8. COMPARISON OF EXPERIMENTAL RESULTS WITH CALCULATED CONDUCTIVITY FOR THE GORRING AND CHURCHILL EQUATION.

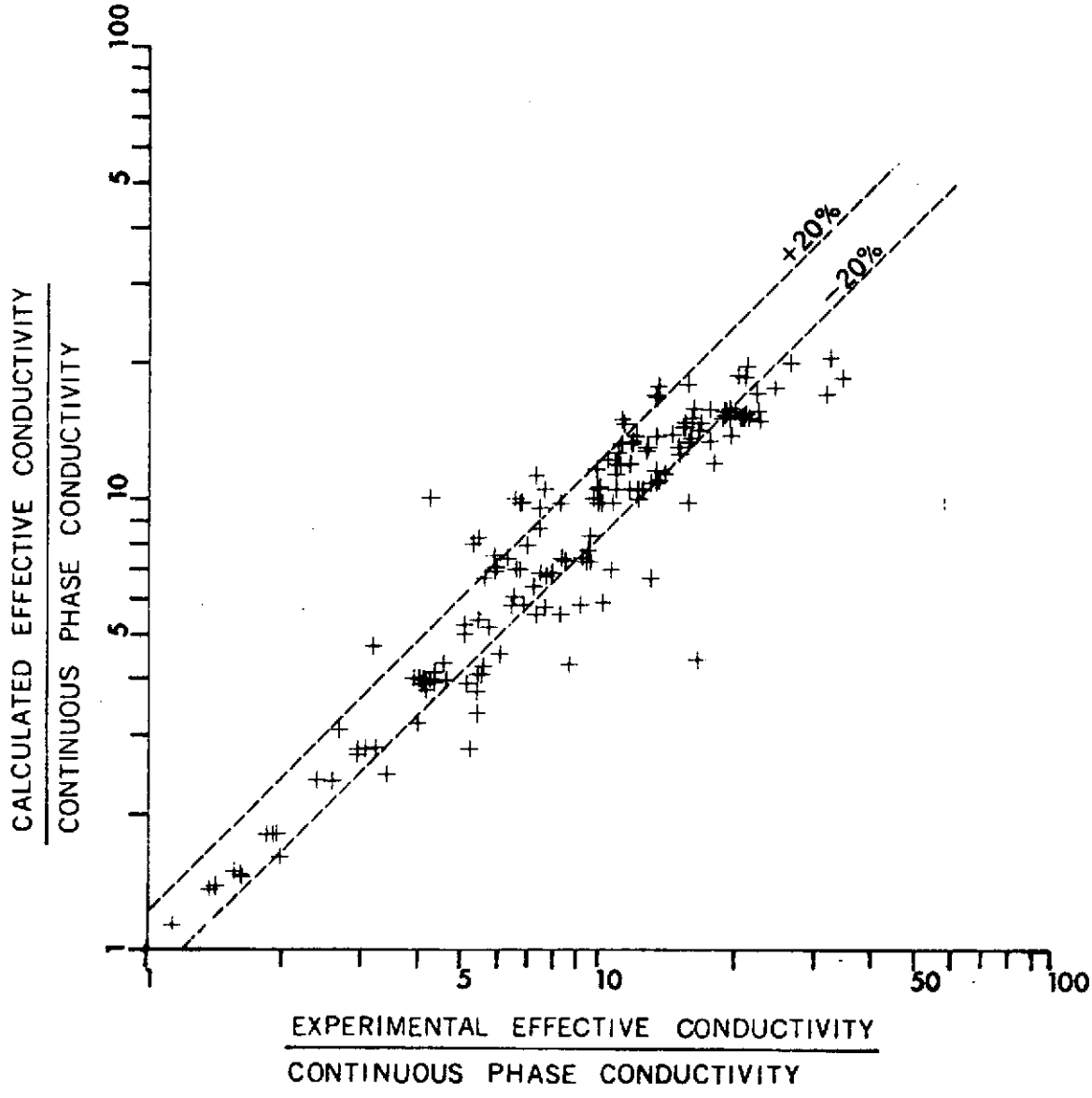

FIGURE 3-9. COMPARISON OF EXPERIMENTAL RESULTS WITH CALCULATED CONDUCTIVITY FOR THE WILLHITE, KUNII AND SMITH EQUATION.

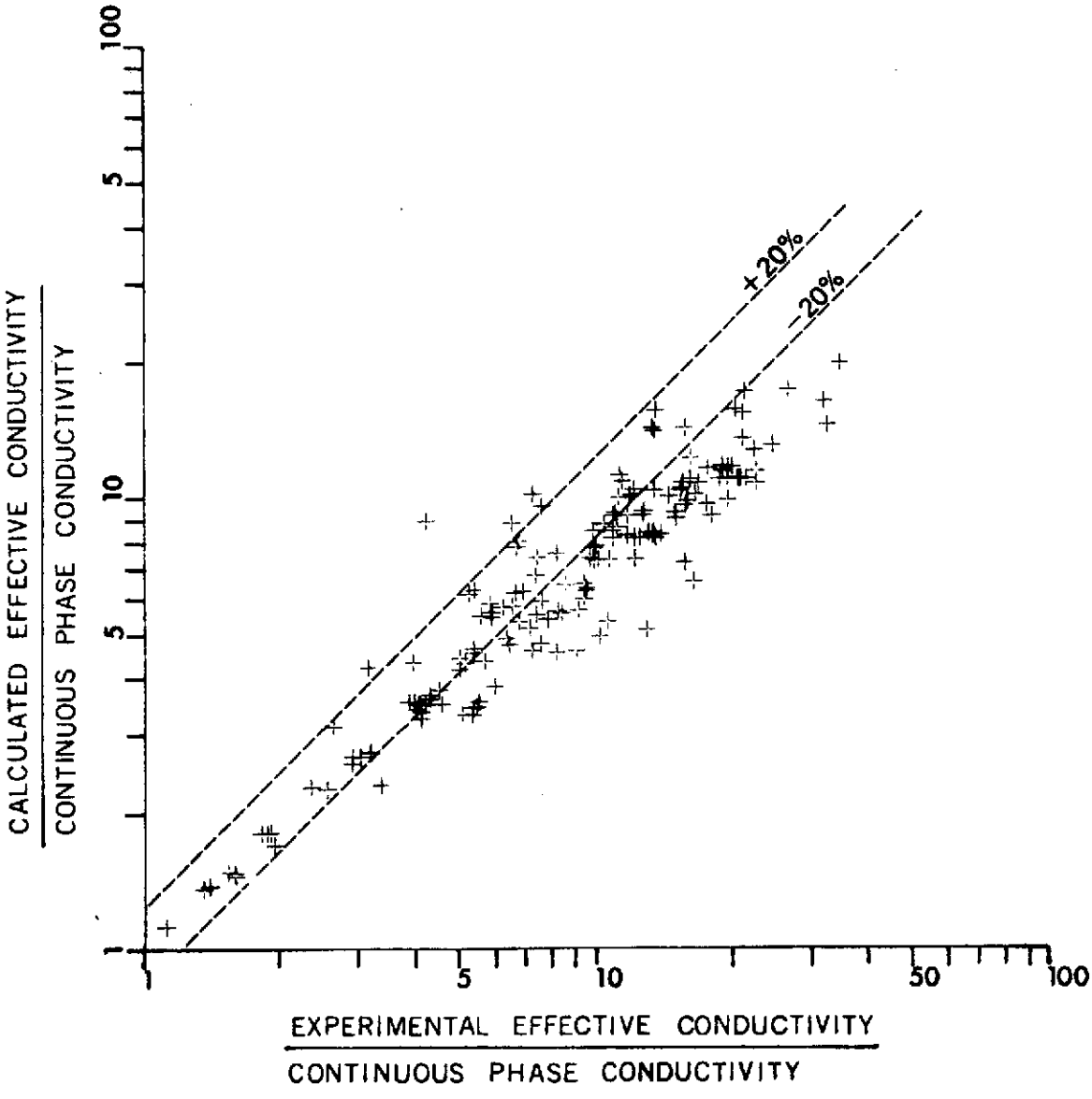

FIGURE 3-10. COMPARISON OF EXPERIMENTAL RESULTS WITH CALCULATED CONDUCTIVITY FOR THE SCHUMANN AND VOSS EQUATION.

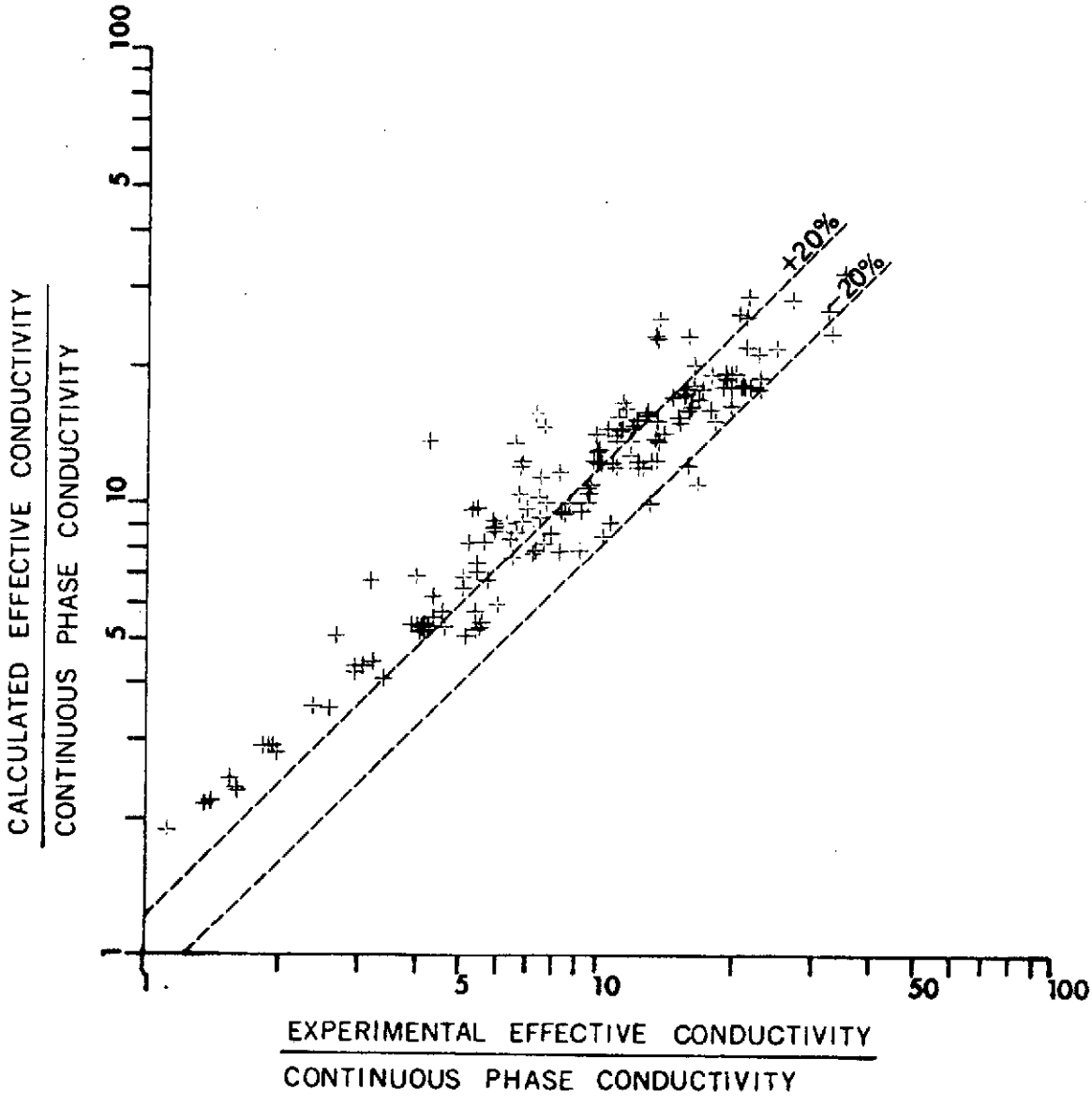

FIGURE 3-11. COMPARISON OF EXPERIMENTAL RESULTS WITH CALCULATED CONDUCTIVITY FOR THE PRESTON EQUATION.

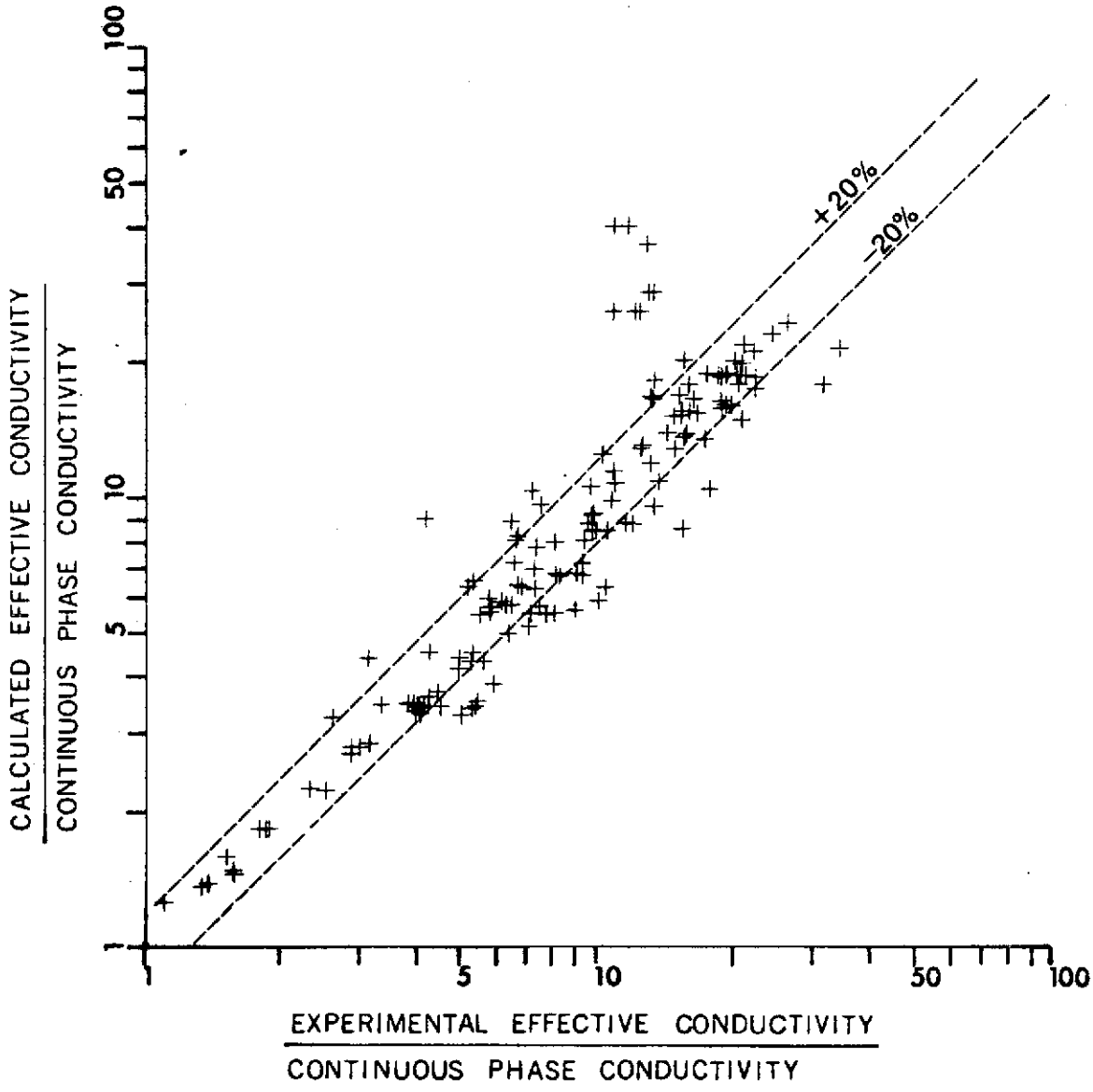

FIGURE 3-12. COMPARISON OF EXPERIMENTAL RESULTS WITH CALCULATED CONDUCTIVITY FOR THE WILHELM ET AL EQUATION.

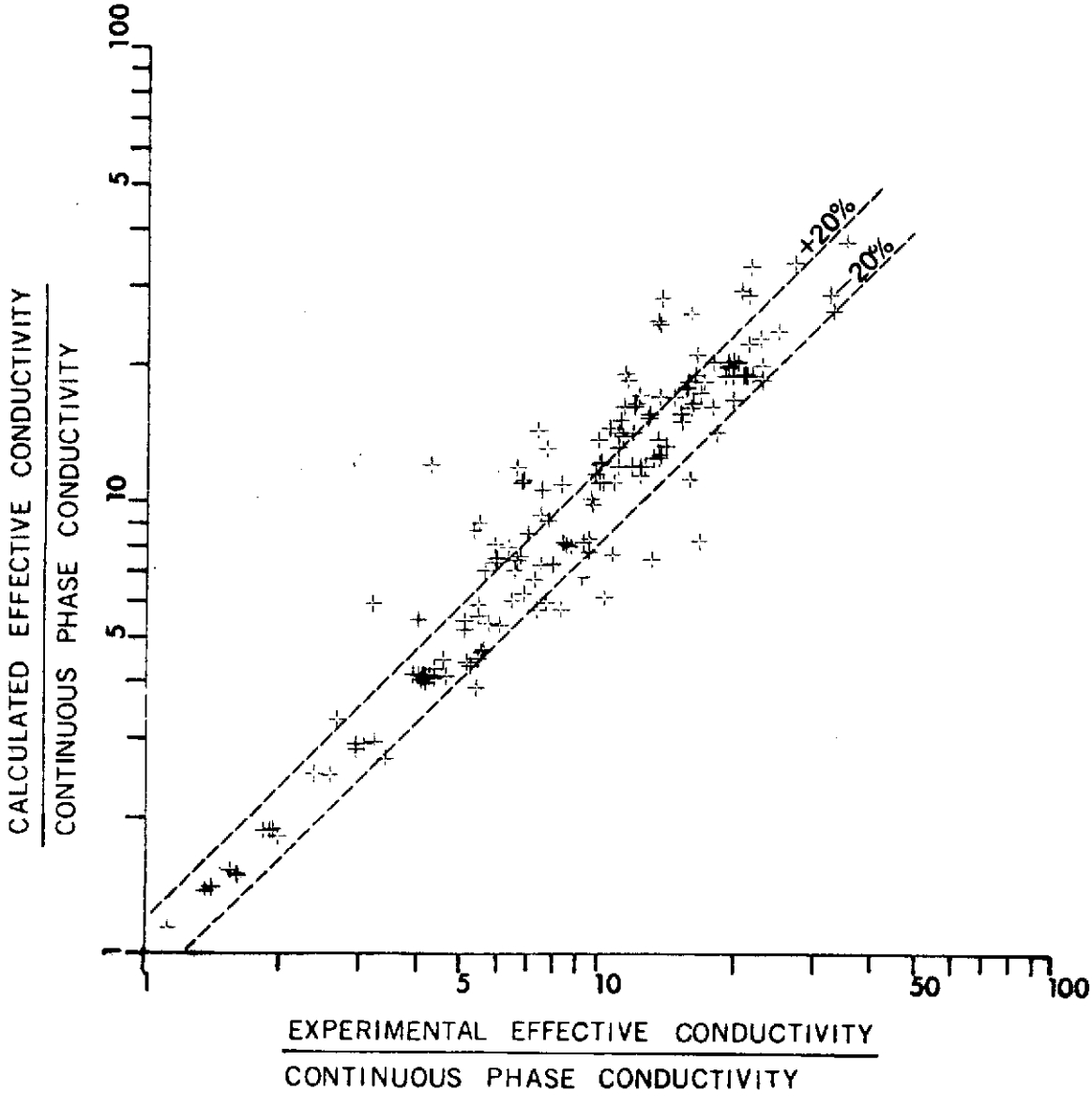

FIGURE 3-13. COMPARISON OF EXPERIMENTAL RESULTS WITH CALCULATED CONDUCTIVITY FOR THE KRUPICZKA EQUATION.

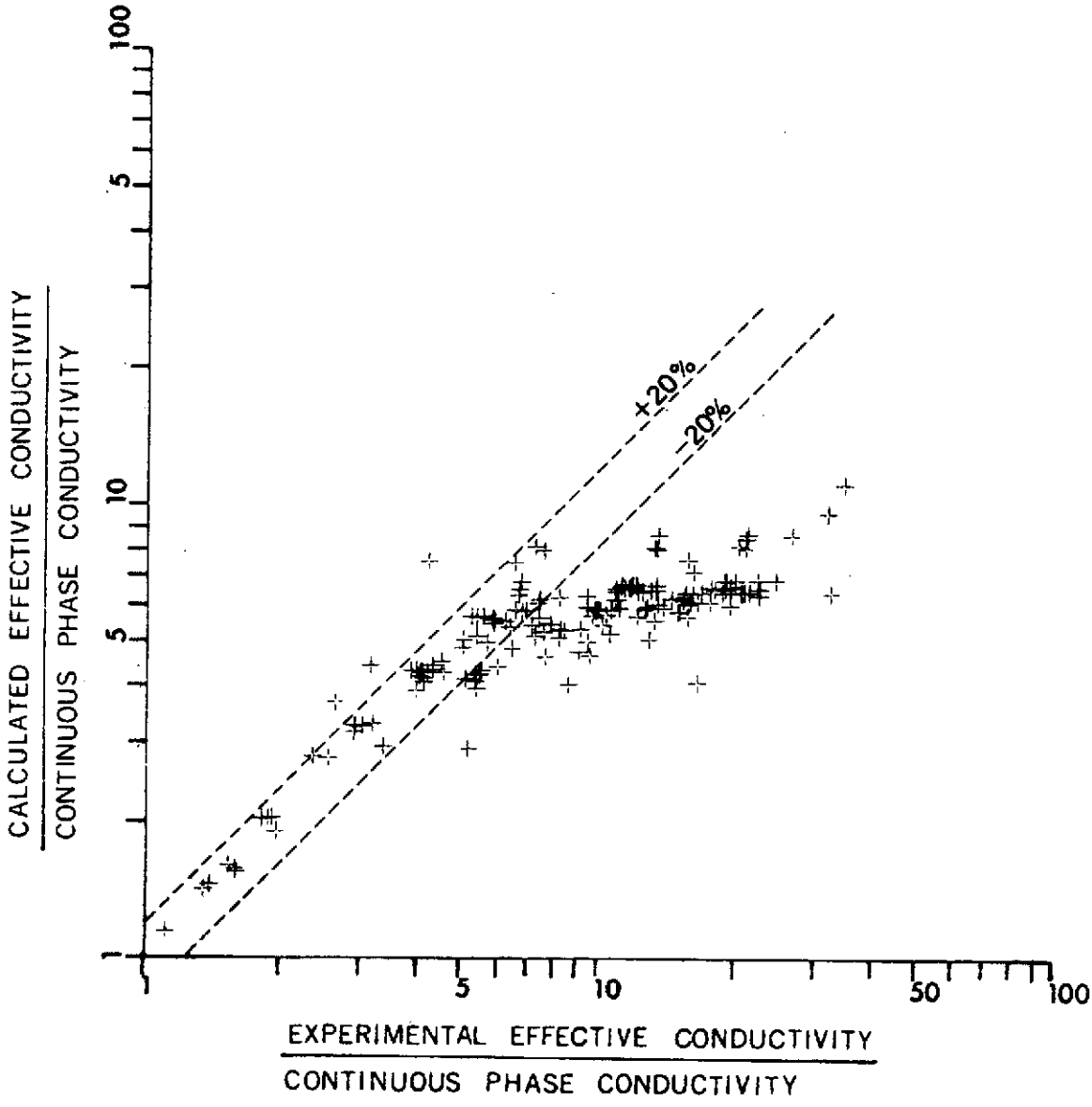

FIGURE 3-14. COMPARISON OF EXPERIMENTAL RESULTS WITH CALCULATED CONDUCTIVITY FOR THE RUSSELL EQUATION.

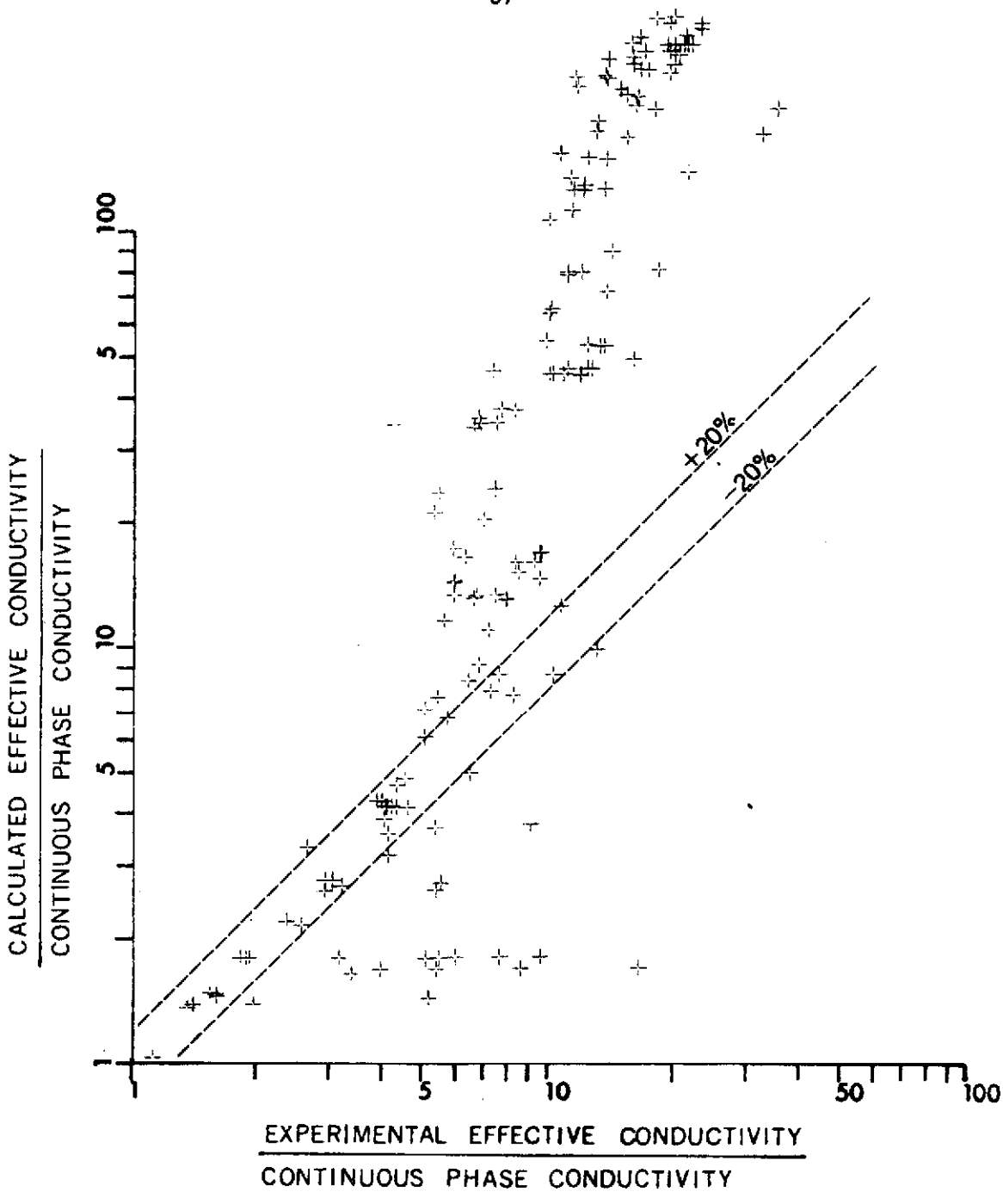

FIGURE 3-15. COMPARISON OF EXPERIMENTAL RESULTS WITH CALCULATED CONDUCTIVITY FOR THE BERNSTEIN EQUATION.

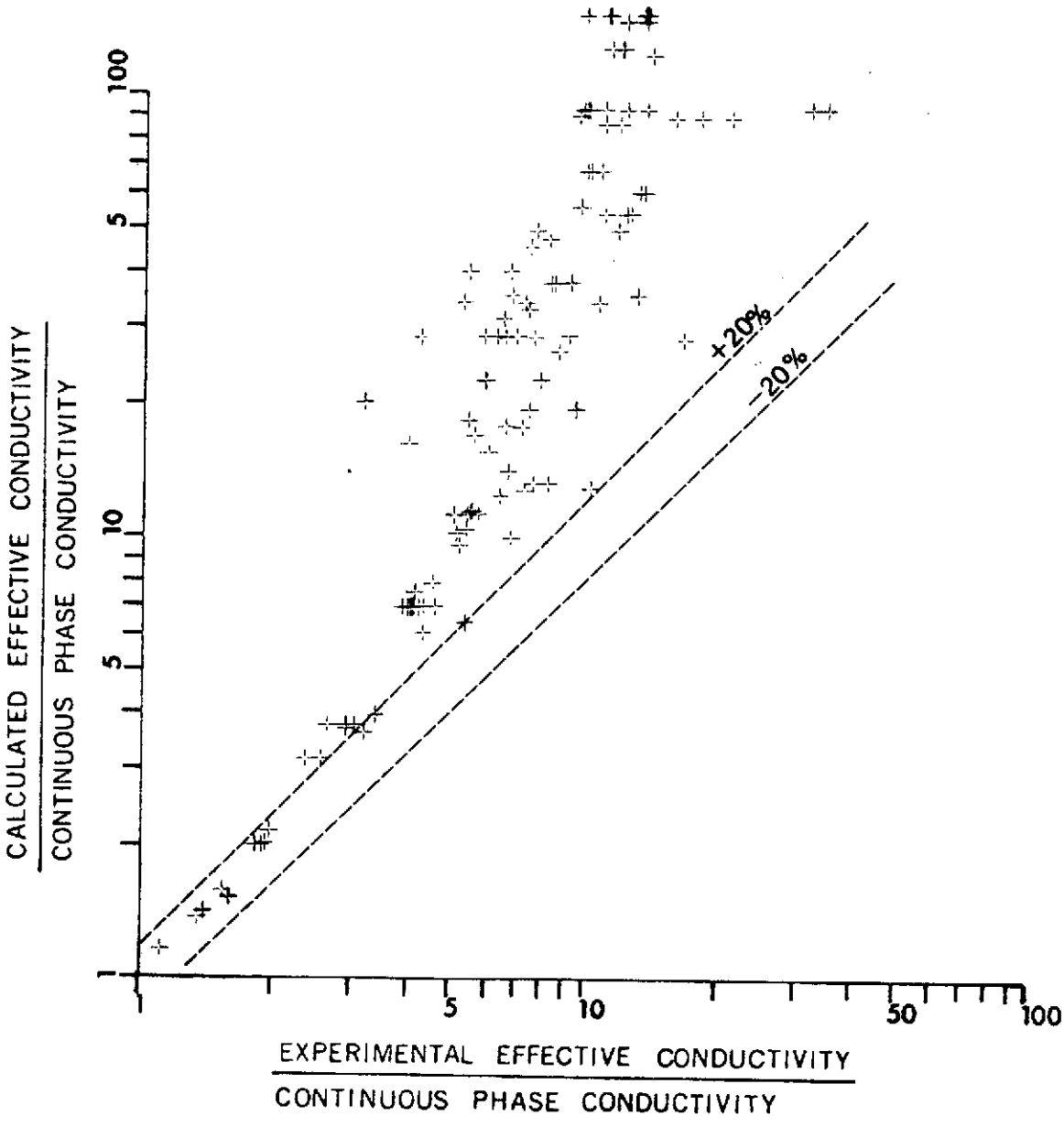

FIGURE 3-16. COMPARISON OF EXPERIMENTAL RESULTS WITH CALCULATED CONDUCTIVITY FOR THE WOODSIDE EQUATION.

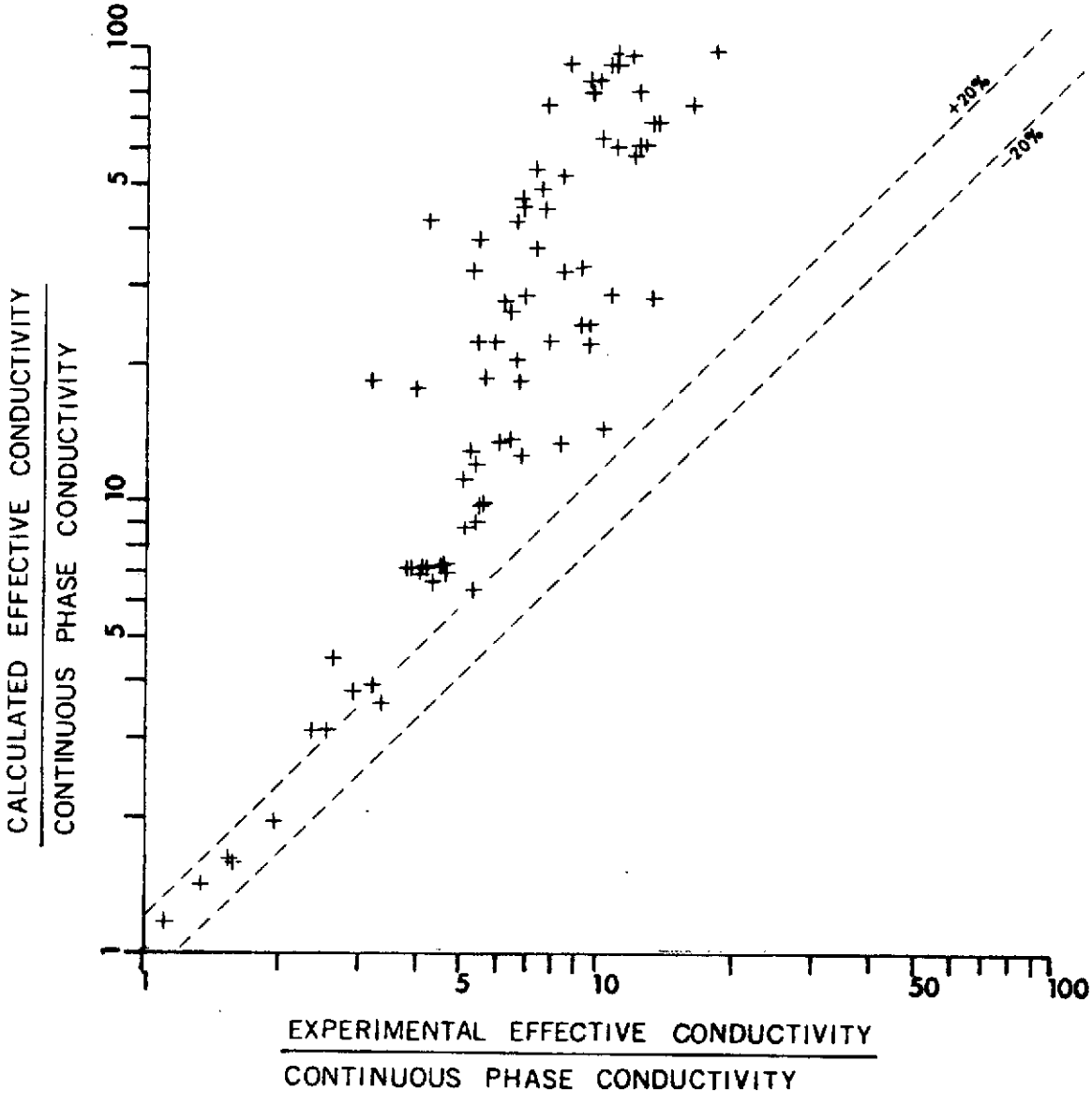

FIGURE 3-17. COMPARISON OF EXPERIMENTAL RESULTS WITH CALCULATED CONDUCTIVITY FOR THE LICHTENECKER 3-D EQUATION.

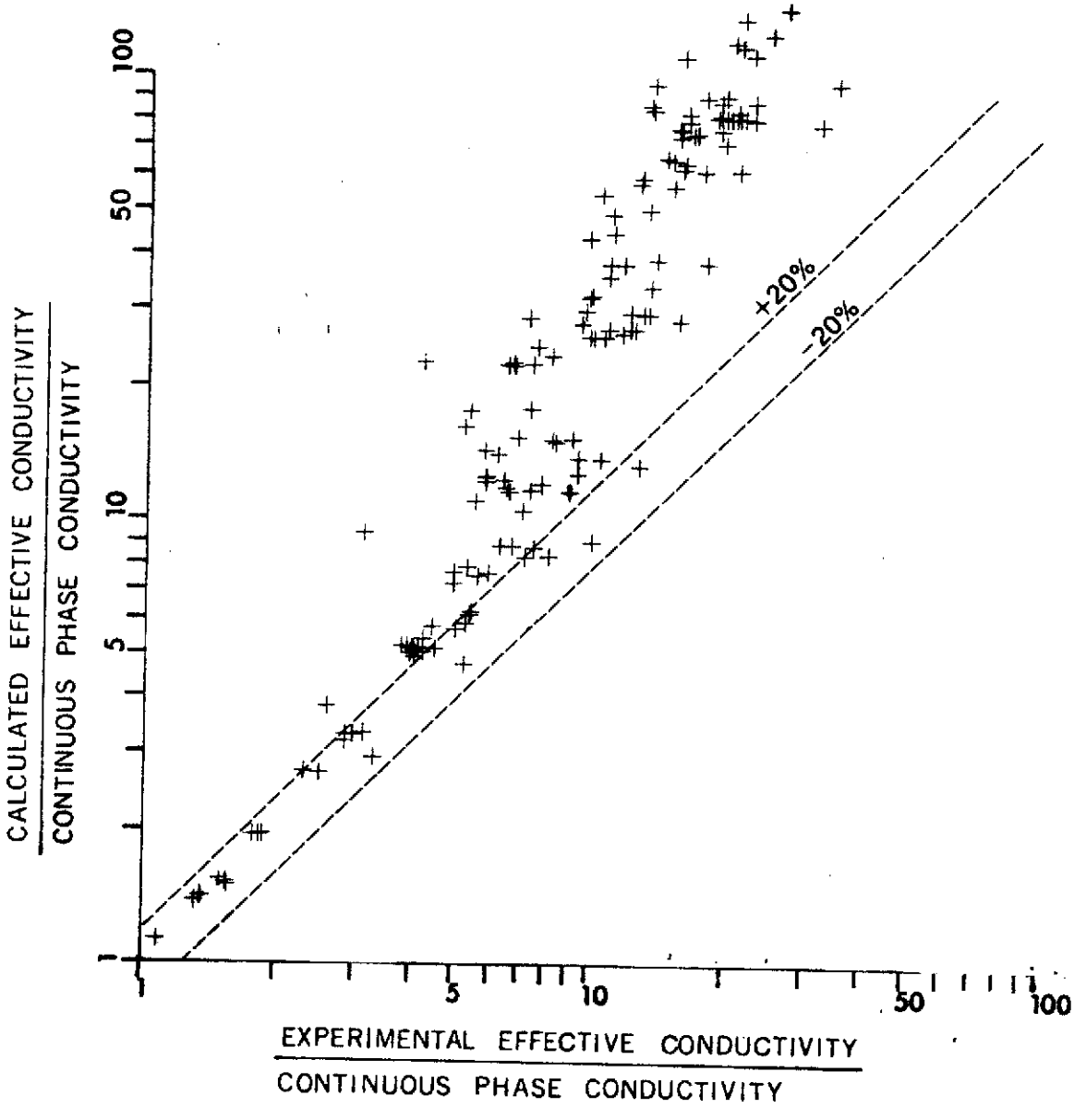

FIGURE 3-18. COMPARISON OF EXPERIMENTAL RESULTS WITH CALCULATED CONDUCTIVITY FOR THE LICHTENECKER 2-D EQUATION.

TABLE 3-I. AVERAGE ERROR, AVERAGE BIAS AND ERROR VARIANCE OF CALCULATED THERMAL CONDUCTIVITY AT ATMOSPHERIC PRESSURE BASED ON SELECTED MODELS

	Av. Bias %	Av. Error %	Error Var.
A. Flux Law Models			
1. Maxwell	-37.9	40.2	0.0606
2. Lord Rayleigh	-24.8	33.7	0.0594
3. Meredith and Tobias	-18.7	34.4	0.0416
4. Bruggeman	23.8	32.9	0.1540
B. Uniform Heat Flux Models			
1. son Frey	-43.8	45.1	0.0599
2. Woodside and Messmer	20.9	34.8	0.0992
3. Kanager	-6.7	18.9	0.0286
4. Gorring and Churchill	-10.7	20.0	0.0192
5. Willhite, Kunii and Smith	-3.6	17.8	0.0268
6. Schumann and Voss	-21.1	25.8	0.0260
7. Preston	26.6	30.5	0.0875
8. Wilhelm et al	-2.1	19.7	0.0373
9. Krupiczka	13.2	21.2	0.0693
C. Parallel Isotherm Models			
1. Russell	-30.3	35.0	0.0566
2. Bernstein	677.9	686.1	85.05
3. Woodside	670.3	670.4	55.16

TABLE 3-I. Continued

D. Weighted Ohm's Law Models			
1. Lichtenecker 3-D	701.1	701.2	48.70
2. Lichtenecker 2-D	194.5	195.0	2.98

IV. CHARACTERISTICS OF PROBABILISTIC MODELS

As indicated in Chapter 2, almost all methods proposed to determine the thermal conductivities of two-phase systems may be grouped into two general classes. The first classification consists of the Ohm's law model equations derived from some special geometries, usually some orderly array of spheres or cubes distributed in a continuous medium.

The second classification consists of the flux law model equations which account for non-linear heat flow. However, most of these equations are based on the assumption that the concentration of particles is small enough so that the field surrounding one particle is not affected by the presence of other particles.

As indicated in [68], published correlations for the thermal conductivity of granular materials, are not applicable to systems composed of different materials for which the thermal conductivities are highly different. This is the case, because the approximations inherent to the assumptions of both classifications mentioned above are no longer valid when the ratio of the component conductivities becomes exceedingly high. The object of this study is the development of a model that will account for non-linear heat flow, that can be extended to a large range of the ratio of thermal conductivities,

and will include the following parameters:

1. Volume fraction of one phase;
2. Particle shape;
3. Particle size distribution;
4. Contact resistance.

The description and analysis of such models is preceded by the development of two Ohm's law models based on the assumption of parallel isotherms and uniform heat flux respectively. Both these models are an outgrowth of Tsao's [8] and Loeb's [69] models supplemented by recent results on the structural properties of packed beds [49, 51]. It should be noted that apart from the heat flow assumptions, the basic proposition utilized in the development of the models is that a granular material can be considered as a random mixture of two phases, in which all particles of the same size and shape have the same probability to occupy each unit volume of the mixture. The validity of this proposition together with its limitations have been discussed extensively by Debbas and Rumpf [51], and it has been utilized in Tsao's [8] model.

The purpose of these preliminary developments is two-fold. First, to indicate that Ohm's law models with realistic geometries provide an upper and lower bound to the effective conductivity of granular materials. Second, to illustrate the need for a probabilistic flux law model that includes particle interaction, so that the unrealistic assumptions concerning the value of the thermal conductivity in the direction perpendicular to the heat flow can be overcome.

Ohm's Law Model - Parallel Isotherms

Consider a unit cube of a granular material subdivided into N^3 cubicles by a three-dimensional grid. Assume that the grid is fine enough, and the two phases are arranged in such a manner that each cubicle is occupied either by the continuous or the discontinuous phase. It has been shown [51] that most granular materials can be thought of as a random mixture of the two phases. Accordingly, the probability that a cubicle is occupied by the continuous phase is P, the volume fraction of the continuous phase. It has been also shown [8, 53] that due to the parallel isotherms assumption, the conductivity of each lamina perpendicular to the heat flow direction depends on the volume fraction of the continuous phase present in the lamina, but is independent of the manner in which the two phases are arranged. Consequently, the effective thermal conductivity of each lamina does not change if the continuous phase is arranged as indicated in Figure (4-1b). Also, since the laminae can be thought of as series resistances to the flow of heat, the effective conductivity of the unit cube does not change if the laminae are rearranged according to decreasing height of the continuous phase as indicated in Figure (4-1c), approximated by a continuous distribution curve indicated in Figure (4-1d). Summation of the series resistances yields the following expression for k_e, the effective conductivity of the unit cube

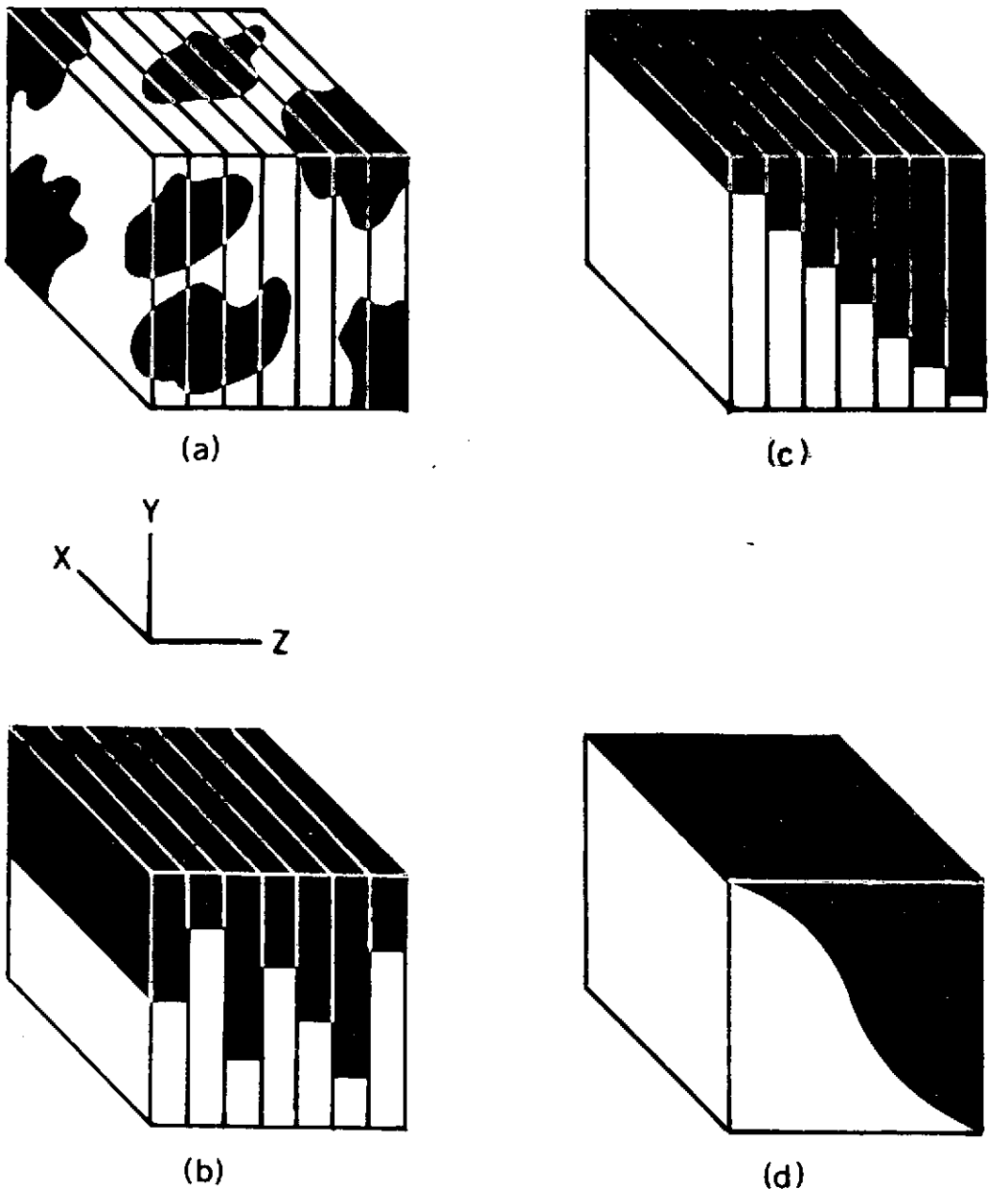

FIGURE 4-1. OHM'S MODEL – LINEAR ISOTHERMS

$$k_e = \frac{1}{\int_0^1 \frac{dz}{k_d + (k_c - k_d)\, y}} \qquad (4\text{-}1)$$

A number of attempts have been made to determine a functional relationship between y and z by either expressing y as a function of z, μ, and σ, where μ is the mean value of z and σ is the standard deviation of z [8, 53], or by approximating the phase distribution curve by a curve by a parabolic function [70]. The method proposed in this study is based on the initial assumption of randomness.

Consider one of the laminae that is perpendicular to the mean heat flow. The probability that exactly rN cubicles, out of the N^2 cubicles present in the lamina, are occupied by the continuous phase is given by the binomial distribution:

$$\Pi(rN) = \frac{(N^2)!}{(N^2)!(N^2 - rN)!} \; P^{rN} \, Q^{N^2 - rN} \qquad (4\text{-}2)$$

where

$$Q = 1 - P \qquad (4\text{-}3)$$

Suppose that the height of the continuous phase in the m^{th} lamina is r/N after the laminae have been rearranged according to decreasing height of the continuous phase, as indicated in Figure 4-1c. It

follows that there are m laminae in which the height of the continuous phase is equal to or greater than r/N, and consequently

$$m = N \sum_{rN}^{N^2} \Pi(rN) \tag{4-4}$$

If N^2 is large enough, $\Pi(rn)$ can be approximated by the normal distribution [71],

$$f(rN) = \frac{1}{\sqrt{2\pi}\ \sqrt{N^2 PQ}} \cdot e^{-\frac{(rN-PN^2)^2}{2(N^2\ PQ)}} \tag{4-5}$$

Substitution of Equation (4-5) into Equation (4-4), and noting that and r/N = y, it follows that

$$z = \tfrac{1}{2}\ (1 - \text{erf}t)\ ,\quad t = \frac{N^2\ (y - P)}{\sqrt{2N^2\ PQ}} \tag{4-6}$$

Equation (4-6) is an expression for z as a function of y in terms of the parameters P and N. The continuous phase volume fraction P is assumed to be known since it is reported in all experimental investigations of granular materials. N is a measure of the fineness of the three-dimensional grid. In other words, it is a measure of the sample size. Although, there is no analytical method to determine N if the size of the cubicles is not selected, a lower bound for N

can be found by the constraint that the total number of cubicles in the unit cube occupied by the continuous phase must be equal to PN^3. In other words

$$\int_0^1 z \, dy = P \tag{4-7}$$

Equation (4-7) is satisfied when N^2 is larger than 8/P and 8/Q. It can be also shown that under this condition, the approximation of the binomial distribution by the normal distribution is also valid.

In view of the discussion above, Equations (4-1) and (4-6) constitute a solution for the effective thermal conductivity of granular materials, provided the model and the assumptions associated with it constitute a realistic approximation of the system. However, it should be noted that the additional resistance to the heat flow from one particle to the other, introduced due to the contact surface of two particles, has not been taken into account in the development. This assumption is certainly justified for unconsolidated porous media, but induces large errors in the case of granular materials [34]. To overcome this discrepancy, an additional term will be introduced in Equation (4-1) to account for contact resistance.

Let N_c be the total number of contact areas in a unit cube. Assuming that these contact areas are randomly distributed and oriented, the number of contact areas in the z-direction, N_{cz} is $N_c/3$. These contact resistances can be distributed over the

laminae shown in Figure (4-1c) in such a manner that the number of contact resistances in a lamina n_{cz} is proportional to the discontinuous phase present in the lamina. That is:

$$\frac{(1 - y)\ (1/N)}{(1 - P)} = \frac{n_{cz}}{N_{cz}} \tag{4-8}$$

Now, taking into account that each lamina is composed of continuous phase cubicles, discontinuous phase cubicles, and cubicles containing contact areas as given by Equation (4-8), summation over the thermal resistances present in each lamina, and integration over all laminae, yields a modified form of Equation (4-1).

$$k_e = \frac{1}{\int_0^1 \frac{dz}{k_d + (k_c - k_d)y - \frac{(1-y)}{(1-P)} \frac{N_{cz}}{N^3} (k_d - k_{cr})}} \tag{4-9}$$

In Equation (4-9), k_{cr} is the contact thermal conductivity associated with a contact area. In the calculations, an expression for k_{cr} is taken from Luikov [34].

It is still necessary to find an expression for the total number of contact areas per unit cube, in order to determine N_{cz}. This can be accomplished by assigning a characteristic volume to each particle and considering the coordination number n which is the average number of contact points per particle. As indicated in [66] the

characteristic volume of each particle is $\epsilon_v d^3$, where ϵ_v is an experimentally determined volumetric parameter that depends on the particle shape, and d is a characteristic particle size obtained from the sieve data. It follows then that the number of particles per unit volume is $\frac{1-P}{\epsilon_v d^3}$. The coordination number is given in [49] as

$$n = 39.39\ (0.571 - P) \tag{4-10}$$

For spherical particles ϵ_v is equal to $\pi/6$. Combination of these expressions yields, for spherical particles

$$N_{cz} = \frac{12.54\ (0.571 - P)}{d^3}\ (1-P) \tag{4-11}$$

Combination of Equations (4-1), (4-9), (4-11) constitute a solution for the effective thermal conductivity of granular materials in terms of the conductivities of the components, the porosity, and the parameters mentioned. The equations have been solved and compared to a number of experimentally determined values. It should be noted that the value of N chosen for each case satisfied the lower bounds mentioned, and was such that the cubicles were smaller than the particles and the voids.

Ohm's Law Model - Uniform Heat Flux

Again, consider a unit cube of a granular material subdivided into N^3 cubicles by a three-dimensional grid. Looking at the parallel-

to-the-heat-flow rectangular tubes, it can be seen that they include continuous phase and discontinuous phase cubicles. Under the assumption of uniform heat flux, the effective thermal conductivity of the rectangular tubes does not change if the cubicles are rearranged in such a manner that the continuous phase is pushed forward [69], as indicated in Figure (4-2b).

The effective thermal resistance of each tube is due to the thermal resistance of the continuous phase and the thermal resistance of the discontinuous phase present in the tube, acting in series. Moreover, since the effective thermal resistances of all tubes are in parallel, summation of all the thermal conductances of the tubes gives the effective thermal conductance of the unit cube. Assuming that the summation can be approximated by integration, the effective thermal conductivity of the unit cube is

$$k_e = \int_0^1 \int_0^1 \frac{dx\,dy}{\frac{1-z}{k_d} + \frac{z}{k_c}} \qquad (4\text{-}12)$$

where z is the height of the discontinuous phase at (x,y). To integrate Equation (4-12), it is necessary to know z as a function of x and y. This can be accomplished by a rearrangement of the rectangular tubes that are parallel to the heat flow as follows:

1. In each parallel to the heat flow x-z lamina, the tubes are rearranged according to decreasing height of the continuous phase in the x-direction (Figure 4-2c).

2. The x-z laminae are rearranged according to the total amount of continuous phase present in each lamina. Further, the rearrangement is such that the continuous phase void fraction of each lamina decreases with y (Figure 4-2d).

This rearrangement of the rectangular tubes does not affect the effective thermal conductivity of the unit cube, since the height of the continuous phase in each tube remains the same, but permits one to express the distribution of the phases in the unit cube by continuous functions. The arguments leading to these distribution functions are the same as the ones presented for the development of Equation (4-6), and will not be repeated here. The results are the following. For each lamina at y, and having thickness dy,

$$x = \tfrac{1}{2}\,(1 - \text{erf}\,t), \qquad t = \frac{N(z - P_y)}{\sqrt{2N\,P_y\,Q_y}} \tag{4-13}$$

where P_y is the ratio of the volume of the continuous phase present in the lamina to the total volume of the lamina, and $Q_y = 1 - P_y$. Analysis of Figure (4-2d) gives,

$$y = \tfrac{1}{2}\,(1 - \text{erf}\,u), \qquad u = \frac{N^2(P_y - P)}{\sqrt{2N^2PQ}} \tag{4-14}$$

Again, the constraint that the total number of cubicles in the unit cube, occupied by the continuous phase, must be equal to PN^3 is satisfied when N is larger than 8/P and 8/Q. Under these conditions

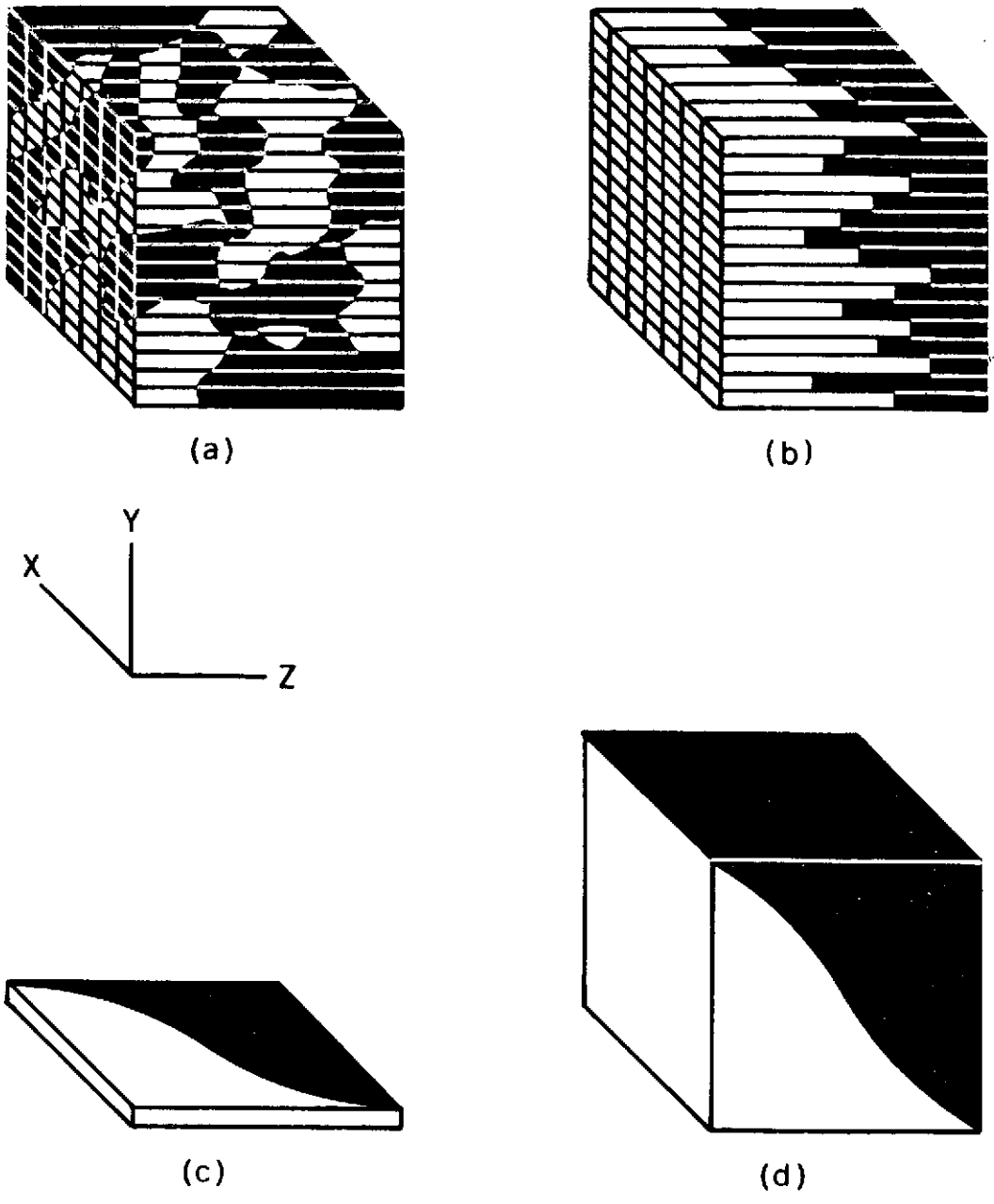

FIGURE 4-2. EQUIVALENT GEOMETRIES FOR UNIFORM HEAT FLUX.

the approximation of the binomial distribution by the normal distribution is also valid.

Combination of Equations (4-12), (4-13) and (4-14) constitutes a solution for the effective thermal conductivity of granular materials in terms of the conductivities of the components and the porosity. The equations have been solved and compared to a number of experimentally determined values. Again, the value of N chosen for each case satisfied the lower bounds mentioned, and was such that the cubicles were smaller than the particles and the voids. It should be noted that in this model the thermal contact resistance, due to the contact areas between particles, has not been introduced. The reason is that the uniform heat flux assumption renders the calculated effective conductivity smaller than the experimental one, and introduction of the contact thermal resistance will increase the discrepancy between calculated and experimental values.

Comparison of the Ohm's Law Models

Equations (4-9) and (4-12) have been obtained to predict the effective thermal conductivity of granular materials as a function of the constituent conductivities, porosity, and the parameters indicated. In both models, a representative unit cube of the granular material has been considered. The basic assumption utilized in order to obtain the distribution of the two phases in the unit cube is that a granular material can be considered a

random mixture of two phases. In view of the evidence given by Debbas and Rumpf [51] and Baxley and Cooper [20], this assumption is in good agreement with experimental results, and consequently it can be concluded that the assumed geometry of the unit cube is quite accurate for most granular materials.

Equations (4-9) and (4-12) have been solved for a number of cases, and some of the results are presented in Figures (4-3) and (4-4), representing granular systems with porosities 0.42 and 0.38, respectively. Wiener's upper and lower bounds are also indicated. The experimentally determined values have been obtained from references [6, 21, 23, 36]. It can be seen that the parallel isotherms model grossly overpredicts the effective thermal conductivity of granular materials, while the uniform heat flux model predicts lower values. The discrepancy increases with the ratio of the constituent conductivities. Although, the region between the upper and lower bounds thus defined is smaller than the region defined by Wiener's bounds, the specific values obtained from Equations (4-9) and (4-12) leave much to be desired.

This difference between calculated and true effective thermal conductivity values can be explained by Laubitz's [17] observation that in the uniform heat flux model it is effectively assumed that the thermal conductivity of the medium in the normal to the heat flow directions is infinite, while in the parallel isotherms model it is

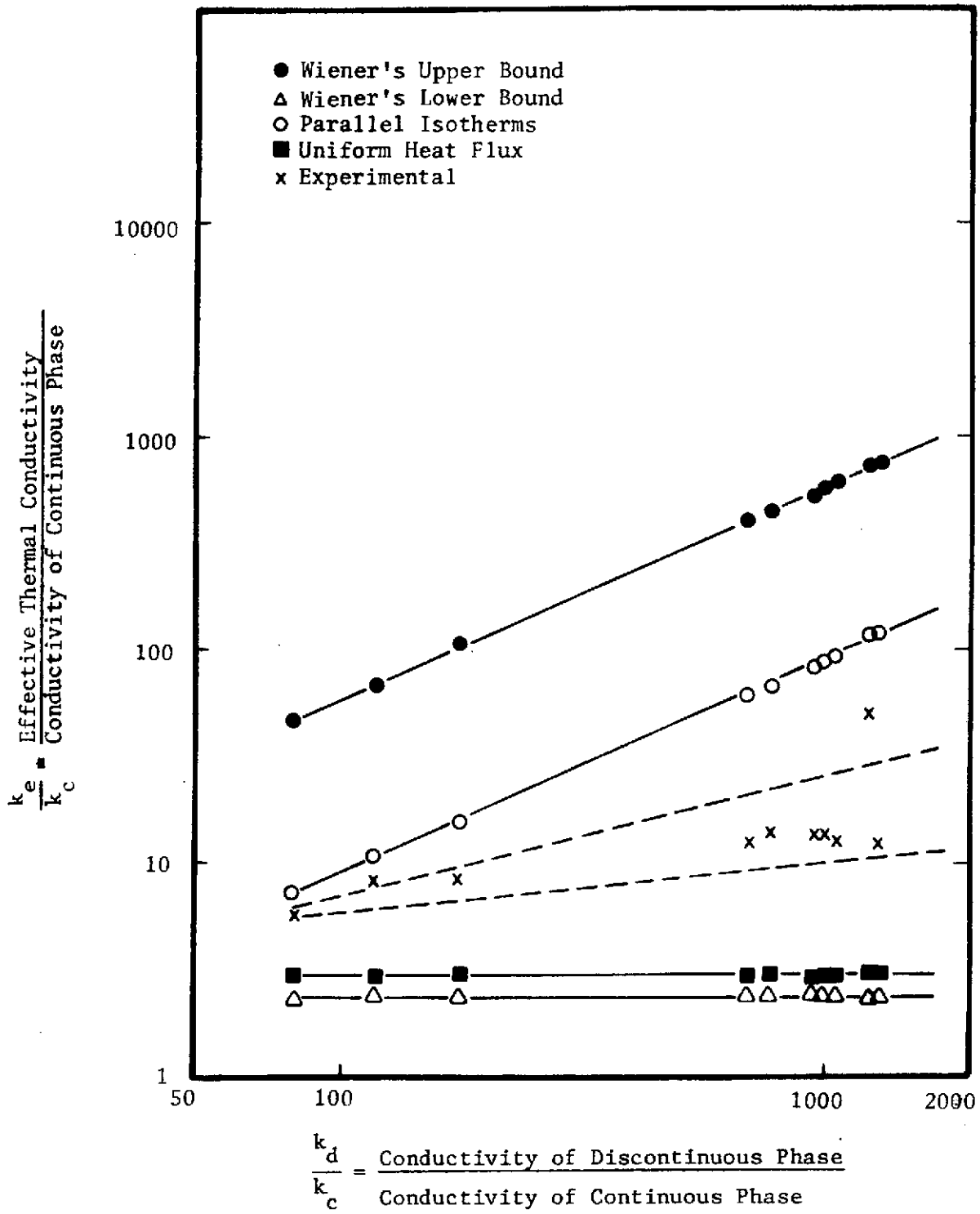

FIGURE 4-3. COMPARISON OF BOUNDING CONDUCTIVITIES WITH EXPERIMENTAL DATA FOR A POROSITY OF 0.42.

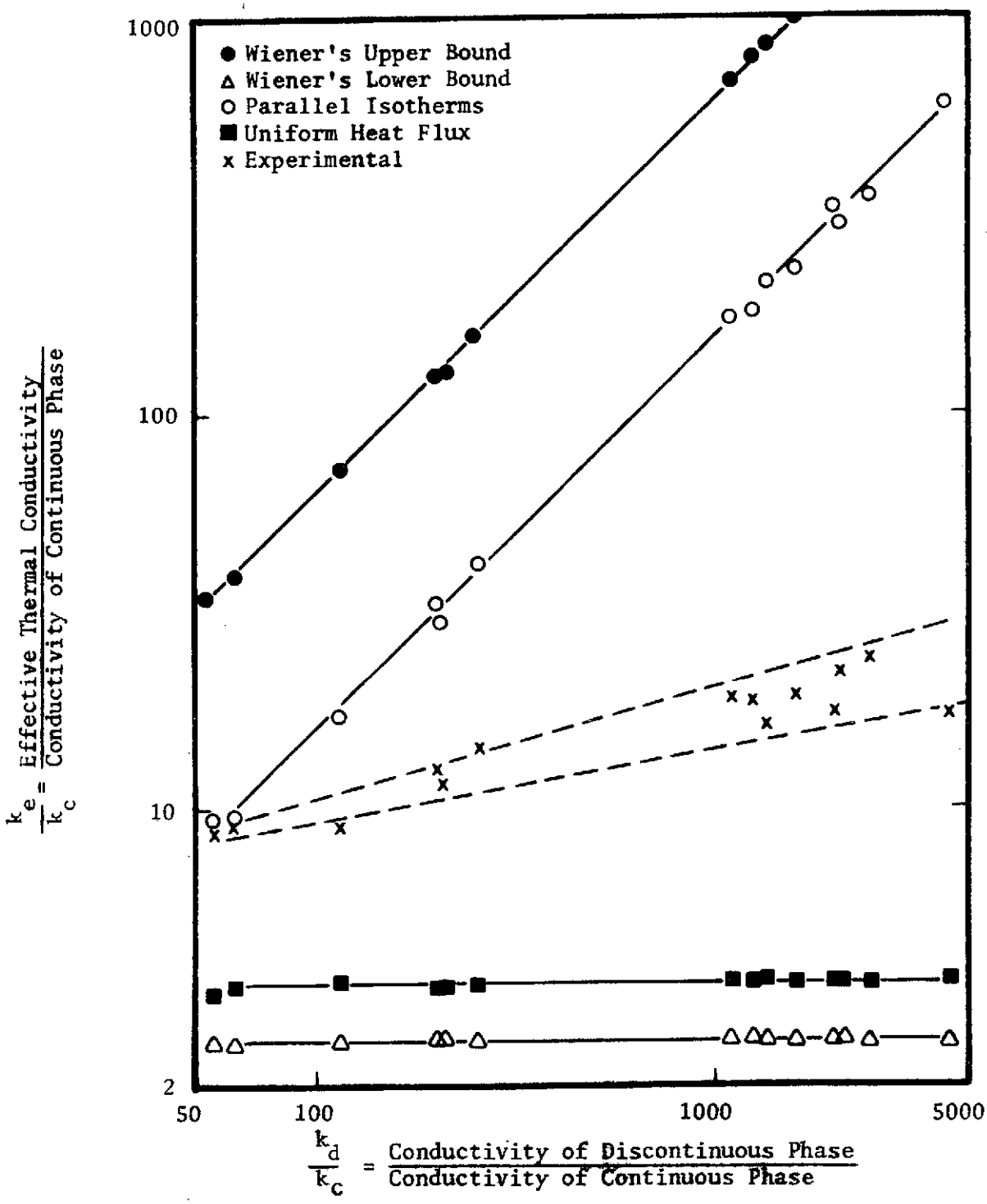

FIGURE 4-4. COMPARISON OF BOUNDING CONDUCTIVITIES WITH EXPERIMENTAL DATA FOR A POROSITY OF 0.38.

vanishingly small. It also provides an explanation as to why previous Ohm's Law models, based upon an assumed regular array, have generally not been successful at higher constituent conductivity ratios. Some of the discrepancy due to the heat flow assumptions has been countered in previous Ohm's law models by assuming a somewhat distorted array. However, at high constituent conductivity ratios, the effect of the heat flow assumptions prevails, and the calculated values continually deviate from the true effective thermal conductivity values.

Since the lateral conductivity of granular materials falls between the limits of zero and infinite lateral conductivity, it can be concluded that Equations (4-9) and (4-12) constitute an upper and lower bound to the true effective thermal conductivity. Numerous correlation forms have been developed in the literature [18] associating the true conductivity of the granular material to the bounding values. However, it does not appear possible to select the correlation which is more consistent with the physical system. Consequently, an alternate approach is suggested, where the geometry of the granular system is the same, while no assumption is made with respect to the heat flow. This constitutes the basic model of this study, and it differs from the Ohm's law models presented in that both the geometry and the heat flow assumptions are realistic. The Ohm's law models will be utilized in the discussion that follows as a criterion for the selection of a number of parameters such as contact resistance, coordination number, etc.

V PARALLEL ISOTHERMS MODEL

The approach specified in this chapter is based upon an extension of the approach originally proposed by Wiener [7] and later extended, first by Russell [43], and later by Tsao [8]. The effective thermal conductivity of the heterogeneous system is determined using the electrical analogy. Probability techniques are used to describe the random distribution of the particles within the system as introduced in Tsao's model. Two statistical parameters are introduced and are determined based upon bulk physical properties.

Consider a unit cube of the heterogeneous system shown in Figure (2-5a). The system is to be divided into a series of fine laminae oriented normal to the direction of heat flux. These elements are sufficiently thin that the cross-sectional area of the solid particles are essentially constant throughout its width. Assuming parallel isotherms within the unit cube, the discontinuous (solid) and continuous phases will act as resistances in parallel within each lamina. The order of the parallel resistances may be changed arbitrarily without affecting the overall resistance of the parallel circuit. Thus the resistances of the solid elements may be combined into a single solid resistance at the bottom of the laminae as shown in Figure (2-5b).

A simple calculation then shows that the equivalent resistance is given by the equation

$$k_e = \frac{1}{\sum_{m=1}^{h} \frac{}{k_c + (k_d - k_c)\bar{\varepsilon}_m}} \qquad (5\text{-}1)$$

In this equation the fraction of solid in the m^{th} lamina is given by $\bar{\varepsilon}_m$ and the width of each lamina is Δx.

Note that the laminae act as resistances in series. Again the order of the resistances does not affect the overall thermal resistance so that the elements may be rearranged in order of decreasing solid fraction as shown in Figure (2-5c). If the width of the laminae is allowed to approach zero then the effective thermal conductivity for Figure (2-5d) becomes

$$k_e = \frac{1}{\int_0^1 \frac{dx}{k_c + (k_d - k_c)\,\bar{\varepsilon}}} \qquad (5\text{-}2)$$

The solution of this equation requires the knowledge of a relationship between the solid area fraction $\bar{\varepsilon}$ and the position x. Such a relationship is given in the form

$$\bar{\varepsilon} = \frac{\int_x^1 e^{-1/2\left(\frac{\rho-\mu}{\sigma}\right)^2} d\rho}{\int_0^1 e^{-1/2\left(\frac{\rho-\mu}{\sigma}\right)^2} d\rho} \qquad (5\text{-}3)$$

In this expression μ and σ represent the mode and the standard deviation of the one dimensional porosity as introduced by Tsao. For the case at hand the mode, μ, will be very close to the bulk solid fraction. The standard deviation, σ, is unknown. In general, it will be a function of the particle shape, size distribution and volume fraction. By restricting consideration to uniform sized particles which are either spherical or semi-spherical the standard deviation becomes a function of the volume fractions only. Or

$$\sigma = f(\bar{\varepsilon}) \tag{5-4}$$

Using the experimental data available from the literature, Equations (5-2) and (5-3) may be solved to determine σ for each case. These data have been curve fitted using a least squares technique to obtain the relation

$$\sigma = 0.32248\ (1 - \bar{\varepsilon}) - 0.092543\ (1 - \bar{\varepsilon})^2 \tag{5-5}$$

The resulting equations may be used to determine the effective thermal conductivity of packed beds with solid fractions between 0.3 to 0.7. Beyond these limits the assumption of random packing of semi-spherical particles no longer holds.

Results

Data describing the effective thermal conductivity of packed beds have been compiled from the literature. Generally, results obtained from Equation (5-2) fall within $\pm$ 20% of the reported values, provided that radiation may be neglected. A representative sample of data

taken from several sources [6, 35, 37, 58] is shown in Figure (5-1). A more extensive comparison between predicted and experimentally determined values for granular materials at atmospheric pressure is included in Chapter 6.

The model has also been extended to the case of particulate basalt in a simulated lunar environment, and the results are shown in Figure (5-2). It is noted that the model predicts a slightly greater dependence of the effective conductivity on packing fraction than is indicated by the experimental data. This could be off-set to some extent by modifying the empirical distribution function used in the correlation; such a modification would be difficult to justify on theoretical grounds and therefore has not been undertaken.

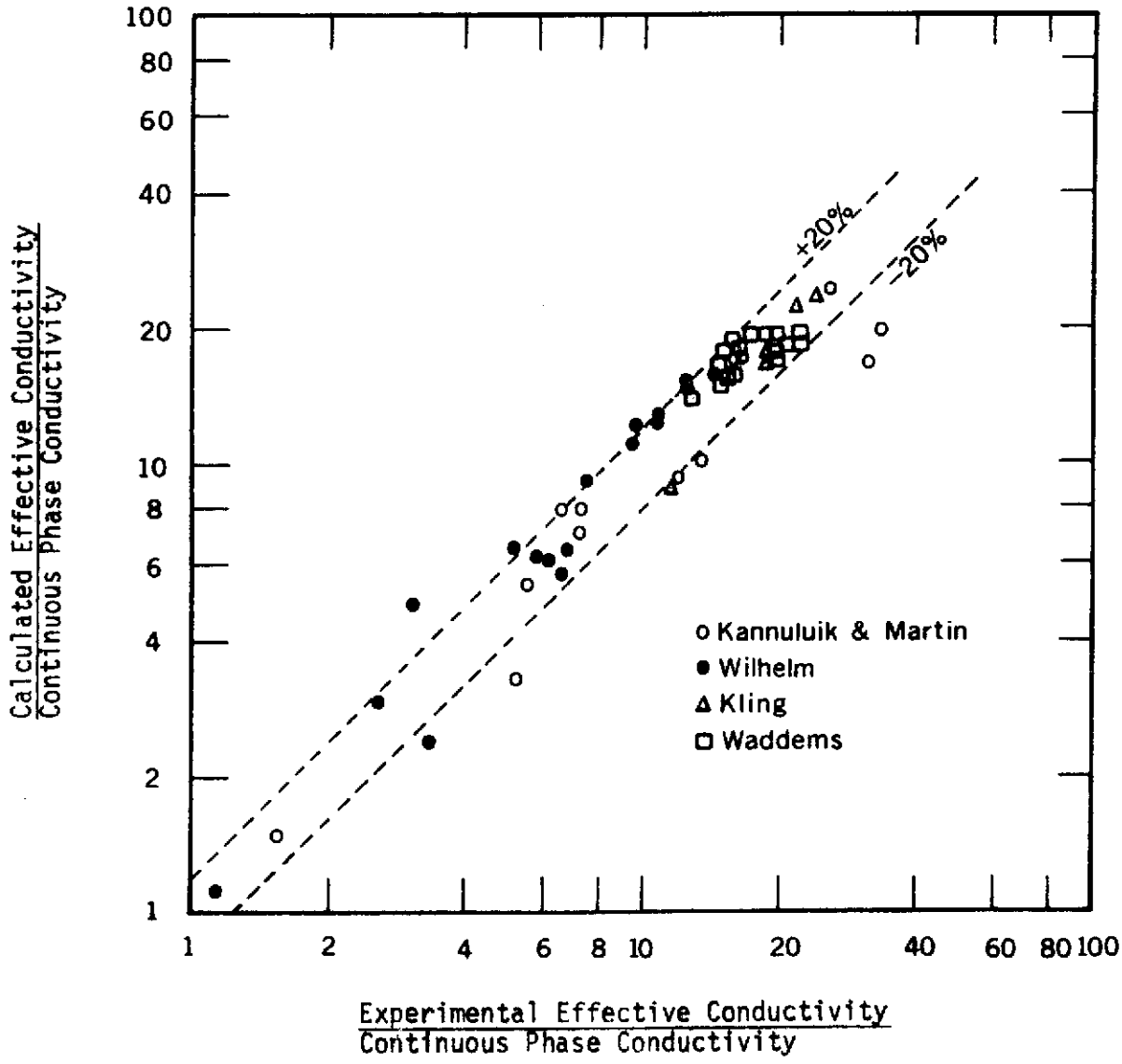

FIGURE 5-1. COMPARISON OF EXPERIMENTAL AND MODEL PREDICTED THERMAL CONDUCTIVITIES.

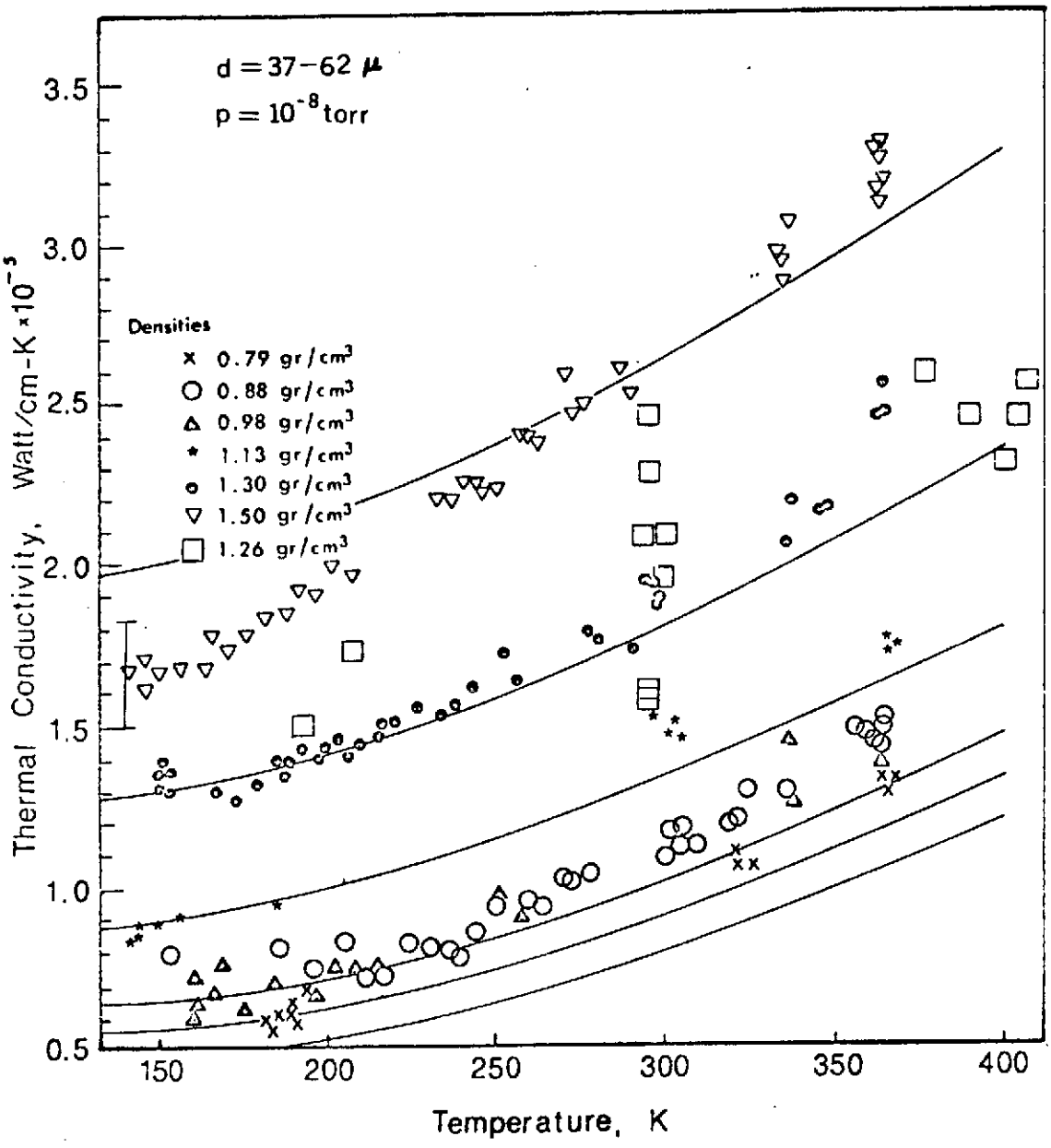

FIGURE 5-2. COMPARISON BETWEEN MODEL PREDICTED AND EXPERIMENTAL THERMAL CONDUCTIVITIES FOR BASALT IN SIMULATED LUNAR ENVIRONMENT.

VI. STOCHASTIC MODEL

Over the past sixty years [7] numerous Ohm's law models have been introduced. Most of these models are based upon a rough approximation of granular materials in terms of solid parallelopipeds or cubically arrayed spheres. Neither geometry bears a close relation to the random dispersions commonly found in nature. The approach described herein avoids these unnatural arrays and unrealistic geometries by assuming a random distribution of arbitrarily shaped solid particles.

As noted in the literature survey, those models incorporating Ohm's law almost universally utilize assumptions of zero or infinite lateral conductivity. In any real substance the lateral conductivity will fall between these two extremes. Consequently these two assumptions lead toward a set of bounding equations for the effective thermal conductivity of the model. These bounding equations set much narrower limits than those originally proposed by Wiener [7]. A comparison of the two sets of equations is shown in Figure (6-1). The effective conductivity of a square array of uniform spheres ($\bar{\epsilon} = 0.5236$) is represented. Note that at a constituent conductivity ratio of 10^6, these new bounding conditions are approximately one order of magnitude above the lower bound and a factor of five below the upper bound established by Wiener. Therefore, a set of such equations, applicable to any packing geometry would represent a considerable improvement over Wiener's formulation.

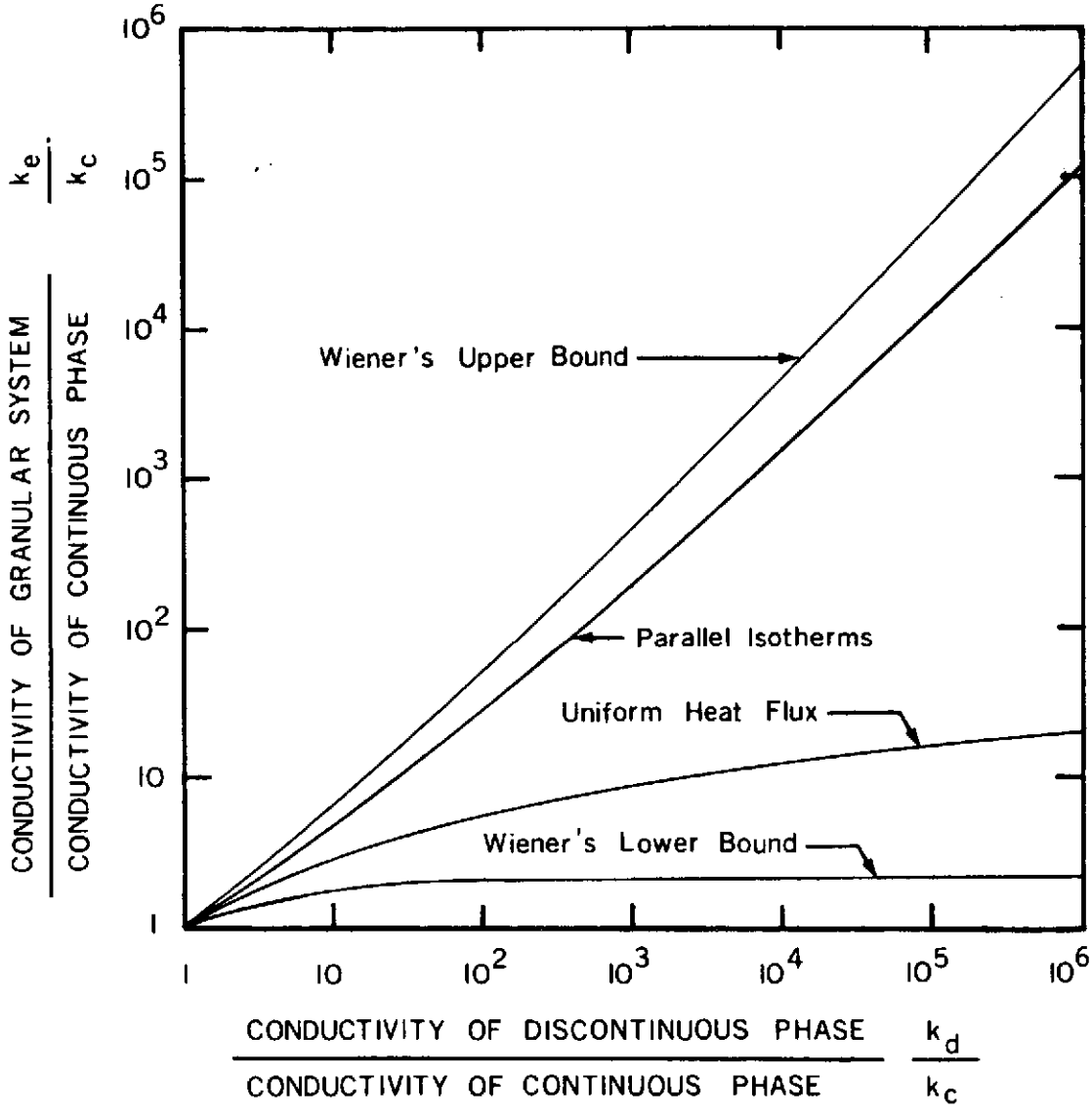

FIGURE 6-1. BOUNDING EQUATIONS FOR A CUBIC ARRAY OF SPHERES

Herein will be developed a set of such equations, generally applicable to any shape particle.

Consider a typical unit cell of the heterogeneous system shown in Figure (6-2a). Divide the unit cell into uniform sized channels by passing both vertical and horizontal planes through the element. These planes are to be oriented parallel to the direction of heat flux and are to be equispaced. If the channels are sufficiently small compared to the dimensions of the solid particles, they will appear as consisting of sections of the continuous and discontinuous phases placed in series. Assuming a uniform heat flux in each channel, the order of the series resistances does not influence the overall resistance. Consequently, the two components may be separated as shown in Figure (6-2b). The resistance of the channel is then given by

$$R_i = \frac{\varepsilon_i}{k_d \Delta A} + \frac{(1-\varepsilon_i)}{k_c \Delta A} \tag{6-1}$$

The channels behave as resistances in parallel. The overall resistance is then given as:

$$\frac{1}{R_e} = \frac{1}{R_1} + \frac{1}{R_2} + \ldots + \frac{1}{R_n} \tag{6-2}$$

The order of these channels and their shape may be altered so long as the individual channel resistances remain unchanged. They may then be distorted to a unit width by changing the vertical dimension while retaining the unit length. They are then arranged in order of decreasing

solid fraction. This geometry is shown in Figure (6-2c). The effective thermal conductivity for the specified element is

$$k_{e_o} = \frac{k_c k_d \Delta A}{\sum_{i=1}^{n} k_c \varepsilon_i + k_d(1-\varepsilon_i)} \tag{6-3}$$

If the area of the channels is allowed to approach zero as the number of channels approaches infinity the summation in Equation (26) may be replaced by an integral.

$$k_{e_o} = \int_A \frac{k_c k_d \quad dA}{k_c \varepsilon + k_d(1-\varepsilon)} \tag{6-4}$$

or,

$$k_{e_o} = \int_0^1 \int_0^1 \frac{k_c k_d}{k_d + \varepsilon\,(k_c - k_d)}\, dxdy$$

$$= \int_0^1 \frac{k_c k_d}{k_d + \varepsilon\,(k_c - k_d)}\, dx \tag{6-5}$$

since the integrand is constant in the horizontal direction. The corresponding geometry is shown in Figure (6-2d).

In a similar manner the effective conductivity has been found assuming infinite lateral conductivity [8, 53]:

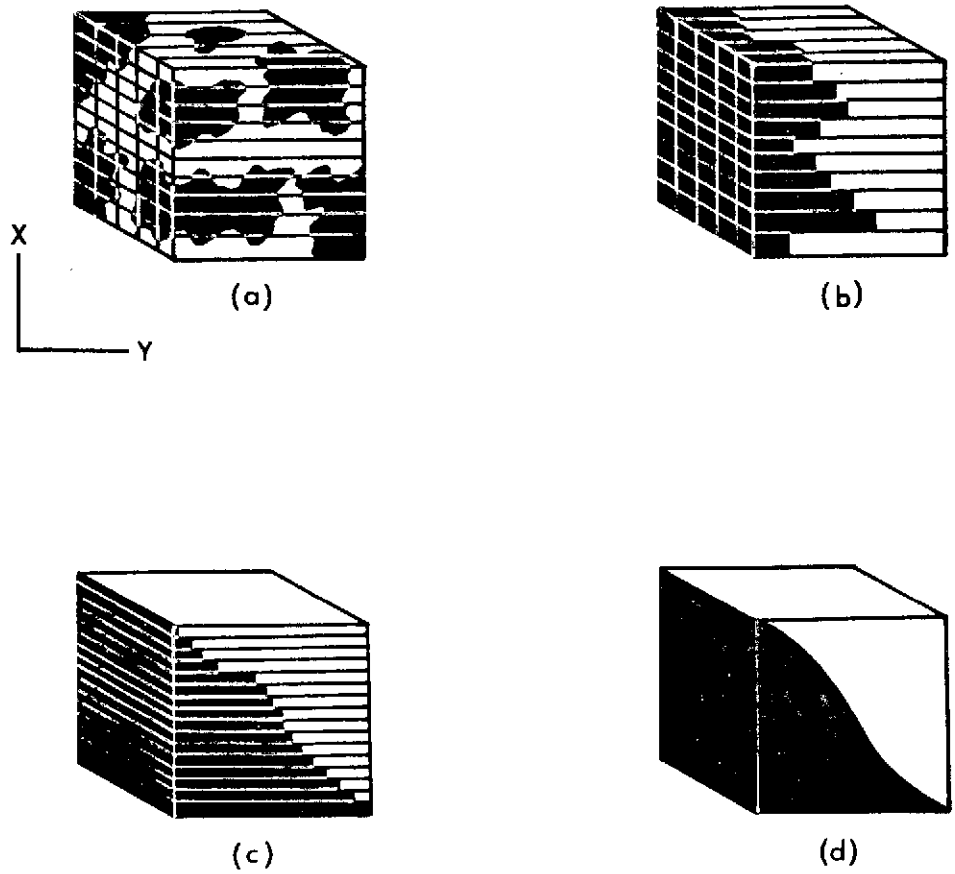

FIGURE 6-2. EQUIVALENT GEOMETRIES FOR UNIFORM HEAT FLUX

$$\frac{1}{k_{e_\infty}} = \int_0^1 \frac{dx}{k_c + \varepsilon(k_d - k_c)} \tag{6-6}$$

Both equations for zero and infinite lateral conductivity require a knowledge of the functional relation between the solid area fraction, ε, and the position, x, to solve the integral. Consider the arbitrary material distribution shown in Figure (6-2c). The verticle position of each lamina is determined by its solid fraction. The portion of the elements below a particular element is then equal to the portion of elements having larger solid fractions.

$$x = P\ (\varepsilon_i > \varepsilon\ )$$

$$= \int_\varepsilon^1 f(\phi)d\phi \tag{6-7}$$

Differentiating this equation,

$$dx = -f(\varepsilon\ )d\varepsilon \tag{6-8}$$

This relationship may be substituted into Equations (6-5) and (6-6) for the thermal conductivity with uniform heat flux and parallel isotherms. The limits of integration must be changed accordingly

$$k_{e_o} = \int_1^0 \frac{k_c k_d f(\varepsilon)}{k_d + \varepsilon(k_c - k_d)}\ d\varepsilon \tag{6-9}$$

$$\frac{1}{k_{e_\infty}} = \int_1^0 \frac{f(\varepsilon)}{k_c + \varepsilon(k_d - k_c)}\, d\varepsilon \qquad (6\text{-}10)$$

Equations (6-9) and (6-10) are entirely general in that no assumptions have yet been made regarding the particle shape or size distribution. The effects of these parameters on the solid area fraction were studied by Debbas and Rumph [51] and Haughey and Beveridge [49]. These sources found experimentally that the distribution of the solid area fraction is Gaussian for most packings. A notable exception occurs after prolonged vibration of a sample. This packing produces large regions of ordered distribution and strong anisotropic effects. Similarly large particle size variations tend to allow sifting of smaller particles into the lower regions of a given sample. This produces a definite bulk porosity gradient in the vertical direction. In such cases the radial distribution remains normal. Neglecting all such non-normal distributions the frequency distribution may be taken as Gaussian.

$$f(t) = \frac{e^{-\frac{1}{2}t^2}}{\int_a^b e^{-\frac{1}{2}t^2} dt} \qquad (6\text{-}11)$$

The integral in the denominator serves to normalize the truncated Gaussian distribution. By replacing the standardized random variable Equation (6-11) may be written in the form:

$$f(\varepsilon) = \frac{+e^{-\frac{1}{2}\left(\frac{\varepsilon-\mu}{\sigma}\right)^2}}{\frac{\sigma\sqrt{\pi}}{\sqrt{2}}\left[\operatorname{erf}\left(\frac{1-\mu}{\sigma\sqrt{2}}\right) - \operatorname{erf}\left(\frac{0-\mu}{\sigma\sqrt{2}}\right)\right]} \tag{6-12}$$

The mode of the distribution, μ, and the standard deviation of the solid area fraction, σ, remain to be evaluated. The mode may be defined implicitly in terms of the standard deviation from the basic geometry of the mixture. The total solid volume is equal to the sum of the elemental solid volumes.

$$\bar{\varepsilon} = \int_0^1 \varepsilon \, dx \tag{6-13}$$

Using the results of Equation (6-8) this expression may be written:

$$\bar{\varepsilon} = \int_1^0 -\varepsilon \, f(\varepsilon) \, d\varepsilon \tag{6-14}$$

Determination of an exact expression for the standard deviation is difficult. Stange [50] reports that the standard deviation is given by the relation,

$$\sigma = \frac{\text{constant}}{\sqrt{M}} \tag{6-15}$$

where M is a measure of the sample size.

The exact value of the standard deviation is difficult to evaluate. However, it may be noted from Figure (6-3) that the effective conductivity tends to reach a fixed value for σ sufficiently large. Consequently a sufficiently large value of σ may be selected for analysis.

Development of an Effective Conductivity Correlation

Equations (6-9) and (6-10) have been obtained to predict the effective thermal conductivity of a two phase mixture as a function of the constituent conductivities and the volume fractions. These expressions are based upon the assumptions of zero and infinite lateral conductivity, respectively. Since the lateral conductivity of the mixture falls between these limits the two equations form a set of bounding limits for the physical case. As noted in the review of literature, numerous authors have proposed correlations which effectively imply that one of these two assumptions is sufficiently close to the physical system that it may be used in obtaining an effective conductivity expression. In spite of arguments presented for proponents of both methods, it does not appear possible to select, a priori, the correlation which is more consistant with physical system. Results from both correlations are then to be compared with experimental results.

Such a comparison has been made and the results are shown graphically in Figures (6-4),(6-5) and (6-6). These figures represent granular systems with porosities of 0.31, 0.43 and 0.58 respectively. The selected values represent a range of packing fractions so that they may be considered as representative of all random packings. The non-dimensionalized effective conductivity is given as a function of the constituent conductivity ratios. The experimental values are taken from a number of independent sources and

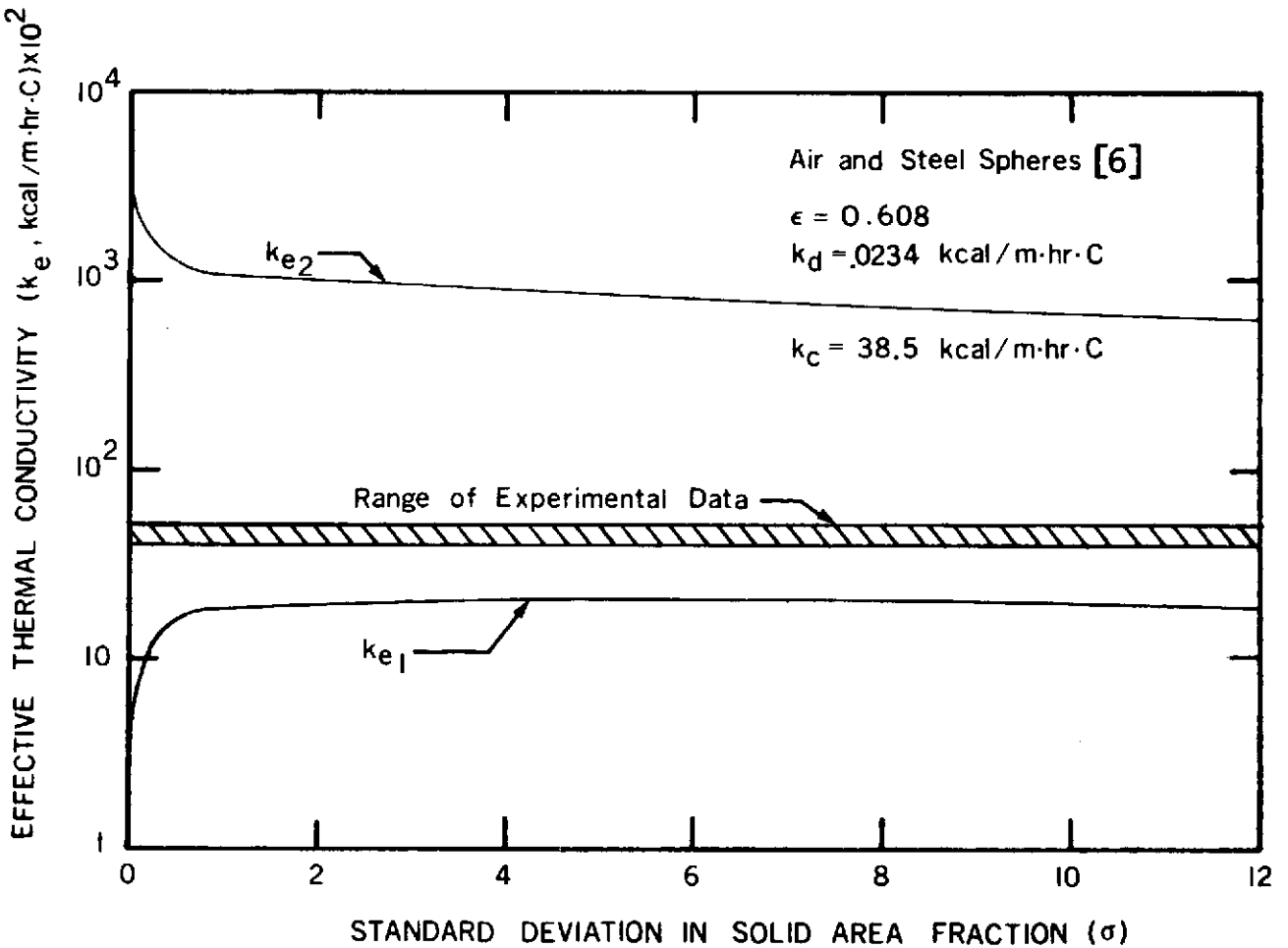

FIGURE 6-3. EFFECT OF STANDARD DEVIATION IN AREA FRACTION UPON EFFECTIVE CONDUCTIVITY

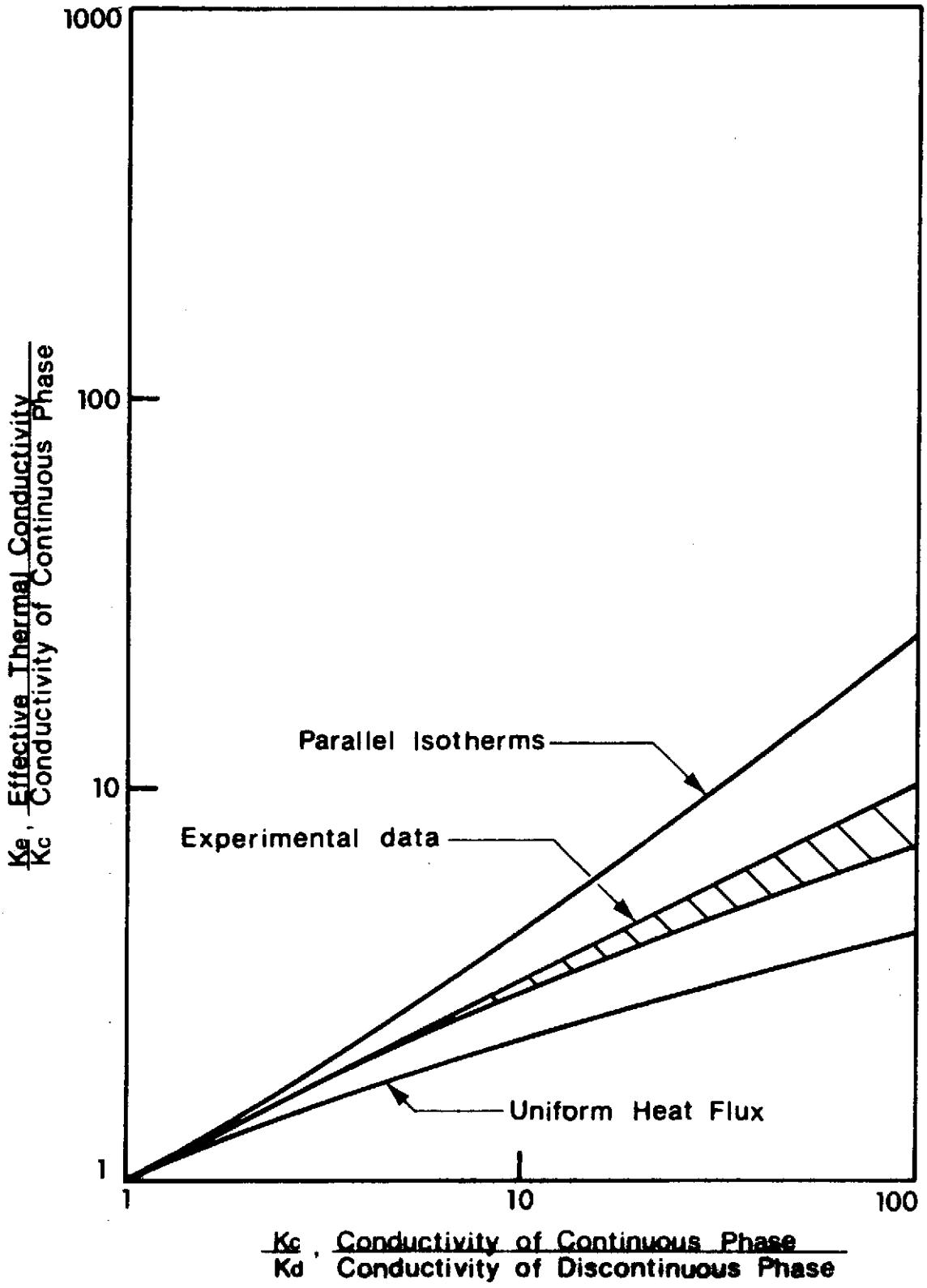

FIGURE 6-4. COMPARISON OF BOUNDING CONDUCTIVITIES WITH EXPERIMENTAL DATA FOR A POROSITY OF 0.31

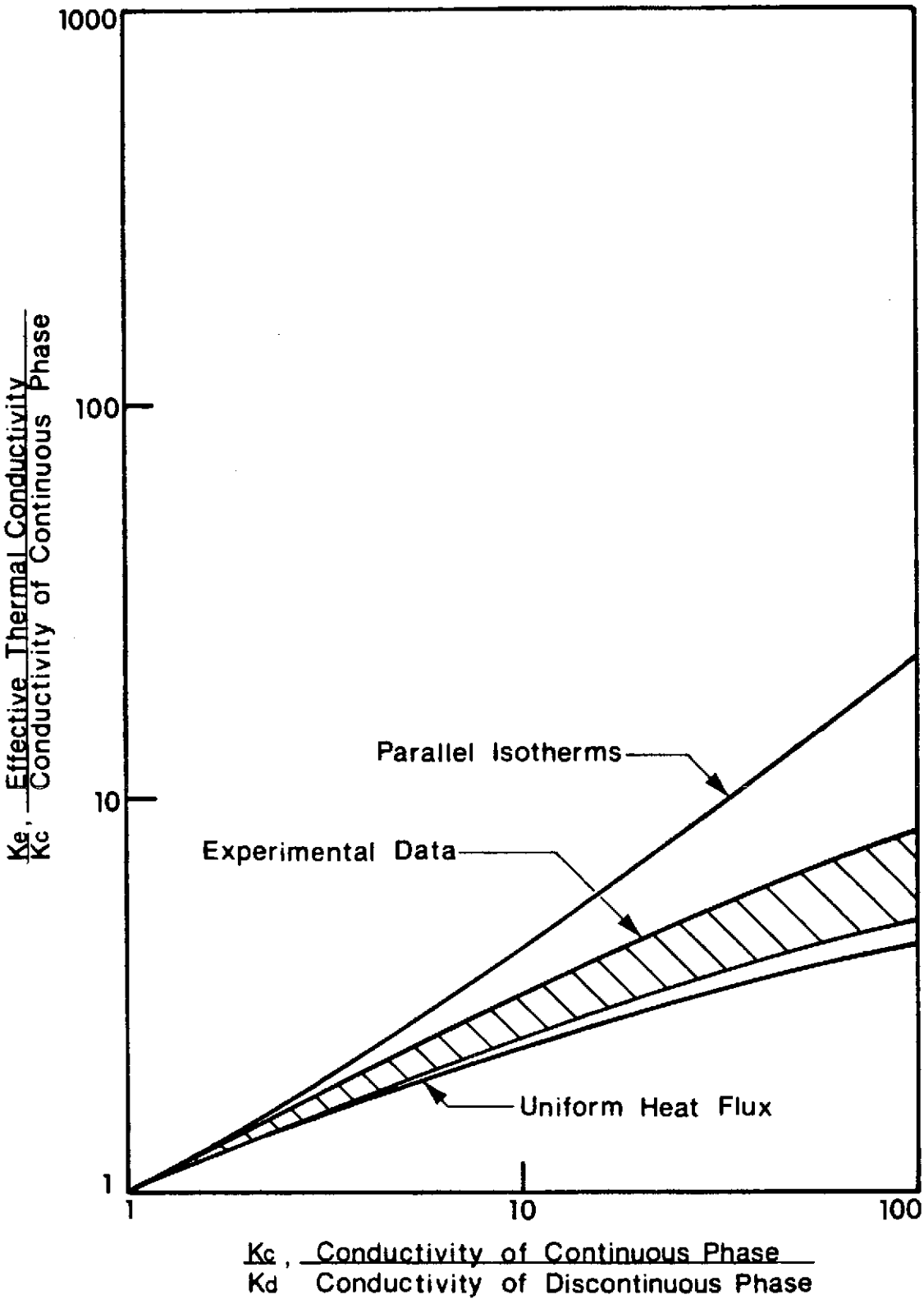

FIGURE 6-5. COMPARISON OF BOUNDING CONDUCTIVITIES WITH EXPERIMENTAL DATA FOR A POROSITY OF 0.43

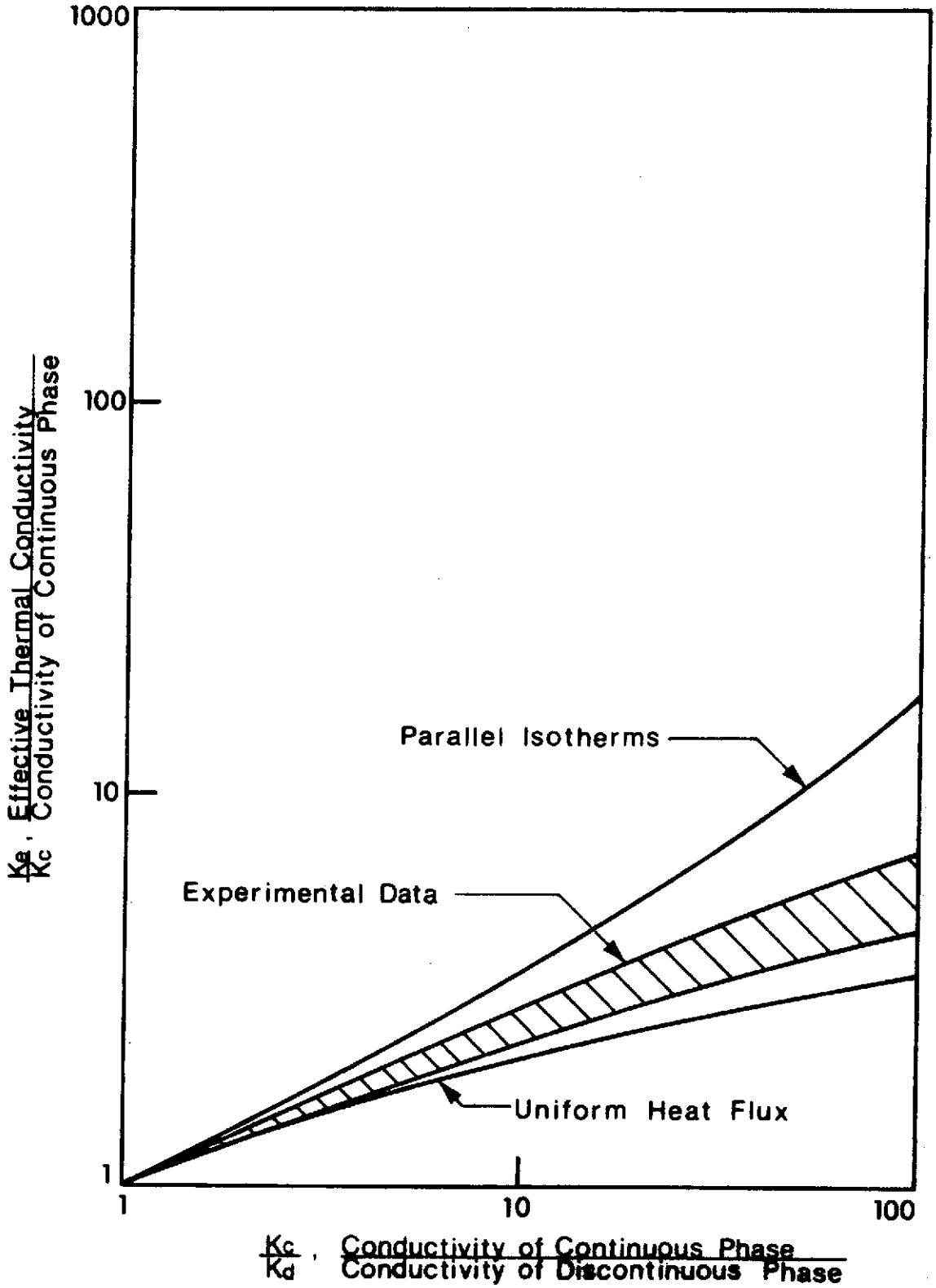

FIGURE 6-6. COMPARISON OF BOUNDING CONDUCTIVITIES WITH EXPERIMENTAL DATA FOR A POROSITY OF 0.58

are listed in Table 6-I. Note that the bulk of these data fall between the two bounding curves as would be anticipated. For a constituent conductivity ratio, $k_d/k_c < 10$ either bounding equation gives reasonably accurate results. For $k_d/k_c > 100$ both bounding equations deviate significantly from the experimental data. This indicates the reason why previous Ohm's law models, based upon an assumed regular array, have generally not been successful at higher constituent conductivity ratios. No doubt, some of the discrepancy has been countered by assuming a somewhat distorted array. Uniform heat flux models have been developed such that an inordinate amount of the higher conductivity material is arranged in series with itself. Thus the calculated conductivities have been raised above the lower bounding curve. Similarly for parallel isotherm models an excessive amount of the higher conductivity material is placed in parallel with itself and in series with the low conductivity phase. This distortion tends to result in a lower calculated conductivity than that of the upper bound.

Rather than assuming both an unrealistic heat flow model and a distorted distribution, three alternate approaches are suggested here. A uniform heat flux model and a parallel isotherm model were developed based upon a theoretical distribution of the granular material which has been experimentally verified. Since only the heat flow model is simplified, an experimentally derived correction factor for the heat flow shall be obtained for each correlation. In addition, an experimentally derived weighting factor shall be obtained for the two correlations. The effective thermal conductivity will then by given by:

$$k_{eff} = F_{\infty} k_{\infty} \tag{6-16}$$

$$k_{eff} = F_{o} k_{o} \tag{6-17}$$

$$k_{eff} = k_{\infty} - F_{w}(k_{\infty} - k_{o}) \tag{6-18}$$

where:

F_{∞} = Correction factor for nonparallel isotherms

F_{o} = Correction factor for nonuniform heat flux

F_{w} = Weighting factor for bounding equations

These correction factors are considered to be, in general, functions of the material solid fraction, constituent conductivity ratio, particle shape and particle size distribution. Unfortunately, previous attempts to describe arbitrary particle shapes with a single parameter have been largely unsuccessful [13]. Various statistical techniques have been proposed for accounting for particle size distribution [45, 54] but sufficient experimental data are not yet available to consider this parameter at this time. For this reason the correction factors are treated as functions of the conductivity ratios and the solid fractions only.

Equations (6-16) through 18) may be solved together with available experimental data to obtain the empirical values of the correction factors. This has been done for a wide range of data from the several sources as listed in Table 6-I. The correction factors listed do, of course, include both experimental error and data scatter. To obtain an easily usuable correlation these factors have been correlated into a polynomial function using a least-squares technique [55]. The fitted correction factors have

been found to be represented by the functional relations:

$$\ln (F_\infty) = 6.038 + 0.28697 \ln(k_d/k_c) - 0.079693 [\ln(k_c/k_d)]^2 - 42.035(1-\bar{\varepsilon}) + 94.701(1-\bar{\varepsilon})^2 - 0.91135(1-\bar{\varepsilon}) \ln(k_d/k_c) + 0.0029629 [\ln(k_d/k_c)]^3 + 0.0040281(1-\bar{\varepsilon}) [\ln(k_d/k_c)]^2 + 0180897(1-\bar{\varepsilon})^2 \ln(k_d/d_c) - 69.049(1-\bar{\varepsilon})^3 \quad (6\text{-}19)$$

$$\ln (F_o) = -2.4006 + 0.83611 \ln(k_d/k_c) - 0.0036959 [\ln(k_d/k_c)]^2 + 12.426(1-\bar{\varepsilon}) - 16.278(1-\bar{\varepsilon})^2 - 3.0926(1-\bar{\varepsilon}) \ln(k_d/k_c) + 0.0019151 [\ln(k_d/k_c)]^3 - 0.034069(1-\varepsilon) [\ln(k_d/k_c)]^2 + 3.3197(1-\bar{\varepsilon})^2 \ln(k_d/k_c) + 2.5768(1-\bar{\varepsilon})^3 \quad (6\text{-}20)$$

$$F_w = 1.5287 + 0.064259 \ln(k_d k_c) - 0.0064623 [\ln(k_d/k_c)]^2 - 6.1759\bar{\varepsilon} + 11.059\bar{\varepsilon}^2 + 0.22176\bar{\varepsilon} \ln(k_d/k_c) + 0.00015041 [\ln(k_d/k_c)]^3 - 0.0042453 \bar{\varepsilon} [\ln(k_d/k_c)]^2 - 0.10921 \bar{\varepsilon}^2 \ln(k_d/k_c) - 7.2252 \bar{\varepsilon}^3 \quad (6\text{-}21)$$

In conclusion, three correlations have been proposed for evaluating the effective thermal conductivity of granular systems. There appears to be no theoretical basis for selecting one solution in preference to the others. Thus, selection of the best correlation must be made solely on the basis of a comparison with experimental results.

Comparison of Available Heat Transfer Models

A number of proposed heat transfer models have been presented in the literature survey. No doubt a number of other correlations may be found through a more exhaustive search of the literature. Nevertheless, the equations which have been presented represent those models which are most prominently used in the current literature and in present engineering practice. Moreover, many of the models are somewhat redundant in that they represent only slight variations of the same basic geometrical assumptions.

The approach to be used in making a comparison of these correlations is to select models representing varying basic geometries and varying heat flow assumptions. Where two models of the same type are particularly well known both are included. Certain prominent models require the input of parameters which are generally unknown; these are, of necessity, excluded from the comparison.

Table 6-II includes a representative sample of correlations based on flux law models. Tables 6-III and 6-IV present Ohm's law models utilizing the assumption of uniform heat flux. Table 6-V presents those Ohm's law models based upon an assumption of parallel isotherms. Table 6-VI includes those Ohm's law models which include a weighting factor or a correction factor to circumvent the simplifying heat flow assumptions. Figure (6-7) presents the results of Equation (5-2) in a graphical form. Figures (6-8) through (6-10) present the results of Equations (6-16) through (6-18)

It should be noted that several of these equations have been extrapolated or extended beyond the range for which they are theoretically applicable. The correlations by Lord Rayleigh, Hengst, and Woodside were derived based on the assumption of a cubical array of uniform sized spheres. The geometrical limits on the solid fraction are then such that $0 \leq \bar{\varepsilon} \leq \pi/6$. Similarly the equation presented by Schumann and Voss and by Preston are limited to solid fractions of $0.5 \leq \bar{\varepsilon} \leq 1$. In order to compare these correlations with the remaining correlations over the same number of cases it was necessary to extrapolate the derived equation beyond its theoretical limits; where extrapolation was not possible, the closest possible value of the solid fraction was taken.

Initial results indicated that the correlation by Gorring and Churchill [4] was in considerable error. It was suspected that a typographical error may have existed in the correlation as published. Following the approach described by the authors Equation (2-17) was rederived and the corrected form of the equation was found to be:

$$\frac{k_e}{k_c} = \frac{\pi}{6\left(1 - \frac{k_c}{k_d}\right) CB}\left[\ln\left(\sqrt{\frac{B^2 - Bx_o + x_o^2}{B + x_o}}\right) + \sqrt{3}\tan^{-1}\left(\frac{2x_o - B}{B\sqrt{3}}\right)\right.$$

$$\left. - \sqrt{3}\tan^{-1}\left(\frac{-1}{\sqrt{3}}\right)\right] + \left[1 - \frac{\pi x_o}{4}\right] \qquad (2\text{-}17a)$$

This equation was found to fit the experimental data much more closely.

In summarizing the results obtained from each correlation, it is found that the major sources of error can be attributed to the following causes:

1. Distorted particle geometry
2. Idealized heat flow
3. Absence of a finite particle contact area.

Not every source of error applies to each correlation. Typically one source will dominate depending upon the ratio of the constituent conductivities, k_d/k_c. It is difficult to define an exact range of k_d/k_c over which one source will dominate as the range will vary between models. However, it is possible to discuss relative ranges.

A system composed of materials of equal conductivities will itself have a conductivity equal to that of the constituents. This is true regardless of the distribution or contact areas. Moreover the assumptions of uniform heat flux and parallel isotherms are both valid for such a system. Consequently each model should be equally valid for $k_d/k_c = 1$. If the ratio k_d/k_c is increased beyond 1.0 the effects of a distorted particle geometry appear as the dominant source of error. At still higher values of k_d/k_c the effects of the heat flow assumption become dominant. At yet higher values of k_d/k_c the effects of the particle contact area predominate.

The tendency of the particle contact area to predominate as a source of error at high constituent conductivity ratios is clearly demonstrated. In granular systems with extremely low gaseous conductivities direct particle to particle conductions will be a major mode of heat

transfer. The effective conductivity of any idealized system having no finite particle contact will approach zero as the conductivity of the gaseous phase approaches zero. An example of such action is shown in the results for a simulated lunar soil. These data are listed in the Tables as cases 159 to 164. The bulk of the correlations yield results far below the experimental values. Those correlations based upon an assumed Gaussian distribution of the two phases are the exception. The reason for this action is attributed to the fact that, while the normalized Gaussian distribution allows only point contact, the granules are in close proximity over a larger area.

The assumption of a uniform heat flux tends to yield results somewhat smaller than the experimental value while the assumption of parallel isotherms tends to yield values which are overly large. This tendency can be offset by a distortion of the material distribution so that the effects are somewhat self compensating. However, the effects of these two factors are not the same overall ranges of k_d/k_c. Therefore, calculational results tend to be high or low depending on which factor predominates.

The results of the comparison between the models is summarized in Table 6-VII. Here a nondimensionalized variance is listed for the results of each model calculated over all 172 cases of Table 6-I. The formula used in determining the variance is:

$$\text{Variance} = \sum_{n=1}^{172} \left(\frac{k_{eff} - k_{exp}}{k_h} \right)^2$$

where k_h is equal to either k_{eff} or k_{exp}, whichever is greater. This method of comparing the variance ensures that calculational results which are either high or low by the same factor are penalized equally for the difference.

It should be noted from Table 6-VII that Equation (5-2) equation together with the Equations (6-16), (6-17) and (6-18) result in the least variance. It is therefore concluded that these equations represent the closest estimation of the experimentally derived effective thermal conductivity.

The major source of error in these formulations is expected to be the failure to account for particle size distribution and shape. Additional experimental work in these areas would provide data from which Equations (6-19), (6-20) and (6-21) could be rederived to more closely fit the actual effect of bending of the heat flux lines.

Failure to account for the contact resistance between particles may or may not be an important source of error. If contact resistance were an important parameter it would be anticipated that the effective thermal conductivity of a system would be a definite function of particle size. Systems of small particles would then have a lower conductivity than systems of large particles, all other parameters being equal. While sufficient data of the necessary kind is not available to draw a definite conclusion, comparisons can be made. Waddams [6] lists the thermal conductivity of 1/8 inch steel spheres in air (Case 84, Table 6-I) as 0.517 kcal/m-hr-K while that of 7/32 inch steel spheres (Case 107, Table 6-I) is given as only 0.403 kcal/m-hr-K; the smaller

diameter, lower density particles are reported to have the larger conductivity in this case. Other data may show similar or opposite trends. Further experimental work will be required before a definite conclusion may be drawn.

The results of Table 6-VI and Table 6-VII indicate that the proposed models each perform well over the range of constituent conductivity ratios of $0 \leq k_d/k_c \leq 10^9$. Further, it is seen that most previous models fail at much lower conductivity ratios. Thus the correlations described herein represent a significant extrapolation of previous models.

TABLE 6-I. COMPARISON OF BOUNDING CONDUCTIVITIES TO EXPERIMENTAL CONDUCTIVITIES

Case	Conductivity, (k_{cal}/m-hr-k) x 100					(k_d/k_c)	$1-\bar{\varepsilon}$	Ref.
	Fluid Phase	Solid Phase	Experiment	Uniform Heat Flux	Parallel Isotherms			
1	Air 2.41	Calcite 310	21.4	12.1	64.8	128.63	.493	6
2	Air 2.41	Steel 1650	22.4	16.1	261.1	684.647	.489	36
3	Helium 11.95	Steel 1650	75.5	60.48	341.2	138.075	.489	36
4	Glycerin 45.4	Steel 1650	246	170.6	456.4	36.343	.489	36
5	Water 51.6	Steel 1650	272	187.4	471.9	31.976	.489	36
6	CO_2 .08016	Basalt 10.76	1.015	.0047	2.259	134.177	.470	3
7	EtOH 15.7	Calcite 310	63.6	49.9	101	19.745	.465	56
8	Air 2.41	Calcite 310	25	11.9	65.7	128.63	.458	6
9	Air 2.13	Calcite 310	17.5	10.6	65.7	145.54	.454	56

TABLE 6-I. Continued

10	EtOH 15.7	Calcite 310.	63.5	48.7	10.3	19.7452	.454	56
11	Water 50.5	Calcite 310	127	103.8	154.3	6.1386	.453	42
12	Air 2.12	Calcite 310	19	10.7	64.7	146.2264	.451	42
13	Air 2.13	Calcite 310	17.2	10.6	65.6	145.54	.451	42
14	Air 2.34	Lead 2950	30.4	16.1	455	1260.6841	.450	6
15	Water 50.8	Calcite 310	118	104.4	154.3	6.1024	.447	42
16	Air 2.38	Quartz 950.1	36.5	14.0	170.1	398.7498	.440	56
17	Air 2.34	Lead 2950	23.85	15.4	475.7	1260.6841	.439	6
18	Water 54.5	Silica 973.9	216.0	154.3	356.0	17.8689	.439	36
19	Air 2.25	Quartz 945	26.8	12.7	176.3	420	.438	35
20	Air 2.25	Coal 36	11.8	6.2	13.6	16	.437	35
21	Hydrogen 16.6	Coal 36	25.3	21.8	27.7	2.1687	.437	35

TABLE 6-I. Continued

22	Air 2.308	Silica 973.9	21.89	13.0	181.7	421.9353	.437	36
23	Air 2.34	Steel 3850	34.1	15.8	604.7	1645.2996	.435	6
24	EtOH 29.34	Silica 973.9	144.7	98.4	302.0	33.198	.434	36
25	Air 2.34	Lead 2950	34.4	15.4	475.7	1260.6841	.433	6
26	Water 54.5	Silica 973.9	244.9	154.3	356.1	17.8689	.431	36
27	IC8 12.29	Glass 93.96	35.14	26.5	44.6	7.6485	.431	36
28	Oil 15.4	Lead 2410	81.5	73.1	533.3	156.4935	.430	42
29	Water 54.5	Silica 973.9	224.9	154.3	356.1	17.8689	.430	36
30	Water 54.5	Silica 973.9	217.4	154.3	356.1	17.8689	.430	36
31	Water 54.5	Silica 973.9	218.9	154.3	356.1	17.8689	.430	36
32	Water 54.5	Silica 973.9	218.9	154.3	356.1	17.8689	.430	36

TABLE 6-I. Continued

33	H_2 14.85	SiC 1550	91	65	371.3	104.3771	.429	37
34	Air 2.08	SiC 1550	20	12.8	266.2	745.1921	.429	37
35	CO_2 1.26	SiC 1550	15.6	8.3	250.6	1230.1594	.429	37
36	IC8 12.29	Silica 973.9	94.4	50.6	247.0	79.2727	.428	36
37	IC8 12.29	Silica 973.9	94.0	50.7	247	79.2727	.428	36
38	Glycerin 46.3	Glass 94	73.3	29.1	73.3	2.0289	.428	36
39	Water 54.5	Silica 973.9	207.0	156.7	350.5	17.8689	.426	36
40	Water 54.5	Silica 973.9	212.9	153.4	358.0	17.8689	.426	36
41	Air 2.31	Silica 973.9	22.3	13	182.6	421.9353	.426	36
42	IC8 12.29	Silica 973.9	70.9	50.4	248.4	79.2727	.426	36
43	Air 2.31	Glass 94.0	18.5	8.1	27.9	40.7097	.426	36

TABLE 6-I. Continued

44	Helium 11.95	SiC 1550	61.5	54.4	357.5	129.7071	.425	3
45	Hydrogen 14.85	SiC 1550	85	64.7	373.3	104.3771	.425	37
46	Air 2.08	SiC 1550	22.6	12.7	267.7	745.1921	.425	37
47	CO_2 1.26	SiC 1550	14.7	8.2	252	1230.1594	.425	37
48	Air 2.31	Silica 973.9	22.6	13	182.6	421.9353	.424	36
49	CO_2 1.2	SiO 700	16.3	7.1	125	583.3333	.424	36
50	Air 2.41	SiO 700	23.8	12.8	139.5	290.4563	.424	36
51	Air 2.41	SiO 700	23.4	12.8	139.5	290.4563	.424	36
52	Air 2.41	SiO 700	25.2	12.8	139.5	290.4563	.424	36
53	Glycerin 26.3	Silica 973.9	205.5	136.6	342.2	21.0289	.424	36
54	Air 2.34	Steel 3850	44.6	15.7	608	1645.2996	.423	6

TABLE 6-I. Continued

55	EtOH 29.3	Silica 973.9	163.8	97.9	303.6	33.1980	.423	36
56	EtOH 29.3	Glass 94.0	55.4	45.3	61.7	3.2030	.423	36
57	Air 2.34	Lead 2950	36	15.3	478.3	1260.6841	.420	6
58	Air 2.41	Glass 93.5	17.1	8.4	28.1	38.7967	.420	36
59	Helium 11.95	Glass 93.5	34.2	25.9	44.3	7.8243	.420	36
60	Helium 11.95	Glass 93.5	35.6	25.9	44.3	7.8243	.420	36
61	EtOH 29.6	Glass 93.5	53.3	45.5	61.8	3.1588	.420	36
62	EtOH 29.6	Glass 93.5	55	45.5	61.8	3.1588	.420	36
63	Glycerol 45.4	Glass 93.5	71.4	58.1	73.8	2.0595	.420	36
64	Water 51.6	Glass 93.5	71.6	62.3	78.1	1.8120	.428	36
65	Water 51.6	Glass 93.5	71.4	62.3	78.1	1.8120	.420	36

TABLE 6-I. Continued

66	Water 51.1	Lead 3000	358	196.1	816.9	58.7084	.420	42
67	IC8 12.3	Silica 973.9	70.7	50.4	248.4	79.2727	.420	36
68	IC8 12.3	Silica 973.9	71.3	50.4	248.4	79.2727	.419	36
69	EtOH 29.3	Silica 973.9	144.4	97.9	303.6	33.198	.418	36
70	Air 2.34	Steel 3850	37.8	15.7	608	1645.2996	.417	6
71	Air 2.48	Lead 2950	42.5	16.1	481.4	1189.5161	.417	57
72	Air 2.25	Quartz 945	29.7	12.7	177.3	420	.416	35
73	Air 2.34	Lead 2950	36.4	15.3	478.3	1260.6841	.416	6
74	Air 2.308	Glass 94.0	17.1	8.1	27.9	40.7097	.414	36
75	Water 54.5	Silica 973.9	230.8	153.4	358.0	17.8689	.414	36
76	Air 2.34	Steel 3850	35.1	15.7	608	1645.2996	.413	6

TABLE 6-I. Continued

77	Hydrogen 14.85	SiC 1550	100.7	64.7	373.3	104.3771	.410	37
78	Air 2.08	SiC 1550	22.4	12.7	267.7	745.1921	.410	37
79	CO_2 1.26	SiC 1550	17.8	82.1	252	1230.1594	.410	37
80	Air 2.86	Sand 187.5	20.7	11.3	49.9	65.6250	.410	29
81	EtOH 29.3	Silica 973.9	154.9	97.9	303.6	33.1980	.410	36
82	Water 54.5	Glass 94	73.1	64.3	80.2	1.7240	.408	36
83	Air 2.31	Silica 973.9	24.6	13	182.6	421.9353	.408	36
84	Air 2.34	Steel 3850	51.7	15.7	608	1645.2996	.406	6
85	Air 2.14	Lead 3000	32.3	14.1	481.1	1401.8694	.406	42
86	Air 2.48	Copper 32950	78.6	18.4	4700	13313.2539	.403	56
87	Air 2.34	Steel 3850	36.8	15.7	608	1645.2996	.402	6

TABLE 6-I. Continued

88	Air 2.34	Steel 3850.	47.5	15.7	608.0	1645.3	.401	6
89	Air 2.14	Lead 3000.	32.5	14.1	481.1	1401.9	.401	42
90	Air 2.25	Lead 3030.	37.0	14.8	487.9	1346.7	.400	35
91	Hydrogen 16.6	Lead 3030.	120.6	80.8	655.2	182.5	.400	35
92	Water 54.5	Lead 3030.	298.0	206.5	835.3	55.6	.400	35
93	Glycerin 24.4	Lead 3030.	176.0	110.1	704.9	124.2	.400	35
94	Hydrogen 12.6	Glass 93.5	39.6	26.7	45.1	7.42	.400	57
95	Air 2.48	Glass 93.5	15.5	8.6	28.3	37.7	.400	57
96	Air 2.91	Steel 4500.	53.2	19.4	714.8	1546.4	.400	29
97	Air 2.91	Steel 4500.	55.4	19.4	714.8	1546.4	.400	29
98	Air 2.91	Steel 4500.	58.5	19.4	714.8	1546.4	.400	29

TABLE 6-I. Continued

99	Air 2.91	Steel 4500.	59.5	19.4	714.8	1546.4	.400	29
100	Air 2.91	Steel 4500.	61.1	19.4	714.8	1546.4	.400	29
101	Air 2.34	Cellite 92.0	23.4	8.2	27.5	39.3	.400	42
102	Air 2.41	Coal 36.0	10.2	6.4	13.9	14.9	.400	42
103	EtOH 15.7	Lead 3000.	126.0	77.0	643.3	191.1	.397	36
104	Air 2.34	Steel 3850.	43.5	15.7	608.0	1645.3	.394	6
105	Air 2.34	Steel 3850.	51.7	15.7	608.0	1645.3	.394	6
106	EtOH 29.3	Copper 33163.	327.6	198.4	5197.1	1130.5	.392	36
107	Air 2.34	Steel 3850.	40.3	16.0	597.1	1645.3	.391	6
108	Water 50.9	Lead 3000.	327.0	193.5	824.8	58.9	.391	42
109	Air 2.34	Steel 3850.	44.6	15.6	614.4	1645.3	.390	6

TABLE 6-I. Continued

110	Air 2.85	Sand 187.6	26.3	11.1	50.4	65.6	.390	29
111	Air 2.38	Quartz 950.1	41.8	13.2	181.7	398.7	.390	56
112	EtOH 29.8	Copper 11500.	318.0	163.7	2210.0	385.9	.388	36
113	EtOH 29.8	Copper 11500.	342.0	163.7	2210.0	385.9	.388	36
114	Glycerin 45.4	Copper 11500.	580.0	232.2	2370.0	253.3	.388	36
115	Glycerin 45.4	Copper 11500.	595.0	232.2	2370.0	253.3	.388	36
116	Water 51.6	Copper 11500.	550.0	257.8	2424.0	222.9	.388	36
117	Water 51.6	Copper 11500.	615.0	257.8	2424.0	222.9	.388	36
118	Water 51.6	Copper 11500.	630.0	257.8	2424.0	222.9	.388	36
119	Water 54.5	Copper 33163.	629.9	321.2	5950.6	608.5	.387	36
120	Water 54.5	Copper 33163.	597.1	321.2	5950.6	608.5	.387	36

TABLE 6-I. Continued

121	EtOH 29.33	Copper 33163.	323.1	321.2	5950.6	1130.5	.386	36
122	Glycerin 46.3	Copper 33163.	607.6	321.2	5950.6	716.1	.386	36
123	Glycerin 46.3	Copper 33163.	549.5	187.5	5499.4	716.1	.385	36
124	Water 54.5	Copper 33163.	634.4	279.4	5818.1	608.5	.384	36
125	Air 2.43	Steel 3030.	45.0	15.7	497.1	1246.9	.380	58
126	Methane 3.0	Steel 3300.	55.8	19.1	548.9	1100.0	.380	58
127	Propane 1.6	Steel 3300.	35.0	10.9	516.5	2062.5	.380	58
128	CO_2 1.35	Steel 3300.	32.4	9.3	509.8	2444.4	.380	58
129	Hydrogen 16.4	Steel 3300.	188.0	80.4	708.4	201.2	.380	58
130	Air 2.34	Steel 2850.	45.7	15.1	468.7	1217.9	.380	6
131	Oil 15.4	Lead 2410.	101.0	72.0	541.9	156.5	.380	57

TABLE 6-I. Continued

132	Air 2.86	Sand 187.6	26.4	11.1	50.4	65.6	.370	29
133	Air 2.25	Steel 2250.	35.6	14.2	378.4	1000.0	.365	35
134	Hydrogen 16.6	Steel 2250.	110.0	75.5	520.0	135.5	.365	35
135	Helium 11.95	Glass 93.5	31.1	25.6	44.8	7.8	.350	37
136	Air 2.12	Glass 93.5	13.8	7.5	27.5	44.1	.350	37
137	Air 2.08	Glass 59.1	13.8	6.61	19.4	28.3	.349	59
138	Air 2.23	Lead 3030.	34.2	14.5	492.6	1358.7	.346	12
139	Hydrogen 14.9	SiC 1548.7	95.4	64.1	377.2	104.0	.328	59
140	Air 2.08	SiC 1548.7	27.3	12.6	270.4	742.8	.328	59
141	CO_2 1.27	SiC 1548.7	26.2	8.2	254.6	1223.5	.328	59
142	Hydrogen 14.9	SiC 1548.7	61.7	64.1	377.2	104.0	.325	59

TABLE 6-I. Continued

143	Air	SiC						
	2.08	1548.7	27.0	12.6	270.4	742.9	.325	59
144	CO_2	SiC						
	1.27	1548.7	25.2	8.2	254.6	1223.5	.325	59
145	Air	Quartz						
	2.38	950.1	49.0	13.4	178.1	398.7	.310	56
146	Hydrogen	SiC						
	14.9	1548.7	110.8	62.5	386.4	104.0	.308	59
147	Air	SiC						
	2.08	1548.7	27.5	12.3	277.0	742.9	.308	59
148	CO_2	SiC						
	1.27	1548.7	26.4	7.97	260.7	1223.5	.308	59
149	Helium	SiC						
	12.0	1548.7	85.2	52.7	260.7	129.2	.308	59
150	Air	Lead						
	2.25	3030.	58.4	14.3	505.1	1346.7	.310	35
151	Air	Quartz						
	2.25	945.0	70.0	12.2	183.5	420.0	.276	37
152	Air	Quartz						
	2.25	945.0	76.0	12.2	183.5	420.0	.241	37
153	Water	S.S.						
	54.5	1795.9	272.5	195.8	496.8	33.0	.501	36

TABLE 6-I. Continued

154	Glycerin 46.3	S.S. 1795.9	248.7	172.9	475.5	38.8	.502	36
155	EtOH 29.3	S.S. 1795.9	172.7	120.7	422.3	61.2	.505	36
156	Hydrogen 14.85	$(C_6H_5)_2NH$ 18.9	16.5	16.7	16.7	1.3	.513	37
157	Air 2.08	$(C_6H_5)_2NH$ 18.9	6.9	5.1	7.5	9.1	.513	37
158	Hydrogen 14.85	SiC 1550.	46.	68.3	322.1	104.4	.518	37
159	CO_2 $.1578x10^{-7}$	Basalt 90.7	.1061	.1280x10	10.53	5.75x10	.540	3
160	CO_2 $.1856x10^{-7}$	Basalt 90.7	.08183	.1760x10	9.0	4.89x10	.600	3
161	CO_2 $.2373x10^{-7}$	Basalt 90.7	.05598	.1933x10	10.47	3.82x10	.654	3
162	CO_2 $.2967x10^{-7}$	Basalt 90.7	.0511	.2747x10	8.90	3.16x10	.683	3
163	CO_2 $.4764x10^{-7}$	Basalt 90.7	.0414	.181x10	19.15	2.23x10	.721	3
164	CO_2 $.1464x10^{-7}$	Basalt 90.7	.1404	.652x10	19.15	6.19x10	.470	37

TABLE 6-I Continued

165	Air 2.08	SiC 1550.	15.6	12.7	218.9	745.2	.518	37
166	CO_2 1.26	SiC 1550.	11.85	8.1	205.6	1230.2	.518	37
167	Air 2.47	Iron 5628.9	39.9	13.2	584.0	2277.1	.575	56
168	Oil 15.4	Copper 32000.	130.	80.6	3365.	2077.9	.580	57
169	Oil 15.4	Steel 3500.	81.5	62.2	512.8	227.3	.580	42
170	Oil 15.4	Glass 61.2	29.8	25.2	31.2	3.974	.580	42
171	Oil 15.4	Lead 2410.	60.	58.7	381.7	156.5	.580	42
172	CO_2 .2013	Basalt 96.8	1.024	.602	18.28	480.7	.720	3

TABLE 6-II COMPARISON OF SELECTED FLUX LAW MODELS

DATA	EFFECTIVE THERMAL CONDUCTIVITY (KCAL/M-HR-K) X 10				
CASE	EXPERIMENTAL	MAXWELL	RAYLEIGH	MEREDITH & TOBIAS	BRUGGEMAN
1	21.39999	9.5 694	10.32832	11.9257	17.31554
2	22.39999	9.898 7	10.85322	12.47 4	19.95781
3	75.5	47.8 798	52.14 9	6 .15923	88.514 8
4	246.	166.67621	173.89758	2 8.61894	254.9 24
5	272.	186.62283	199.79781	233.31593	278.58374
6	1. 15	.33894	.37632	.43272	.654 5
7	63.59999	56. 1492	6 .14163	7 .91235	77.23344
8	25.	1 .54335	11.86223	13.59271	2 .83421
9	17.5	9.47892	1 .723 3	12.25495	19.18465
1	63.5	57.58 96	62.29413	73.55556	8 .91877
11	127.	130.42792	134.33577	158.94153	143.49553
12	19.	9.5229	1 .81323	12.341 7	19.4223 4
13	17.2	9.56628	1 .8623 1	12.39723	19.5 473
14	.39999	10.87482	12.47522	14.11478	25. 7587

TABLE 6-II CONTINUED

DATA CASE	EFFECTIVE THERMAL CONDUCTIVITY (KCAL/M-HR-K) X 10[illegible]				
	EXPERIMENTAL	MAXWELL	RAYLEIGH	MEREDITH & TOBIAS	BRUGGEMAN
16	113.	132.23[illegible]15	136.36444	161.78436	145.45194
1c	36.5 [illegible]	11.31429	13.12894	14.79832	25.9[illegible]7
17	23.84999	11.26248	13.12744	14.74412	26.96[illegible]9
18	31o.[illegible]	2[illegible]3.2 45	221.369 6	262.35938	278.5[illegible]317
1[illegible]	26.79999	1 .77105	12.53937	14.11[illegible]4	24.89319
2[illegible]	11.F[illegible]	8.21585	8.91648	1[illegible].59934	1[illegible].98189
21	25.29[illegible]99	25.9333[illegible]	26.[illegible]1422	28.591[illegible]3	26.13719
22	21.89[illegible]	11.[illegible]8524	12.92428	14.53338	25.[illegible]222
23	34. 9999	11.41934	13.39832	14.99745	27.84776
24	144.7[illegible]	123.84[illegible]36	139.1313[illegible]	161.94485	198.329[illegible]6
25	34.39999	11.48218	13.51[illegible]69	15.1[illegible]1	28.[illegible]5673
26	244.89999	2[illegible]7.3[illegible]269	227.28355	269.5[illegible]562	285.592[illegible]4
27	35.14[illegible]	36.[illegible]6357	37.77673	45.36514	41.25337
28	81.5[illegible]	74.[illegible]1193	86.59778	97.54688	16[illegible].52133

TABLE 6-II CONTINUED

DATA	EFFECTIVE THERMAL CONDUCTIVITY (KCAL/M-HR-K) X 10**				
CASE	EXPERIMENTAL	MAXWELL	RAYLEIGH	MEREDITH & TOBIAS	BRUGGEMAN
29	224.89999	207.82314	228.04282	270.41699	286.46747
30	217.39999	207.82314	228.04282	270.41699	286.35205
31	216.89999	207.82314	228.04282	270.41699	286.36499
32	218.89999	207.82314	228.04282	270.41699	286.36499
33	91.[illegible]	73.38913	82.81788	92.81613	144.37750
34	2[illegible]	10.3 813	12.19656	13.60151	25.16855
35	15.6[illegible]	6.26272	7.41785	8.26378	15.52164
36	94.39999	57.51353	66.76503	75.87054	112.61105
37	94.39999	57.51353	66.76503	75.87054	112.61105
38	78.29999	70.08798	7 .26729	76.85507	7 .51149
39	2[illegible]	219.92188	231.12563	274.19352	289.76667
40	212.89999	219.92188	231.12563	274.19352	289.84961
41	22.29999	11.49583	13.64046	15.21807	27.59543
42	7[illegible].89999	57.86711	67.37192	76.46379	113.76636

TABLE 6-II. CONTINUED

DATA CASE	EFFECTIVE THERMAL CONDUCTIVITY (KCAL/M-HR-K) X 10[illegible]				
	EXPERIMENTAL	MAXWELL	RAYLEIGH	MEREDITH & TOBIAS	BRUGGEMAN
43	15.5[illegible]	1[illegible].24[illegible]56	11.69946	13.5[illegible]178	17.37811
44	61.5[illegible]	57.93112	68.15[illegible]16	76.65494	124.[illegible]1643
45	35.[illegible]	71.27[illegible]94	83.55272	94.28864	147.49832
46	22.59999	1[illegible].443[illegible]2	12.44179	13.82354	25.86356
47	15.7[illegible]	6.34491	7.56726	8.39893	15.94831
48	22.59999	11.56858	13.77651	15.32526	27.95589
49	16.29999	6.[illegible]3185	7.19293	7.99[illegible]74	14.83859
50	23.79999	11.99753	14.25591	15.89282	28.22928
51	23.39999	11.99753	14.25591	15.89282	28.22726
52	25.2[illegible]	11.99753	14.25591	15.89282	28.233[illegible]
53	2[illegible]5.5[illegible]	185.74664	2[illegible]6.64229	243.69896	267.73511
54	44.59999	11.87461	14.219[illegible]3	15.74392	3[illegible].24588
55	163.79999	127.58[illegible]6	145.15849	168.41991	2[illegible]7.[illegible]2396
56	55.39999	57.76814	58.43582	67.42899	59.36821

TABLE 6-II. CONTINUED

DATA	EFFECTIVE THERMAL CONDUCTIVITY (KCAL/M-HR-K) X 10[illegible]				
CASE	EXPERIMENTAL	MAXWELL	RAYLEIGH	MEREDITH & TOBIAS	BRUGGEMAN
57	36.[illegible]	11.97962	14.417[illegible]	15.9213[illegible]	3[illegible].67448
58	17.[illegible]9999	1[illegible].8[illegible]734	12.42[illegible]18	14.31884	18.3[illegible]139
59	34.2[illegible]	36.13893	38.[illegible]7352	45.94[illegible]64	41.589[illegible]
60	35.59999	36.13893	38.[illegible]7352	45.94[illegible]64	41.59145
61	53.29999	58.[illegible]6[illegible]36	58.721[illegible]7	67.75734	59.6[illegible]811
62	55.[illegible]	58.[illegible]6[illegible]36	58.721[illegible]7	67.75734	59.6[illegible]846
63	71.39999	69.69447	69.89546	76.79613	7[illegible].13719
64	71.59999	73.42126	73.53889	79.45815	73.66144
65	71.39999	73.42126	73.53889	79.45815	73.68317
66	358.[illegible]	239.48276	279.155[illegible]3	317.83447	447.21973
67	7[illegible].7[illegible]	58.99115	69.3[illegible]759	78.34[illegible]39	117.33726
68	71.29999	59.17392	69.63153	78.64911	117.93312
69	144.39999	129.4[illegible]219	149.14[illegible]	171.56953	21[illegible].78299
70	37.79999	12.11177	14.66577	16.1357[illegible]	31.52858

TABLE 6-II. CONTINUED

DATA CASE	EFFECTIVE THERMAL CONDUCTIVITY (KCAL/M-HR-K) X 1[illegible]				
	EXPERIMENTAL	MAXWELL	RAYLEIGH	MEREDITH & TOBIAS	BRUGGEMAN
71	42.5[illegible]	12.81913	15.51392	17.[illegible]7814	33.[illegible]92[illegible]7
72	29.7[illegible]	11.56561	13.97381	15.42[illegible]64	28.67444
73	36.29999	12.13889	14.72[illegible]56	16.18491	31.54257
74	17.[illegible]9999	1[illegible].59676	12.3[illegible]149	14.11691	18.3[illegible]182
75	23[illegible].79999	21[illegible].34837	24[illegible].84163	285.57251	3[illegible].92358
76	35.[illegible]9999	12.27368	14.97875	16.4[illegible]419	32.44339
77	2[illegible].7[illegible]	74.72[illegible]79	89.82[illegible]99	1[illegible].09573	159.95567
78	22.39999	1[illegible].972[illegible]8	13.[illegible]4718	14.7[illegible]15	28.63178
79	17.79999	6.66732	8.16226	8.93278	17.7[illegible]522
80	2[illegible].7[illegible]	13.94991	16.5717[illegible]	18.67726	27.15118
81	154.[illegible]9999	132.39192	153.15465	176.77412	217.64229
82	73.[illegible]9999	75.78584	75.88779	81.73167	75.99522
83	24.59999	12.19252	14.9653[illegible]	16.36278	91.[illegible]6195
84	51.7[illegible]1	12.56468	15.55835	16.88857	34.[illegible]9999

TABLE 6-II. CONTINUED

DATA CASE	EXPERIMENTAL	EFFECTIVE THERMAL CONDUCTIVITY (KCAL/M-HR-K) X 1.[illegible] MAXWELL	RAYLEIGH	MEREDITH & TOBIAS	BRUGGEMAN
85	32.29999	11.46351	14.21559	15.43543	31.[illegible]2811
86	76.59999	13.49535	16.94593	18.19315	37.76892
87	36.79999	12.7355[illegible]	15.9[illegible]930	17.174[illegible]	35.[illegible]5396
88	47.5[illegible]	12.77873	15.99943	17.24638	35.24[illegible]92
89	32.5[illegible]	11.679[illegible]3	14.61817	15.76233	32.19775
9[illegible]	37.[illegible]	12.31887	15.45297	16.63954	34.[illegible]5927
91	12[illegible].59999	88.336[illegible]7	1[illegible]9.36789	119.34586	212.[illegible]8203
92	298.[illegible]	27[illegible].12842	324.582[illegible]3	364.7[illegible]2[illegible]	514.5[illegible]122
93	176.[illegible]	127.89821	157.29483	172.79655	289.11646
94	39.59999	38.751[illegible]	41.[illegible]5339	49.93776	44.295[illegible]1
95	15.5[illegible]	11.74639	13.87323	15.83[illegible]2	2[illegible].21[illegible]43
96	53.2[illegible]	15.94177	2[illegible].[illegible]313	21.53299	44.2[illegible]741
97	55.39999	15.94177	2[illegible].[illegible]313	21.5329[illegible]	44.18[illegible]83
98	58.5[illegible]	15.94177	2[illegible].[illegible]313	21.53299	44.1[illegible]741

TABLE 6-II. CONTINUED

DATA CASE	EFFECTIVE THERMAL CONDUCTIVITY (KCAL/M-HP-K) X 10[illegible] EXPERIMENTAL	MAXWELL	RAYLEIGH	MEREDITH & TOBIAS	BRUGGEMAN
99	59.5	15.94177	2[illegible]313	21.53290	44.[illegible]7776
1	61.[illegible]999	15.94177	2[illegible]313	21.53297	44.22619
1 1	23.39999	11.14626	13.19173	15.[illegible]3186	19.4[illegible]2[illegible]5
1 2	1[illegible].2[illegible]	9.46[illegible]87	1[illegible].54435	12.59192	12.64756
1 3	126.[illegible]	84.5[illegible]438	1[illegible]5.37512	114.45631	2[illegible]5.92126
1 4	43.5[illegible]	13.[illegible]8748	16.6591[illegible]	17.76472	37.21918
1 5	51.7[illegible]	13.[illegible]8748	16.65919	17.76472	37.22635
1 6	327.53985	164.718[illegible]3	21.[illegible].52751	223.961[illegible]3	466.13599
1 7	4[illegible].29999	13.22317	16.95822	17.99335	37.98955
1 8	327.[illegible]	26[illegible].924 7	319.54712	355.12183	511.55884
1 9	44.59999	13.26886	17.[illegible]6[illegible]26	18.[illegible]7[illegible]39	38.34334
11	26.29999	14.6[illegible]45[illegible]	19.24736	2[illegible].16972	29.88664
111	42.79999	13.336[illegible]3	17.[illegible]4173	18.16583	35.99596
112	218.[illegible]	168.[illegible]2546	215.[illegible]4771	229.27646	454.3[illegible]2[illegible]3

TABLE 6-II. CONTINUED

DATA CASE	EXPERIMENTAL	MAXWELL	RAYLEIGH	MEREDITH & TOBIAS	BRUGGEMAN
		EFFECTIVE THERMAL CONDUCTIVITY (KCAL/M-HR-K) X 10			
113	342.[illegible]	168. 3546	215.74771	229.27646	454.94434
114	59[illegible]	253.84285	324.5[illegible]	346.4[illegible]8	658.894[illegible]4
115	595.[illegible]	253.84285	324.5[illegible]	346.4[illegible]8	658.91260
116	55.[illegible]	287.54614	366.95[illegible]1	392.414[illegible]6	733.746[illegible]9
117	615.[illegible]	287.54614	366.958[illegible]1	392.414[illegible]6	734.41235
118	63[illegible]	287.54614	366.958[illegible]1	392.414[illegible]6	734.46753
119	629.8999	31[illegible].217[illegible]4	4[illegible].58[illegible]6	423.5835[illegible]	87[illegible].687[illegible]1
120	597.[illegible]9985	31[illegible].217[illegible]4	4[illegible].58[illegible]8	423.5835[illegible]	869.52905
121	323. 9985	166.33691	218.5[illegible]992	23[illegible].[illegible]2142	489.[illegible]3589
122	6[illegible]7.59985	265.[illegible]3931	343.4292[illegible]	362.18555	754.62207
123	549.5[illegible]	265.95825	345.538.9	363.74438	759.[illegible]3125
124	634.3999[illegible]	313.45[illegible].44	4[illegible]7.98486	429.[illegible]7178	889.40552
125	45.[illegible]	14.2493[illegible]	18.81113	19.568[illegible]4	42.45663
126	56.79999	17.57947	23.19819	24.14169	52.1[illegible]484

TABLE 6-II. CONTINUED

DATA CASE	EFFECTIVE THERMAL CONDUCTIVITY (KCAL/M-HR-K) X 10				
	EXPERIMENTAL	MAXWELL	RAYLEIGH	MEREDITH & TOBIAS	BRUGGEMAN
127	35.[illegible]	9.4 169	12.42641	12.91 25	28.43169
128	22.39999	7.9365	1 .49296	1 .89827	24. 1172
129	188.[illegible]	93.6284	121.76 38	128.65332	241.37253
13	45.7[illegible]	13.71985	18.11 89	18.841 2	4 .93221
131	1 1.[illegible]	87.13061	112.76949	119.75 14	215.79996
132	26.39999	15.8399	2 .41969	21.97133	33. 4515
133	35.59999	13.89732	19.2 981	19.328 6	43.73842
134	11 .[illegible]	98.25 15	132.1279	136.81972	246.3 835
135	31. 4999	41.46146	45.4 475	56.1776	48. 9766
136	13.9[illegible]	11.97224	15.84873	16.92 73	22.85046
137	13.8[illegible]	1 .941 9	13.93198	15.45854	18.13 58
138	34.2[illegible]	14.795 1	22. 3165	2 .91229	51.26269
139	95.39999	99. 739	151. 1283	142.69764	253.6 451
14	27.2 999	14.7 9 4	23.81555	21.12596	53.2673

TABLE 6-II. CONTINUED

DATA	EFFECTIVE THERMAL CONDUCTIVITY (KCAL/M-HR-K) X 100				
CASE	EXPERIMENTAL	MAXWELL	RAYLEIGH	MEREDITH & TOBIAS	BRUGGEMAN
141	26.2[illegible]	9.[illegible]1769	14.66218	12.94813	33.74352
142	61.7[illegible]	1[illegible].[illegible]9858	154.81667	144.67279	258.38135
143	27.[illegible]	14.881[illegible]7	24.5[illegible]314	21.42986	54.6[illegible]3[illegible]4
144	25.2[illegible]	9.12357	15.[illegible]8942	13.13482	34.59[illegible]
145	49.[illegible]	17.89517	32.[illegible]5487	26.13841	64.99879
146	11[illegible].79999	1[illegible]6.64858	19[illegible].6[illegible]283	156.68[illegible]53	284.81616
147	27.5[illegible]	15.91946	29.3[illegible]2	23.27493	63.[illegible]2864
148	26.39999	9.76224	18.[illegible]7634	14.26836	4[illegible].26196
149	85.2[illegible]	87.16588	15[illegible].16927	127.94313	248.[illegible]59
15[illegible]	58.39999	17.[illegible]669[illegible]	31.34285	25.[illegible]4462	7[illegible].51279
151	7.[illegible]	19.5[illegible]879	48.68428	29.4[illegible]662	82.[illegible]6227
152	76.[illegible]	22.89493	13[illegible].57375	35.69896	11[illegible].92848
153	272.5[illegible]	191.64548	2[illegible]3.74248	237.47173	283.51660
154	248.7[illegible]	165.27722	176.[illegible]8318	2[illegible]4.93[illegible]89	251.63412

TABLE 6-II. CONTINUED

DATA CASE	EFFECTIVE THERMAL CONDUCTIVITY (KCAL/M-HR-K) X 10				
	EXPERIMENTAL	MAXWELL	RAYLEIGH	MEREDITH & TOBIAS	BRUGGEMAN
155	172.7	1 7.73157	115.24449	133.64227	175.524 2
156	16.9	16.73445	16.73523	17. 769	16.7366
157	6.9	5.5177	5.66798	6.58252	6.36967
158	46.	54.1 468	57.62999	66.59724	91.57744
159	.1361				
160	.8183				
161	.5593				
162	.513				
163	. 414				
164	.14 4				
165	15.6	7.84149	8.39758	9.67169	14.6 451
166	11.15	4.76 8	5.1 28	5.87268	8.9 119
167	39.99999	7.93444	8.23735	9.4 89	12.91767
168	13	43.772 5	52993	66266	78.35597

TABLE 6-II. CONTINUED

DATA CASE	EFFECTIVE THERMAL CONDUCTIVITY (KCAL/M-HR-K) X 10				
	EXPERIMENTAL	MAXWELL	RAYLEIGH	MEREDITH & TOBIAS	BRUGGEMAN
169	81.5	48.1 748	49.7762	56.79507	74.95 3
17	29.79999	27.61348	27.74 28	3 .3 795	28.56239
171	67.	47.778 9	49.4 659	56.37567	73.31424
172	1. 24	.43413	.43656	.47197	.53364

TABLE 3-III. COMPARISON OF SELECTED UNIFORM HEAT FLUX MODELS

DATA	EFFECTIVE THERMAL CONDUCTIVITY (KCAL/M-HR-K) X 1[illegible]				
CASE	EXPERIMENTAL	SCHEFFEY	WOODSIDE & MESSMER	HENGST	GORRING & CHURCHILL
1	21.39[illegible]	8.216 5	21.59131	27.81955	9.68224
2	22.[illegible]	8.5 7 7	24.[illegible]4747	39.61765	17.98637
3	75.5	41.33388	1[illegible]9.26685	141.4[illegible]97	49.78612
4	346.[illegible]	146.78038	322.41919	372.84497	114.44376
5	272.[illegible]	164.86118	352.13623	4[illegible]6.8[illegible]713	123.79[illegible]30
6	1.[illegible]15	.29447	.77575	[illegible].97724	[illegible].34656
7	43.[illegible]	5 .47438	84.6.9[illegible]	1[illegible]9.92197	32.43243
8	25.[illegible]	[illegible].19536	24.[illegible]7825	29.74[illegible]4	1[illegible].55274
9	17.[illegible]	8.26423	21.84[illegible]9[illegible]	27.269[illegible]4	9.96445
10	43.[illegible]	52. 2 31	97.[illegible]682	112.18112	33.[illegible]687
11	127.[illegible]	123.41541	162.51231	22[illegible].49751	63.22[illegible]73
12	19.[illegible]	8.3 843	21.64783	27.32[illegible]34	9.9[illegible]542
13	17.[illegible]	8.34694	22.[illegible]4125	27.41888	9.93447
14	3[illegible].39[illegible]	9.43198	25.[illegible]6537	45.9[illegible]691	24.[illegible]5783

TABLE 5-III. CONTINUED

DATA CASE	EFFECTIVE THERMAL CONDUCTIVITY (KCAL/M-HR-K) X 10				
	EXPERIMENTAL	SCHREY	WOODSIDE & MESSMER	HENGST	GORING & CHURCHILL
15	119.[illegible]	125.67723	164.32[illegible]	226.6629[illegible]	63.642[illegible]3
16	36.5[illegible]	9.85696	27.358[illegible]6	38.78313	16.59296
17	23.84999	9.79678	27.8[illegible]275	46.325[illegible]4	24.77[illegible]1[illegible]
18	216.[illegible]	184.86432	332.36 59	385.83325	112.37578
19	26.79999	9.358[illegible]4	26.[illegible]8746	37.15984	16.[illegible]6[illegible]78
2	11.8[illegible]	7.5[illegible]763	13. 5321	15.34[illegible]29	4.43499
21	25.29999	25.674[illegible]7	26.91245	43.9[illegible]685	1[illegible].63655
22	21.89[illegible]	9.66385	26.84[illegible]93	38.22[illegible]93	16.54385
23	34. 9999	9.84242	28.24911	49.18425	27.51242
24	144.7[illegible]	11 .79533	233.355[illegible]6	259.31[illegible]55	79.22112
25	34.99999	1 .[illegible]4 9	28.33229	47.32585	25.15863
26	244.89999	198.96 85	338.[illegible]5991	391.33496	113.71243
27	35.14[illegible]	34. 18[illegible]	47.15613	62.53662	17.38632
28	81.5	64.91 23	17[illegible].95238	2[illegible]9.34[illegible]68	77.48856

TABLE 6-III. CONTINUED

DATA CASE	EFFECTIVE THERMAL CONDUCTIVITY (KCAL/M-HR-K) X 100				
	EXPERIMENTAL	SUN PREY	WOODSIDE & MESSMER	HENGST	GORRING & CHURCHILL
29	224.[illegible]	189.481 5	338.77515	392.[illegible]2271	113.87953
30	217.[illegible]	189.481 5	338.77515	392.[illegible]2271	113.87953
31	218.[illegible]	189.481 5	338.77515	392.[illegible]2271	113.87953
32	218.[illegible]	189.481 5	338.77515	392.[illegible]2271	113.87953
33	91.[illegible]	61.94331	157.14453	183.37791	64.[illegible]7443
34	2[illegible]	3.99619	25.24947	38.783[illegible]4	18.[illegible]
35	15.[illegible]	5.46259	15.442[illegible]3	25.56157	13.56719
36	94.[illegible]	5.[illegible]7246	124.56232	141.5739[illegible]	47.7[illegible]596
37	94.[illegible]	5.[illegible]7246	124.56232	141.5739[illegible]	47.7[illegible]596
38	73.[illegible]	69.52[illegible]7	72.25192	119.72414	27.[illegible]8932
39	2[illegible]7.[illegible]	191.58[illegible]84	341.64[illegible]38	394.77393	114.54784
4	213.[illegible]	191.58[illegible]84	341.64 38	394.77393	114.54784
41	2[illegible]2.[illegible]	1[illegible].[illegible]5[illegible]9	27.7861[illegible]	38.994[illegible]6	17.[illegible]264
42	7[illegible].[illegible]	51.[illegible]1237	125.25269	142.[illegible]3886	47.9[illegible]417

TABLE 6-III. CONTINUED

DATA	EFFECTIVE THERMAL CONDUCTIVITY (KCAL/M-HR-K) X 10⁵				
CASE	EXPERIMENTAL	SUM & REY	WOODSIDE & MESSMER	HENGST	GORRING & CHURCHILL
43	18.5	9.14 37	2 .2167	22. 7112	6.88360
44	61.5	5 .94296	131.74825	156.75896	56.57709
45	85.	62.7874	158.93935	184.66257	64.62695
46	22.59959	9.12391	25.56296	39. 5473	18.89276
47	15.7	6.54 35	15.6349	25.74 63	13.7 532
48	22.59999	1 .121 1	27.95583	39.12991	17. 8449
49	16.29999	5.27346	14.69415	21.69397	9.99637
5	23.79999	1 .5 795	28.62161	37.89958	15.52456
51	23.39994	1 .5 795	28.62161	37.89958	15.52456
53	25.2	1 .5 795	28.62161	37.89958	15.52456
53	2 5.5	168.7 114	314.54698	356.98 4	1 4.8 246
54	44,59999	1 .37231	29.32655	5 .22885	28.37459
55	1 3.7 99	114.46762	239.46548	264.1 522	8 .71844
56	55.39999	56.55273	62.95851	98.81178	25.57965

TABLE 6-III. CONTINUED

DATA CASE	EFFECTIVE THERMAL CONDUCTIVITY (KCAL/M-HR-K) X 1[illegible] EXPERIMENTAL	SON FREY	WOODSIDE & MESSMER	HENGST	GORRING & CHURCHILL
57	36.[illegible]	1[illegible].4748[illegible]	29.498[illegible]	48.41[illegible]	26.[illegible]
58	17.[illegible]	9.67121	2[illegible].89[illegible]	22.92738	7.11912
59	34.[illegible]	34.12347	47.36348	62.62257	17.25584
60	35.59999	34.12347	47.36348	62.62257	17.25584
61	52.29999	56.88243	63.1[illegible]475	99.5[illegible]975	25.53238
62	55.[illegible]	56.88243	63.1[illegible]475	99.50975	25.53238
63	71.29999	69.12439	71.91624	12[illegible].[illegible]4974	26.61925
64	71.59999	73.[illegible]1462	74.96863	126.46695	25.[illegible]4327
65	71.39999	73.[illegible]1462	74.96863	126.46695	25.[illegible]4327
66	358.[illegible]	212.72653	496.72485	549.67188	178.83778
67	7[illegible].7[illegible]	52.1913[illegible]	127.4174[illegible]	143.63956	48.52255
68	71.29999	52.36739	127.76588	143.98718	48.62169
69	144.39999	116.256[illegible]3	242.3562[illegible]	266.3938[illegible]	81.42799
70	37.79999	1[illegible].59711	29.87333	5[illegible].75116	28.8[illegible]548

TABLE 6-III. CONTINUED

DATA CASE	EFFECTIVE THERMAL CONDUCTIVITY (KCAL/M-HR-K) X 10				
	EXPERIMENTAL	SONNEVEY	WOODSIDE & MESSMER	HENGST	GORRING & CHURCHILL
71	42.5	11.21879	31.52399	51.78989	27.19
72	29.7	1 .141	27.89 72	38.6145	16.93538
73	36.39999	1 .6259	29.86176	48.74478	26.2594
74	17. 9999	9.4887	2 .61638	22.519 4	7. 3276
75	2 .79999	1 6493	35 .27 2	4 3.8271	116.55283
76	35. 9999	1 .75 3	3 .24 95	51. 994	29. 9288
77	1 .7	66.1 1 3	165.75314	199.47987	66.69872
78	22.99999	9.62628	25.75684	4 .7353	19.59247
79	17.79999	5.84626	16.36954	26.41212	14.22331
8	2 .7	12.4 59	29.2765	32.2778	1 .67211
81	154.89999	119.19899	247. 516	27 .5542	82.56298
82	73. 9999	75.44955	77. 941	132.3438	23. 3883
83	24.59999	1 .71463	29.33125	4 .21684	17.73851
84	51.7	11. 2745	3 .89	51.7 874	29.59578

TABLE 6-III. CONTINUED

DATA CASE	EXPERIMENTAL	EFFECTIVE THERMAL CONDUCTIVITY (KCAL/M-HR-K) X 10^ SON FREY	WOODSIDE & MESSMER	HENGST	GORRING & CHURCHILL
86	32.29999	1[illegible].77968	28.19328	46.11787	25.56139
86	76.59999	11.84763	33.37509	72.95583	65.64183
87	36.79999	11.19[illegible]9	31.26418	52.[illegible]5698	29.88309
88	47.5[illegible]	11.23128	31.35809	52.14400	29.95494
89	32.5[illegible]	1[illegible].26589	28.62[illegible]0	46.5[illegible]6[illegible]	25.87[illegible]7
9[illegible]	37.[illegible]	1[illegible].83176	3[illegible].16437	48.66629	26.87482
91	12[illegible].59999	76.[illegible]5263	2[illegible]4.[illegible]7242	246.[illegible]2983	94.63369
92	298.[illegible]	241.49158	55[illegible].44[illegible]43	597.11328	193.80983
93	176.[illegible]	113.29666	287.[illegible]6[illegible]79	33[illegible].49585	119.78264
94	39.59999	36.8[illegible]632	49.77415	66.71267	18.[illegible]235
95	15.5[illegible]	1[illegible].57513	22.35555	24.19[illegible]51	7.49979
96	53.2[illegible]	14.[illegible]1585	39.[illegible]8441	64.33[illegible]81	36.52295
97	55.39999	14.[illegible]1585	39.[illegible]8441	64.33[illegible]81	36.52295
98	58.5[illegible]	14.[illegible]1585	39.[illegible]8441	64.33[illegible]81	36.52295

TABLE 5-III. CONTINUED

DATA	EFFECTIVE THERMAL CONDUCTIVITY (KCAL/M-HR-K) X 10				
CASE	EXPERIMENTAL	SUN FREY	WOODSIDE & MESSMER	HENGST	GORRING & CHURCHILL
99	59.5	14.11545	39.78441	64.33781	36.52295
1	61.99999	14.11545	39.78441	64.33781	36.52295
1 1	23.39999	1 .12616	21.38562	23.12411	7.2 296
1 2	1 .2	8.74336	14.52395	17. 592	4.84294
1 3	126.	74.71269	195.49753	236.26627	91.67732
1 4	43.5	11.52577	32. 1976	52.75337	3 .45782
1 5	61.7	11.52577	32. 1976	52.75337	3 .45782
1 6	327.99995	145.12892	4 1.15942	624.39941	334.98853
1 7	4 .29999	11.65537	32.3 559	53. 1453	3 .67331
1 8	327.	233.63985	533.677	575.53516	188.54 97
1 9	44.59999	11.69913	32.4 115	53.1 158	3 .74516
11	26.29999	13.23942	3 .75471	33.29242	11. 6783
111	41.79999	11.78171	31.77673	42.24588	18.65 44
112	219.	148.55 2	399.529 8	527.19482	231.6 94

TABLE 6-III. CONTINUED

DATA CASE	EFFECTIVE THERMAL CONDUCTIVITY (KCAL/M-HR-K) X 10[illegible]				
	EXPERIMENTAL	SON FREY	WOODSIDE & MESSMER	HENGST	GORRING & CHURCHILL
113	342.[illegible]	144.55 2[illegible]	399.528[illegible]8	527.19482	231.6[illegible]94
114	58[illegible]	224.72 38	593.5[illegible]537	737.2[illegible]19[illegible]	3[illegible]1.[illegible]1343
115	595.[illegible]	224.72 38	593.5 537	737.2[illegible]19[illegible]	3[illegible]1.[illegible]1343
116	59[illegible]	254.69652	667.9458[illegible]	815.22681	325.8[illegible]
117	615.[illegible]	254.69652	667.9458[illegible]	815.22681	325.8[illegible]
118	63[illegible]	254.69652	667.9458[illegible]	815.22681	325.8[illegible]
119	629.8999[illegible]	274.[illegible]5371	746.15283	1[illegible]52.25757	5[illegible]2.66479
12[illegible]	597.[illegible]9985	274.[illegible]5371	746.15283	1[illegible]52.25757	5[illegible]2.66479
121	323.[illegible]9985	148.63745	4[illegible]8.7[illegible]557	631.1[illegible]156	339.873[illegible]5
122	4[illegible]7.59985	234.15.19	639.17944	922.36353	454.59473
123	549.5[illegible]	235.[illegible]3156	641.[illegible]4[illegible]4	923.86597	455.61694
124	634.3999[illegible]	277.15259	752.66968	1[illegible]57.4[illegible]674	5[illegible]6.[illegible]3979
125	45.[illegible]	12.6[illegible]28[illegible]	34.515[illegible]1	53.64485	29.57269
126	55.79999	15.54999	42.52984	64.98873	34.89153

TABLE 6-III. CONTINUED

DATA CASE	EFFECTIVE THERMAL CONDUCTIVITY (KCAL/M-HR-K) X 10^2				
	EXPERIMENTAL	SONFREY	WOODSIDE & MESSMER	HENGST	GORRING & CHURCHILL
127	35.[illegible]	8.31253	22.86977	38.19576	23.32364
128	32.99999	7.[illegible]1661	19.32559	33.[illegible]4791	2[illegible].9[illegible]578
129	186.[illegible]	83.1662[illegible]	215.19414	256.68781	1[illegible]1.24123
130	45.7[illegible]	12.13477	33.22412	51.462[illegible]5	28.23676
131	1 1.[illegible]	77.5[illegible]923	196.97273	227.7[illegible]387	86.22366
132	26.39999	14.24799	32.42883	34.47119	11.5[illegible]799
133	35.59999	12.34881	33.23314	49.[illegible]6239	26.13159
134	11 .[illegible]	87.8669[illegible]	217.2[illegible]74[illegible]	243.[illegible]2867	[illegible].48[illegible]83
135	31.[illegible]4999	39.66171	52.69141	7[illegible].18[illegible]48	18.27229
136	13.8[illegible]	1 .8[illegible]926	22.59[illegible]16	23.5[illegible]623	7.46198
137	13.8[illegible]	1 .[illegible]5478	18.89433	2[illegible].19761	6.[illegible]3471
138	34.2[illegible]	13.21836	34.93283	52.64954	3[illegible].15294
139	95.29999	89.7282[illegible]	2[illegible]5.8[illegible]371	216.31229	78.15236
140	27.29999	13.22277	33.78964	45.63637	23.41[illegible]51

TABLE 6-III. CONTINUED

DATA CASE	EXPERIMENTAL	EFFECTIVE THERMAL CONDUCTIVITY (KCAL/M-HR-K) X 10[illegible] SON FREY	WOODSIDE & MESSMER	HENGST	GORRING & CHURCHILL
141	26.2[illegible]	8.1[illegible]6	2[illegible].86414	3[illegible].27881	17.13559
142	61.7[illegible]	9[illegible].8[illegible]51	2[illegible]7.32312	217.27795	78.56728
143	27.[illegible]	13.3[illegible]986	34.[illegible]6313	45.84[illegible]1[illegible]	23.55[illegible]45
144	25.2[illegible]	8.2[illegible]482	21.[illegible]3415	3[illegible].41397	17.23967
145	49.[illegible]	16.19675	39.55229	47.78639	21.94421
146	11[illegible].79999	97.25[illegible]79	216.[illegible]248[illegible]	222.75[illegible]18	8[illegible].93[illegible]69
147	27.5[illegible]	14.39546	35.63449	46.99461	24.34775
148	26.39999	8.82587	22.[illegible]11[illegible]2	31.17998	17.83273
149	85.2[illegible]	79.34776	18[illegible].23277	189.21664	71.22829
15[illegible]	58.39999	15.5[illegible]932	38.857[illegible]6	55.96614	32.62816
151	7[illegible].[illegible]	17.84613	4[illegible].87521	47.87144	22.66267
152	76.[illegible]	21.18156	44.51111	5[illegible].18568	24.55772
153	272.5[illegible]	168.7[illegible]651	368.51343	423.66528	129.13[illegible]16
154	248.7[illegible]	144.91[illegible]72	323.16113	378.1731[illegible]	116.45776

TABLE 6-III. CONTINUED

DATA CASE	EFFECTIVE THERMAL CONDUCTIVITY (KCAL/M-HR-K) X 1[illegible]				
	EXPERIMENTAL	SONNEREY	WOODSIDE & MESSMER	HENGST	GORRING & CHURCHILL
155	172.7[illegible]	93.6[illegible]571	226.[illegible]159	272.27515	86.88446
156	16.5[illegible]	16.71394	16.791A[illegible]	24.55[illegible]5	3.55[illegible]39
157	6.9[illegible]	5.[illegible]867[illegible]	7.65523	9.76947	2.93787
158	46.[illegible]	46.57545	119.69844	154.79541	51.782[illegible]6
159	[illegible].1 61	[illegible]	[illegible]	[illegible]	[illegible]2
160	[illegible].9193	[illegible]	[illegible]	[illegible]	[illegible]2
161	[illegible].[illegible]593	[illegible]	[illegible]	[illegible]	[illegible]1
162	[illegible].[illegible]511[illegible]	[illegible]	[illegible]	[illegible]	[illegible]1
163	[illegible].414[illegible]	[illegible]	[illegible]	[illegible]	[illegible]1
164	[illegible].14[illegible]4[illegible]	[illegible]	[illegible]	[illegible]	[illegible]3
165	15.6	6.694[illegible]9	18.[illegible]675	32.738[illegible]7	14.55421
166	11.85[illegible]	4.[illegible]6138	11.48297	21.57736	1[illegible].49382
167	29.89999	6.69278	18.28589	41.[illegible]2341	2[illegible].55[illegible]72
168	13.[illegible]	41.1[illegible]8[illegible]6	111.72429	249.32[illegible]14	121.63942

TABLE 6-III. CONTINUED

DATA CASE	EFFECTIVE THERMAL CONDUCTIVITY (KCAL/M-HR-K) X 1[illegible]				
	EXPERIMENTAL	SUN FREY	WOODSIDE & MESSMER	HENGST	GORRING & CHURCHILL
169	81.5[illegible]	4[illegible].71188	1[illegible]6.3[illegible]	167.68166	58.[illegible]75[illegible]1
17	2[illegible].7[illegible]	26.412[illegible]3	31.45314	42.29439	15.41329
171	6[illegible].[illegible]	4[illegible].51416	1[illegible]3.88419	154.25[illegible]96	51.28328
172	1.[illegible]24[illegible]	[illegible].36333	[illegible].77145	1.6997[illegible]	[illegible].44762

TABLE 6-IV. COMPARISON OF SELECTED UNIFORM HEAT FLUX MODELS

DATA CASE	EFFECTIVE THERMAL CONDUCTIVITY (KCAL/M-HR-K) X 100				
	EXPERIMENTAL	WILLHITE, KUNII & SMITH	SCHUMANN & VOSS	PRESTON	KRUPICZKA
1	21.39999	30.58623	10.94355	18.70827	16.19852
2	22.39999	47.55049	14.85457	25.07813	24.24138
3	75.50000	163.22572	55.93527	89.43590	82.96125
4	246.00000	400.29590	158.42358	242.72166	209.98410
5	272.00000	432.23389	174.36879	266.10303	228.48177
6	1.01500	1.37111	0.40426	0.79117	0.58865
7	63.59999	133.91194	50.24249	80.68788	61.53003
8	25.00000	46.32814	12.68302	21.55121	18.21974
9	17.50000	44.25276	11.69747	19.94258	16.93826
10	63.50000	146.90202	51.99330	83.38252	62.99168
11	127.00000	224.19444	112.45572	174.73199	124.08296
12	19.00000	45.44478	11.80254	20.11433	17.06645
13	17.20000	45.59529	11.84647	20.18613	17.12315
14	30.39999	83.85548	19.15024	31.99532	31.86885

TABLE 6-IV. CONTINUED

DATA CASE	EFFECTIVE THERMAL CONDUCTIVITY (KCAL/M-HR-K) X 1CC				
	EXPERIMENTAL	WILLHITE, KUNII & SMITH	SCHUMANN & VOSS	PRESTON	KRUPICZKA
15	118.00000	232.31764	114.24954	177.40428	125.47821
16	36.50000	74.12903	16.92627	28.42311	26.38243
17	23.84999	93.82394	20.22913	33.72197	33.77486
18	216.00000	541.22119	183.03313	278.77075	217.02795
19	26.79999	72.28941	16.30099	27.41541	25.49240
20	11.80000	21.24489	7.33154	12.74100	8.59804
21	25.29999	31.74640	24.32825	40.24960	25.07823
22	21.89000	74.93779	16.81395	28.24219	26.29956
23	34.09999	102.45132	21.47824	35.71642	36.33392
24	144.70000	418.10156	120.99857	187.44221	150.96895
25	34.39999	99.40475	20.84666	34.70860	34.88362
26	244.89999	572.65503	187.48227	285.26611	220.84439
27	35.14000	73.13052	31.21465	51.11766	34.42345
28	81.50000	408.71387	95.18149	148.90633	136.89030

TABLE 6-IV. CONTINUED

DATA CASE	EFFECTIVE THERMAL CONDUCTIVITY (KCAL/M-HR-K) X 100				
	EXPERIMENTAL	WILLHITE, KUNII & SMITH	SCHUMANN & VOSS	PRESTON	KRUPICZKA
29	224.89999	576.60229	188.04678	286.08984	221.33124
30	217.39999	576.60229	188.04678	286.08984	221.33124
31	218.89999	576.60229	188.04678	286.08984	221.33124
32	218.89999	576.60229	188.04678	286.08984	221.33124
33	91.00000	349.10938	84.12898	132.28313	116.49580
34	20.00000	82.54218	17.37775	29.14975	28.26201
35	15.60000	55.29848	11.40983	19.47205	19.10077
36	94.39999	264.32520	65.42412	103.93791	88.21062
37	94.39999	264.32520	65.42412	103.93791	88.21062
38	73.29999	84.76138	66.28185	105.24437	67.93713
39	207.00000	592.43018	190.32243	289.40918	223.30064
40	212.89999	592.43018	190.32243	289.40918	223.30064
41	22.29999	82.85297	17.72032	29.70062	27.68407
42	70.89999	268.62280	65.94923	104.73782	88.80655

TABLE 6-IV. CONTINUED

DATA CASE	EXPERIMENTAL	EFFECTIVE THERMAL CONDUCTIVITY (KCAL/M-HR-K) X 100 WILLHITE, KUNII & SMITH	SCHUMANN & VOSS	PRESTON	KRUPICZKA
43	18.50000	38.45332	10.38729	17.79535	13.12635
44	61.50000	311.97437	72.38222	114.51656	102.07315
45	85.00000	360.78979	85.53532	134.40306	118.17538
46	22.59999	85.55513	17.72148	29.70250	28.84357
47	15.70000	57.34253	11.64175	19.85146	19.52393
48	22.59999	84.30673	17.88850	29.97090	27.94415
49	16.29999	47.21161	9.85118	16.91360	15.76856
50	23.79999	80.12569	17.38402	29.15985	26.34326
51	23.39999	80.12569	17.38402	29.15985	26.34326
52	25.20000	80.12569	17.38402	29.15985	26.34326
53	205.50000	560.34937	171.63145	262.09570	203.90205
54	44.59999	114.48170	22.88257	37.95303	38.89476
55	163.79999	453.54956	125.76273	194.51445	155.36868
56	55.39999	85.36807	52.36089	83.94774	54.60246

TABLE 6-IV. CONTINUED

DATA	EFFECTIVE THERMAL CONDUCTIVITY (KCAL/M-HR-K) X 100				
CASE	EXPERIMENTAL	WILLHITE, KUNII & SMITH	SCHUMANN & VOSS	PRESTON	KRUPICZKA
57	36.00000	111.82214	22.29712	37.02130	37.47093
58	17.09999	41.02596	10.93644	18.69662	13.68109
59	34.20000	76.87021	31.42694	51.45102	34.42252
60	35.59999	76.87021	31.42694	51.45102	34.42252
61	53.29999	85.84662	52.72963	84.51462	54.87790
62	55.00000	85.84662	52.72963	84.51462	54.87790
63	71.39999	85.76227	65.91762	104.68968	67.41853
64	71.59999	85.66153	70.29794	111.35236	71.57538
65	71.39999	85.66153	70.29794	111.35236	71.57538
66	358.00000	1041.73608	260.21729	390.65063	338.67065
67	70.70000	281.75488	67.68922	107.38646	90.68391
68	71.29999	283.93408	67.95511	107.79092	90.99518
69	144.39999	469.97510	127.91452	197.70503	157.51135
70	37.79999	120.64456	23.57863	39.05948	40.27139

TABLE 6-IV. CONTINUED

DATA CASE	EFFECTIVE THERMAL CONDUCTIVITY (KCAL/M-HR-K) X 100				
	EXPERIMENTAL	WILLHITE, KUNII & SMITH	SCHUMANN & VOSS	PRESTON	KRUPICZKA
71	42.30000	120.25105	23.76529	39.35597	39.88403
72	29.70000	87.76758	18.10641	30.32092	28.23933
73	36.39999	115.72844	22.74287	37.73077	38.32213
74	17.09999	41.93744	10.84972	18.55441	13.58416
75	230.79999	640.26025	197.46478	299.81689	229.43102
76	35.09999	124.80501	24.05841	39.82138	41.22763
77	100.70000	405.39233	91.10527	142.78535	124.84547
78	22.39999	97.12326	19.09396	31.90515	31.18739
79	17.79999	65.19725	12.56905	21.36546	21.23581
80	20.70000	65.61769	15.58228	26.25514	20.38972
81	154.89999	496.46704	131.46788	202.96892	161.05682
82	73.09999	87.70724	73.14787	115.67809	74.00459
83	24.59999	96.18216	19.31223	32.25484	30.16379
84	51.70000	132.18263	24.92836	41.20128	42.97977

TABLE 6-IV CONTINUED

DATA CASE	EFFECTIVE THERMAL CONDUCTIVITY (KCAL/M-HR-K) X 100				
	EXPERIMENTAL	WILLHITE, KUNII & SMITH	SCHUMANN & VOSS	PRESTON	KRUPICZKA
85	32.29999	117.29691	22.23698	36.92557	37.98433
86	78.59999	199.33517	35.51990	57.86070	64.84431
87	36.79999	136.45222	25.44284	42.01639	44.02840
88	47.50000	137.52550	25.57341	42.22316	44.29619
89	32.50000	122.02280	22.80809	37.83456	39.12225
90	37.00000	128.29848	23.94914	39.64790	41.00870
91	120.59999	584.87109	121.11996	187.62265	174.98882
92	298.00000	1251.81348	294.91113	440.46875	377.66968
93	176.00000	760.24341	162.79938	249.14752	226.25079
94	39.59999	85.96399	33.90945	55.34254	36.56947
95	15.50000	47.73401	11.97573	20.39729	14.75896
96	53.20000	170.37206	31.65918	51.81555	54.68451
97	55.39999	170.37206	31.65918	51.81555	54.68451
98	56.50000	170.37206	31.65918	51.81555	54.68451

TABLE 6-IV. CONTINUED

DATA CASE	EXPERIMENTAL	EFFECTIVE THERMAL CONDUCTIVITY (KCAL/M-HR-K) X 100			
		WILLHITE, KUNII & SMITH	SCHUMANN & VOSS	PRESTON	KRUPICZKA
99	59.50000	170.37206	31.65918	51.81555	54.68451
100	61.09999	170.37206	31.65918	51.81555	54.68451
101	23.39999	45.95647	11.44436	19.52858	14.16165
102	10.20000	27.48444	8.53562	14.74131	9.68186
103	126.00000	573.10449	117.28314	181.91917	170.16017
104	43.50000	145.10443	26.51057	43.70592	46.23676
105	51.70000	145.10443	26.51057	43.70592	46.23676
106	327.59985	1715.02881	315.72998	470.24634	537.74292
107	40.29999	148.38657	26.92435	44.35989	47.10522
108	327.00000	1271.44189	289.85645	433.22607	371.82324
109	44.59999	149.48515	27.06407	44.58066	47.39987
110	26.29999	75.03748	16.80733	28.23152	21.79857
111	41.79999	111.82056	21.44038	35.65605	33.45587
112	318.00000	1407.88379	269.20239	403.57739	418.94873

TABLE 6-IV. CONTINUED

DATA CASE	EFFECTIVE THERMAL CONDUCTIVITY (KCAL/M-HR-K) X 100				
	EXPERIMENTAL	WILLHITE, KUNII & SMITH	SCHUMANN & VOSS	PRESTON	KRUPICZKA
113	342.00000	1407.88379	269.20239	403.57739	418.94873
114	580.00000	1916.31787	375.79736	555.72754	560.92163
115	595.00000	1916.31787	375.79736	555.72754	560.92163
116	550.00000	2099.59497	415.35303	611.70728	611.90381
117	615.00000	2099.59497	415.35303	611.70728	611.90381
118	630.00000	2099.59497	415.35303	611.70728	611.90381
119	629.99990	2894.58716	540.02856	786.80811	877.19165
120	597.09985	2894.58716	540.02856	786.80811	877.19165
121	323.09985	1792.87500	325.79004	484.60596	557.69434
122	607.59985	2570.67017	475.26123	696.08081	783.57446
123	549.50000	2588.86743	477.62915	699.40625	787.97876
124	634.39990	2956.20654	548.06128	798.02905	891.69800
125	45.00000	158.02725	28.29333	46.52072	49.08374
126	55.79999	190.22292	34.20032	55.79771	58.74028

TABLE 6-IV. CONTINUED

DATA CASE	EFFECTIVE THERMAL CONDUCTIVITY (KCAL/M-HR-K) X 100				
	EXPERIMENTAL	WILLHITE, KUNII & SMITH	SCHUMANN & VOSS	PRESTON	KRUPICZKA
127	35.00000	114.50127	20.19646	33.66980	36.33409
128	32.39999	99.59148	17.48831	29.32759	31.80313
129	188.00000	683.11768	133.78758	206.40227	195.06731
130	45.70000	151.46167	27.13866	44.69846	46.99364
131	101.00000	593.08423	118.45277	183.65854	168.09543
132	26.39999	84.99678	18.23677	30.53023	23.48619
133	35.59999	154.58116	27.24794	44.87105	47.12100
134	110.00000	669.15698	131.65253	203.24222	183.83636
135	31.04999	105.88724	36.88158	59.98622	38.93994
136	13.80000	58.70363	12.93406	21.96014	15.85690
137	13.80000	45.93121	10.94369	18.70853	12.81330
138	34.20000	183.41197	31.51228	51.58502	57.44498
139	95.39999	668.09253	129.35771	199.84351	175.85689
140	27.29999	166.50456	28.89240	47.46490	50.64946

TABLE 6-IV. CONTINUED

DATA CASE	EXPERIMENTAL	EFFECTIVE THERMAL CONDUCTIVITY (KCAL/M-HR-K) X 100 WILLHITE, KUNII & SMITH	SCHUMANN & VOSS	PRESTON	KRUPICZKA
141	26.20000	113.17999	19.36655	32.34183	35.98036
142	61.70000	678.12842	131.05650	202.35971	178.34129
143	27.00000	169.20699	29.34781	48.18216	51.67146
144	25.20000	115.03691	19.68065	32.84468	36.76106
145	49.00000	179.21666	31.78062	52.00621	52.57718
146	110.79999	735.47627	141.22476	217.39323	193.58580
147	27.50000	184.69882	32.10506	52.51523	58.07330
148	26.39999	125.68794	21.58565	35.88768	41.67722
149	85.20000	642.29883	121.19238	187.73024	171.18640
150	58.39999	224.99965	38.52536	62.54784	75.00726
151	70.00000	201.06511	36.36180	59.17522	63.78119
152	76.00000	232.15498	44.17183	71.31412	83.49115
153	272.50000	399.69238	178.60139	272.29443	237.12428
154	248.70000	356.15112	157.72446	241.69421	212.07919

TABLE 6-IV. CONTINUED

DATA CASE	EXPERIMENTAL	EFFECTIVE THERMAL CONDUCTIVITY (KCAL/M-HR-K) X 100 WILLHITE, KUNII & SMITH	SCHUMANN & VOSS	PRESTON	KRUPICZKA
155	172.70000	252.44057	110.58070	171.93726	153.71112
156	16.50000	16.85527	16.46114	27.67363	16.72668
157	6.90000	7.48778	4.74239	8.39002	5.55099
158	46.00000	121.25670	62.07175	98.82504	87.33781
159	0.10610	0.00000	0.00000	0.00000	0.00000
160	0.08183	0.00000	0.00000	0.00000	0.00000
161	0.05598	0.00000	0.00000	0.00000	0.00000
162	0.05110	0.00000	0.00000	0.00000	0.00000
163	0.04140	0.00000	0.00000	0.00000	0.00000
164	0.14040	0.00000	0.00000	0.00000	0.00000
165	15.60000	25.68503	12.15019	20.68217	18.75803
166	11.85000	16.91458	7.90069	13.68808	12.28974
167	39.89999	10.58609	15.94372	26.83890	20.00317
168	130.00000	64.80984	97.74626	152.75218	121.11963

TABLE 6-IV. CONTINUED

DATA CASE	EXPERIMENTAL	EFFECTIVE THERMAL CONDUCTIVITY (KCAL/M-HR-K) X 100			
		WILLHITE, KUNII & SMITH	SCHUMANN & VOSS	PRESTON	KRUPICZKA
169	81.50000	50.49634	70.56497	111.75790	89.70921
170	29.79999	24.32439	25.85866	42.67471	27.67903
171	60.00000	48.08287	66.04495	104.88356	83.26828
172	1.02400	0.54938	0.85596	1.62444	0.85991

TABLE 6-V. COMPARISON OF SELECTED PARALLEL ISOTHERMS MODELS

DATA CASE	EFFECTIVE THERMAL CONDUCTIVITY (KCAL/M-HR-K) X 10				
	EXPERIMENTAL	RUSSELL	BERNSTEIN	WOODSIDE	Equation 5-2
1	21.39999	11.35[illegible]84	9.[illegible]5587	34.11279	13.[illegible]40
2	22.39[illegible]99	11.91[illegible]25	41.[illegible]0717	1[illegible]7.35464	23.42773
3	75.5[illegible]	57.[illegible]2879	59.5[illegible]623	185.24553	68.[illegible]7611
4	246.[illegible]	193.6767[illegible]	122.72449	257.73462	173.96[illegible]13
5	272.[illegible]	215.93658	134.169[illegible]4	265.81763	19[illegible].39352
6	1.[illegible]15[illegible]	[illegible].4[illegible]1[illegible]	[illegible].79519	1.3951[illegible]	[illegible].47514
7	63.59999	63.[illegible]55[illegible]5	49.49434	58.13519	52.52979
8	25.[illegible]	12.41196	3[illegible].42108	4[illegible].47348	14.54256
9	17.5[illegible]	11.1493[illegible]3	32.36168	39.668[illegible]6	13.51[illegible]1
10	63.5[illegible]	64.57969	55.65683	58.13519	53.69958
11	127.[illegible]	137.792[illegible]8	107.82751	78.63356	115.[illegible]479
12	19.[illegible]	11.18736	34.17848	39.63994	13.57578
13	17.2[illegible]	11.23781	34.1963[illegible]	39.668[illegible]6	13.61926
14	3[illegible].39999	12.88216	299.2[illegible]859	279.97795	32.[illegible]816

TABLE 5-V. CONTINUED

DATA CASE	EFFECTIVE THERMAL CONDUCTIVITY (KCAL/M-HR-K) X 10				
	EXPERIMENTAL	RUSSELL	BERNSTEIN	WOODSIDE	Equation 5-2
15	118.	139.46962	11[illegible].93158	78.77039	117.15749
16	36.5[illegible]	13.31256	118.19025	1[illegible]4.51558	22.[illegible]1546
17	33.84999	13.27931	364.[illegible]586	279.97715	33.94925
18	216.[illegible]	225.79[illegible]7	2[illegible]9.44612	186.88631	186.[illegible]5870
19	26.79999	12.66572	121.11266	1[illegible]3.21956	21.32[illegible]31
20	11.0	9.[illegible]7918	8.23765	7.[illegible]9029	7.43614
21	25.29999	26.19[illegible]4	24.39537	12.93435	24.85637
22	21.89[illegible]	13.[illegible]2919	126.73624	1[illegible]6.34[illegible]9[illegible]	21.97264
23	34.[illegible]9999	13.44579	5[illegible]4.56934	354.25293	38.64723
24	144.7[illegible]	14[illegible].56415	177.99951	163.15637	123.33[illegible]4
25	34.35[illegible]99	13.5[illegible]4[illegible]8	399.34961	279.977[illegible]5	34.65524
26	244.89999	229.76244	223.37694	186.88631	189.11176
27	35.14[illegible]	38.36937	31.7[illegible]35[illegible]	22.33326	31.64961
28	61.5[illegible]	66.25[illegible]27	363.71973	3[illegible]4.82275	1[illegible]6.79[illegible]85

TABLE 6-V. CONTINUED

DATA CASE	EFFECTIVE THERMAL CONDUCTIVITY (KCAL/M-HR-K) X 100				
	EXPERIMENTAL	RUSSELL	BERNSTEIN	WOODSIDE	Equation 5-2
29	224.89999	23[illegible].26491	225.11832	186.88631	189.49945
30	217.39999	23[illegible].26491	225.11832	186.88631	189.49945
31	218.89999	23[illegible].26491	225.11832	186.88631	189.49945
32	218.89999	23[illegible].26491	225.11832	186.88631	189.49945
33	91.[illegible]	81.64751	245.34[illegible]85	219.56[illegible]84	9[illegible].58546
34	2[illegible]	12.[illegible]9319	223.66454	156.78442	25.147[illegible]8
35	15.6[illegible]	7.35292	222.26[illegible]59	147.33360	18.72270
36	94.39999	66.42775	161.[illegible]1998	138.11543	68.85420
37	94.39999	66.42775	161.[illegible]1988	138.11543	68.85420
38	73.29999	7[illegible].64775	66.64334	34.64285	67.55347
39	2[illegible]7.[illegible]	232.29[illegible]62	232.[illegible]8362	186.88631	191.[illegible]6364
40	212.89999	232.29[illegible]62	232.[illegible]8362	186.88631	191.[illegible]6364
41	22.29999	13.4473[illegible]	148.[illegible]6400	196.31741	22.73305
42	7[illegible].89999	66.78267	164.81833	138.11543	69.21696

TABLE 6-V. CONTINUED

DATA CASE	EFFECTIVE THERMAL CONDUCTIVITY (KCAL/M-HR-K) X 10				
	EXPERIMENTAL	RUSSELL	BERNSTEIN	WOODSIDE	Equation 5-2
43	18.5	11.65616	17.75331	15.11711	14.54553
44	61.5	67.25276	252.65945	252.57339	79.14689
45	85.	82.53639	257.51537	259.56084	91.57344
46	22.59999	12.23	236.73130	156.78442	25.47963
47	15.7	7.43699	234.64037	147.33360	18.98404
48	22.59999	13.52346	151.94125	196.31741	22.87326
49	16.29999	7.05777	178.43171	73.16948	13.46762
50	23.79999	14.07364	119.47327	89.59071	26.91824
51	23.39999	14.07364	119.47327	89.59071	26.91824
52	25.2	14.07364	119.47327	89.59071	26.91824
53	25.5	206.76819	222.99376	189.03682	172.39056
54	44.59999	13.91175	596.85693	354.25293	49.33975
55	163.79999	144.22986	198.10822	163.10674	126.37257
56	55.39999	59.01506	52.27281	29.39241	53.32962

TABLE 6-V. CONTINUED

DATA CASE	EXPERIMENTAL	EFFECTIVE THERMAL CONDUCTIVITY (KCAL/M-HR-K) X 10[illegible] RUSSELL	BERNSTEIN	WOODSIDE	Equation 5-2
57	36.[illegible]	14.[illegible]1232	475.92822	279.977[illegible]5	36.25958
58	17.[illegible]9999	12.25793	18.9[illegible]6	15.17392	1[illegible].99409
59	34.2[illegible]	38.4[illegible]248	32.76[illegible]91	22.13[illegible]75	31.61661
60	35.59999	38.4[illegible]248	32.76[illegible]91	22.13[illegible]75	31.61661
61	53.29999	59.26619	52.73[illegible]62	29.3[illegible]298	53.66516
62	55.[illegible]	59.26619	52.73[illegible]62	29.3[illegible]299	53.66516
63	71.39999	7[illegible].25677	66.3[illegible]217	34.26784	67.[illegible]7533
64	71.59999	73.81848	7[illegible].82[illegible]22	36.[illegible]4248	71.438[illegible]3
65	71.39999	73.81848	7[illegible].82[illegible]22	36.[illegible]4248	71.438[illegible]3
66	358.[illegible]	274.26123	564.41[illegible]16	449.33862	265.78369
67	7[illegible].7[illegible]	67.916[illegible]6	176.23[illegible]38	138.13518	7[illegible].36467
68	71.29999	68.[illegible]9929	178.12949	138.13518	7[illegible].55255
69	144.39999	146.[illegible]2[illegible]61	2[illegible]7.27832	163.1[illegible]674	127.853[illegible]1
7[illegible]	37.79999	14.15291	642.99976	354.25293	41.21[illegible]10

TABLE 6-V. CONTINUED

DATA CASE	EXPERIMENTAL	EFFECTIVE THERMAL CONDUCTIVITY (KCAL/M-HR-K) X 10[illegible] RUSSELL	BERNSTEIN	WOODSIDE	Equation 5-2
71	42.5[illegible]	14.97444	493.83391	281.79614	37.97573
72	29.7[illegible]	13.47485	162.49513	103.21956	22.81739
73	36.39999	14.17487	499.49072	279.97775	36.77461
74	17.[illegible]	12.[illegible]739	19.89945	15.10771	10.84967
75	231.79999	238.52497	252.97986	186.88631	195.99224
76	35.[illegible]	14.31813	673.76245	354.25293	41.81262
77	1[illegible].7[illegible]	86.[illegible]	313.12256	209.55384	95.44477
78	32.39999	12.77[illegible]26	282.4[illegible]649	156.78442	26.78778
79	17.79999	7.76587	281.[illegible]647[illegible]	147.33367	20.[illegible]1439
80	2[illegible].7[illegible]	15.94651	38.36993	27.51478	15.81591
81	154.89999	148.95731	221.95[illegible]5[illegible]	163.11674	139.28931
82	73.[illegible]9999	76.11324	73.59721	36.96539	74.[illegible]1647
83	24.59999	14.15834	182.95847	106.31741	24.[illegible]4616
84	51.7[illegible]	14.61435	727.59741	354.25293	42.89624

TABLE 6-V. CONTINUED

DATA	EFFECTIVE THERMAL CONDUCTIVITY (KCAL/M-HR-K) X 10[illegible]				
CASE	EXPERIMENTAL	RUSSELL	BERNSTEIN	WOODSIDE	Equation 5-2
85	32.29999	13.35525	567.47266	28[illegible].96582	36.51816
86	78.59999	15.68976	6396.20297	2443.18774	145.43269
87	36.79999	14.78839	758.36[illegible]11	354.25293	43.53212
88	47.5[illegible]	14.83294	766.[illegible]5[illegible]29	354.25293	43.69395
89	32.5[illegible]	13.55441	597.42969	28[illegible].96582	37.189[illegible]3
90	37.[illegible]	14.29[illegible]47	6[illegible]9.59668	284.8916[illegible]	38.55194
91	12[illegible].59999	1[illegible]1.81[illegible]12	632.41584	374.[illegible]2497	132.[illegible]7474
92	299.[illegible]	3[illegible]6.62998	691.65918	458.49316	293.43774
93	176.[illegible]	146.91357	644.728[illegible]3	397.89697	17[illegible].77969
94	39.59999	4[illegible].9[illegible]118	36.46587	22.46[illegible]28	33.77589
95	15.5[illegible]	13.21395	22.56546	15.26178	11.77[illegible]22
96	53.2[illegible]	18.49576	9[illegible]4.65259	416.99780	53.[illegible]3323
97	55.39999	18.49576	9[illegible]4.65259	416.99780	53.[illegible]3323
98	58.5[illegible]	18.49576	9[illegible]4.65259	416.99780	53.[illegible]3323

TABLE 6-V. CONTINUED

DATA CASE	EFFECTIVE THERMAL CONDUCTIVITY (KCAL/M-HR-K) X 10^0				
	EXPERIMENTAL	RUSSELL	BERNSTEIN	WOODSIDE	Equation 5-2
00	59.5	18.4957	914.65259	416.99781	53.03323
1	61.99999	18.49577	914.65259	416.99781	53.03323
1 1	23.39999	12.55259	22.05112	14.89195	11.25849
1 2	17.7	10.39619	17.81486	7.29878	8.38487
1 3	126.[illegible]	97.31678	642.89176	367.71773	127.99695
1 4	43.5	15.14726	819.88511	354.25293	44.84638
1 5	51.7	15.14726	819.88511	354.25293	44.84638
1 6	327.59985	193.41157	7209.17938	3185.28442	478.98633
1 7	47.29999	15.28532	842.95728	354.25293	45.35347
1 8	327.	295.49 97	732.27954	449.02368	286.15188
1 9	44.59999	15.33187	851.64722	354.25293	45.52478
11	26.29999	16.79286	45.65143	27.51196	16.65929
111	41.79999	15.36889	212.72542	104.51558	25.72656
112	318.	193.46802	2622.12915	1270.93921	320.17505

TABLE 6-V. CONTINUED

DATA CASE	EXPERIMENTAL	EFFECTIVE THERMAL CONDUCTIVITY (KCAL/M-HR-K) X 10^ RUSSELL	BERNSTEIN	WOODSIDE	Equation 5-2
113	342.[illegible]	193.46[illegible]2	2622.12915	127[illegible].93921	32[illegible].17585
114	58[illegible]	291.728[illegible]3	2646.18384	135[illegible].791[illegible]2	419.15674
115	595.[illegible]	291.728[illegible]3	2646.18384	135[illegible].791[illegible]2	419.15674
116	55[illegible]	33[illegible].22461	2655.72559	1376.92456	455.653[illegible]8
117	615.[illegible]	33[illegible].22461	2655.72559	1376.92456	455.653[illegible]8
118	63[illegible]	33[illegible].22461	2655.72559	1376.92456	455.653[illegible]8
119	629.89999	357.48779	7579.[illegible]8594	3446.13[illegible]13	7[illegible].10938
12[illegible]	597.[illegible]9985	357.48779	7579.[illegible]8594	3446.13[illegible]13	7[illegible].10938
121	323.[illegible]9985	194.11241	76[illegible]6.42578	3188.54565	489.92489
122	6[illegible]7.59985	3[illegible]5.4[illegible]4[illegible]5	7632.61719	3374.64258	637.78329
123	949.5[illegible]	3[illegible]6.33749	7698.75781	3374.64258	64[illegible].84639
124	634.3[illegible]	36[illegible].76929	7777.414[illegible]6	3446.13[illegible]13	7[illegible]7.43596
125	45.[illegible]	16.39252	73[illegible].88989	287.87524	43.33[illegible]41
126	55.79999	2[illegible].22[illegible]55	796.55566	318.[illegible]1571	5[illegible].62471

TABLE 6-V. CONTINUED

DATA CASE	EFFECTIVE THERMAL CONDUCTIVITY (KCAL/M-HR-K) X 10**				
	EXPERIMENTAL	RUSSELL	BERNSTEIN	WOODSIDE	Equation 5-2
127	35.[illegible]	1[illegible].82755	794.43[illegible]18	295.87476	35.92[illegible]18
128	32.39589	[illegible].13533	794.[illegible]578	289.82[illegible]04	32.87917
129	1[illegible]8.[illegible]	1[illegible]7.1[illegible]872	816.8[illegible]444	4[illegible]1.246[illegible]9	143.29[illegible]3
13[illegible]	4[illegible].7[illegible]	15.783[illegible]	687.55298	271.42334	41.29378
131	1[illegible]1.[illegible]	99.49986	6[illegible]1.65918	3[illegible]4.82275	123.51195
132	26.39999	17.82768	52.94521	27.52713	17.66586
133	35.59999	15.88542	61[illegible].78149	21[illegible].37628	38.53224
134	11[illegible].[illegible]	111.38135	631.55811	291.23584	132.75174
135	31.[illegible]999	43.4[illegible]933	42.[illegible]884 8	22.13[illegible]75	35.75244
136	13.8[illegible]	13.27157	3[illegible].95219	14.79249	12.118[illegible]6
137	13.9[illegible]	11.99142	2[illegible].65315	1[illegible].22888	1[illegible].22176
138	34.2	16.78769	936.32373	284.83989	47.14157
139	95.29999	11[illegible].33 95	552.11499	2[illegible].51463	122.22845
14	27.23[illegible]99	16.55669	535.47754	156.78442	36.2[illegible]37[illegible]

TABLE 6-V. CONTINUED

DATA	EFFECTIVE THERMAL CONDUCTIVITY (KCAL/M-HR-K) X 10[illegible]				
CASE	EXPERIMENTAL	RUSSELL	BERNSTEIN	WOODSIDE	Equation 5-2
141	26.2[illegible]	1[illegible].15738	534.41724	147.54761	27.48863
142	61.7[illegible]	111.41768	561.22998	2[illegible]9.51463	123.41405
143	27.[illegible]	16.73 3[illegible]	544.74463	156.78442	36.64189
144	25.20[illegible]	1[illegible].26433	543.69434	147.54761	27.82973
145	49.[illegible]	19.97[illegible]25	363.98169	1[illegible]4.51558	34.28934
146	11[illegible].79999	117.936.8	612.88218	2[illegible]9.51463	13[illegible].50111
147	27.5[illegible]	17.77635	597.25952	156.78442	39.28493
148	26.3[illegible]999	1[illegible].9.893	596.26392	147.54761	29.88408
149	35.2[illegible]	96.59285	6[illegible]9.37[illegible]85	2[illegible]2.[illegible]7487	113.45471
15	58.39999	19.2[illegible]45	1154.18774	284.8916[illegible]	54.95262
151	7[illegible].[illegible]	21.48741	425.83789	1[illegible]3.21956	38.16228
152	76.[illegible]	24.88144	491.67358	1[illegible]3.21956	44.83087
153	272.5[illegible]	222.[illegible]7977	1[illegible]5.69698	274.77612	197.92854
154	246.7[illegible]	193.4 34[illegible]	9[illegible].[illegible]9673	261.72681	175.95125

TABLE 6-V. CONTINUED

DATA	EFFECTIVE THERMAL CONDUCTIVITY (KCAL/M-HR-K) X 10^				
CASE	EXPERIMENTAL	RUSSELL	BERNSTEIN	WOODSIDE	Equation 5-2
155	172.7	127.73595	57.37563	226.[illegible]69	126.26[illegible]59
156	15.5	10.7538[illegible]	16.58563	8.49812	16.65686
157	6.[illegible]	6.[illegible]4223	3.7[illegible]421	4.[illegible]6507	4.99119
158	46.[illegible]	65.1[illegible]677	28.89368	149.47769	72.52258
159	.[illegible]1617	.[illegible]	[illegible]	[illegible]	[illegible]10854
160	.[illegible]8183	.[illegible]	.[illegible]	[illegible]	[illegible]47389
161	.[illegible]8599	.[illegible]	.[illegible]	[illegible]	[illegible]05266
162	.[illegible]511	.[illegible]	[illegible]	[illegible]	[illegible]04411
163	.[illegible]4140	.[illegible]	.[illegible]	[illegible]	[illegible]03523
164	.14.4[illegible]	.[illegible]	5.442[illegible]	[illegible]06	[illegible].17131
165	15.6[illegible]	9.5566[illegible]	4.[illegible]7974	51.[illegible]4829	19.17526
166	11.99[illegible]	5.8[illegible]77	2.47266	35.36[illegible]68	14.[illegible]3751
167	35.[illegible]999	9.93.2	4.56765	34.1132[illegible]	29.69441
168	13.[illegible]	61.17 55	28.32355	2[illegible].1810[illegible]	175.598[illegible]1

TABLE 6-V. CONTINUED

DATA CASE	EFFECTIVE THERMAL CONDUCTIVITY (KCAL/M-HR-K) X 10[illegible]				
	EXPERIMENTAL	RUSSELL	BERNSTEIN	WOODSIDE	Equation 5-2
169	81.5[illegible]	59.92964	29.22266	14[illegible].48701	81.95348
17[illegible]	29.79996	28.95757	23.13467	16.43518	25.94375
171	8[illegible]	59.32135	28.17171	124.2811[illegible]	73.52748
172	1.[illegible]24[illegible]	.57686	.31350	[illegible].95478	[illegible].90038

TABLE 6-VI COMPARISON OF SELECTED WEIGHTED OHM'S LAW MODELS

DATA	EFFECTIVE THERMAL CONDUCTIVITY (KCAL/M-HR-K) X 100				
CASE	EXPERIMENTAL	EQUATION 6-16	EQUATION 6-17	EQUATION 6-18	LICHTENKER
1	21.40000	18.26809	17.83623	20.88347	59.00730
2	22.40000	29.24886	27.50689	30.67581	206.36506
3	75.50000	93.65003	91.99059	107.58758	314.29590
4	246.00000	232.27410	241.86344	252.00923	448.36002
5	272.00000	252.41523	264.36643	272.00594	464.56322
6	1.01500	0.66111	0.67829	0.77075	2.26094
7	63.60000	67.37439	75.83169	72.35299	107.45101
8	25.00000	20.38193	21.50933	23.97093	69.58905
9	17.50000	18.96925	20.11296	22.43993	68.91376
10	63.50000	68.78856	79.14794	74.64435	110.90501
11	127.00000	132.90186	158.07349	135.94636	155.17180
12	19.00000	19.10030	20.38149	22.64880	69.81630
13	17.20000	19.16223	20.45052	22.72027	69.89026
14	30.40000	39.26373	40.27656	33.26539	408.71057

TABLE 6-VI. CONTINUED

DATA CASE	EFFECTIVE THERMAL CONDUCTIVITY (KCAL/M-HR-K) X 100				
	EXPERIMENTAL	EQUATION 6-16	EQUATION 6-17	EQUATION 6-18	LICHTENKER
15	118.00000	133.97484	161.11842	137.83734	157.10994
16	36.50000	30.15233	32.32900	35.23028	181.32992
17	23.85000	41.26558	43.65939	35.34461	439.41410
18	216.00000	235.94091	279.92522	258.02148	372.71004
19	26.80000	29.16821	31.40180	33.97493	180.36430
20	11.80000	9.33043	11.14216	10.15881	14.24098
21	25.30000	25.78623	31.08171	25.81932	26.30080
22	21.89000	30.10430	32.44405	35.05504	186.72458
23	34.10000	45.50702	48.14179	31.81032	554.84475
24	144.70000	165.32420	192.19444	186.89323	326.60048
25	34.40000	42.16504	45.30069	36.36206	456.89007
26	244.90000	238.63294	285.40920	261.98245	380.91525
27	35.14000	36.77445	44.65680	38.57387	45.87782
28	81.50000	152.07631	166.76405	181.94245	589.76435

TABLE 6-VI. CONTINUED

DATA CASE	EFFECTIVE THERMAL CONDUCTIVITY (KCAL/M-HR-K) X 100				
	EXPERIMENTAL	EQUATION 6-16	EQUATION 6-17	EQUATION 6-18	LICHTENKER
29	224.90000	242.84768	281.59641	262.72258	381.94926
30	217.40000	243.84827	280.68852	262.89725	381.94926
31	218.90000	246.64020	277.63526	263.15639	381.94926
32	218.90000	242.37366	282.55591	262.87220	381.94926
33	91.00000	129.46813	141.89911	152.53862	414.18049
34	20.00000	32.98888	35.18421	34.81148	275.61703
35	15.60000	23.07759	24.45273	20.01663	247.63950
36	94.40000	97.42206	107.97547	113.73614	276.64474
37	94.40000	97.42206	107.97547	113.73614	276.64474
38	73.30000	69.88891	82.74999	69.85542	70.84719
39	207.00000	257.25429	267.99600	265.11636	386.10388
40	212.90000	257.25429	267.99600	265.11636	386.10388
41	22.30000	33.17131	31.66056	36.50808	198.39167
42	70.90000	103.75744	102.17270	114.86331	278.87070

TABLE 6-VI. CONTINUED

DATA CASE	EFFECTIVE THERMAL CONDUCTIVITY (KCAL/M-HR-K) X 100				
	EXPERIMENTAL	EQUATION 6-16	EQUATION 6-17	EQUATION 6-18	LICHTENKER
43	18.50000	15.25530	15.40108	16.37681	30.95555
44	61.50000	114.81826	120.61396	133.78939	403.13726
45	89.00000	135.23735	137.66891	154.02988	421.27522
46	22.60000	35.39034	33.52736	35.34213	282.25755
47	15.70000	24.76877	23.33712	20.18501	254.04953
48	22.60000	33.36160	31.75435	36.66610	200.56221
49	16.30000	19.03756	18.10594	20.06048	134.88290
50	23.60000	31.17224	29.72937	35.05696	155.47729
51	23.40000	31.17224	29.72937	35.05696	155.47729
52	25.20900	31.17224	29.72937	35.05696	155.47729
53	205.50000	235.25228	242.43308	243.88625	373.68603
54	44.60000	50.14001	47.26900	32.66897	601.03429
55	163.80000	179.51593	182.11988	190.52539	338.40064
56	55.40000	60.50910	64.11924	58.35769	60.60930

TABLE 6-VI. CONTINUED

DATA CASE	EFFECTIVE THERMAL CONDUCTIVITY (KCAL/M-HR-K) X 100				
	EXPERIMENTAL	EQUATION 6-16	EQUATION 6-17	EQUATION 6-18	LICHTENKER
57	36.00000	46.42386	44.45473	37.69998	496.56298
58	17.10000	15.68087	15.89289	16.80524	31.74458
59	34.20000	38.77132	41.26020	38.53062	46.34372
60	35.60000	38.77132	41.26020	38.53062	46.34372
61	53.30000	60.48748	64.27804	58.47467	60.80183
62	55.00000	60.48748	64.27804	58.47467	60.80183
63	71.40000	73.26926	76.86735	70.64043	70.49702
64	71.60000	77.41596	80.76813	74.73293	73.88966
65	71.40000	77.41596	80.76813	74.73293	73.88966
66	358.00000	388.95095	388.27393	425.23792	934.81427
67	70.70000	104.28636	103.06313	115.53438	285.66888
68	71.30000	104.28372	103.25560	115.60843	286.80489
69	144.40000	179.31822	183.37059	190.95476	343.90477
70	37.80000	50.29759	48.41836	33.46267	625.19866

TABLE I-VI. CONTINUED

DATA CASE	EXPERIMENTAL	EFFECTIVE THERMAL CONDUCTIVITY (KCAL/M-HR-K) X 100 EQUATION 6-16	EQUATION 6-17	EQUATION 6-18	LICHTENKER
71	42.50000	48.44803	46.88942	40.97817	512.13830
72	29.70000	32.53211	31.63679	36.06000	203.35508
73	36.40000	46.52268	45.14170	38.15535	509.27668
74	17.10000	15.29368	15.61938	16.48975	32.23886
75	230.80000	257.46974	270.49073	266.56968	398.74598
76	35.10000	50.43168	49.22279	34.06481	641.71144
77	100.70000	138.76442	138.65102	156.33456	448.62784
78	22.40000	35.63231	35.29717	36.38001	308.21786
79	17.80000	24.97200	24.71508	21.10048	279.20431
80	20.70000	22.67456	22.93893	25.06121	59.33500
81	154.90000	179.21011	185.36218	191.69065	352.83431
82	73.10000	78.77325	82.64781	76.88286	76.15786
83	24.60000	33.57004	33.32753	37.49713	218.55021
84	51.70000	50.72692	50.70768	35.26633	671.39497

TABLE 5-VI. CONTINUED

DATA CASE	EXPERIMENTAL	EFFECTIVE THERMAL CONDUCTIVITY (KCAL/M-HR-K) X 100 EQUATION 6-16	EQUATION 6-17	EQUATION 6-18	LICHTENKER
85	32.30000	44.22812	44.29449	34.89893	539.94730
86	78.60000	101.09844	107.61176	25.89379	3839.37706
87	36.80000	49.60256	53.10404	36.21983	688.81107
88	47.50000	51.67617	51.35218	36.27270	693.21712
89	32.50000	47.99164	42.17589	35.85984	557.12542
90	37.00000	56.05673	39.32221	39.14365	570.58757
91	120.60000	227.28975	157.62872	228.19567	825.91706
92	298.00000	493.66227	349.73652	471.72746	1026.50052
93	176.00000	294.26019	204.87509	292.15431	885.54253
94	39.60000	47.86938	35.61040	41.92740	48.82971
95	15.50000	19.33748	13.85331	18.10140	34.11394
96	53.20000	75.55705	52.95738	47.29458	825.22139
97	55.40000	75.55705	52.95738	47.29458	825.22139
98	58.50000	75.55705	52.95738	47.29458	825.22139

TABLE 6-VI. CONTINUED

DATA CASE	EFFECTIVE THERMAL CONDUCTIVITY (KCAL/M-HR-K) X 100				
	EXPERIMENTAL	EQUATION 6-16	EQUATION 6-17	EQUATION 6-18	LICHTENKER
99	59.50000	75.55705	52.95738	47.29458	825.22139
100	61.10000	75.55705	52.95738	47.29458	825.22139
101	23.40000	18.55058	13.27307	17.40321	33.29460
102	10.20000	12.71516	9.34998	11.38894	15.90991
103	126.00000	194.07769	172.08793	212.10419	822.21901
104	43.50000	55.37533	50.30533	37.92990	724.64669
105	51.70000	55.37533	50.30533	37.92990	724.64669
106	327.60000	621.64499	568.03096	542.55222	6773.54644
107	40.30000	55.61382	51.00951	38.71766	738.43325
108	327.00000	420.38800	382.06988	440.48026	1038.46366
109	44.60000	55.69790	51.24874	38.99000	743.07128
110	26.30000	24.54554	22.27846	25.86402	63.90143
111	41.80000	37.21594	33.64014	40.32416	236.51583
112	318.00000	462.40538	419.48245	502.89521	2909.23004

TABLE 6-VI. CONTINUED

DATA CASE	EXPERIMENTAL	EFFECTIVE THERMAL CONDUCTIVITY (KCAL/M-HR-K) X 100 EQUATION 6-16	EQUATION 6-17	EQUATION 6-18	LICHTENEKER
113	342.00000	462.40538	419.48245	502.89521	2909.23004
114	580.00000	619.09245	558.39753	680.84295	3128.44173
115	595.00000	619.09245	558.39753	680.84295	3128.44173
116	550.00000	675.81458	608.94645	743.07338	3197.92937
117	615.00000	675.81458	608.94645	743.07338	3197.92937
118	630.00000	675.81458	608.94645	743.07338	3197.92937
119	629.90000	969.77173	889.60602	1011.09310	7789.99876
120	597.10000	969.77173	889.60602	1011.09310	7789.99876
121	323.10000	627.66939	583.42334	558.45987	7020.76531
122	607.60000	866.10024	799.05327	880.03270	7612.86973
123	549.50000	867.41892	802.21736	882.93277	7655.19008
124	634.40000	974.09676	899.78815	1020.03510	7917.56551
125	45.00000	54.11049	51.20005	47.10582	653.27948
126	55.80000	64.34005	60.76265	58.97540	727.19873

TABLE 6-VI. CONTINUED

DATA CASE	EFFECTIVE THERMAL CONDUCTIVITY (KCAL/M-HR-K) X 1CC				
	EXPERIMENTAL	EQUATION 6-16	EQUATION 6-17	EQUATION 6-18	LICHTENKER
127	35.CCCCC	41.54685	39.44183	24.98846	651.05339
128	32.40000	36.96911	35.08021	17.48121	631.57698
129	188.CCCCC	210.03414	191.43568	231.29989	968.31840
130	45.70000	51.73979	48.94081	45.52054	616.59663
131	101.CCCCC	181.62449	165.29476	198.75663	737.09537
132	26.40000	25.17274	23.15149	26.44550	68.74687
133	35.60000	48.45411	47.33002	47.83672	548.95760
134	110.CCCCC	191.22090	176.21498	207.79861	749.89525
135	31.05000	43.00424	39.24361	40.23275	52.95140
136	13.80000	16.63020	15.22358	16.81157	39.01617
137	13.80000	13.63439	12.47190	13.43961	26.49543
138	34.20000	55.90693	57.34914	54.08713	784.56546
139	95.40000	173.82155	156.94868	178.85411	618.86684
140	27.30000	46.56551	47.08640	51.44201	480.59426

TABLE 6VI. CONTINUED

DATA CASE	EXPERIMENTAL	EFFECTIVE THERMAL CONDUCTIVITY (KCAL/M-HR-K) X 100 EQUATION 6-16	EQUATION 6-17	EQUATION 6-18	LICHTENER
141	26.20000	33.16844	34.68392	35.04215	449.82873
142	61.70000	175.90408	158.08702	179.92768	625.75569
143	27.00000	47.21751	47.79587	52.29997	487.91652
144	25.20000	33.64918	35.27914	35.85971	457.15207
145	49.00000	47.89173	45.75384	52.19388	347.16633
146	110.80000	190.25043	164.78573	186.60326	665.64385
147	27.50000	51.67708	52.16730	57.69110	530.74884
148	26.40000	36.93366	38.97973	41.00819	500.11590
149	85.20000	165.94268	145.43751	165.60189	649.41849
150	58.40000	66.74942	71.02539	73.34132	956.51049
151	70.00000	58.07241	51.68107	59.01005	398.32499
152	76.00000	81.74598	61.62668	70.87885	459.77048
153	272.50000	262.01689	267.10996	280.01328	480.93223
154	248.70000	234.70536	237.01759	252.82006	457.18135

TABLE 6-VI. CONTINUED

DATA CASE	EFFECTIVE THERMAL CONDUCTIVITY (KCAL/M-HR-K) X 100				
	EXPERIMENTAL	EQUATION 6-16	EQUATION 6-17	EQUATION 6-18	LICHTENKER
155	172.70000	171.02733	168.08607	188.14054	396.68016
156	16.50000	18.09448	17.80534	16.71334	16.74108
157	6.90000	6.07512	6.30359	6.00097	7.36559
158	46.00000	97.87946	91.63376	109.30790	277.44236
159	0.10610	0.08101	0.08228	0.03170	0.03203
160	0.08183	0.06274	0.04555	0.04203	0.00773
161	0.05598	0.06051	0.03174	0.08234	0.00207
162	0.05110	0.02694	0.05470	0.04489	0.00105
163	0.04140	0.03160	0.02755	0.02220	0.00046
164	0.14040	0.10830	0.13498	0.17819	0.15300
165	15.60000	23.09515	20.32662	23.63961	156.30005
166	11.95000	15.94027	13.75262	13.68524	134.58651
167	39.90000	29.98027	22.82285	16.35257	253.52111
168	130.00000	181.94301	137.55627	110.98691	1428.90519

TABLE 6-VI. CONTINUED

DATA CASE	EFFECTIVE THERMAL CONDUCTIVITY (KCAL/M-HR-K) X 100				
	EXPERIMENTAL	EQUATION 6-16	EQUATION 6-17	EQUATION 6-18	LICHTENKER
169	81.50000	103.96177	85.07619	116.02943	349.59322
170	29.80000	29.54646	25.51770	28.03818	29.64116
171	60.00000	94.51779	78.11311	104.96805	275.08724
172	1.02400	1.08128	0.97622	0.97847	2.61458

TABLE 6-VII. DIMENSIONLESS VARIANCE OF CALCULATED THERMAL CONDUCTIVITY BASED ON SELECTED MODELS

A.	Flux Law Models	
	1. Maxwell	42.9
	2. Lord Rayleigh	32.1
	3. Meredith and Tobias	29.8
	4. Bruggemen	17.8
B.	Uniform Heat Flux Models	
	1. son Frey	50.2
	2. Woodside and Messmer	19.2
	3. Kanager	13.1
	4. Gorring and Churchill	14.8
	5. Willhite, Kunii and Smith	13.3
	6. Schumann and Voss	20.1
	7. Preston	16.4
	8. Wilhelm et al	13.8
	9. Krupiczka	13.1
C.	Parallel Isotherm Models	
	1. Russell	35.2
	2. Bernstein	87.4
	3. Woodside	70.7
	4. Equation 5-2	7.0
D.	Weighted Ohm's Law Models	
	1. Equation 6-16	10.6
	2. Equation 6-17	9.7
	3. Equation 6-18	13.0
	4. Lichtenecker 3-D	98.4
	5. Lichtenecker 2-D	56.8

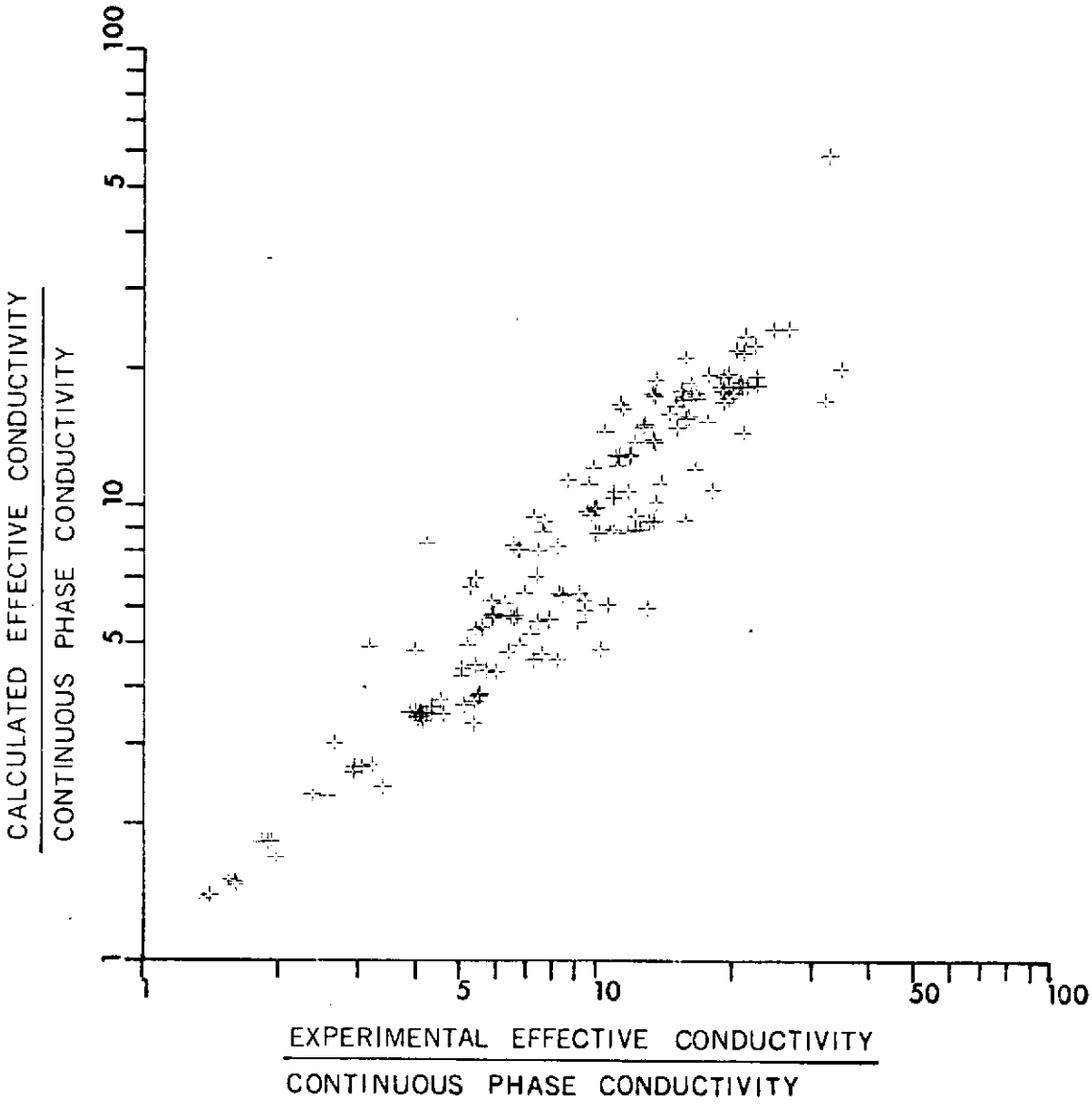

FIGURE 6-7. COMPARISON OF EXPERIMENTAL RESULTS WITH CALCULATED CONDUCTIVITY FOR EQUATION 5-2.

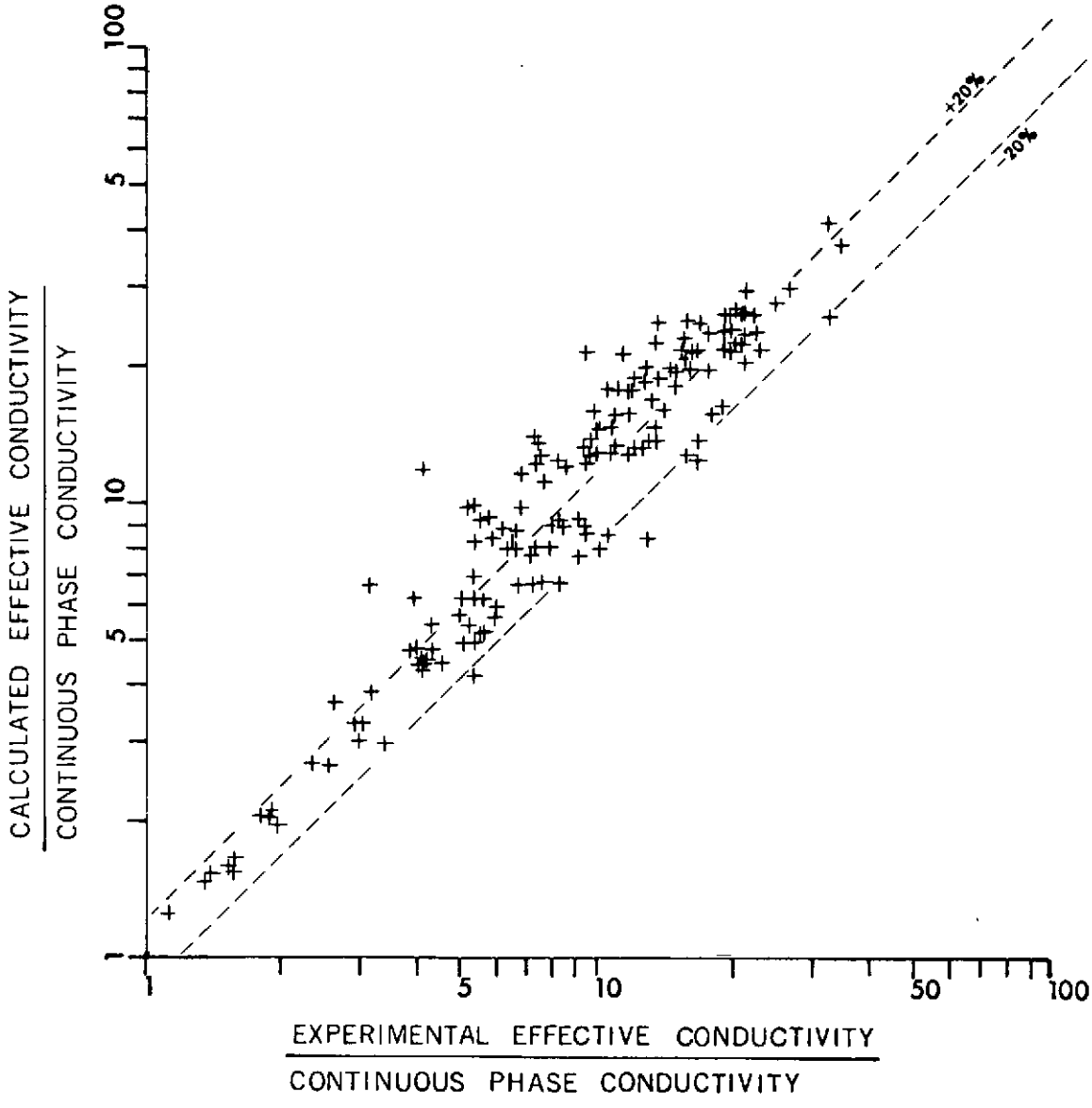

FIGURE 6-8. COMPARISON OF EXPERIMENTAL RESULTS WITH CALCULATED CONDUCTIVITY FOR EQUATION 6-16.

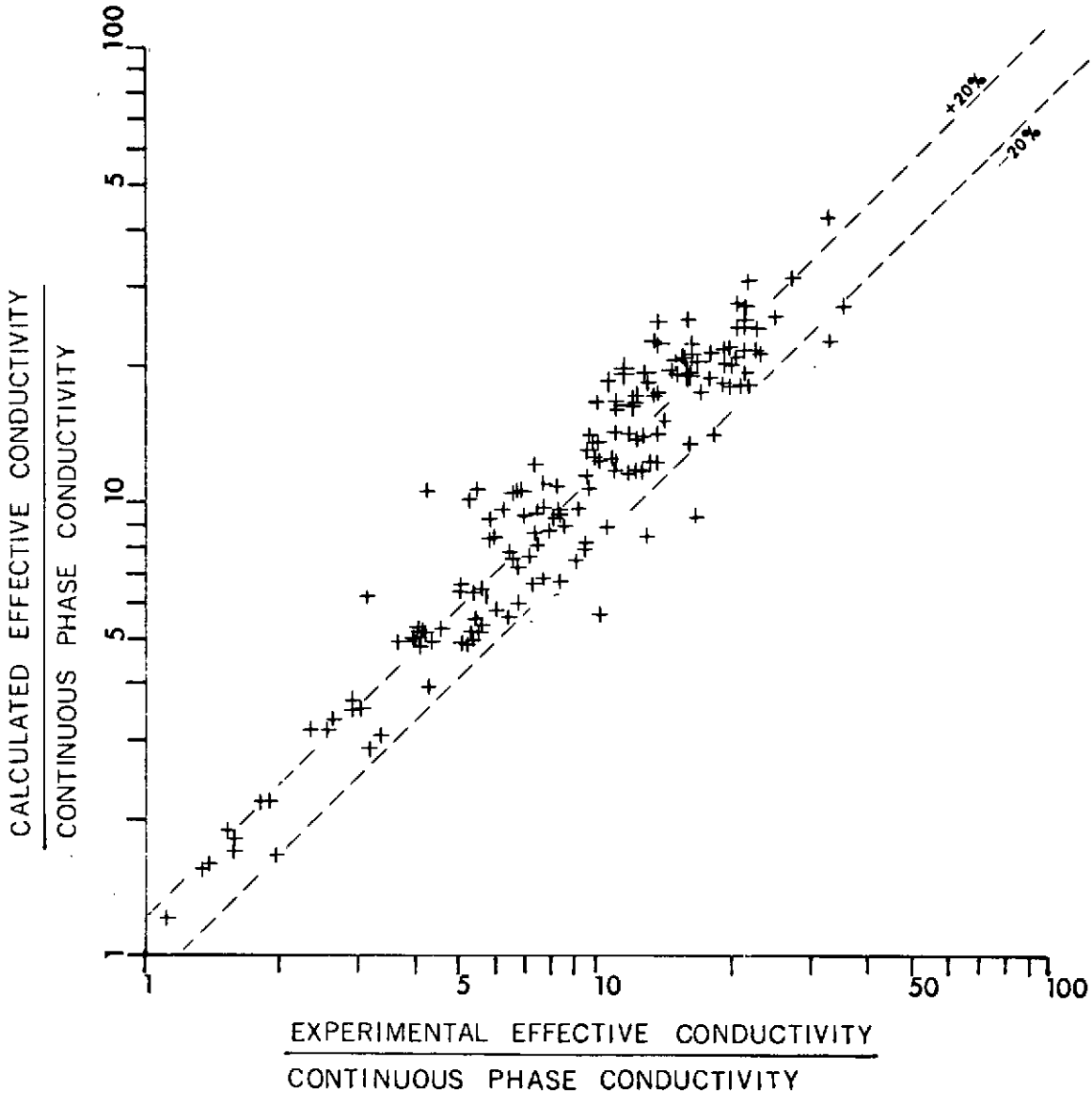

FIGURE 6-9. COMPARISON OF EXPERIMENTAL RESULTS WITH CALCULATED CONDUCTIVITY FOR EQUATION 6-17.

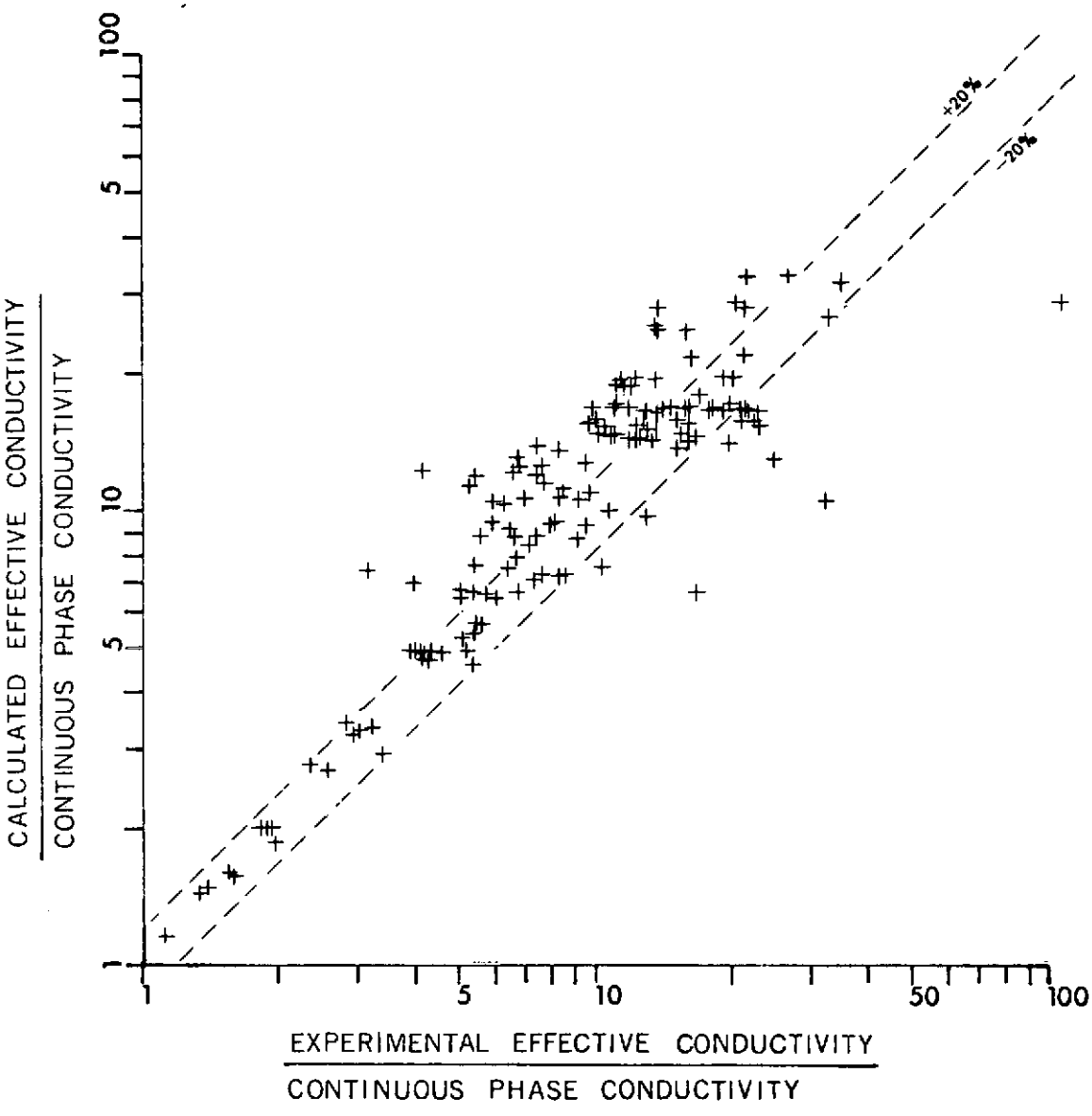

FIGURE 6-10. COMPARISON OF EXPERIMENTAL RESULTS WITH CALCULATED CONDUCTIVITY FOR EQUATION 6-18.

VII. MODEL BASED ON NON-LINEAR HEAT FLOW

Consider a representative unit cube of the granular material, subdivided by a three-dimensional grid into N^3 cubicles, as indicated in Figure (7-1a). Assume that the two faces normal to the z-direction are isothermal, and the other four faces are insulated, so that application of a constant temperature potential gives rise to a net conduction heat transfer in the z-direction. In order to determine the effective thermal conductivity of such a system, without any additional simplifying assumptions regarding the flow of heat, it is first necessary to find the temperature distribution in the unit cube. Once this has been accomplished, the heat flow rate in the z-direction can be determined, and an effective thermal conductivity can be assigned to the material by the Fourier-Biot law.

The solution proposed in this study consists of the following steps:

1. System synthesis;
2. Determination of the average working thermal conductivities;
3. Computation of the actual temperature distribution;
4. Determination of the heat flows and the effective thermal conductivity.

The above four steps will now be discussed in detail.

System Synthesis

A representative unit cube of a granular material is shown in Figure (7-1a) and in Figure (7-1b). The distribution of the continuous and discontinuous phases is modified is such a manner that each cubicle is occupied either by the continuous or the discontinuous phase. Effectively, any irregular shaped particle can be built to any degree of approximation by arranging a number of cubicles according to a predetermined format, as indicated in [20]. These particles can then be placed in the unit cube according to a specified statistical distribution. This way, the basic assumption of a regularly repeated elementary cell of spatial configuration, common to most previous models, is avoided.

The method of placing continuous phase cubicles in the unit cube, is based on the assumption that the granular material can be considered as a random mixture of the two phases. Then, in order to place a continuous phase cubicle in the system, three random numbers are generated by the 0-1.0 constant density function random number generator, and these random numbers are associated with three coordinates, defining the position of a cubicle in the system. If the cubicle thus defined, is already occupied by the continuous phase, another triplet of random numbers is generated. This process continues until the total number of continuous phase cubicles is equal to the continuous phase solid fraction of the granular system times the total number of cubicles in the unit cube. The geometry

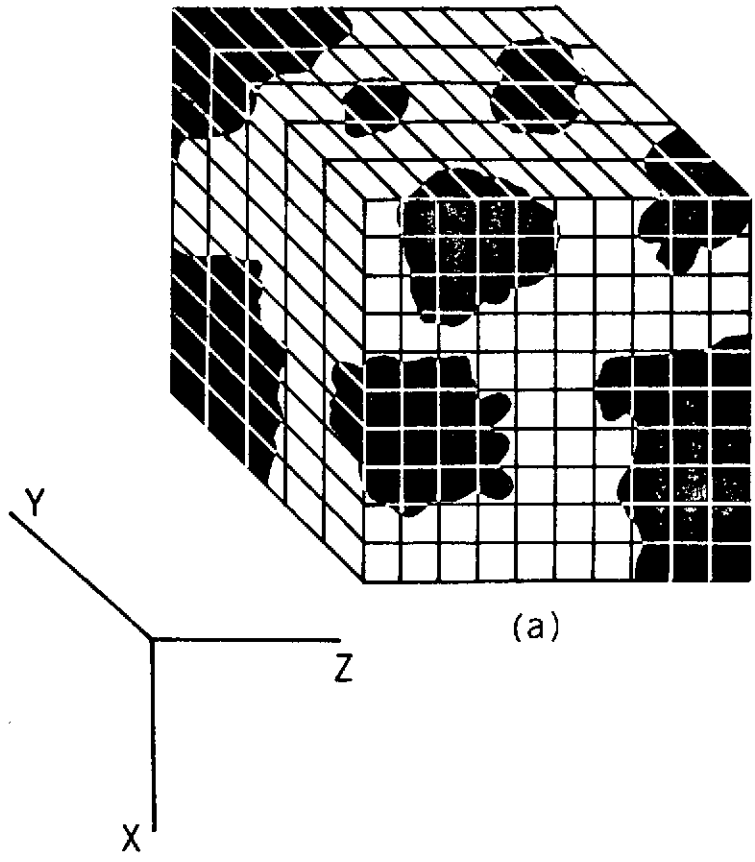

(a)

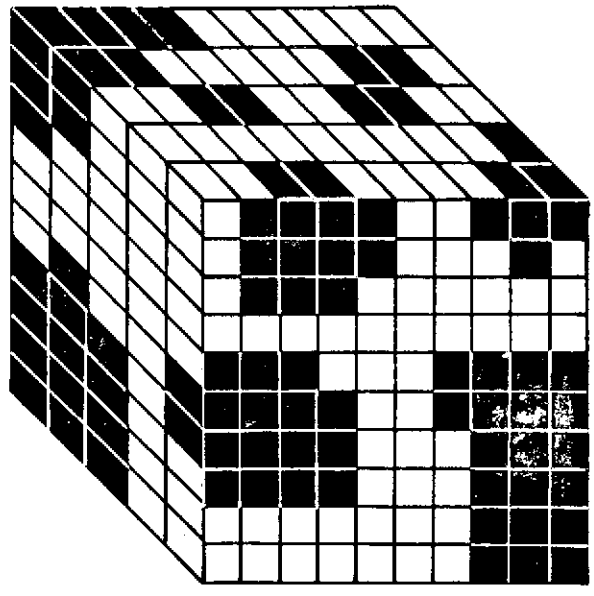

(b)

FIGURE 7-1. EQUVALENT GEOMETRIES FOR UNIT CUBE.

of the system thus defined, represents a random mixture of two phases, and, effectively, in this system the probability that a particular cubicle is occupied by the continuous phase is equal to the volume fraction of the continuous phase.

Determination of the Average Working Thermal Conductivities

As illustrated by Trezek and Witwer [72], there are a number of choices in selecting the average working conductivities between adjacent cubicles, but the series model yields the most accurate results on each side of the interface. According to [72] then,

$$k_{ij} = k_i k_j / (0.5\ k_i + 0.5\ k_j) \tag{7-1}$$

where k_{ij} is the average working thermal conductivity between the adjacent cubicles i and j. k_i and k_j are the conductivities of the cubicles. A scanning process can now be defined such that looking at a particular cubicle the composition of its neighbors can be determined, and consequently it is possible to assign an average working thermal conductivity between any two adjacent cubicles.

At this point, it should be noted that the working thermal conductivities thus defined, require that the adjacent cubicles are in perfect contact with each other. However, physical granular systems contain randomly distributed and oriented contact areas between neighboring particles that provide additional resistance to the heat flow from one particle to the other. Further, when the voids between particles are evacuated, these contact areas provide the only path

of heat transfer, other than radiation heat transfer, from one particle to the other. Consequently, as indicated in [34], failure to account for these contact areas induces large errors in the calculation of the effective thermal conductivity of granular materials, especially when the ratio of the constituent conductivities is high.

In order to incorporate the effect that these contact areas have on the flow of heat in the physical model presented, it is necessary to associate a contact conductivity with each contact area, and to know the number of contact points in the unit cube. As indicated in the Literature Review, a number of expressions have been developed relating the contact resistance to the contact area between two particles. In the calculations, the expressions given in reference [34] have been used because they are in good agreement with Kanager's [73] analytical development. The number of contact points in the cube, N_c, can be determined, as indicated in the Ohm's Law Models section, as a function of the unit cube size, a characteristic particle size obtained from sieve analysis of the granular material, and the coordination number.

To complete the determination of the working thermal conductivities, it is necessary to randomly distribute N_c contact conductivities between adjacent cubicles occupied by the discontinuous phase. Again a triplet of random numbers is generated, and is associated with three coordinates, defining the position of a cubicle in the system. If the cubicle is occupied by the discontinuous phase, the

composition of its neighbors is determined, and the working conductivity between the first pair of solid cubicles is replaced by k_{cr}. The process is repeated until N_c such replacements have been executed. A point of importance is that since contact points at the boundaries of the unit cube should also be included, it is necessary to determine the composition of the cubicles surrounding the six faces of the unit cube.

Determination of the Actual Temperature Distribution

When a steady-state temperature field is desired for a region in which the thermal conductivity is dependent upon the spatial location, a solution must be obtained for the following equation

$$\nabla(k\nabla T) = 0 \tag{7-2}$$

When each cubicle is considered separately, the condition which must be met is the Laplace equation

$$\frac{\partial^2 T}{\partial x^2} + \frac{\partial^2 T}{\partial y^2} + \frac{\partial^2 T}{\partial z^2} = 0 \tag{7-3}$$

Also, each temperature in the unit cube must be bounded by the temperatures applied at the two opposite faces of the unit cube. Laplace's equation requires that the temperature at every cubicle remain constant. That is the net heat accumulation in each cubicle should be equal to zero. In order to write a conduction heat balance for each cubicle, it is first assumed that the cubicle is

isothermal and is lumped into a single node, and all the nodes are connected by the average working thermal conductivities described in the previous paragraph. The basic system unit around which each heat balance is written is shown in Figure (7-2). Under the assumption that heat flow to the center cube is positive, the resulting heat balance is

$$\sum_{i=1}^{6} k_{i7} (T_i - T_7) A/L = R_7 \tag{7-4}$$

Application of Equation (7-4) to all cubicles results in $N^3 = m$ simultaneous, linear equations. The coefficients of this system of linear equations are functions of the average working conductivities, and the unknowns are the node temperatures. As indicated in [74] one of the most efficient methods of solving such a system of equations is a successive overrelaxation technique in conjunction with an iterative scheme. The steps involved in this method are the following.

Consider the system of linear equations

$$\begin{aligned}
&b_{11} x_1 + b_{12} x_2 + \cdots\cdots\cdots + b_{1m} x_m = u_1 \\
&b_{21} x_1 + b_{22} x_2 + \cdots\cdots\cdots + b_{2m} x_m = u_2 \\
&\quad\vdots \qquad\qquad\qquad\qquad\qquad\quad \vdots \\
&b_{m1} x_1 + b_{m2} x_2 + \cdots\cdots\cdots + b_{mm} x_m = u_m
\end{aligned} \tag{7-5}$$

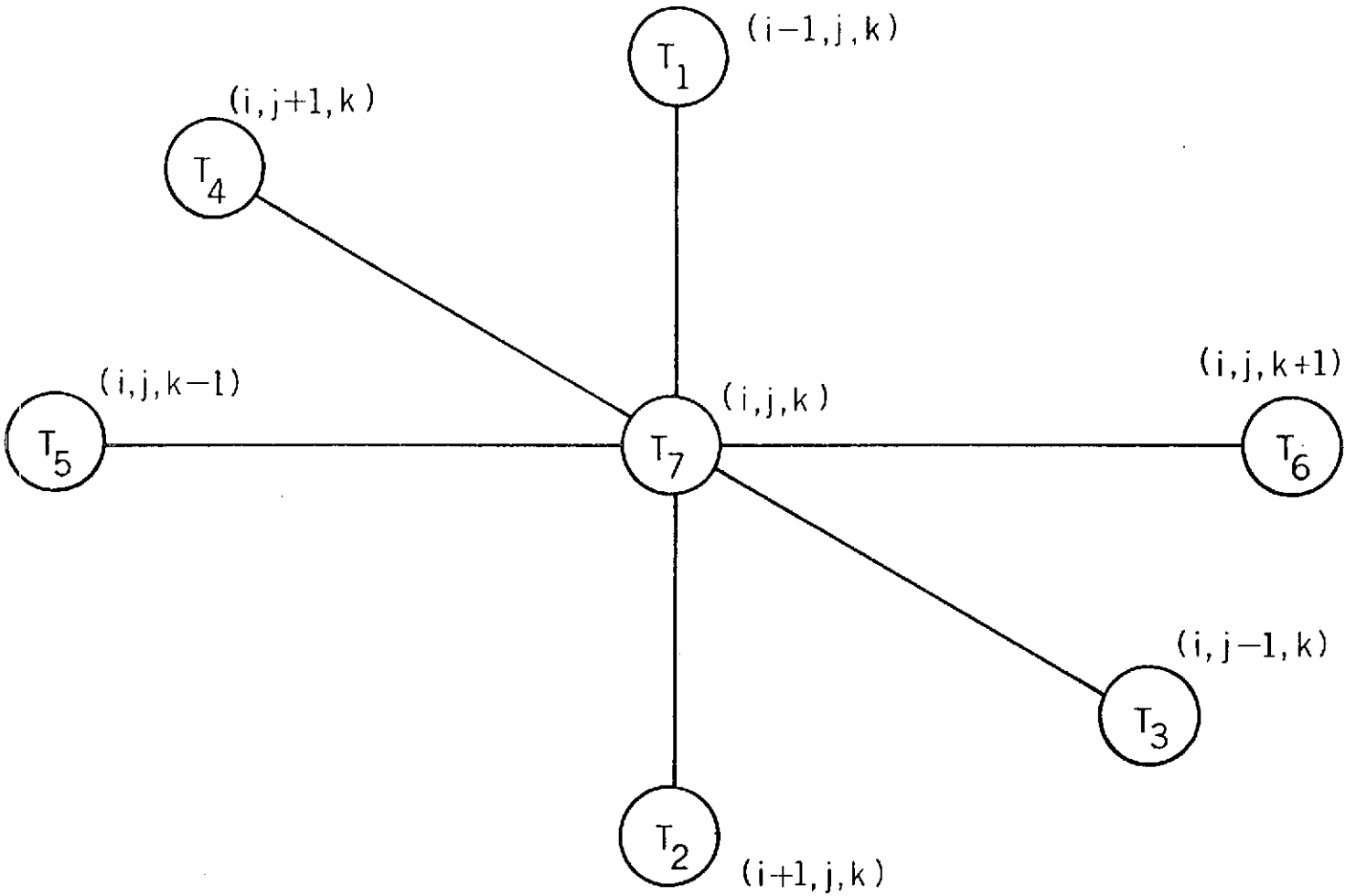

FIGURE 7-2. HEAT BALANCE BASIC NODAL ORIENTATION

or

$$[B]\,\bar{x} = \bar{u} \tag{7-6}$$

First define the ith component of an auxilliary vector iterate $\bar{x}'^{n}$ by

$$b_{ii}\, x'_i{}^{n+1} = -\sum_{j=1}^{i-1} b_{ij}\, x_j^{n+1} - \sum_{j=i+1}^{m} b_{ij}\, x_j^{n} + u_i \tag{7-7}$$

Then, the (n+1) approximation of the ith component of the solution vector for the successive overrelaxation method is defined from

$$x_i^{n+1} = x_i^{n} + w\,[x'_i{}^{n+1} - x_i^{n}] = (1-w)\, x_i^{n} + w x'_i{}^{n+1} \tag{7-8}$$

The quantity w is called the overrelaxation factor, and $1 < w < 2$. It is seen from Equation (7-8) that x_i^{n+1} is a weighted mean of x_i^{n} and $x'_i{}^{n+1}$, the weights depending only on w. Combination of Equations (7-7) and (7-8) into a single equation yields

$$b_{ii}\, x_i^{n+1} = b_{ii}\, x_i^{n} + w\left[-\sum_{j=1}^{i-1} b_{ij}\, x_j^{n+1} - \sum_{j+1}^{m} b_{ij}\, x_j^{n} + u_i - b_{ii}\, x_i^{n}\right] \tag{7-9}$$

Then, from Equation (7-9) the (n+1) approximation of the ith component of the solution vector is

$$x_i^{n+1} = x_i^{n} + \frac{w}{b_{ii}}\left[-\sum_{j=1}^{i-1} b_{ij}\, x_j^{n+1} - \sum_{j+1}^{m} b_{ij}\, x_j^{n} + u_i - b_{ii}\, x_i^{n}\right] \tag{7-10}$$

It is seen that in the iterations, the newly-computed components of the $\bar{x}$ vector are always used in the righthand sides as soon as they are obtained.

Comparison of Equation (7-10) with the heat balance equation for each cubicle indicates that the term in brackets is equal to the negative of the thermal residue. Also, b_{ii} is the negative of the sum of the average working conductivities between the node at which heat balance is executed and the surrounding nodes. As a result, for the particular problem in question, Equation (7-10) takes the form

$$T^{n+1} = T^{n} + \frac{w}{\sum_{i=1}^{i=6} k_{i7}} \left[\sum_{i=1}^{i=6} k_{i7} \, (T_i - T_7) \right] \qquad (7\text{-}11)$$

Equation (7-11) gives a better estimate of the temperature at each node in terms of previous estimates. It can be seen that a positive thermal residue, resulting from T_7 being too low, will increase the new value of T_7.

Exactly the same iterative scheme can be obtained by writing the finite-difference representation of Equation (7-2), and treating the conductivity variation according to Equation (7-1).

The steady-state temperature field in the unit cube can now be obtained, provided that an initial temperature field is defined. A reasonable selection for the initial temperature field is to assume

that planes of nodes normal to the direction of the heat flow are isothermal, and the temperature of each plane is proportional to its distance from the surface of the cube. Also, the imposed boundary conditions dictate that the temperatures of the nodes on the front and back faces, which are normal to the direction of the heat flow, remain constant, and the heat flow away from nodes associated with the other four faces is zero. Application of Equation (7-11) coupled with the assumed initial temperature distribution and the boundary conditions, gives the actual temperature distribution in the unit cube. In the calculations, the iteration process cut-off point is when the sum of the absolute values of the thermal residues becomes less than or equal to 1.0.

Determination of the Heat Flows and the Effective Thermal Conductivity

After the steady-state temperature field has been determined, three orthogonal heat flux vectors can be defined at each node. However, since the net heat flow is in the z-direction only, this is the rate of heat flow on which the effective thermal conductivity should be based. To find the rate of heat flow Q in the z-direction, the heat flows in the z-direction between all nodes in any two successive planes are summed. This process is repeated for all successive planes, and Q is the average value of these sums. The effective thermal conductivity of the granular material,

as defined by the Fourier-Biot law, is given by:

$$k_e = \frac{Q}{N\Delta T} \qquad (7\text{-}12)$$

where ΔT is the difference between the temperatures of the back and front faces of the unit cube that are normal to the net heat flow direction.

The method of solution described in the preceding paragraphs can be applied to any granular system for which the fluid in the voids is at atmospheric pressure. In this case, the solid particles and the voids are approximated by the arrangement of a number of cubicles according to the statistical distribution chosen; heat balances at each node should give the temperature distribution since both phases are in the domain of a continuum. However, when the medium in the voids is a rarefied gas, which is the case for both lunar and martian environments, a dominant mode of heat transfer in the voids may be radiation between particle surfaces [1], as shown in Fig. (7-3). Also, when the molecular mean free path is greater than the void diameter, conduction in the voids takes place by direct exchange of energy between particle surfaces. Consequently, for extremely rarefied gases it is not possible to determine a working effective conductivity between nodes that belong to gaseous cubicles located in the same void. However, if the chosen grid size is coarse enough so that the volume of each cubicle is equal to the mean void equivalent hole volume, then each void is approximated by a cubicle and the working effective con-

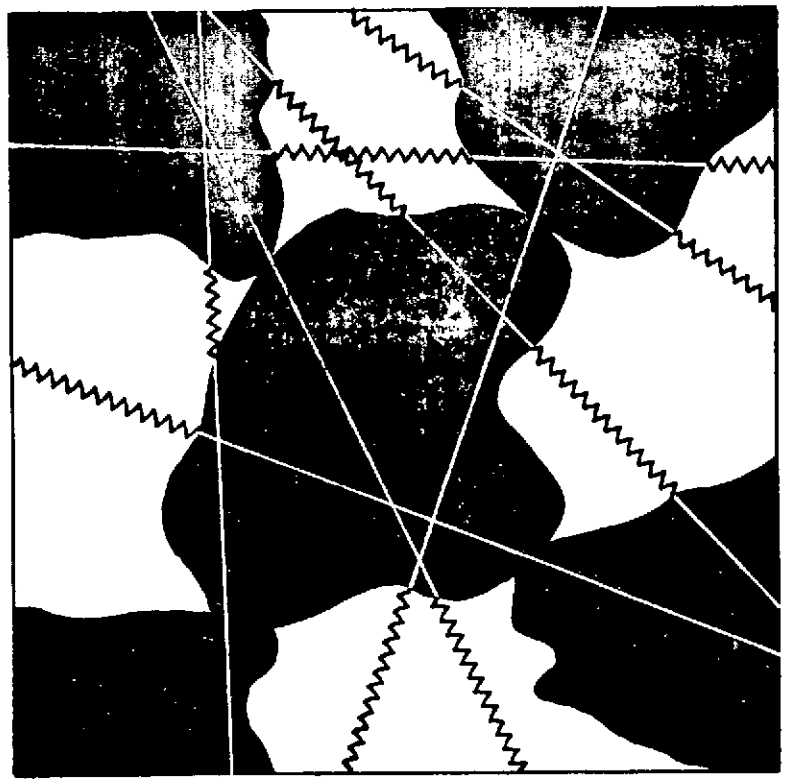

FIGURE 7-3. HEAT CONDUCTED THROUGH GRAINS AND TRANSFERRED BY CONDUCTION AND RADIATION AT BOUNDRIES.

ductivity of each cubicle occupied by the continuous phase can be approximated by the effective radiative and gaseous conductivities discussed in the literature survey.

Comparison of Calculated Effective Conductivity to Experimental Data.

The effective thermal conductivity has been calculated and compared to experimentally determined values for a number of granular materials at atmospheric pressures, as indicated on Table 7-I. The range of porosities and constituent conductivities is 0.31 - 0.59 and 1.67 - 2444.4 respectively. For all these cases the conductivities of the constituents were assumed to be constant, independent of temperature distribution in the unit cube. The mechanical properties of the solid phase, required for the calculation of the contact resistance, are shown on Table 7-IX.

In addition to the model presented in this study, the effective conductivity predicted by a number of selected models was also determined, and the calculated values are presented in Tables 7-II and 7-III. The column "Case" in these Tables refers to the granular system described in Table 7-I. It should be noted that a number of these models, such as the Maxwell, Rayleigh and Jefferson models, have been extended to porosities beyond the range for which they are theoretically applicable.

The percentage error between experimental thermal conductivities and those predicted by all selected models is shown on Tables 7-IV and 7-V. Table 7-VI summarizes the mean error, mean bias and the variance of percentage error between the experimental and model

predicted thermal conductivities. From this Table it is seen that the model of this study predicts the experimental thermal conductivities with a mean of 15.8%, an error variance of 1.63, and is biased below the experimental values by 5.8%. This is slightly better than the Krupiczka model, for which a mean error of 17.5% has been calculated. The mean error of all other models is in the range of 30.1% - 42.2%. A graphical representation of the effective thermal conductivity predicted by the model described in this study is shown in Figure (7-4).

It is interesting to observe the performance of some of the models as compared to the assumptions introduced in their developments. It would be expected that models utilizing the parallel isotherm assumption would overpredict the effective thermal conductivity. Jefferson's model (6 in Table 7-VI) generally conforms to this expectation. However Russel's model (5 in Table 7-VI) predicts lower conductivities than the experimental ones, and the discrepancy increases with the ratio of constituent conductivities. The most probably explanation for this behavior is that the effects of the assumed simplified geometry, and the absence of contact areas between particles, dominate over the assumption of infinite conductivity in the lateral-to-the-heat-flow direction, thus rendering the calculated conductivities low.

On the other hand, it would be expected that models utilizing the uniform heat flux assumption would predict low values for the effective thermal conductivity. This is the case for Lichtenecker's

model (8 in Table 7-VI) which, as expected, predicts lower values than Russell's model. However, the Krupiczka and Woodside and Messmer models (7 and 9 in Table 7-VI) are generally biased above the experimental effective thermal conductivity, thus strengthening the indication that the effects of particle shape and spatial distribution, and the bending of the heat flow lines in granular materials are too complex to be analyzed separately, and should be incorporated in a single unified model. Therefore, an analysis of a simplified geometrical configuration or an unrealistic heat flow assumption do not provide sufficient information to deduce whether a particular model will predict high or low conductivities for real granular materials.

Models based on non-linear heat flow are generally biased below the experimental thermal conductivity, as seen from Tables 7-IV, 7-V and 7-VI. A surprising result is that the conductivities predicted by Maxwell's and Rayleigh's equations are very close for the total range of porosities and ratios of constituent conductivities. This is probably due to Rayleigh's failure to include a larger number of terms in his solution, and for this reason Meredith and Tobias' equation provides a marked improvement of the predicted values.

For the model described in this study, the effective conductivity in each case was determined by considering five or more random placements of the continuous phase in a unit cube, and finding the average of the calculated values. The variance of the calculated values was less than 0.1 for 78 cases and its highest value vas 0.587.

Whenever the variance was exceedingly high, more random placements were considered, so that a more representative average could be obtained for the effective thermal conductivity.

In Fig.(7-5) the calculated effective thermal conductivity shown in Table 7-VII, is compared to experimental data obtained by Fountain and West [3] for particulate basalt in a simulated lunar environment. The thermal conductivity of solid basalt was assumed to be a function of temperature given by:

$$k(\text{Basalt})=0.01091+9.09\times10^{-6}T \quad \text{Watt/cm-K} \tag{7-13}$$

where T is in ^{o}K. Equation (7-13) is a least squares fit of the data given in Reference [64]. The effective thermal conductivity of the gaseous phase was calculated according to Equation (A-1), and the effective radiant conductivity for the transfer of heat between particle surfaces was calculated according to Equation (B-13). In both cases the effective pore size was assumed to be given by Equation (D-6). Then, the effective conductivity of the continuous phase is the sum of the gaseous conductivity and the radiant conductivity.

As indicated in Fig. (7-5), the calculated conductivities are lower than the experimental. Probably the source of error is due to two factors. First, the semi-empirical equation for the contact resistance used in this study probably predicts low values for the contact conductivity. Evidence to this effect is that calculated conductivities at low pressures, in which case heat transfer from particle to particle is a dominant mode, are generally low. A second source of error is

failure to include radiation heat transfer as a photon diffusion process. Evidence to this effect is that the discrepancy between calculated and experimental values generally increases with temperature. Nevertheless, it is seen that the model predicts fairly well the increase in slope with decreasing porosity, and the increase in slope with temperature, due to the increase of the relative influence of radiant heat transfer with decreasing porosity and increasing temperature. The maximum error of the calculated thermal conductivities is 23.6% and the mean error is 15.9%.

In Fig. (7-6) the calculated effective thermal conductivity is compared to experimental data obtained by Fountain and West [3] for particulate basalt in a simulated martian environment. In this case the gaseous conductivity and the radiant conductivity are of the order of magnitude 3×10^{-5} and 10^{-7} Watt/cm^{o}K respectively. Consequently, radiation can be neglected. Again the predicted values are lower than the experimental, and the maximum error and mean error are 25.2% and 20.8% respectively. The slight increase of the effective thermal conductivity with temperature is due to the simultaneous increase of the conductivity of the solid and gaseous phases with temperature, and not to radiation heat transfer.

A case in which the calculated values are not in good agreement with experimental values is shown in Fig. (7-7). The experimental data in this Figure were obtained from Reference [93]. Here, experimental and calculated thermal conductivities are compared for glass spheres

in a simulated lunar environment, and the maximum and mean errors are 48.3% and 39.4% respectively. The discrepancy increases with increasing temperature. The most probable explanation for the low predicted thermal conductivities is that this case does not satisfy the assumptions stated in the development of the model. Radiation heat transfer has been incorporated in the model through the effective radiant conductivity of the voids, which accounts for the radiation heat transfer between particle surfaces. It has been necessary to make this assumption because of the lack of information about the extinction coefficient of granular materials and powders, which is required for the complete description of the radiation heat transfer process. Consequently, it has been effectively assumed that the solid particles are opaque to thermal radiation, and that the pure radiation heat transfer process can be neglected. However, there exists evidence [2,85] that this is not always the case, and for very small particles the pure radiation process is generally more effective than the conduction-radiation process. It appears that failure to account for the pure radiation process has rendered the calculated values much lower than the experimental values is this case of glass spheres.

The experimental and calculated thermal conductivities of particulate basalt in air, lead shot in air, and glass beads in air are compared in Figures (7-8), (7-9) and (7-10) respectively, as a function of pressure. It is observed that the model predicted values are generally in good agreement with the experimental values, although somewhat lower con-

ductivities are predicted at low pressures. This relatively good agreement is attributed to the choice of Equation (D-6) for the effective pore size associated with the conduction heat transfer in the voids. The maximum and mean errors corresponding to Figures (7-8),(7-9) and (7-10) are 28.4 and 19.4, 37 and 18.5, 23 and 17.6 respectively.

Table 7-VIII summarizes the mean error and the variance of percentage error for all low pressure cases.

Summarizing the comparisons between calculated and experimental thermal conductivities, it is seen that the performance of the model described in this study is sufficiently good for granular materials at atmospheric pressures. For granular materials at low pressures, the predicted thermal conductivities are generally low, but the change of the thermal conductivity with temperature and pressure is in good agreement with the changes observed in the experimental values.

The major sources of error in the calculated effective thermal conductivity values are as follows:

1. Low values for the contact conductivity predicted by Equation (C-7);
2. Failure to account for the pure radiation process;
3. Incomplete description of the particle and pore size and shape distribution by the random placement method.

The first factor is of particular importance in cases where the ratio of the constituent conductivities is large, and could explain the low calculated values at low pressures. The third factor is a manifestation of the lack of information associated with the generalized geometry of granular materials.

TABLE 7-1 COMPARISON OF CALCULATED CONDUCTIVITIES TO EXPERIMENTAL CONDUCTIVITIES

Case (1)	Conductivity, (k_{cal}/m-hr - °k) x 100				k_d/k_c (6)	P (7)	Ref. (8)
	Fluid Phase (2)	Solid Phase (3)	Experimental (4)	Calculated (5)			
1	h-Heptane 11	Quartz 720	57.6	61.6	65.5	0.590	23
2	Helium 11.5	Quartz 720	63	61.7	62.6	0.590	23
3	Hydrogen 14.7	Quartz 720	74	73.8	49	0.590	23
4	Water 54	Quartz 720	180	152.6	13.3	0.590	23
5	EtOH 29.3	S. Steel 1793	172.7	181.2	61.2	0.505	36
6	Air 2.3	S. Steel 1793	22	24.2	779.6	0.502	36
7	Glycerine 46.3	S. Steel 1793	248.3	211.9	38.7	0.502	36
8	Water 54.5	S. Steel 1793	272	228.3	32.9	0.501	36
9	Helium 15.6	S. Steel 1785	117.4	114.4	114.5	0.500	21

TABLE 7-1 Continued

(1)	(2)	(3)	(4)	(5)	(6)	(7)	(8)
10	Helium 18.5	S. Steel 1670	122	133.5	90.3	0.500	21
11	Argon 1.62	S. Steel 1883	38.7	30.6	1162.3	0.500	21
12	Argon 2.01	S. Steel 1720	41.6	48.7	855.7	0.500	21
13	Iso-Octane 12.3	S. Steel 1793	80.5	73.3	145.8	0.476	36
14	Air 2.41	Lead 2950	30.4	27.0	1224.1	0.450	6
15	Water 54.5	Silica 973	216	191.9	17.9	0.439	36
16	Air 2.25	Quartz 947	26.8	34.5	420.9	0.438	35
17	Air 2.3	Silica 973	21.9	16.9	423.0	0.437	36
18	Air 2.25	Coal 36	11.8	8.9	16.0	0.437	35
19	Hydrogen 16.6	Coal 36	25.3	22.1	2.17	0.437	35
20	EtOH 29.3	Silica 973	144.6	122.3	33.2	0.434	36

TABLE 7-1 Continued

(1)	(2)	(3)	(4)	(5)	(6)	(7)	(8)
21	EtOH 29.3	Silica 973	146.5	124.6	33.2	0.433	36
22	Air 2.3	Silica 973	23.8	22.5	423.0	0.433	36
23	Iso-Octane 12.3	Glass 93.9	35.1	42.2	7.63	0.431	36
24	Water 54.5	Silica 973	218.5	177.5	17.9	0.430	36
25	Glycerine 46.3	Glass 93.9	73.2	61.1	2.03	0.428	36
26	Iso-Octane 12.3	Silica 973	94.1	81.9	79.1	0.428	36
27	Iso-Octane 12.3	Silica 973	70.9	78.9	79.1	0.426	36
28	Air 2.3	Silica 973	22.3	25.9	423.0	0.426	36
29	Water 54.5	Silica 973	210	159.1	17.9	0.426	36
30	Air 2.3	Silica 973	22.6	26.3	423.0	0.424	36
31	Glycerine 46.3	Silica 973	205.5	180.3	21.0	0.424	36

Table 7-1 Continued

(1)	(2)	(3)	(4)	(5)	(6)	(7)	(8)
32	Air 2.41	Steel 3850	44.6	53.2	1597.5	0.423	6
33	EtOH 29.3	Glass 93.9	55.4	41.1	3.2	0.423	36
34	EtOH 29.3	Silica 973	163.8	134.5	33.2	0.423	36
35	Iso-Octane 12.3	Silica 973	74.6	77.7	79.1	0.423	36
36	Air 2.41	Lead 2950	36	41.2	1224.1	0.420	6
37	Iso-Octane 12.3	Silica 973	70.6	66.9	79.1	0.420	36
38	Helium 15.6	MgO 2750	132.5	151.7	176.3	0.420	21
39	Helium 18.6	MgO 2160	152	127.2	116.1	0.420	21
40	Air 2.68	MgO 2820	33.5	30.5	1052.2	0.420	21
41	Air 3.20	MgO 2200	40.2	52.7	687.5	0.420	21
42	Argon 2.16	MgO 2750	26.8	19.5	1273.2	0.420	21

Table 7-1 Continued

(1)	(2)	(3)	(4)	(5)	(6)	(7)	(8)
43	Argon 2.23	MgO 2200	29.8	24.1	986.6	0.420	21
44	Air 2.74	Al_2O_3 2600	36.1	31.3	948.9	0.420	45
45	Iso-Octane 12.3	Silica 973	71.2	69.3	79.1	0.419	36
46	EtOH 29.3	Silica 973	144.2	114.2	34.2	0.418	36
47	Air 2.25	Quartz 947	29.7	19.4	420.9	0.416	35
48	Air 2.3	Glass 93.9	17.1	13.9	40.8	0.414	36
49	Water 54.5	Silica 973	230.5	157.7	17.9	0.414	36
50	Air 2.41	Steel 3850	35.1	29.8	1597.5	0.413	6
51	Air 2.41	Steel 3850	33.6	29.8	1597.5	0.413	6
52	EtOH 29.3	Silica 973	154.9	115.6	33.2	0.410	36
53	Air 3.0	Sand 160	23.1	16.7	53.3	0.410	56

Table 7-1 Continued

(1)	(2)	(3)	(4)	(5)	(6)	(7)	(8)
54	Water 54.5	Glass 93.9	73.1	69.7	1.72	0.408	36
55	Air 2.41	Steel 3850	36.7	41.6	1597.5	0.402	6
56	Air 2.25	Lead 3040	37.1	42.8	1351.1	0.400	35
57	Hydrogen 16.6	Lead 3040	120.7	128.7	183.1	0.400	35
58	Water 55	Lead 3040	299.5	273.1	55.3	0.400	35
59	Glycerine 24.5	Lead 3040	176	204.9	124.1	0.400	35
60	Air 2.41	Steel 3850	42.5	40.9	1597.5	0.394	6
61	EtOH 29.3	Copper 33200	327.5	251.3	1133.1	0.392	36
62	Air 2.41	Steel 3850	40.3	45.9	1597.5	0.391	6
63	Air 2.41	Steel 3850	45.6	48.2	1597.5	0.390	6
64	Air 3.0	Sand 160	29.4	22.4	53.3	0.390	56

Table 7-1 Continued

(1)	(2)	(3)	(4)	(5)	(6)	(7)	(8)
65	Water 54.5	Copper 33200	613	639.0	609.2	0.387	36
66	Glycerine 46.3	Copper 33200	607	529.1	717.1	0.386	36
67	Glycerine 46.3	Copper 33200	549	463.2	717.1	0.385	36
68	Water 54.5	Copper 33200	635	553.2	609.2	0.384	36
69	Argon 1.46	Lead 2950	25	29.4	2020.6	0.380	23
70	Air 2.18	Lead 2950	36	31.2	1353.2	0.380	23
71	Helium 11.5	Lead 2950	162	205.8	256.5	0.380	23
72	Hydrogen 14.7	Lead 2950	183	214.3	200.7	0.380	23
73	Water 54	Lead 2950	470	377.7	54.6	0.380	23
74	Air 2.43	Steel 3030	45	59.1	1246.9	0.380	58
75	Methane 3.0	Steel 3300	55.8	72.5	1100.0	0.380	58

Table 7-1 Continued

(1)	(2)	(3)	(4)	(5)	(6)	(7)	(8)
76	CO_2 1.35	Steel 3300	32.4	42.1	2444.4	0.380	58
77	Hydrogen 16.4	Steel 3300	188	191.2	201.2	0.380	58
78	Freon-12 0.78	Glass 90	3.96	3.19	115.4	0.379	23
79	Argon 1.46	Glass 90	13.3	11.2	61.6	0.379	23
80	Air 2.18	Glass 90	18	16.2	41.3	0.379	23
81	Water 54	Glass 90	75.5	66.2	1.67	0.379	23
82	Air 2.24	Quartz 1175	35.7	41.8	524.6	0.377	34
83	Air 3.0	Sand 160	29.4	22.2	53.3	0.370	56
84	Helium 13.1	Quartz 680	94.5	72.6	51.9	0.369	60
85	Helium 13.1	Quartz 680	91.5	72.6	51.9	0.369	60
86	Helium 12.2	Quartz 830	97.8	78.0	68.0	0.369	60

Table 7-1 Continued

(1)	(2)	(3)	(4)	(5)	(6)	(7)	(8)
87	Helium 12.2	Quartz 830	94	78.0	68.0	0.369	60
88	Air 2.25	Steel 2250	35.6	29.6	1000.0	0.365	35
89	Hydrogen 16.6	Steel 2250	110	106.3	135.5	0.365	35
90	Air 2.58	ZrO_2 172	25	20.2	66.7	0.360	45
91	Air 2.24	Quartz 1175	37.8	42.8	524.6	0.354	34
92	Air 2.25	Lead 3040	58.3	62.7	1351.1	0.310	35

TABLE 7-II EXPERIMENTAL AND PREDICTED THERMAL CONDUCTIVITIES FOR VARIOUS MODELS

CASE	EXPE	MODEL	KRUPIC.	RUSSELL	LICHT.	JEFFERSON
1	0.5760	0.6160	0.4752	0.3965	0.3283	0.3731
2	0.6300	0.6170	0.4914	0.4132	0.3424	0.3873
3	0.7400	0.7380	0.5900	0.5174	0.4313	0.4751
4	1.8000	1.5260	1.4804	1.5330	1.3468	1.3232
5	1.7270	1.8120	1.5364	1.2773	1.0900	1.3735
6	0.2200	0.2420	0.1994	0.0958	0.0802	0.1550
7	2.4830	2.1190	2.1197	1.9338	1.6698	1.9570
8	2.7200	2.2830	2.3700	2.2294	1.9349	2.2114
9	1.1740	1.1440	0.9955	0.7184	0.6082	0.8620
10	1.2200	1.3350	1.1025	0.8403	0.7136	0.9693
11	0.3870	0.3060	0.1701	0.0781	0.0654	0.1319
12	0.4160	0.4870	0.2006	0.0967	0.0810	0.1569
13	0.8050	0.7330	0.9056	0.6081	0.5180	0.8095
14	0.3040	0.2700	0.3264	0.1327	0.1131	0.2986
15	2.1600	1.9190	2.1695	2.2576	2.0391	2.2112
16	0.2680	0.3450	0.2551	0.1267	0.1088	0.2442
17	0.2190	0.1690	0.2623	0.1299	0.1115	0.2519
18	0.1180	0.0690	0.0860	0.0908	0.0824	0.0879
19	0.2530	0.2210	0.2508	0.2619	0.2447	0.2543
20	1.4460	1.2230	1.5079	1.4039	1.2450	1.5260
21	1.4650	1.2460	1.5119	1.4073	1.2484	1.5319
22	0.2380	0.2250	0.2671	0.1313	0.1129	0.2603
23	0.3510	0.4220	0.3443	0.3838	0.3582	0.3551
24	2.1850	1.7750	2.2125	2.3022	2.0848	2.2721
25	0.7320	0.6110	0.6790	0.7060	0.6584	0.6884
26	0.9410	0.8190	0.8823	0.6648	0.5802	0.8855
27	0.7090	0.7890	0.8883	0.6683	0.5838	0.8948
28	0.2230	0.2590	0.2759	0.1339	0.1155	0.2762
29	2.1000	1.5910	2.2321	2.3224	2.1056	2.2998
30	0.2260	0.2630	0.2785	0.1347	0.1162	0.2810
31	2.0550	1.8030	2.0382	2.0673	1.8649	2.1000
32	0.4460	0.5320	0.3983	0.1433	0.1234	0.4247
33	0.5540	0.4110	0.5457	0.5898	0.5578	0.5591
34	1.6380	1.3450	1.5531	1.4422	1.2835	1.5925
35	0.7460	0.7770	0.8973	0.6737	0.5891	0.9091
36	0.3600	0.4120	0.3835	0.1443	0.1244	0.4104
37	0.7060	0.6690	0.9065	0.6792	0.5945	0.9238
38	1.3250	1.5170	1.4965	0.9027	0.7835	1.5197
39	1.5200	1.2720	1.5616	1.0549	0.9190	1.5869
40	0.3350	0.3050	0.4127	0.1603	0.1383	0.4380
41	0.4020	0.5270	0.4466	0.1907	0.1646	0.4649
42	0.2680	0.1950	0.3466	0.1294	0.1116	0.3718
43	0.2980	0.2410	0.3385	0.1333	0.1150	0.3580
44	0.3610	0.3130	0.4123	0.1638	0.1413	0.4353
45	0.7120	0.6930	0.9097	0.6810	0.5963	0.9288
46	1.4420	1.1420	1.5745	1.4601	1.3016	1.6241
47	0.2970	0.1940	0.2826	0.1348	0.1166	0.2948
48	0.1710	0.1390	0.1355	0.1197	0.1063	0.1402

TABLE 7-II EXPERIMENTAL AND PREDICTED THERMAL CONDUCTIVITIES FOR VARIOUS MODELS

CASE	EXPT.	MODEL	KRUPIC.	RUSSELL	LICHT.	JEFFERSON
49	2.3050	1.5770	2.2934	2.3848	2.1696	2.3857
50	0.3510	0.2980	0.4221	0.1475	0.1275	0.4841
51	0.3360	0.2980	0.4221	0.1475	0.1275	0.4841
52	1.5450	1.1960	1.6100	1.4894	1.3312	1.6764
53	0.2310	0.1670	0.1981	0.1635	0.1446	0.2059
54	0.7310	0.6970	0.7396	0.7606	0.7052	0.7487
55	0.3670	0.4160	0.4506	0.1523	0.1322	0.5688
56	0.3710	0.4280	0.4104	0.1429	0.1242	0.5165
57	1.2070	1.2870	1.7518	1.0183	0.8901	1.8939
58	2.9950	2.7310	3.8028	3.0925	2.7420	4.0181
59	1.7600	2.0490	2.2712	1.4752	1.2936	2.4285
60	0.4250	0.4090	0.4731	0.1560	0.1358	0.6492
61	3.2750	2.5130	5.3789	1.9043	1.6595	7.1256
62	0.4030	0.4590	0.4820	0.1574	0.1372	0.6849
63	0.4560	0.4820	0.4850	0.1579	0.1377	0.6977
64	0.2540	0.2240	0.2199	0.1826	0.1627	0.2359
65	6.1300	6.3900	8.7746	3.5753	3.1246	11.1084
66	6.0700	5.2910	7.8344	3.0524	2.6678	10.2277
67	5.4900	4.6320	7.8784	3.0617	2.6769	10.3734
68	6.3500	5.5320	8.9197	3.6081	3.1568	11.5586
69	0.2300	0.2940	0.3300	0.0987	0.0864	0.5856
70	0.3600	0.3120	0.4492	0.1471	0.1288	0.7099
71	1.6200	2.0580	1.4818	0.7573	0.6655	1.7757
72	1.8300	2.1430	1.7469	0.9600	0.8448	2.0476
73	3.7000	3.7770	3.9764	3.2027	2.8600	4.3449
74	0.4500	0.5910	0.4908	0.1639	0.1435	0.7599
75	0.5580	0.7250	0.5874	0.2022	0.1770	0.8827
76	0.3240	0.4210	0.3180	0.0914	0.0799	0.6022
77	1.8600	1.9120	1.9507	1.0712	0.9426	2.2870
78	0.0356	0.0319	0.0767	0.0497	0.0439	0.0868
79	0.1330	0.1120	0.1132	0.0881	0.0785	0.1244
80	0.1660	0.1620	0.1437	0.1246	0.1119	0.1560
81	0.7550	0.6620	0.7286	0.7487	0.6962	0.7383
82	0.3570	0.4180	0.3651	0.1512	0.1327	0.4891
83	0.2940	0.2220	0.2266	0.1824	0.1635	0.2516
84	0.9450	0.7260	0.9818	0.7960	0.7142	1.0911
85	0.9190	0.7260	0.9818	0.7960	0.7142	1.0911
86	0.9780	0.7800	1.0204	0.7658	0.6839	1.1494
87	0.9460	0.7800	1.0204	0.7658	0.6839	1.1494
88	0.3560	0.2960	0.4712	0.1589	0.1399	0.8521
89	1.1000	1.0630	1.8384	1.1139	0.9883	2.2069
90	0.2500	0.2020	0.2215	0.1659	0.1487	0.2546
91	0.3780	0.4820	0.4156	0.1626	0.1439	0.7013
92	0.5830	0.6270	0.7508	0.1920	0.1724	-2.5897

TABLE 7-III EXPERIMENTAL AND PREDICTED THERMAL CONDUCTIVITIES FOR VARIOUS MODELS

CASE	EXKE	MAXWELL	RAYLEIGH	W AND M	M AND T
1	0.5760	0.3226	0.3213	0.6489	0.3771
2	0.6300	0.3365	0.3352	0.6736	0.3933
3	0.7400	0.4241	0.4226	0.8240	0.4951
4	1.8000	1.3371	1.3339	2.0233	1.5349
5	1.7270	1.0772	1.0733	2.2594	1.3363
6	0.2200	0.0791	0.0788	0.1919	0.0987
7	2.4830	1.6525	1.6469	3.2302	2.0490
8	2.7200	1.9161	1.9098	3.6333	2.3742
9	1.1740	0.6007	0.5983	1.3496	0.7494
10	1.2200	0.7050	0.7021	1.5492	0.8791
11	0.3870	0.0646	0.0643	0.1572	0.0807
12	0.4160	0.0800	0.0796	0.1941	0.1000
13	0.8050	0.5123	0.5097	1.1786	0.6511
14	0.3040	0.1120	0.1115	0.2764	0.1454
15	2.1600	2.0316	2.0142	3.3220	2.6230
16	0.2680	0.1077	0.1062	0.2608	0.1411
17	0.2190	0.1105	0.1089	0.2675	0.1448
18	0.1180	0.0822	0.0680	0.1305	0.1060
19	0.2530	0.2593	0.2554	0.2691	0.2859
20	1.4460	1.2368	1.2231	2.3307	1.6173
21	1.4650	1.2403	1.2264	2.3364	1.6233
22	0.2380	0.1119	0.1103	0.2708	0.1472
23	0.3510	0.3607	0.3427	0.4715	0.4537
24	2.1850	2.0778	2.0587	3.3862	2.7035
25	0.7320	0.7004	0.6968	0.7220	0.7679
26	0.9410	0.5755	0.5677	1.2462	0.7592
27	0.7090	0.5791	0.5711	1.2531	0.7652
28	0.2230	0.1144	0.1127	0.2767	0.1514
29	2.1000	2.0988	2.0788	3.4149	2.7404
30	0.2260	0.1152	0.1134	0.2784	0.1526
31	2.0550	1.8571	1.8379	3.1442	2.4365
32	0.4460	0.1223	0.1218	0.3019	0.1621
33	0.5540	0.5773	0.5677	0.6291	0.6738
34	1.6380	1.2756	1.2602	2.3939	1.6840
35	0.7460	0.5844	0.5761	1.2635	0.7742
36	0.3600	0.1234	0.1227	0.3037	0.1640
37	0.7060	0.5899	0.5813	1.2740	0.7834
38	1.3250	0.7770	0.7726	1.8045	1.0325
39	1.5200	0.9116	0.9053	2.0503	1.2111
40	0.3350	0.1371	0.1363	0.3369	0.1822
41	0.4020	0.1632	0.1620	0.3985	0.2169
42	0.2680	0.1106	0.1099	0.2723	0.1470
43	0.2980	0.1140	0.1132	0.2800	0.1515
44	0.3610	0.1401	0.1392	0.3438	0.1862
45	0.7120	0.5917	0.5830	1.2774	0.7864
46	1.4420	1.2938	1.2775	2.4228	1.7155
47	0.2970	0.1157	0.1137	0.2789	0.1542
48	0.1710	0.1056	0.0927	0.2056	0.1407

TABLE 7-III EXPERIMENTAL AND PREDICTED THERMAL CONDUCTIVITIES FOR VARIOUS MODELS

CASE	EXPE	MAXWELL	RAYLEIGH	W AND M	M AND T
49	2.3050	2.1634	2.1407	3.5011	2.8550
50	0.3510	0.1264	0.1258	0.3114	0.1689
51	0.3360	0.1264	0.1258	0.3114	0.1689
52	1.5490	1.3237	1.3058	2.4692	1.7675
53	0.2310	0.1436	0.1317	0.2922	0.1922
54	0.7310	0.7574	0.7548	0.7704	0.8167
55	0.3670	0.1312	0.1305	0.3219	0.1769
56	0.3710	0.1232	0.1224	0.3017	0.1664
57	1.2070	0.8835	0.8781	2.0414	1.1936
58	2.9950	2.7245	2.7100	5.5466	3.6783
59	1.7600	1.2842	1.2766	2.8821	1.7350
60	0.4250	0.1348	0.1341	0.3297	0.1829
61	3.2750	1.6472	1.6462	4.0117	2.2396
62	0.4030	0.1362	0.1354	0.3326	0.1853
63	0.4560	0.1366	0.1359	0.3336	0.1861
64	0.2940	0.1618	0.1603	0.3221	0.2203
65	6.1300	3.1022	3.1002	7.4618	4.2359
66	4.0700	2.6487	2.6470	6.3880	3.6196
67	5.4000	2.6579	2.6562	6.4066	3.6351
68	6.3500	3.1345	3.1325	7.5270	4.2908
69	0.2500	0.0858	0.0851	0.2086	0.1178
70	0.3800	0.1279	0.1269	0.3100	0.1756
71	1.6250	0.6610	0.6561	1.5391	0.9082
72	1.8300	0.8392	0.8329	1.9284	1.1531
73	4.7000	2.8440	2.8255	5.7066	3.9087
74	0.4500	0.1425	0.1414	0.3452	0.1957
75	0.5520	0.1758	0.1746	0.4252	0.2414
76	0.3240	0.0794	0.0788	0.1933	0.1090
77	1.9800	0.9363	0.9301	2.1519	1.2865
78	0.0396	0.0437	0.0356	0.0961	0.0601
79	0.1330	0.0781	0.0645	0.1595	0.1074
80	0.1800	0.1114	0.0932	0.2127	0.1531
81	0.7550	0.7462	0.7434	0.7569	0.8073
82	0.3570	0.1318	0.1292	0.3140	0.1815
83	0.2940	0.1627	0.1444	0.3227	0.2256
84	0.9450	0.7105	0.6894	1.4021	0.9863
85	0.9150	0.7105	0.6894	1.4021	0.9863
86	0.9750	0.6832	0.6628	1.3986	0.9443
87	0.9400	0.6802	0.6628	1.3986	0.9443
88	0.3960	0.1390	0.1374	0.3323	0.1933
89	1.1000	0.9825	0.9720	2.1721	1.3682
90	0.2500	0.1479	0.1305	0.3010	0.2070
91	0.3780	0.1431	0.1397	0.3350	0.2009
92	0.5830	0.1717	0.1693	0.3886	0.2505

TABLE 7-IV PERCENTAGE ERROR BETWEEN PREDICTED AND EXPERIMENTAL THERMAL CONDUCTIVITIES

CASE	MODEL	KRUPIC.	RUSSELL	LICHT.	JEFFERSON
1	6.944	-17.497	-31.156	-43.005	-35.217
2	-2.064	-22.003	-34.411	-45.648	-38.520
3	-0.270	-20.265	-30.082	-41.717	-35.802
4	-15.222	-17.755	-14.833	-25.180	-26.487
5	4.922	-11.039	-26.041	-36.886	-20.470
6	10.000	-9.349	-56.450	-63.551	-29.558
7	-14.660	-14.632	-22.120	-32.749	-21.183
8	-16.066	-12.869	-18.037	-28.863	-18.697
9	-2.555	-15.201	-38.807	-48.198	-26.578
10	9.496	-9.632	-31.120	-41.505	-20.550
11	-20.930	-56.042	-79.813	-83.098	-65.923
12	17.067	-51.777	-76.743	-80.519	-62.283
13	-8.944	12.497	-24.456	-35.650	0.561
14	-11.184	7.365	-56.360	-62.780	-1.770
15	-11.157	0.438	4.517	-5.597	2.372
16	28.731	-4.828	-52.734	-59.421	-8.894
17	-22.831	19.750	-40.704	-49.075	15.039
18	-24.576	-27.135	-23.054	-30.181	-25.482
19	-12.648	-0.877	3.520	-3.299	0.497
20	-15.422	4.280	-2.910	-13.900	5.534
21	-14.949	3.201	-3.936	-14.782	4.568
22	-5.462	12.223	-44.828	-52.547	9.384
23	20.228	-1.913	9.337	2.048	1.173
24	-18.764	1.257	5.364	-4.585	3.987
25	-16.530	-7.241	-3.548	-10.059	-5.959
26	-12.965	-6.238	-29.354	-38.338	-5.901
27	11.283	25.283	-5.736	-17.665	26.210
28	16.143	23.717	-39.951	-48.218	23.853
29	-24.238	6.293	10.593	0.266	9.517
30	16.372	23.222	-40.412	-48.578	24.345
31	-12.263	-0.815	0.600	-9.248	2.188
32	19.283	-10.703	-67.878	-72.336	-4.772
33	-25.812	-1.493	6.461	0.678	0.919
34	-17.688	-5.181	-11.956	-21.641	-2.775
35	4.155	20.285	-9.690	-21.035	21.868
36	14.444	6.531	-59.916	-65.431	14.011
37	-5.241	28.406	-3.801	-15.796	30.848
38	14.491	12.947	-31.872	-40.867	14.695
39	-16.316	2.737	-30.597	-39.540	4.401
40	-8.955	23.197	-52.144	-58.721	30.738
41	31.095	11.095	-52.554	-59.046	15.645
42	-27.239	29.331	-51.730	-58.373	38.737
43	-19.128	13.599	-55.256	-61.402	20.151
44	-13.296	14.217	-54.630	-60.860	20.570
45	-2.669	27.761	-4.355	-16.251	30.443
46	-20.804	9.192	1.253	-9.738	12.628
47	-34.680	-4.864	-54.624	-60.727	-0.736
48	-18.713	-20.762	-29.995	-37.832	-18.003

TABLE 7-IV PERCENTAGE ERROR BETWEEN PREDICTED AND EXPERIMENTAL THERMAL CONDUCTIVITIES

CASE	MODEL	KRUPIC.	RUSSELL	LICHT.	JEFFERSON
49	-31.583	-0.503	3.461	-5.874	3.499
50	-15.100	20.243	-57.989	-63.685	37.913
51	-11.310	25.611	-56.114	-62.063	44.070
52	-25.371	3.936	-3.846	-14.059	8.225
53	-27.706	-14.239	-29.205	-37.402	-10.851
54	-4.651	1.178	4.053	-3.535	2.415
55	13.351	22.781	-58.500	-63.979	54.998
56	15.364	10.617	-61.477	-66.534	39.226
57	6.628	45.133	-15.632	-26.256	56.913
58	-8.815	26.973	3.256	-8.446	34.159
59	16.420	29.043	-16.181	-26.502	37.983
60	-3.765	11.322	-63.295	-68.047	52.760
61	-23.267	64.240	-41.854	-49.327	117.577
62	13.696	19.595	-60.938	-65.956	69.961
63	5.702	6.353	-65.374	-69.812	52.996
64	-23.810	-25.196	-37.908	-44.650	-19.776
65	4.241	43.142	-41.676	-49.027	81.213
66	-12.834	29.067	-49.713	-56.050	68.496
67	-15.628	43.305	-44.231	-51.240	68.952
68	-12.602	40.468	-43.180	-50.287	82.026
69	17.650	32.019	-60.505	-65.446	134.239
70	-13.333	24.774	-59.126	-64.228	97.181
71	27.037	-8.532	-53.251	-58.920	9.610
72	17.104	-4.541	-47.538	-53.837	11.893
73	-19.636	-15.395	-31.857	-39.149	-7.556
74	31.333	9.075	-63.569	-68.114	68.862
75	29.028	5.269	-63.759	-68.276	58.193
76	25.538	-1.842	-71.802	-75.333	85.873
77	1.702	3.759	-43.022	-49.864	21.650
78	-19.444	93.720	25.497	10.956	119.219
79	-15.789	-14.890	-33.762	-40.953	-6.454
80	-10.000	-20.168	-30.779	-37.819	-13.344
81	-12.313	-3.501	-0.836	-7.793	-2.214
82	17.587	2.268	-57.645	-62.834	36.997
83	-24.490	-22.939	-37.951	-44.375	-14.405
84	-23.175	3.896	-15.770	-24.428	15.459
85	-20.656	7.302	-13.008	-21.950	19.244
86	-20.245	4.333	-21.702	-30.069	17.524
87	-17.021	8.550	-18.536	-27.242	22.275
88	-16.454	32.362	-55.374	-60.714	139.360
89	-3.364	67.124	1.244	-[illegible].152	100.628
90	-19.200	-11.413	-33.646	-40.532	1.610
91	27.513	9.952	-56.975	-61.927	85.528
92	7.547	28.788	-67.062	-70.424	-544.204

TABLE 7-V PERCENTAGE ERROR BETWEEN PREDICTED AND EXPERIMENTAL THERMAL CONDUCTIVITIES

CASE	MAXWELL	RAYLEIGH	W AND M	M AND T
1	-44.001	-44.211	12.648	-34.526
2	-46.593	-46.792	6.914	-37.568
3	-42.690	-42.897	11.352	-33.095
4	-25.715	-25.894	12.405	-14.727
5	-37.626	-37.849	30.829	-22.625
6	-64.033	-64.184	-12.765	-55.117
7	-33.447	-33.674	30.091	-17.481
8	-29.555	-29.788	33.577	-12.712
9	-48.835	-49.039	14.961	-36.166
10	-42.209	-42.453	26.983	-27.942
11	-83.320	-83.388	-59.391	-79.154
12	-80.774	-80.860	-53.352	-75.973
13	-36.365	-36.689	46.406	-19.123
14	-63.162	-63.315	-9.087	-52.187
15	-5.945	-6.748	53.798	21.435
16	-59.806	-60.372	-2.676	-47.345
17	-49.556	-50.254	22.149	-33.865
18	-30.374	-42.345	10.620	-10.175
19	2.503	0.944	6.373	13.008
20	-14.468	-15.414	61.185	11.850
21	-15.341	-16.285	59.485	10.803
22	-52.986	-53.659	13.794	-38.165
23	2.771	-2.359	34.333	29.266
24	-4.907	-5.782	54.977	23.732
25	-4.311	-4.809	-1.366	4.906
26	-38.838	-39.670	32.437	-19.316
27	-18.325	-19.456	76.747	7.922
28	-48.679	-49.461	24.080	-32.122
29	-0.059	-1.009	62.613	30.495
30	-49.031	-49.821	23.180	-32.480
31	-9.629	-10.566	53.001	18.564
32	-72.582	-72.694	-32.301	-63.648
33	4.214	2.466	13.559	21.626
34	-22.122	-23.068	46.147	2.806
35	-21.657	-22.770	69.373	3.779
36	-65.732	-65.919	-15.647	-54.457
37	-16.448	-17.666	80.446	10.957
38	-41.360	-41.687	36.191	-22.077
39	-40.029	-40.442	34.888	-20.325
40	-59.081	-59.314	0.556	-45.617
41	-59.401	-59.696	-0.863	-46.043
42	-58.737	-58.978	1.615	-45.160
43	-61.738	-62.016	-6.049	-49.149
44	-61.201	-61.440	-4.778	-48.435
45	-16.896	-18.118	79.415	10.455
46	-10.274	-11.410	68.015	18.963
47	-61.057	-61.722	-6.083	-48.077
48	-38.227	-45.792	20.236	-17.706

TABLE 7-V PERCENTAGE ERROR BETWEEN PREDICTED AND EXPERIMENTAL THERMAL CONDUCTIVITIES

CASE	MAXWELL	RAYLEIGH	W AND M	M AND T
49	-6.143	-7.128	51.892	23.863
50	-63.990	-64.151	-11.296	-51.871
51	-62.382	-62.550	-7.336	-49.723
52	-14.542	-15.699	59.409	14.105
53	-37.825	-42.998	26.511	-16.795
54	3.607	3.263	5.388	11.718
55	-64.264	-64.440	-12.294	-51.810
56	-66.795	-67.005	-18.691	-55.149
57	-26.806	-27.246	69.127	-1.111
58	-9.032	-9.516	85.196	22.815
59	-27.035	-27.464	63.754	-1.421
60	-68.288	-68.455	-22.433	-56.955
61	-49.704	-49.735	22.494	-31.614
62	-66.210	-66.393	-17.468	-54.021
63	-70.035	-70.198	-26.845	-59.191
64	-44.973	-50.252	9.564	-25.063
65	-49.393	-49.426	21.726	-30.899
66	-56.364	-56.392	5.238	-40.370
67	-51.586	-51.618	16.695	-33.786
68	-50.637	-50.670	18.535	-32.429
69	-65.686	-65.952	-16.542	-52.881
70	-64.476	-64.751	-13.881	-51.217
71	-59.196	-59.502	-4.995	-43.939
72	-54.144	-54.484	5.377	-36.990
73	-39.696	-39.882	21.418	-16.836
74	-68.335	-68.573	-23.300	-56.515
75	-68.496	-68.713	-23.798	-56.735
76	-75.504	-75.675	-40.353	-66.363
77	-50.198	-50.528	14.465	-31.567
78	10.252	-10.087	142.802	51.674
79	-41.292	-51.476	19.923	-19.231
80	-38.133	-48.199	18.180	-14.944
81	-1.166	-1.531	0.251	6.931
82	-63.085	-63.802	-12.035	-49.168
83	-44.665	-50.889	9.775	-23.251
84	-24.615	-27.047	48.375	4.374
85	-22.350	-24.655	53.240	7.797
86	-30.459	-32.233	43.003	-3.444
87	-27.641	-29.493	48.784	0.459
88	-60.963	-61.411	-6.648	-45.708
89	-10.681	-11.640	97.461	24.381
90	-40.838	-47.792	20.392	-17.180
91	-62.149	-63.042	-11.373	-46.845
92	-70.554	-70.956	-33.346	-57.041

TABLE 7-VI AVERAGE ERROR, BIAS AND VARIANCE BETWEEN PREDICTED AND EXPERIMENTAL THERMAL CONDUCTIVITIES

Model	Average Error %	Average Bias %	Variance of % Error
1. This Study	-5.78	15.8	1.63
2. Maxwell [9]	-40.59	41.1	4.99
3. Rayleigh [14]	-42.05	42.2	4.96
4. Meredith & Tobias [16]	-22.46	31.34	3.56
5. Russell [43]	-32.65	34.37	4.90
6. Jefferson [78]	13.80	37.59	38.58
7. Krupiczka [42]	6.76	17.48	2.63
8. Lichtenecker [24]	-40.52	40.82	4.93
9. Woodside & Messmer [23]	19.10	30.12	6.68

TABLE 7-VII CONDUCTIVITY OF PARTICULATE BASALT IN SIMULATED LUNAR ENVIRONMENT

Conductivity (Kcal/m-hr-^{o}K)

Solid Phase	Experimental x10^{3}	Calculated x10^{3}	T(^{o}K)	P	Ref.
1.078	1.50	1.46	180	0.470	3
1.125	1.82	1.67	240	0.470	3
1.156	2.09	1.86	280	0.470	3
1.188	2.42	2.12	320	0.470	3
1.219	2.84	2.28	360	0.470	3
1.078	1.17	1.04	180	0.540	3
1.125	1.36	1.20	240	0.540	3
1.156	1.53	1.37	280	0.540	3
1.188	1.78	1.46	320	0.540	3
1.219	2.06	1.63	360	0.540	3
1.078	0.86	0.69	180	0.600	3
1.125	1.01	0.86	240	0.600	3
1.156	1.14	1.00	280	0.600	3
1.188	1.31	1.12	320	0.600	3
1.219	1.50	1.24	360	0.600	3
1.078	0.51	0.43	180	0.721	3
1.125	0.63	0.57	240	0.721	3
1.156	0.77	0.62	280	0.721	3
1.188	0.93	0.71	320	0.721	3
1.219	1.10	0.86	360	0.721	3

TABLE 7-VIII AVERAGE ERROR, BIAS AND VARIANCE BETWEEN PREDICTED AND EXPERIMENTAL THERMAL CONDUCTIVITIES

Case	Average Error %	Average Bias %	Variance of % Error
Figure 17	-15.9	15.9	8.7
Figure 18	-20.8	20.8	2.1
Figure 19	-39.4	39.4	7.5
Figure 20	-9.4	19.4	2.4
Figure 21	11.8	18.5	1.2
Figure 22	-17.6	17.6	1.1

TABLE 7-IX MECHANICAL PROPERTIES AND DENSITY OF SOLID MATERIALS

Solid	Young's Modulus Newtons/$m^2 x 10^{10}$	Poisson's Ratio	Specific weight Newtons/$m^3 x 10^4$
Aluminum	6.90	0.33	2.52
Basalt	5.73	0.25	2.78
Coal	5.00	0.25	1.36
Copper	10.80	0.33	8.72
Glass	6.90	0.24	2.52
Iron	8.96	0.28	6.95
Lead	1.57	0.43	11.10
MgO	21.00	0.25	3.51
Quartz (SiO_2)	7.00	0.14	2.60
Sand	7.00	0.14	2.70
Silica	7.00	0.14	2.45
Stainless Steel	20.70	0.31	7.86
Steel	20.70	0.3	7.65

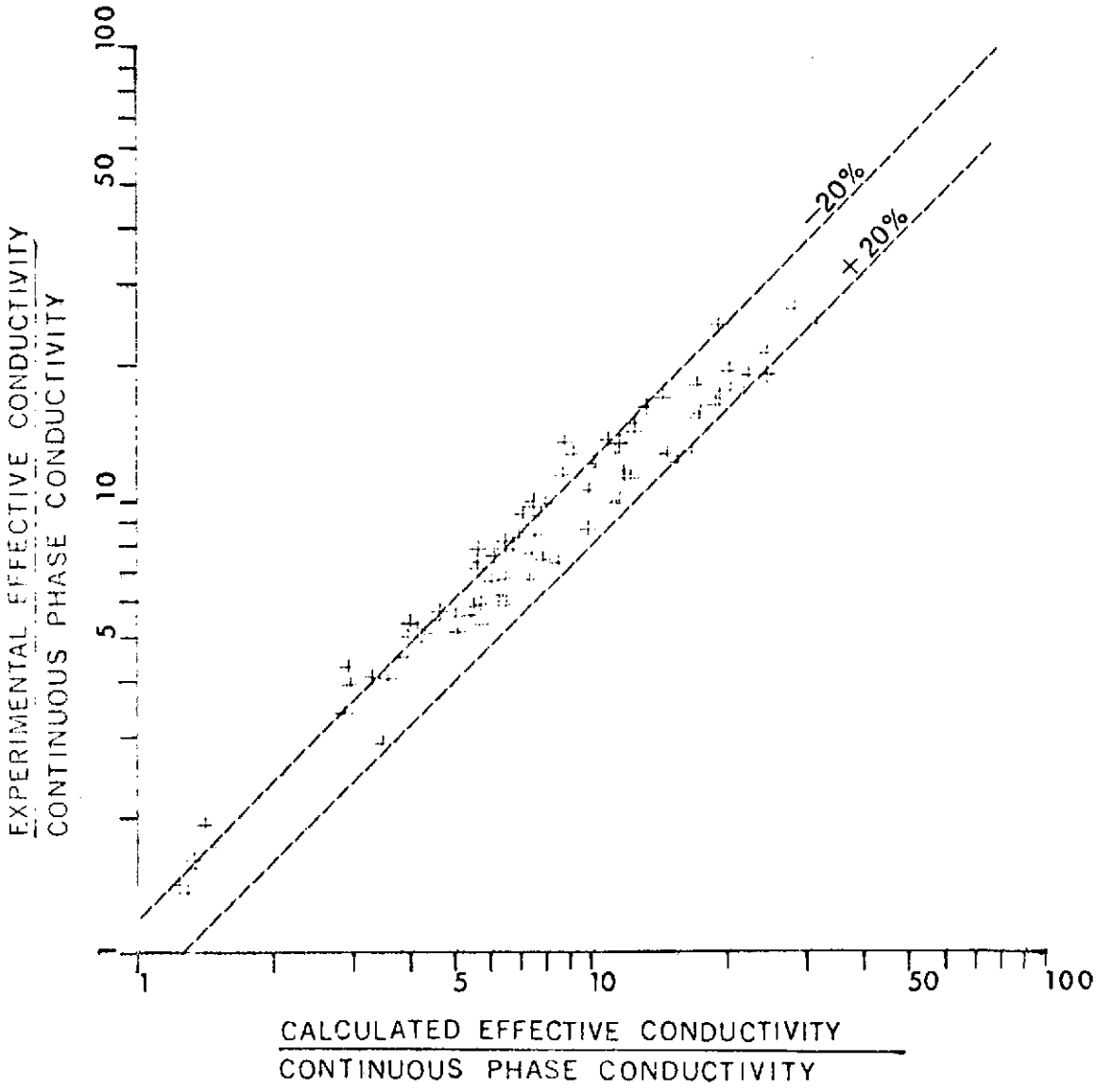

FIGURE 7-4. COMPARISON OF EXPERIMENTAL AND MODEL PREDICTED THERMAL CONDUCTIVITIES.

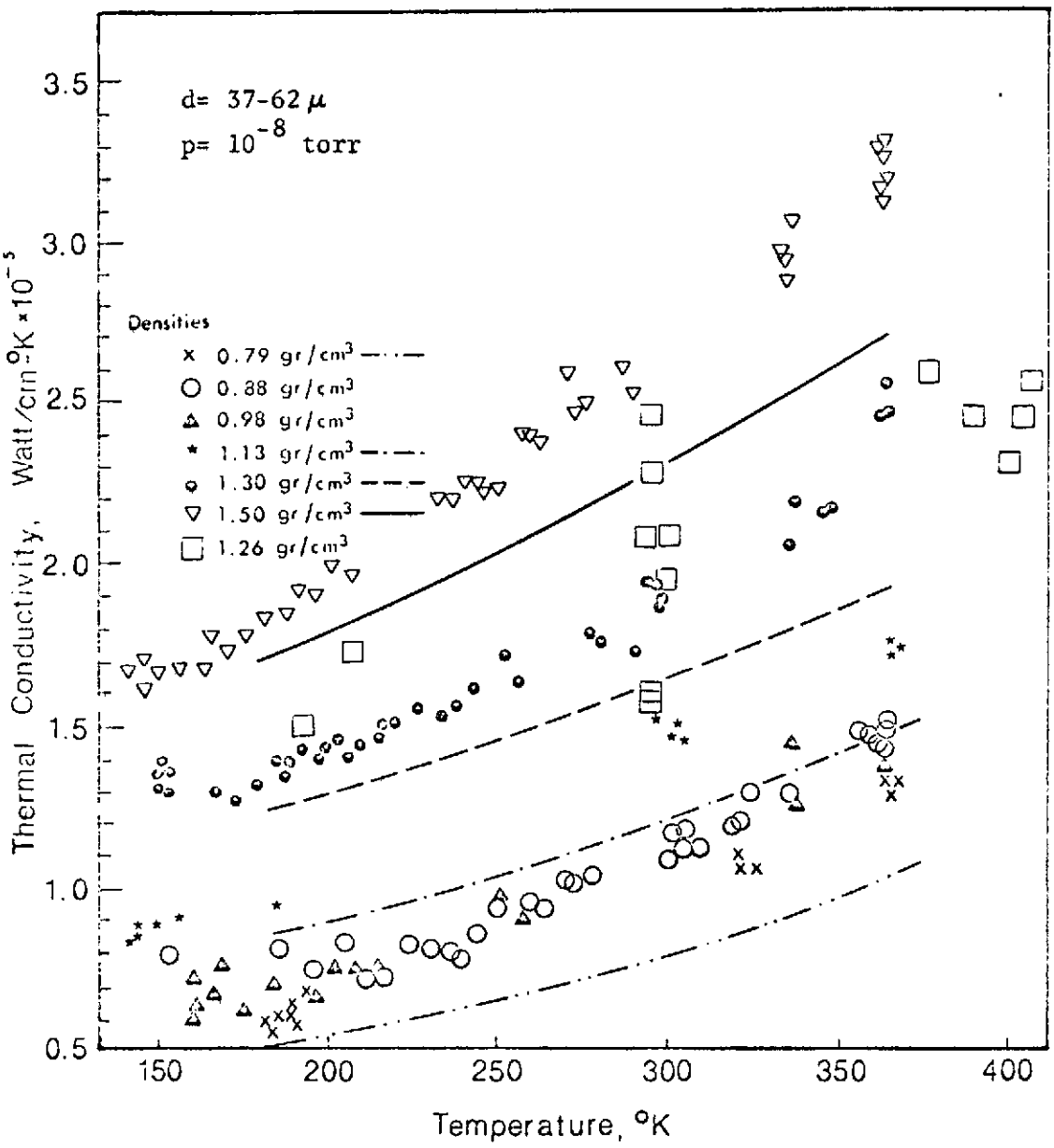

FIGURE 7-5. EXPERIMENTAL AND CALCULARED CONDUCTIVITY OF PARTICULATE BASALT IN SIMULATED LUNAR ENVIRONMENT.

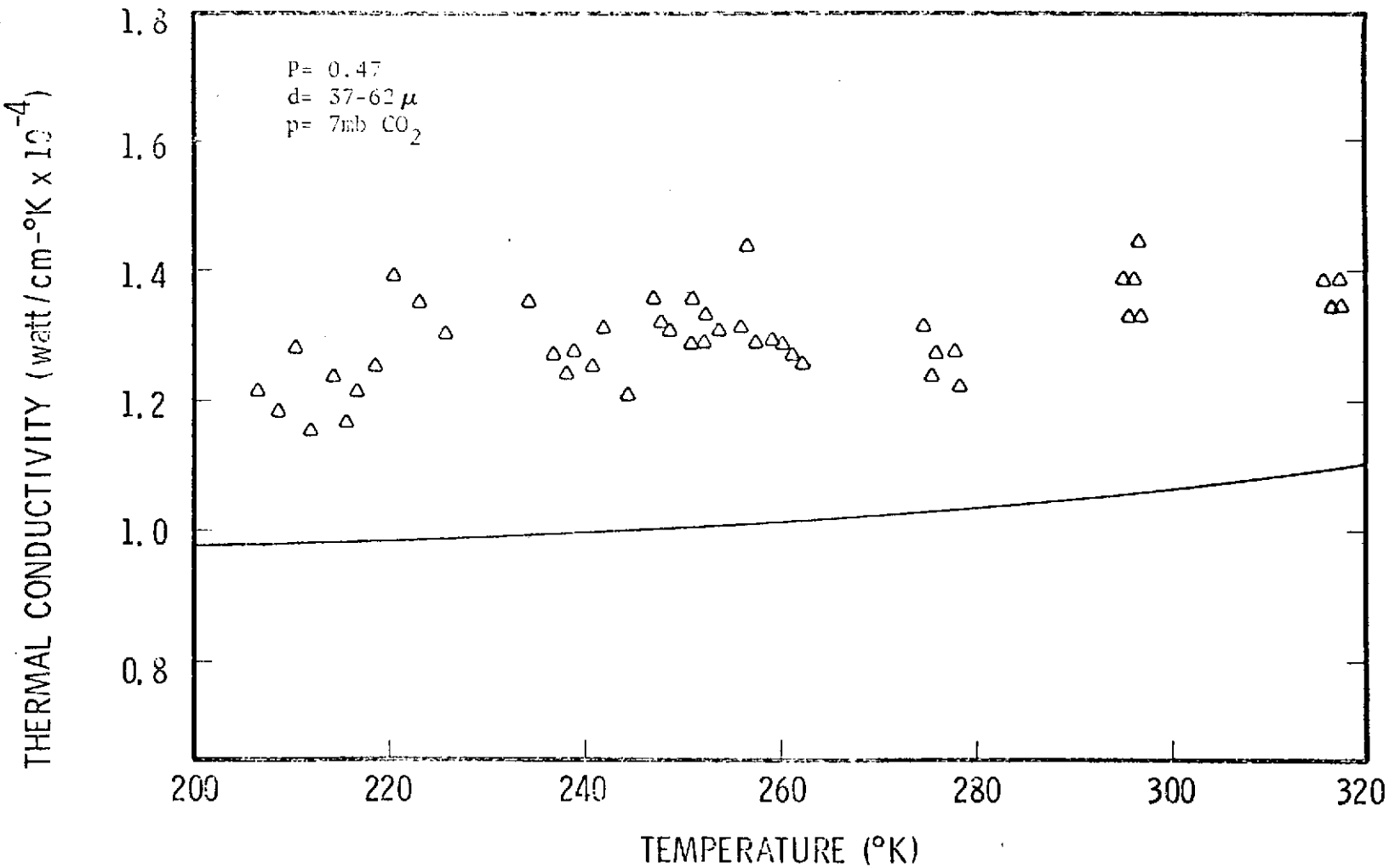

FIGURE 7-6. EXPERIMENTAL AND CALCULATED CONDUCTIVITY OF PARTICULATE BASALT IN SIMULATED MARTIAN ENVIRONMENT.

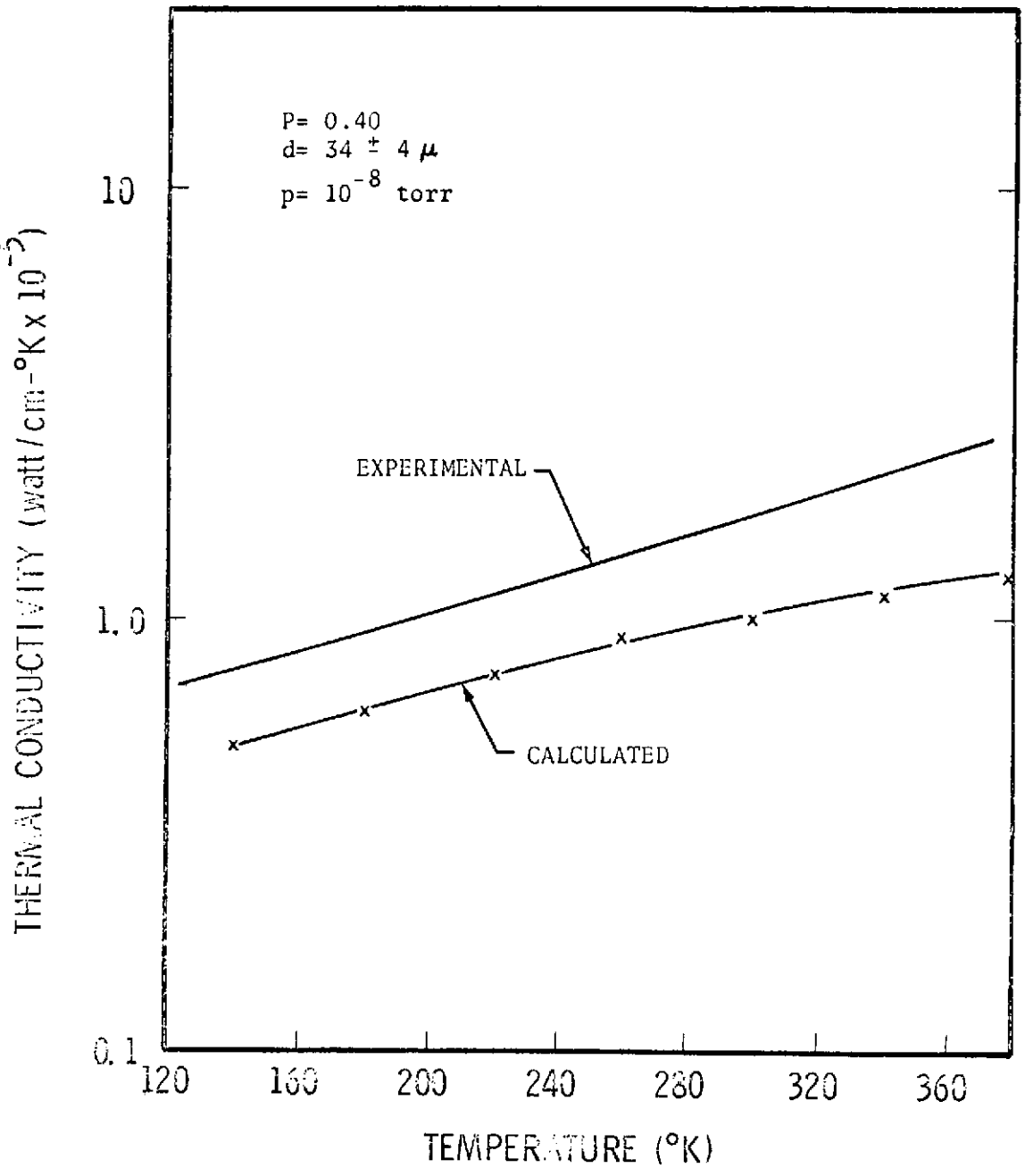

FIGURE 7-7. EXPERIMENTAL AND CALCULATED THERMAL CONDUCTIVITY OF PARTICULATE GLASS IN SIMULATED LUNAR ENVIRONMENT.

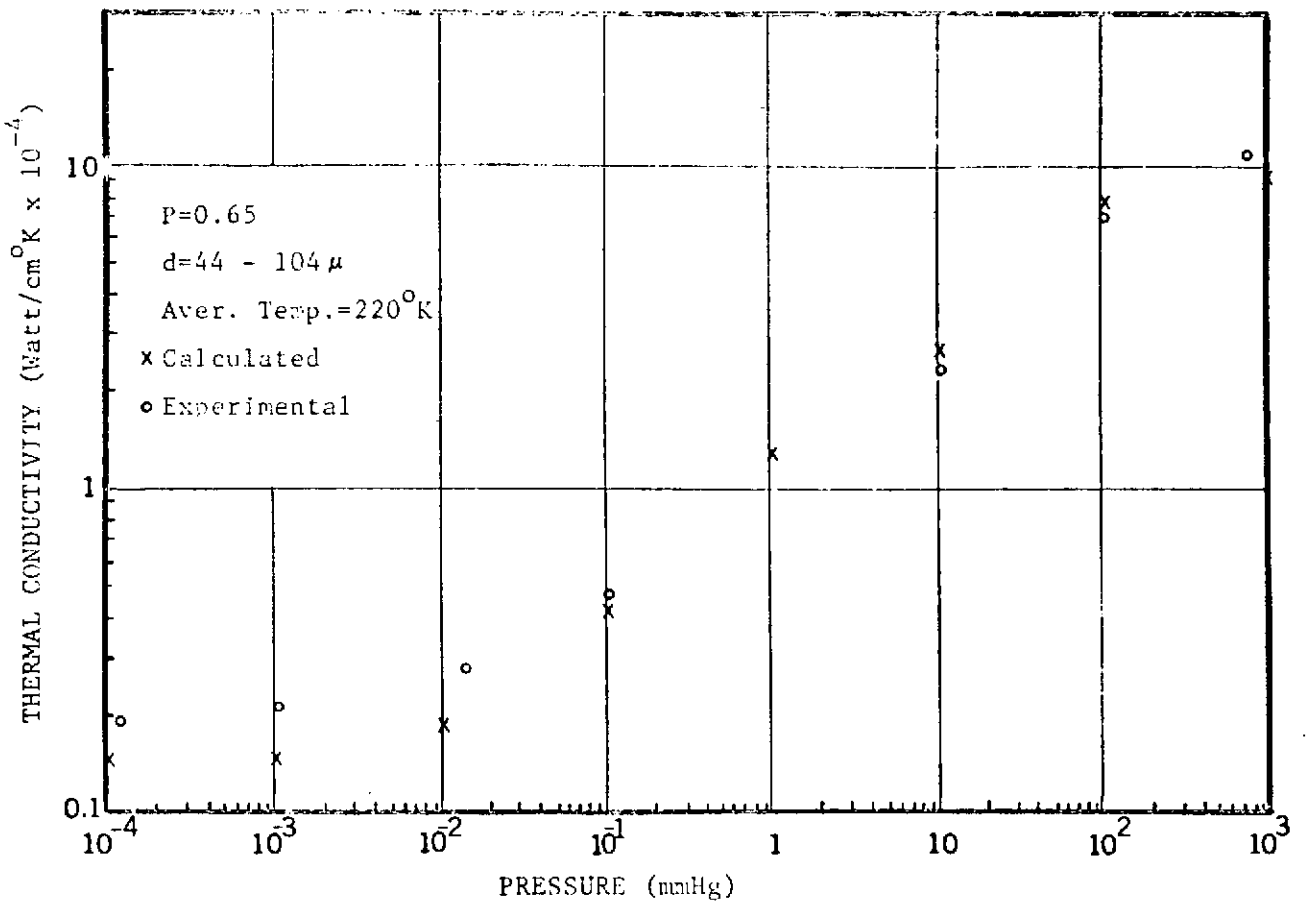

FIGURE 7-8. EXPERIMENTAL AND CALCULATED THERMAL CONDUCTIVITY OF PARTICULATE BASALT IN AIR.

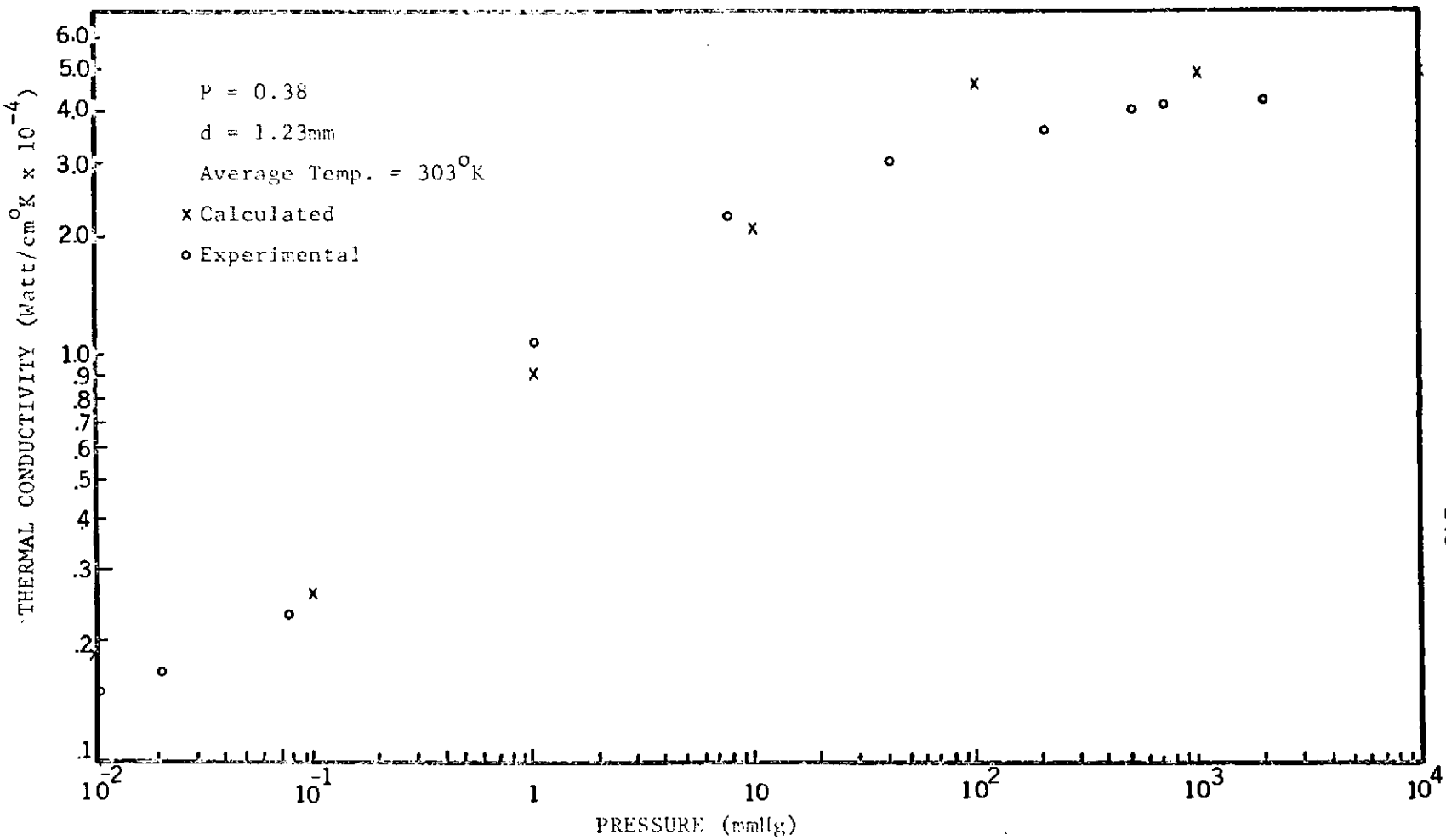

FIGURE 7-9. EXPERIMENTAL AND CALCULATED THERMAL CONDUCTIVITY OF LEAD SHOT IN AIR.

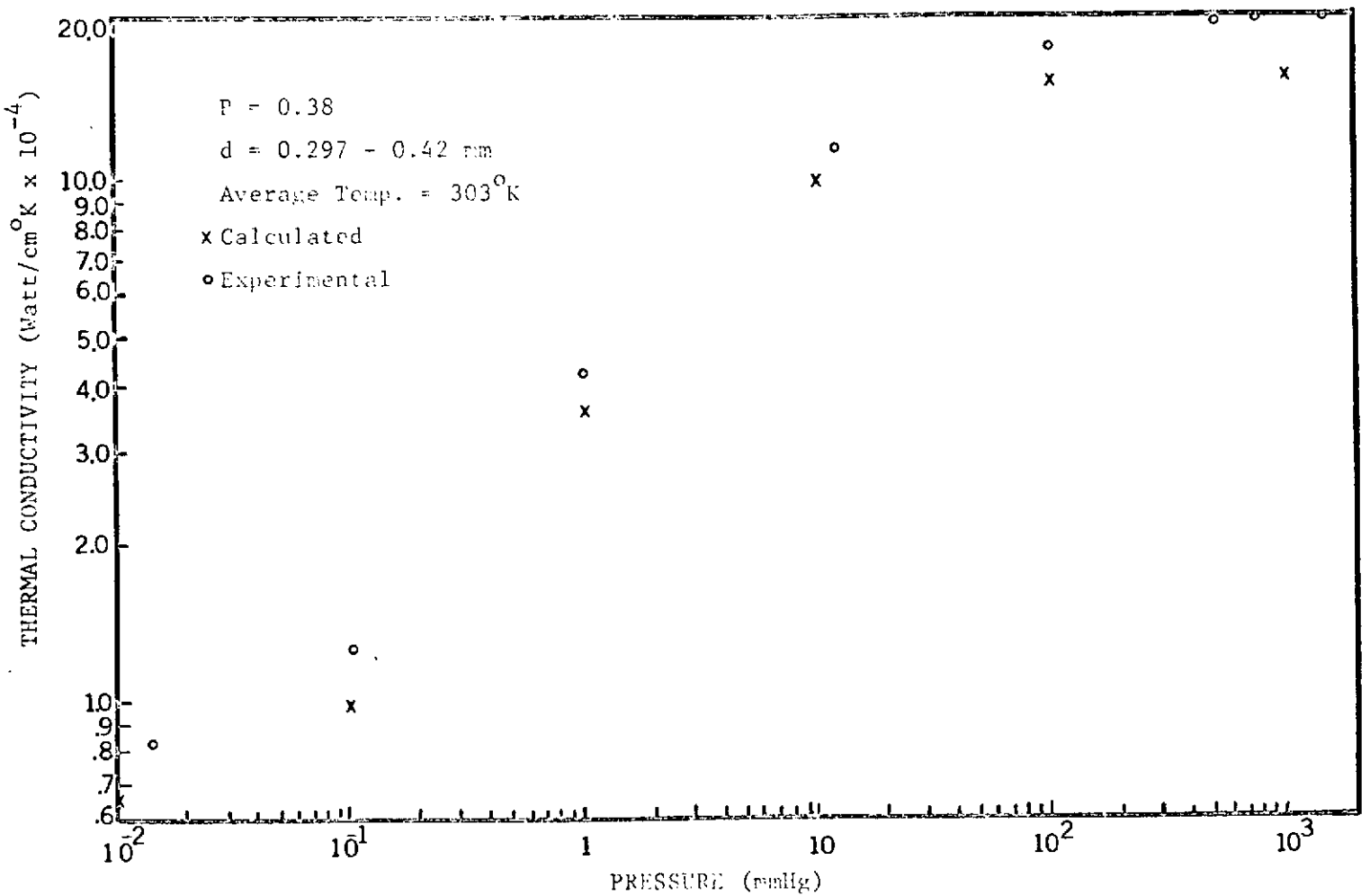

FIGURE 7-10. EXPERIMENTAL AND CALCULATED THERMAL CONDUCTIVITY OF GLASS BEADS IN AIR.

VIII. LUNAR MODEL

Introduction

Interest in the thermal conductivity of lunar soils under lunar environmental conditions has stimulated analytical and experimental research on thermal conductivity. A problem of particular interest is the effect of lunar soil depth on the effective thermal conductivity of lunar soil samples. This section presents a model for the thermal conductivity of lunar soil as a function of soil depth as measured from the lunar surface and compares values calculated using the model with experimental data.

Before a study of thermal conductivity can be undertaken on any material the character of the material must be known. The character of the lunar surface and soil has been a mystery to man until recent years when Luna 9, Ranger 7, 8 and 9, [94] Surveyor flights [95-98] microwave and radar studies [99] and the Apollo flights have in successive steps established the character of lunar soil to some degree. The results of lunar studies to date indicate:

1. the density of the lunar outermost layer is a function of depth [100, 101].
2. the soil has a particulate structure with a mean particle size of 0.1 to 1000 m [102, 103 and 119].
3. the effective thermal conductivity as determined experimentally [105] is a function of temperature and density and below

10^{-3} torr there is negligible gaseous conduction or conduction in the voids of the soil mixture.

The papers cited above suggest the lunar soil is a heterogeneous mixture and several studies on conductivity of mixtures germane to this paper can be found in the literature. The studies [45, 106 and 107] to date, however, involve the case where conduction in the gaseous voids in the mixture is not negligible whereas conduction through the points of particulate contact is neglected. The model presented herein neglects conduction in the gaseous voids and accounts for conduction at the points of particulate contact as well as radiant interchange between particles, and conduction in the particles. The model yields effective thermal conductivity values as a function of depth, temperature, porosity, particle dimension and mechanical-thermal properties of the particles.

Mathematical Model

The model accounts for conductive and radiative transfer in the mixture. Figure (8-1) depicts these modes [85] and it is seen that conduction occurs in the solid particles and at the points of particulate contact which give rise to contact resistance. Radiative transfer occurs between adjacent particles as well as between particles viewing each other through the voids.

Consider a unit cell taken from the bed at a depth Z, which has the same average bed porosity P. The unit cell has an effective area A, and height ΔZ as shown in Figure (8-2). If the system is regarded

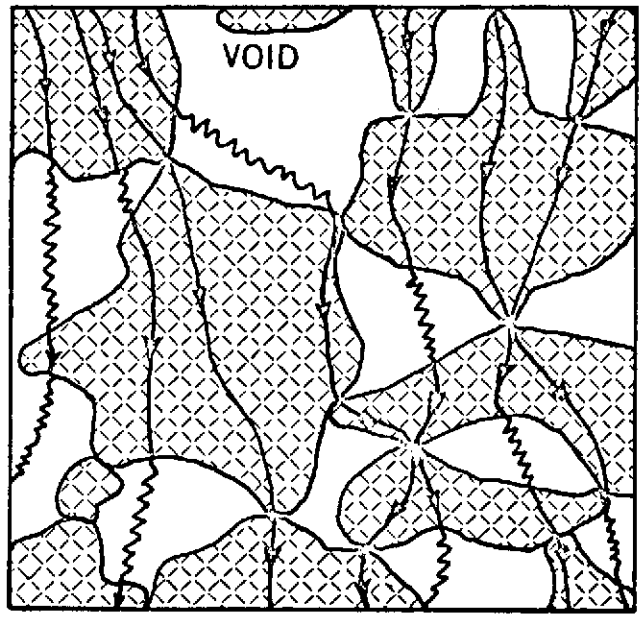

FIGURE 8-1. POSSIBLE MODES OF HEAT TRANSFER IN LUNAR SOIL.

as homogeneous, the heat flux can be expressed by Fourier-Biot relation

$$\frac{Q}{A} = - k_e \frac{\Delta t}{\Delta Z} \qquad (8\text{-}1)$$

where k_e is the effective thermal conductivity. This effective thermal conductivity is a function of

a. particle size
b. porosity
c. depth below the surface
d. solid particle mechanical-thermal properties

The heat flux equation must account for the heat transfer modes shown in Figure (8-1) and therefore the effective conductivity is the equivalent of two conductances in parallel. These two parallel conductances are

1. Conduction through and between solids consisting of
   a. conduction in the solid and
   b. conduction at the points of "particulate contact in series"
2. Radiation between surfaces.

Each of these conductances in terms of their reciprocals will be developed and then synthesized to yield the effective thermal conductivity. In order to obtain a simplified system which will permit calculations of these conductances the particles will be simulated by spheres with an effective diameter d.

Conduction Through and Between Solids

Conduction in the Solid.

The resistance in the solid is obtained from the integration of the resistance through a disk of thickness dZ, as seen in Figure (8-2).

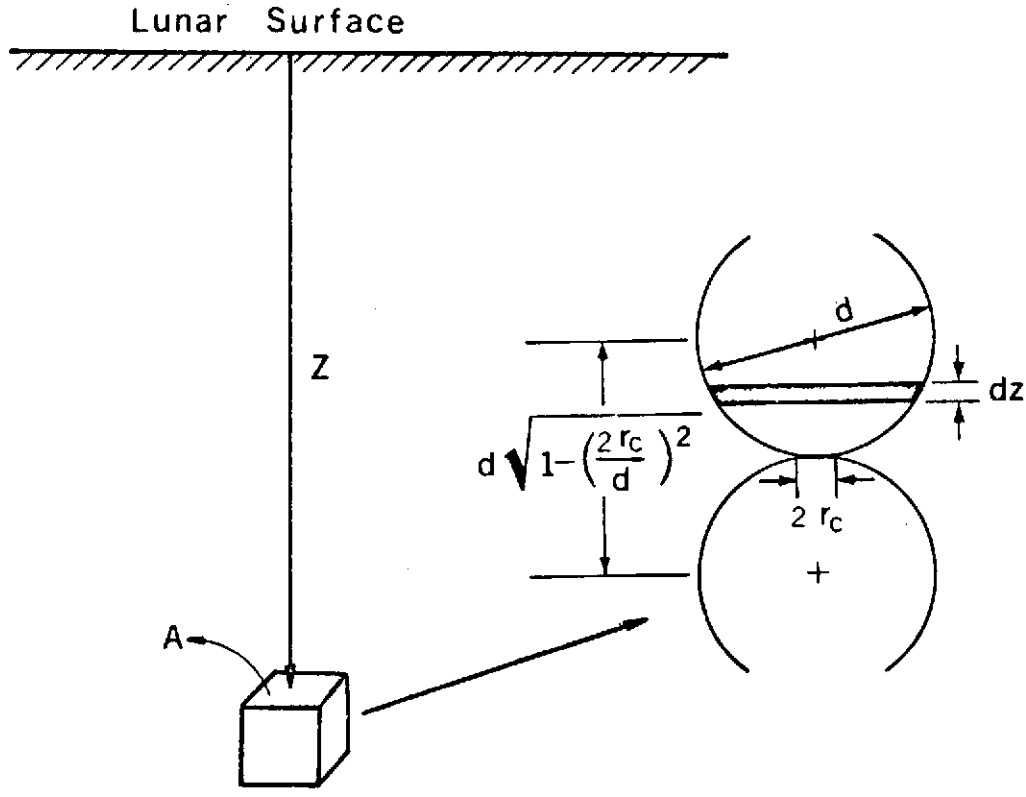

FIGURE 8-2. MODEL FOR THE STUDY OF THE THERMAL CONDUCTIVITY OF LUNAR SOIL.

Thus

$$R_1 = \int_{-Z_1}^{Z_1} \frac{dZ}{k_s \pi \left(d^2/4 - Z^2\right)} = \frac{4}{\pi k_s d} \text{LN}\left(\frac{1 + \sqrt{1 - (2r_c/d)^2}}{1 - \sqrt{1 - (2r_c/d)^2}}\right) \quad (8\text{-}2)$$

where Z is measured normal to the contact surface from the center of the sphere and $Z_1 = \frac{d}{2}\sqrt{1 - (2r_c/d)^2}$, when deformation of the particle is neglected.

Conduction at the Points of Particulate Contact

The expression for thermal resistance at the point of particulate contact can be determined from the solution of the temperature distribution using the Hankel transformation and the analysis yields the same result as that appearing in the classical work of electric contacts [108] and will not be elaborated here. The contact resistance can be written as

$$R_c = \frac{1}{2k_s r_c} \quad (8\text{-}3)$$

where r_c is the radius of the contact area and an expression for r_c will be developed later. Equation (8-3) will give erroneous results if the ratio, $2r_c/d$ is large since equation (8-3) is derived based on the assumption of a semi-infinite body. This problem can be overcome by considering the analogous case of electrostatic capacitance [109] and one can write the equation for thermal contact resistance as

$$R_c = \frac{1}{2k_s r_c}\left(1 - \frac{2r_c}{d}\right) \quad (8\text{-}4)$$

The radius of the contact area must be determined. This radius is a function of the depth of the particles below the surface of the material for the case of lunar soils. The analysis to determine the radius of the contact area was made by assuming the area of contact to be small compared with the size of the spheres. This assumption is reflected in Equation (8-4) and allows one to consider the contact area to be that of the contact between two semi-infinite solids. Also, it was assumed that the spheres had smooth surfaces. Considering material deformations to be elastic under small applied loads, Hertz's equation [110],

$$r_c = \left[\frac{3}{8} \frac{F_1 (1-\nu^2)\, d}{E}\right]^{1/3} \tag{8-5}$$

gives the radius of the contact area. F_1 is due to the weight of the particles above the contact plane. However, studies of the lunar soil density by Jones [101] show that the density is also a function of depth due to the change in material, packing and porosity. Accordingly F_1, will be given as

$$F_1 = A \int_0^Z \rho(Z)\, g\, dZ \tag{8-6}$$

where A is the effective area depending on the porosity of the material and will be determined. Substituting this relation into Equation (8-5) gives the radius of contact area as

$$r_c = \left[\frac{3d\ g(1-\nu^2)}{8E} A \int_0^Z \rho(Z)dZ\right]^{1/3} \tag{8-7}$$

with the contact area as an implicit function of the depth Z. However for paactical calculations the density function for relatively small depths of soil can be replaced by an average density, $\bar{\rho}$, to give

$$\frac{r_c}{d} = \left[\frac{3g\ A\ \bar{\rho}(1-\nu^2)}{8E\ d^2}\right]^{1/3} Z^{1/3} \tag{8-8}$$

Combining Equation (8-8) with Equation (8-4) yields the expression for contact resistance as

$$R_c = \frac{1}{k_s\ d}\left[\frac{1}{S} - 1\right] \tag{8-9}$$

where

$$S = 2\left[\frac{3g\ \bar{\rho}\ A\ (1-\nu^2)}{8E\ d^2}\right]^{1/3} Z^{1/3} \tag{8-10}$$

Radiation Between Surfaces

For beds of small sized particles in a vacuum the solid conductivity is small, however the relative contribution of radiation to the heat transfer may be quite significant even at low temperature ranges (100°K - 500°K). When radiant energy impinges on particulate media, it may be reflected, transmitted through the particles or void space, absorbed by the particles and later re-radiated or scattered by the

particle surface. In the case of small particles, scattering of radiation is likely to occur. The phenomenon of absorption is intimately tied to the physical properties of the material and is influenced by the emissivity of the particle and the "absorption cross section". Similary, the transmission of energy depends on the physical characteristics of the material. The complexity of the geometry over which these transmission processes take place is one of significant difficulty in evaluating the contribution of the radiant mechanisms. However, many investigators have analyzed radiation through porous and particulate media and obtained the effective contribution of radiation made without considering the phenomena of abosrption and scattering in detail [111]. Instead an approximate analysis is considered for evaluating the radiative transport by using the "discrete model" of Wesselink [1]

$$q_r = \frac{4\sigma_b\, e(T)\, T^3}{[2 - e(T)]} D_p \frac{\Delta t}{\Delta Z} \qquad (8\text{-}11)$$

where D_p is the mean spacing between particles and is related to the pore size. The size of a pore is difficult to specify in a system of particles in general because of the complex shapes of these particles. Even in the simplest system comprised of uniform regularly packed spheres, there is no single dimension which will characterize the cross-section of the pore. However based on Reference [1] L can be related to the porosity of the material by

$$D_p = \frac{d}{(1-P)} \tag{8-12}$$

which yields a radiative thermal conductivity component k_r, as

$$k_r = \frac{4\sigma_b\, d}{(1-P)} \; \frac{e(T)\, T^3}{[2 - e(T)]} \tag{8-13}$$

Effective Thermal Conductivity

The effective thermal conductivity compatible with Equation (8-1) can now be written remembering that the expressions for the resistance in each particle and the contact resistance are summed and the result is then taken in parallel with the resistance accounting for radiative transfer between particles. First the sum of the conductive resistances is written using Equation (8-2) and (8-9) to give

$$R_c = R_1 + R_c = \frac{1}{k_s d} \left[\frac{4}{\pi} \, LN \left(\frac{1 + \sqrt{1-S^2}}{1 - \sqrt{1-S^2}} \right) + \left(\frac{1}{S} - 1 \right) \right] \tag{8-14}$$

Equation (8-14) must be summed from 0 to Z to account for the interaction of all particles from the surface to the point in question. Thus,

$$\overline{R}_c = \frac{1}{Z} \int_0^Z R_c(Z)\, dZ \tag{8-15}$$

gives the mean conduction resistance which yields

$$k_c = \frac{\Delta Z}{A\, \overline{R}_c(Z)} = \frac{d \sqrt{1 - S^2}}{A\, \overline{R}_c(Z)} \tag{8-16}$$

for the conduction component of the thermal conductivity k_e.

The area A is determined from the unit cube shown in Figure (8-2). The porosity by definition is $1 - V_s/V$ where V_s is the volume of solid material and V is the composite volume. Since ΔZ is taken as $d\sqrt{1 - S^2}$, the area of this cube is related to the porosity by

$$P = 1 - \frac{\pi}{6} \frac{d^2}{A\sqrt{1-S^2}} \tag{8-17}$$

where

$$A = \frac{1}{6} \frac{\pi d^2}{(1-P)\sqrt{1-S^2}} \tag{8-18}$$

Equations (8-16) and (8-18) result in

$$k_c = \frac{3(1-P)\ (1-C^2\ Z^{2/3})\ k_s}{\left[\frac{\pi}{2}\left(\frac{3}{2C\ Z^{1/3}} - 1\right) + (4-1.2C^2\ Z^{2/3})\right]} \tag{8-19}$$

where

$$C = 2\left[\frac{q\ \bar{\rho}\ (1-\nu^2)}{16E\ (1-P)}\right]^{1/3} \tag{8-20}$$

Combining this result with that for the expression for the radiative thermal conductivity component, Equation (8-13) yields the effective thermal conductivity k_e as

$$k_e = \frac{3(1-P)\ (1-C^2\ Z^{2/3})\ k_s}{\left[\frac{\pi}{2}\left(\frac{3}{2C\ Z^{1/3}} - 1\right) + (4-1.2\ C^2\ Z^{2/3})\right]}$$

$$+ \frac{4\sigma_b\ d}{(1-P)}\ \frac{e(T)\ T^3}{\left[2 - e(T)\right]} \qquad (8\text{-}21)$$

Application of the Model

Equation (8-21) was compared with experimental data taken with lunar soil samples from the Apollo 11 and 12 flights. Application of the model is dependent on knowing the values of certain physical properties and characteristics of the sample to be evaluated. The only property or characteristic of the lunar soil directly measured in the Apollo experiments applicable in Equation (8-21) was the sample density. Thus the values of the other properties and characteristics had to be approximated. The approximation process was based on the similarity of lunar soil to terrestrial basalt. This similarity has been demonstrated by Snoddy et al. [112], the Surveyor alpha-scattering experiments [113] and as a result of Apollo 12 [114] studies. Table 8-I compares the major and minor elements of Apollo 12 samples and terrestrial basalt and shows that there is substantive evidence to support the approximations. The properties and characteristics selected for inclusion in Equation (8-21) were

1. Solid particles density, modulus of elasticity, solid thermal conductivity and Poisson's ratio.

   ρ = 2830 dg/m^3 Reference [64]

   E = 2.2 x 10" N/m^3 calculated from data given in Reference [115]

TABLE 8-I. COMPARISON OF MAJOR AND MINOR ELEMENTS OF APOLLO 12 SAMPLES AND TERRESTRIAL BASALT.

Element Oxide	Lunar Fines %	Basalt %
S_iO_2	47.2	51
Al_2O_3	14.3	14
Fe_2O_3	0.0	3.4
Fe O	14.2	8.8
Mg O	9.28	4.4
CaO	10.6	8.
Na_2O	0.66	3.4
K_2O	0.41	1.7
H_2O	0.0	0.86
T_iO_2	2.48	2.7
P_2O_5	0.52	1.4
M_nO	0.19	0.25
Cr_2O_3	0.32	
CO_2		0.03
S		0.004

K_s = 1.324 watt/m K Reference [64]

ν = 0.2 Reference [116]

2. Emissivity

The hemispherical emittance as function of the temperature given by Reference [121] was used. It shows that the emissivity changes from approximately 0.98 at 80 K to 0.92 at 440 K.

3. Depth-density relationship

Matveev [100] proposed a model for the relation between the density of the outermost lunar layer and the depth as

$$\rho = \rho_\infty \left[1 + \left(\frac{\rho_0}{\rho_\infty} - 1\right) \exp - \frac{Z}{Z_0}\right] \tag{8-22}$$

while Jones [101] modified this model to an approximate similar equation as

$$\rho = \rho_\infty \Big/ \left[1 + \left(\frac{\rho_\infty}{\rho_0} - 1\right) \exp - \frac{Z}{Z_0}\right] \tag{8-23}$$

where ρ_∞, ρ_0 and Z_0 are given constants [101]. Each model seems to satisfy the known physical requirements indicated by the presently available experimental data. These models together with the experimental data of Jaffe [94], Christensen et al. [97], Campbell et al. [122] were used to approximate the depth Z, for a given density.

4. Particle Diameter

Unfortunately, there is no method developed in the literature to specify the particle diameter to be used in conjunction with any theoretical model for the thermal conductivity of a natural sample of granular material with a diverse range of particle sizes. As an example, Figure (8-3) shows different arrangements A and B of six particles of two different sizes which will give different porosities and thermal conductivities while they give the same particle size distributions. It is an important fact that when the system of granular material is modeled theoretically, the size of the particle should be based on an experimental simulation of the natural sample. If, for example, one needs a representative particle diameter to calculate the thermal conductivity of a lunar sample of particle sizes from 0.1 to 1000 μm [119], one should conduct the following experiment: 1) Determine experimentally the conductivity of the lunar sample; 2) Separate the lunar sample into n samples with each of the n samples having the same particle size; 3) Determine experimentally the conductivity of each of the n samples; 4) Compare the conductivity value of the original lunar sample with each of the n samples and 5) Select a representative particle diameter for the original sample on the basis of the closest agreement of the original sample conductivity with the conductivity of one of the n samples. This diameter is then correlated to one of the statistically defined particle sizes obtained from the natural sample size-distribution data (the median, the mean, the mode, etc.). In this way, a correlation will specify the particle diameter to be used in the theoretical equation

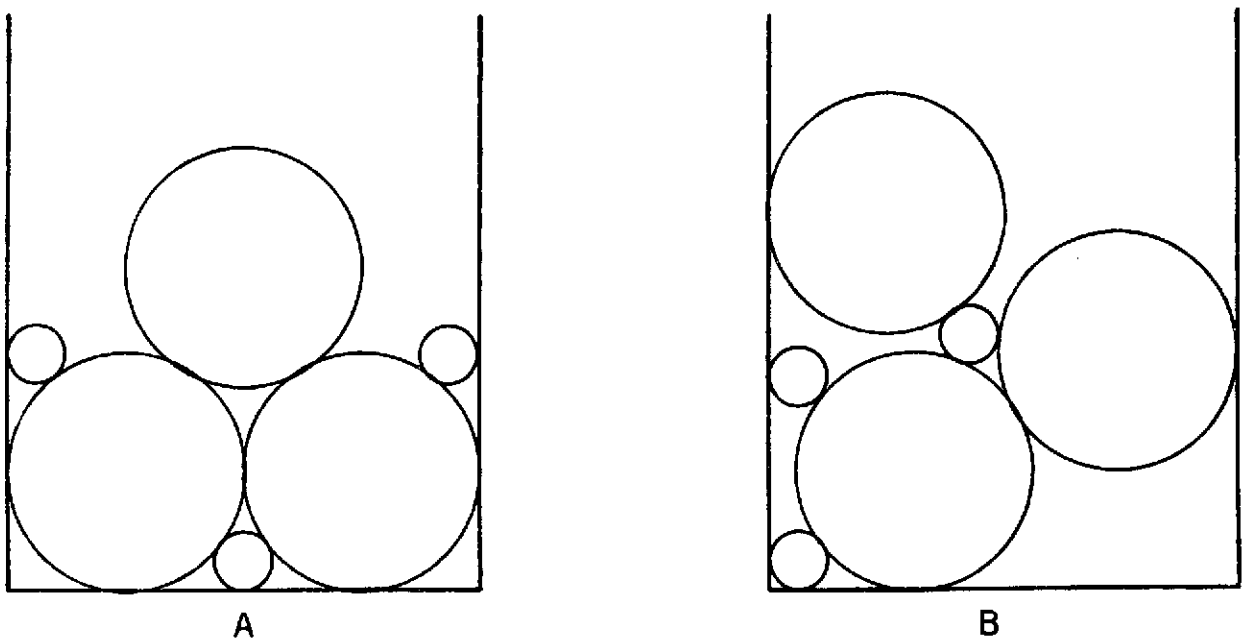

FIGURE 8-3. DIFFERENT ARANGEMENTS OF SIX PARTICLES OF TWO DIFFERENT SIZES.

for determining the thermal conductivity of any other natural sample or material in site without the necessity of performing the previously described experiment again. The experimental values of Fountain and West [123] for basalt samples of particle sizes from 37 to 62 μm diameter and density of 1.3 g/cm^3, showed fairly good agreement with lunar sample data of Apollo 11 [105] at a density of 1.265 g/cm^3. Since the range of the particle sizes of [123] is very narrow compared to the lunar material range, an average diameter of 50 μm was used in the theoretical model. It is noted that the diameter chosen is approximately in the range of the median diameter (50%) based on a weight distribution of lunar samples analyzed by [124], [125] and [126].

Values of conductivity from equation (8-21) using the aforementioned physical properties and characteristics are compared with the data from Apollo 12 lunar soil samples in Figure (8-4). The Apollo 12 data are for sample 12001/9 having a density of 1.3 gr/cm^3 as determined by Cremers and Birkebak [105]. The depth at which this density most probably would occur was calculated to be 1.02 cm. This depth was based on the average value for the depth obtained using Equation (8-22) and (8-23). The data for Apollo 11 are shown in Figure (8-5) with the results of Equation (8-21). The Apollo 11 sample had a density of 1.265 gr/cm^3 as determined by Cremers et al. [127] and this density corresponds to a lunar soil depth of .96 cm. The model is seen to give satisfactory results.

A critical evaluation of the model requires considerable

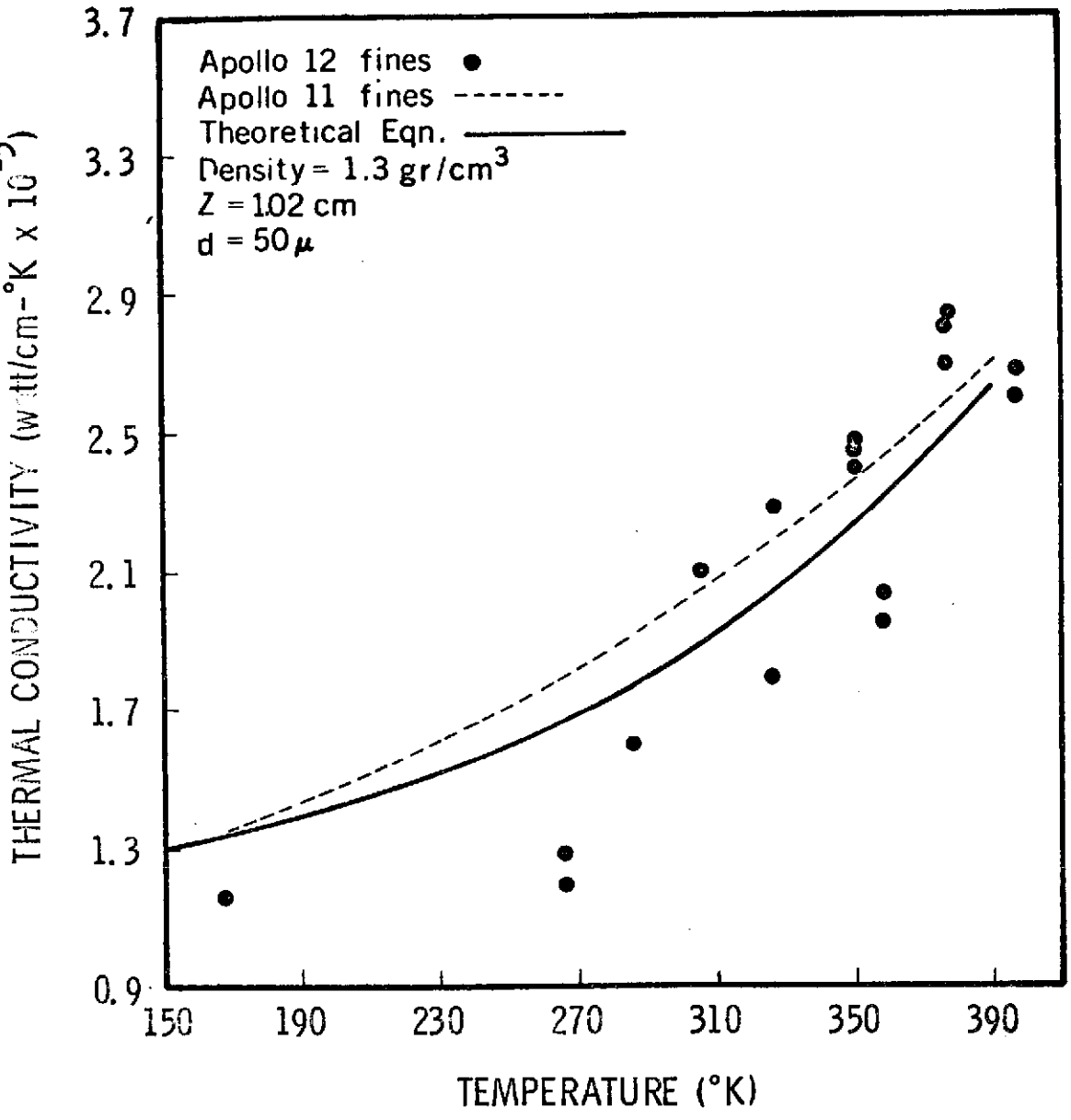

FIGURE 8-4. THERMAL CONDUCTIVITY OF APPOLO 12 FINES COMPARED WITH THE THEORY AT A DENSITY OF 1.3 GR/CM^3.

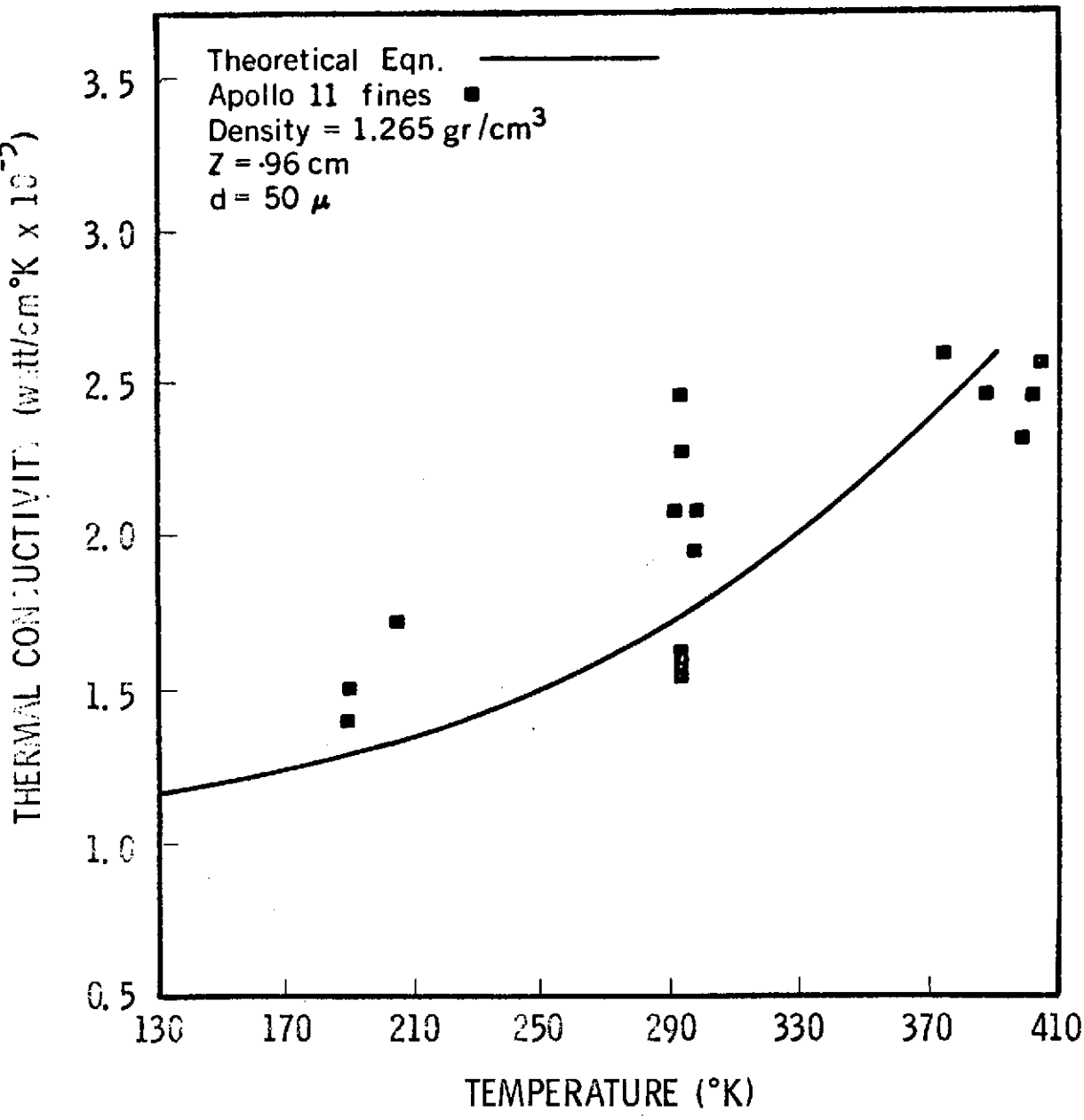

FIGURE 8-5. THERMAL CONDUCTIVITY OF APPOLO 11 FINES COMPARED WITH THE THEORY AT A DENSITY OF 1.265 GR/CM.

additional data. However the model can be examined from a number of viewpoints. Figures (8-6), (8-7), and (8-8) display thermal conductivity for lunar soils as a function of the variables. Figure (8-6) represents the behavior of the effective thermal conductivity at constant temperature as the depth and density increase. As one expects as the depth increases the contact area between particles increases due to the increase in the loading and consequently smaller thermal contact resistance results and in turn thermal conductivity increases. For fixed temperature, the effective thermal conductivity is plotted against the density for various depths in Figure (8-7). For high values of z and the density, the effective loading increases and in turn increases the effective conductivity of the soil. Figure (8-7) shows the thermal conductivity as a function of the temperature with the density as a parameter. As one notices from Equation (8-21) the dependance on the temperature is a consequence of radiation effects, which result in higher values of conductivity at high values of temperature. As seen from Figure (8-8) curves of different densities cross each other at different temperature. This is explained by the fact that the radiation in a system of small density (high porosity) is more effective than for a system of high density. Also the model indicates that radiation is a strong function of the particle diameter which was indicated by Watson [128]. Additionally Equation (8-21) shows that the effective thermal conductivity is dependent on the gravitational constant, g. Accordingly a lunar sample will possess higher values of thermal conductivity under the gravitational influence of earth, than it will under the lunar gravitational environment.

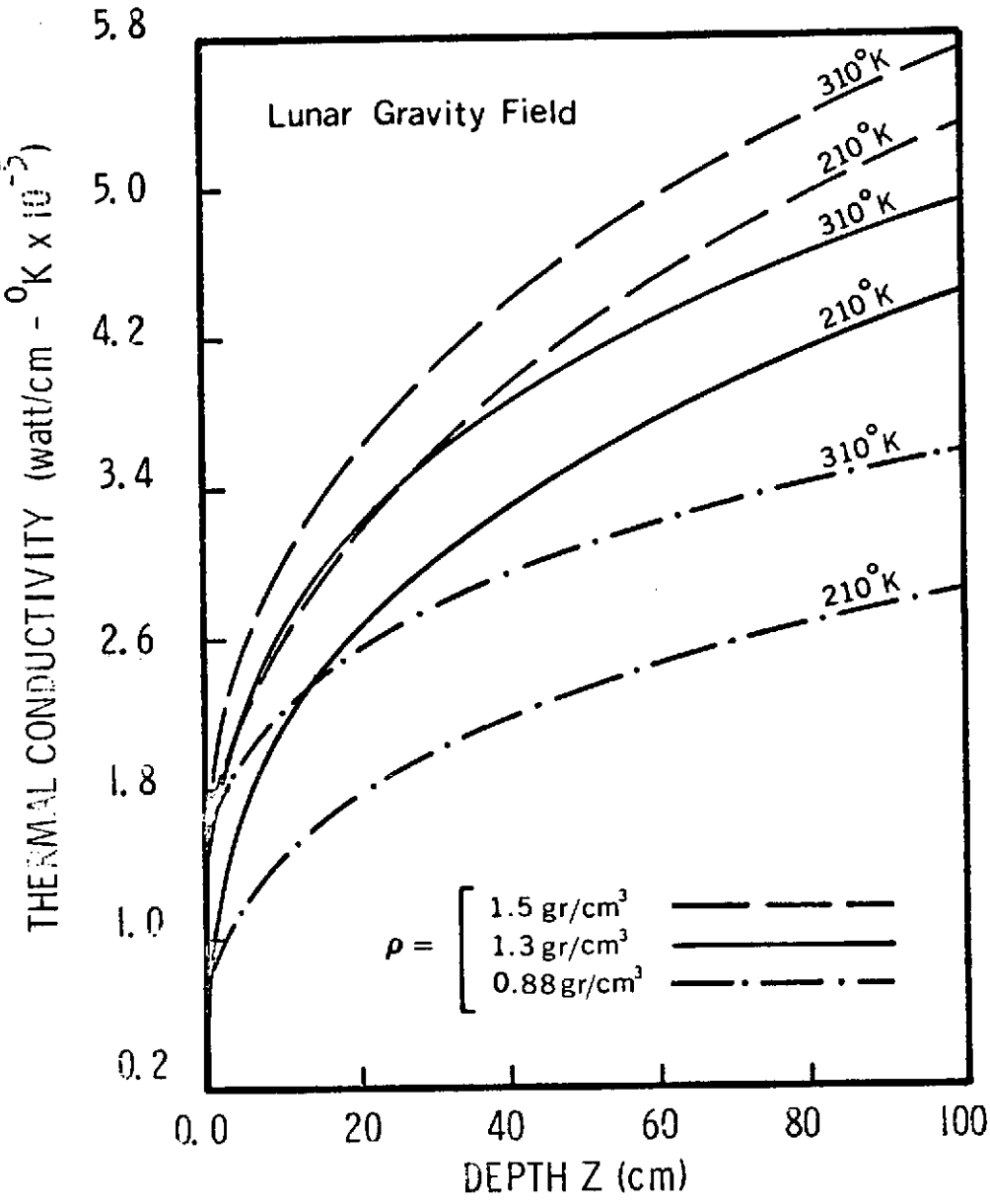

FIGURE 8-6. LUNAR CONDUCTIVITY AS A FUNCTION OF DEPTH AT CONSTANT TEMPERATURE AND DENSITY.

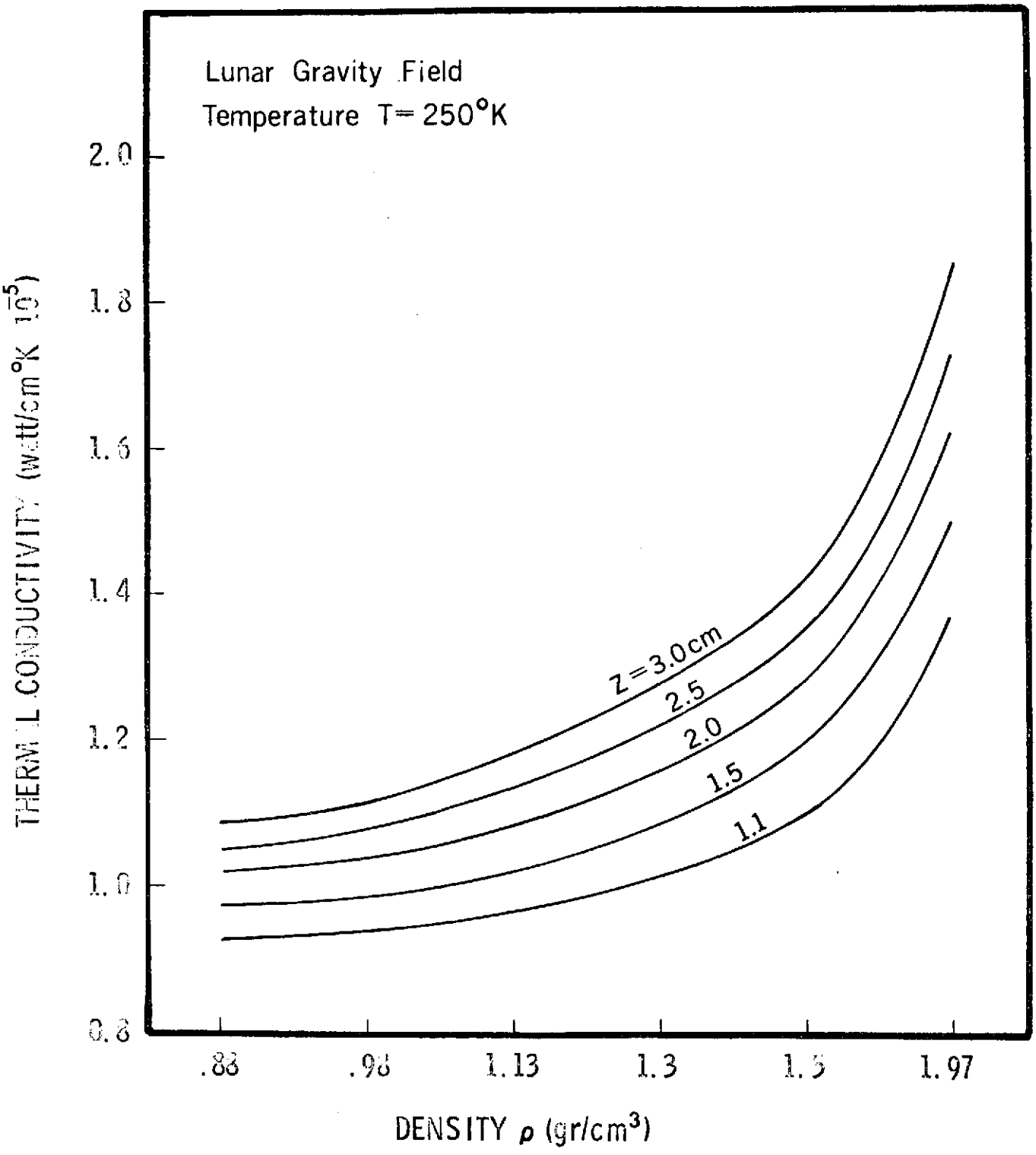

FIGURE 8-7. LUNAR THERMAL CONDUCTIVITY AS A FUNCTION OF DENSITY AT CONSTANT TEMPERATURE OF 250 K.

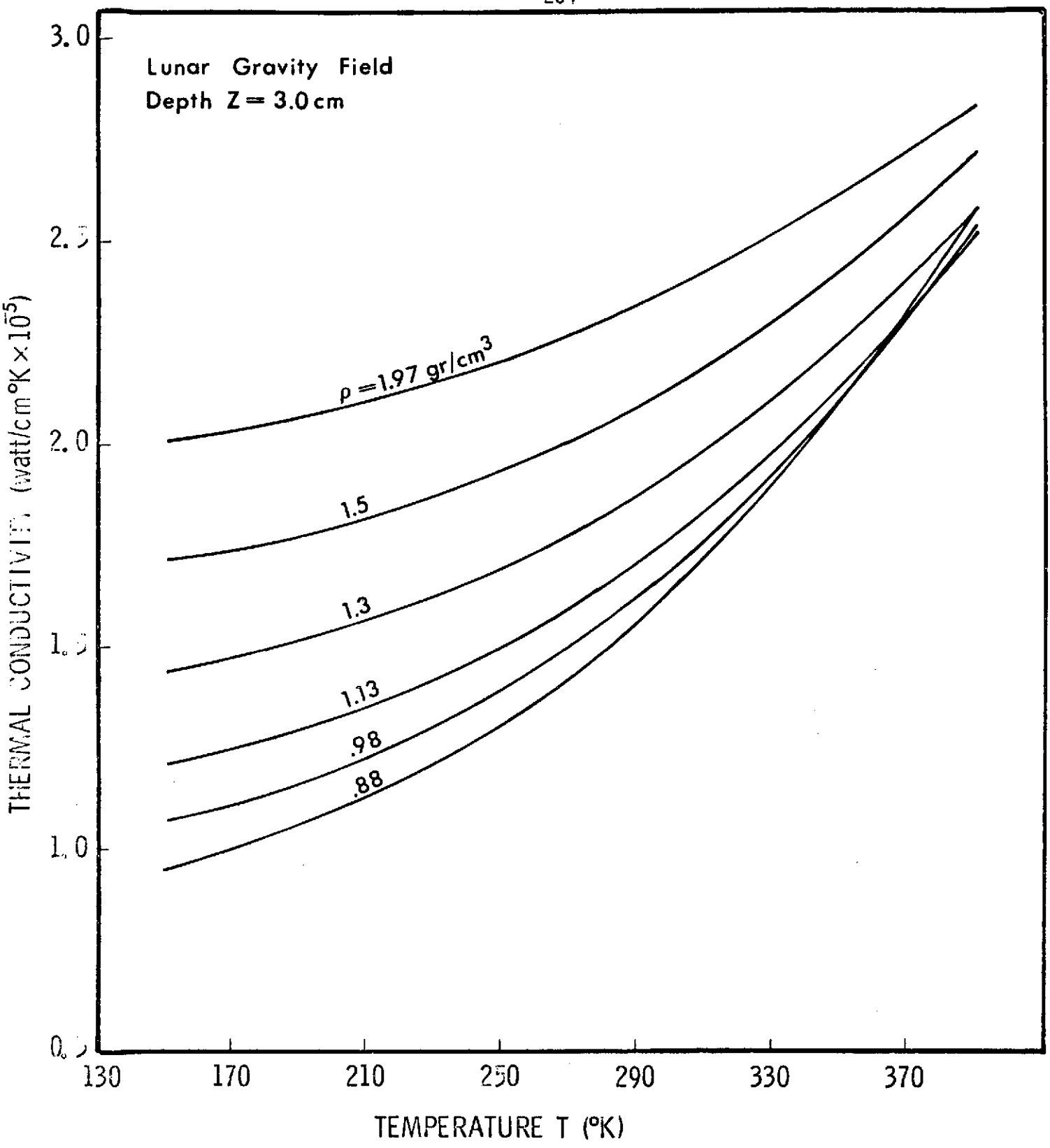

FIGURE 8-8. LUNAR THERMAL CONDUCTIVITY AS A FUNCTION OF TEMPERATURE AT CONSTANT DEPTH AND DENSITY.

The theory assumed that the particles are arranged in a simple square lattice which results in two contact areas in the direction of the heat flow, however by knowing the nature of packing of the soil, a more realistic approximation of the number of contacts can be found. With a complete analysis of the forces between particles, a more accurate estimation of the contact area can be obtained.

IX. GENERAL COMPARISON AND DISCUSSION

Four models have been developed in this study, each utilizing different propositions. The parallel isotherms model, the stochastic model, and the nodular model have been applied to a wide range of granular materials at pressures ranging from atmospheric to vacuum. The lunar model has been developed and applied specifically to granular materials at a simulated lunar environment and to lunar fines. Each of these models will now be evaluated with respect to the assumptions introduced in its development and with respect to the discrepancy between experimental and predicted thermal conductivities.

A careful review of the previously published correlations showed that the discrepancy between the analytical model and the physical granular system could be attributed to one of the following causes:

1. Failure to account for solid to solid contact;
2. Failure to utilize a realistic distribution of the two phases;
3. Failure to utilize realistic heat flow assumptions.

It is thus expected that for any new model to constitute an improvement over existing ones, these causes of failure should be eliminated. Consequently, the models presented on this study will be discussed on this basis.

The parallel isotherms model has utilized results of the packing theory to the problem of heat transfer in granular materials so that an accurate distribution of the two phases may be obtained. The description of heterogeneous materials as random mixtures of the two phases has been verified experimentally [5, 51], and has been applied by Tsao [8] to the problem of heat transfer. Two statistical parameters are introduced in the final expression for the effective conductivity, namely the mode, μ, and the standard deviation,σ, of the one dimensional porosity. The mode μ is set equal to the bulk solid fraction on the basis of physical arguments. In order to determine σ, the experimental data on the effective conductivity available from the literature have been used, and have been curve fitted to obtain σ as a function of the bulk solid fraction. Consequently in this model a realistic material distribution, as outlined in the packing theory has been introduced. In addition, good agreement between calculated and experimental thermal conductivities indicates that the unrealistic heat flow assumption has been countered by the experimentally based selection of σ.

This model has been applied to granular materials at atmospheric pressures and to basalt fines in a simulated lunar environment. For the granular materials listed in Table 6-I the average error, bias, and variance of the calculated values is 17.8%, -3.7% and 0.0236, respectively. For the data on basalt fines given by Fountain and West [3] the average error, bias and variance of the calculated values is 11.3%, -8.5% and 0.0061 respectively, as indicated in Table 9-I.

Finally, it should be noted that for granular materials at atmospheric pressures the only data required by this model is the conductivities of the constituents, and the bulk porosity of the material. At reduced pressures, the average particle diameter, the gas pressure, the gas Prandtl number, the solid emissivity and the temperature are additional required data.

The stochastic model utilizes essentially the same expressions for the distribution of the two phases in granular materials. Moreover, it is noted that the parallel isotherms and uniform heat flux assumptions are analogous to that of assuming zero and infinite resistances, respectively, normal to the direction of the bulk temperature gradient. It is then argued that since the transverse thermal conductivity of granular materials lies somewhere between the limits of zero and infinity, it follows that the true effective thermal conductivity of such materials can be represented as a weighted average of the conductivities calculated utilizing the parallel isotherms and uniform heat flux assumptions.

The standard deviation σ is still an unknown. However it has been demonstrated that as σ increases, both limiting conductivities approach a constant value which depends on the constituent conductivities and the bulk solid fraction only. As a result three correlations have been developed relating calculated conductivities to experimental data. The first is expressed as a correction factor for nonparallel isotherms, the second as a correction factor for nonuniform heat flux, and the third is a weighting factor for the bounding equations.

Consequently, the stochastic model introduces (1) at least point contact between particles, (2) a realistic material distribution as outlined by packing theory and (3) it overcomes the previous unrealistic heat flow assumptions. The model has been applied to granular materials at atmospheric pressures and to basalt fines in a simulated lunar environment. The comparison between predicted and experimental thermal conductivity values is summarized in Table 9-I. The input data required for the calculation of the effective conductivities are exactly the same as the data required for the parallel isotherms model.

In the nodular model developed in Chapter 7, the geometry of a unit cube of the heterogeneous mixture was characterized by the random distribution of the two phases. It was effectively assumed that no cubicle is more likely to be occupied by the solid phase than another. Further, it was noted that application of the three-dimensional Fourier conduction equation to each cubicle simply requires that the temperature of each cubicle remain constant. The cubicles were then lumped into nodes, connected with the neighboring nodes by resistances, the value of which depends on the conductivity of the neighboring nodes. Contact resistance was included in all cases, and radiant conductivity was included only for granular materials at reduced pressures. A heat balance equation was then written for each node, and this system of equations was solved by a successive overrelaxation technique, superimposing on it an iterative scheme, to determine the temperature of each node. Finally, the heat flow in each lamina perpendicular to the mean heat flow direction was determined, and the mean heat flow value in conjunction

with the Fourier-Biot law were used to find the effective thermal conductivity of the heterogeneous mixture.

It is evident that in this manner all causes contributing to the failure of previously published models have been eliminated since this model introduces (1) solid to solid contact resistance, (2) realistic distribution of the two phases based on the packing theory and (3) realistic three-dimensional heat flow as defined by the Fourier equation for steady-state heat conduction. The model has been applied to granular materials for pressures ranging from atmospheric to vacuum, and the comparison between predicted and experimental thermal conductivity values are summarized in Table 9-I. In addition to the input data required by the previous models, knowledge of the depth, density of the solid phase, Young's modulus and Poisson's ratio of the solid particles is required.

As is has already been mentioned, for granular materials "in vacuo" the modes of heat transfer are

1. Conduction in the solid particles;
2. Conduction at the contact areas between particles;
3. Radiation between particle surfaces.

The lunar model developed in Chapter 8 has synthesized these modes to yield the effective thermal conductivity. For the mathematical analysis of the model a regular array of spherical particles was assumed, and the calculation of the conduction in the solid particles was based on parallel isotherms. Further, the effect of depth on the effective thermal conductivity of granular materials was included both in the calculation

of the contact resistance, and through published expressions correlating the density of lunar fines to the depth from the surface of the moon. Thus, the final expressions include both the effect of lunar soil depth and the effect of temperature on the effective thermal conductivity of lunar fines.

The lunar model has been applied to Apollo 11 and 12 lunar fines. Comparisons between predicted and experimental conductivity values are summarized in Table 9-I.

Although the models presented in this study are applicable, and have been applied to granular materials over a wide range of environments, there exists a number of limitations due to the assumptions introduced in the development of the models. The causes of these limitations will now be discussed.

1. Phase distribution - The geometry of three of the models has been based on the assumption that irregular packed beds can be considered as a random mixture of the two phases. It has been shown [49, 50, 51] that for granular materials in which the particle sizes are not much different, and in which the particles can be approximated by spheres, this is a valid assumption. That is, for such beds, the distribution of the local bed properties can be approximated by a normal distribution. For packed beds consisting of irregularly shaped particles no generalized conclusions have been reached in the literature concerning the distribution of the local properties. It has been shown, however, that the geometry of packed beds of irregularly

shaped particles does not satisfy the randomness criteria when the particle size distribution is narrow [51]. It is therefore possible that the geometry of certain classes of granular materials is different than the assumed geometry.

2. Particle size distribution - Calculations for the unit cube size, pore size, etc. have been based on a characteristic particle size. For packed beds in which the particle size distribution is narrow, it has been assumed by all models in this study that the characteristic particle size is equal to the mean volume diameter [66]. However, no set method exists in the literature for calculating the characteristic particle size for beds having a broad particle size distribution. Further, as indicated in Chapter 8 and in Appendix F the mean volume diameter is not a satisfactory description of the characteristic particle size for such beds.

3. Particle shape - The geometrical parameters utilized in the development of the models such as pore size, coordination number, etc., and the equations for contact resistance have been based on equations given in the literature for randomly packed beds of equal sized spheres. It follows that none of the models presented in this study is applicable in the case of heterogeneous mixtures containing highly irregular shaped particles such as Rashing rings, Berl saddles, etc.

4. Solid-liquid heterogeneous mixtures at high temperatures - The equations for the radiant conductivity used by all models have been based on the assumption that the medium in the voids is transparent.

Consequently, when the continuous phase in the voids is a liquid these equations are not valid, and radiant conductivity cannot be taken into account.

5. Convection - As indicated in the Introduction, convection heat transfer in the voids has been neglected. Consequently, the models of this study are only applicable on stagnant packed beds.

6. Anisotropy - In all models of this study, granular materials have been treated as equivalent homogeneous and isotropic single phases, so that no change in the thermal conductivity with direction is predicted. The assumption of random mixtures of the two phases justifies this treatment. It appears that for such systems, the only factor contributing to the variation of the thermal conductivity with direction is the pressure tensor, and consequently the different values of the contact resistance in the vertical and horizontal directions. This case has not been examined in this study.

7. Wall effects - As indicated in [49] and [120] both the local property variation, and the thermal conductivity of heterogeneous mixtures change at short distances from the walls of the container. Again, this case has not been examined in this study.

It can be seen that all limitations are basically due to two factors: (1) Insufficient knowledge of the geometric configuration of packed beds and (2) insufficient knowledge of the parameters associated with radiation heat transfer in packed beds. All assumptions introduced in the development of the models is an attempt to circumvent these difficulties in such a manner that the models constitute a

realistic approximation to the actual physical phenomena.

A comparison between Tables 9-I and 9-II indicates that for granular materials at atmospheric pressures the models presented in this study are generally more accurate than previously published models. This is probably due to the attempt undertaken in this study to combine a realistic geometry with realistic heat flow. It is also a strong indication that the flexible random phase distribution constitutes a better approximation to the actual geometry of granular systems than the fixed arrangement of spherical or near spherical particles utilized by previously published models.

Table 9-I also indicates that for granular materials at reduced interstitial gas pressure, thermal conductivities predicted by the models of this study are generally low. The sources of error are as follows:

1. Exclusion of pure radiation heat transfer at very low pressures;
2. Low calculated values for the contact resistance;
3. Deviation of the actual distribution of the two phases from the assumed random phase distribution.

As indicated in Appendix B, lack of experimental data on the extinction coefficient of granular materials prohibits an exact analysis of the radiation heat transfer process. As a result, only radiation heat transfer between particle surfaces has been included in the models. As indicated in [84, 85] this is a sufficiently accurate approximation when the solid particles are opaque to thermal radiation, but results in low calculated values for packed beds of particles having small

diameters. Consequently, since at very low pressures radiation is a dominant mode of heat transfer, exclusion of pure radiation heat transfer results in low calculated values for the effective thermal conductivity of packed beds.

For all models, the calculated thermal conductivities at low pressures and low temperatures are consistantly lower than the experimentally determined thermal conductivities. Since under these conditions the dominant mode of heat transfer is through contact areas between particles, the only explanation for this behavior is that the calculated values for the contact conductances are low. It should be noted that low calculated contact conductances influence the effective thermal conductivity only at low pressures and temperatures. At higher pressures and temperatures, and in particular at atmospheric pressures, the calculated effective thermal conductivity is relatively insensitive to the contact conductance.

Finally, it is noted that although at reduced pressures the calculated effective thermal conductivities are generally low, the slope of the calculated thermal conductivity versus pressure curves is in very good agreement with experimental data. Since for a major portion of these curves the only variable is the thermal conductivity of the interstitial gas, it can be concluded that Kennard's Equation (A-1) combined with the experimentally determined effective pore size given by Equation (D-6) yield accurate results for the variation of the gas conductivity with pressure. Consequently, as indicated in Appendix D, the conduction effective pore size is much smaller than the geometric pore size.

TABLE 9-I

AVERAGE ERROR, AVERAGE BIAS AND ERROR VARIANCE

BETWEEN PREDICTED AND EXPERIMENTAL THERMAL

CONDUCTIVITY VALUES FOR ALL MODELS OF THIS STUDY

	Average Error %	Average Bias %	Error Variance
1. Parallel Isotherms Model			
a. Granular Materials at Atmospheric Pressures (Table 6-I)	17.8	-3.7	0.0236
b. Simulated Lunar Data	11.3	-8.5	0.0061
2. Stochastic Model			
i. Equation (6-16)			
a. Granular Materials at Atmospheric Pressures (Table 6-I)	30.1	25.3	0.0707
b. Simulated Lunar Data	24.8	-22.1	0.0131
ii. Equation (6-17)			
a. Granular Materials at Atmospheric Pressures (Table 6-I)	27.7	20.9	0.0558
b. Simulated Lunar Data	25.8	-23.4	0.0260
iii. Equation (6-18)			
a. Granular Materials at Atmospheric Pressures (Table 6-I)	32.3	23.1	0.0956
b. Simulated Lunar Data	41.8	-17.2	0.0333
3. Nodular Model			
a. Granular Materials at Atmospheric Pressures (Table 7-I)	15.8	-5.8	0.0163
b. Granular Materials at Reduced Pressures	18.5	-5.1	0.0157
c. Simulated Lunar Data	15.9	-15.9	0.0870
d. Simulated Martian Data	20.8	-20.8	0.0210

TABLE 9-I. Continued

4. Lunar Model			
a. Apollo 11 Lunar Fines	13.7	-6.8	0.0044
b. Apollo 12 Lunar Fines	12.8	5.1	0.0090

TABLE 9-II

AVERAGE ERROR, AVERAGE BIAS AND ERROR VARIANCE BETWEEN PREDICTED AND EXPERIMENTAL THERMAL CONDUCTIVITY VALUES FOR GRANULAR MATERIALS AT ATMOSPHERIC PRESSURE (TABLE 6-I)

	Average Error %	Average Bias %	Error Variance
A. Flux Law Models			
1. Maxwell	40.2	-37.9	0.0606
2. Lord Rayleigh	33.7	-24.8	0.0594
3. Meredith and Tobias	34.4	-18.7	0.0416
4. Bruggeman	32.9	23.8	0.1540
5. Modular Model (this study)	15.8	-5.8	0.0163
B. Uniform Heat Flux Models			
1. son Frey	45.1	-43.8	0.0599
2. Woodside and Messmer	34.8	20.9	0.0992
3. Kanager	18.9	-6.7	0.0286
4. Gorring and Churchill	20.0	-10.7	0.0192
5. Willhite, Kunii & Smith	17.8	-3.6	0.0268
6. Schumann and Voss	25.8	-21.1	0.0260
7. Preston	30.5	26.6	0.0875
8. Wilhelm et al	19.7	-2.1	0.0373
9. Krupiczka	21.2	13.2	0.0693
10. Equation (6-16) (this study)	30.1	25.3	0.0707
11. Bernstein	686.1	677.9	85.05
C. Parallel Isotherm Models			
1. Russell	35.0	-30.3	0.0566
2. Woodside	670.4	670.3	55.16
3. Equation (5-2) (this study)	17 8	-3.7	0.0236
Equation (6-17) (this study)	27.7	20.9	0.0558

TABLE 9-II. Continued

D. Weighted Ohm's Law Models			
1. Lichtenecker 3-D	701.2	701.1	48.70
2. Lichtenecker 2-D	195.0	194.5	2.98
3. Equation (6-18) (this study)	32.3	23.1	0.0956

X. CONCLUSIONS AND RECOMMENDATIONS

The problem of predicting the effective thermal conductivity of heterogeneous mixtures has received the attention of numerous investigators over the past sixty years. Unfortunately, the complexity of the mechanisms contributing toward heat flow is such that no truly satisfactory model has been obtained. The continued proliferation of alternate models attests to these difficulties. The scope of this study has been to utilize all available information on the subject and extend the analytical techniques of predicting the variable thermal conductivity of heterogeneous mixtures over as wide a range of environments as possible.

Initially a study was made of the published models with respect to the geometry and heat flow assumptions utilized by each one. Further, a number of published equations for the effective thermal conductivity were applied to a large group of granular materials, and the results were evaluated in relation to the geometry and heat flow assumptions utilized in the development of each equation. The results of this analysis can be summarized in that the sources of error in the predicted thermal conductivities can be attributed to one or more of the following causes:

1. Failure to account for solid to solid contact;
2. Failure to utilize a realistic distribution of the two phases;
3. Failure to utilize realistic heat flow assumptions.

It was therefore concluded that for any new model to constitute an improvement over existing ones, these causes of failure should be eliminated.

Since the possibility of assuming that the heat flow process in granular materials is approximately linear simplifies considerably the problem of heat transfer, this possibility was examined separately for random heterogeneous mixtures having a realistic phase distribution. The analysis presented in Chapter 4 resulted in the conclusion that a parallel isotherms assumption yields too high values for the effective thermal conductivity whereas a uniform heat flux assumption yields values that are too low. Also, the error in the predicted thermal conductivity increases rapidly with the ratio of the constituent conductivities. Consequently, either no assumption should be made regarding the flow of heat in granular materials, or weighting factors should be associated with the linear heat flow assumptions.

Four models have been developed in this study, each utilizing different approximations regarding the geometry and the flow of heat in granular materials. In the development of the models the most recent results of the packing theory have been used regarding the distribution of the phases, effective pore size, coordination number etc. The resulting equations enable one to calculate the effective

thermal conductivity as a function of interstitial gas pressure, temperature and loading conditions. These models have been successfully applied to large groups of granular materials and the results are summarized in Table 9-I. Comparison between Tables 9-I and 6-VII indicates that these models constitute a considerable improvement over previously published models. The error in the effective thermal conductivity values predicted by the equations developed in this study can be attributed to the following causes:

1. Exclusion of pure radiation heat transfer at very low pressures;
2. Low calculated values for the contact resistance;
3. Deviation of the actual distribution of the two phases from the assumed random phase distribution;
4. Uncertainty regarding the mean particle size in cases of granular materials having broad particle size range.

The reason it is not possible to eliminate these sources of error at this time is lack of experimental evidence. However, once more accurate expressions are found, they can be readily incorporated in the models. In spite of the above mentioned limitations to the accuracy of the models, it is now possible to predict the effective thermal conductivity of granular materials over a wide range of environments with a high degree of confidence, as attested by the successful application of the models to large groups of heterogeneous mixtures. It is evident from the discussion of the previously published models, and from the models presented in this study that the most serious drawbacks in the analysis of the thermal conductivity of heterogeneous mixtures are (a) a sufficiently accurate description

of the geometry of granular materials and (b) the radiation heat transfer process. Since the effective thermal conductivity of granular systems is very sensitive to the conductivity of the gaseous phase, it is expected that knowledge of the mean void volume and void volume distribution should provide accurate calculated thermal conductivities. Towards this end, an analysis is presented in Figure 10-1. This analysis is based on a unit cube of a heterogeneous mixture, and is similar to the analysis of the nodular model.

The geometry of a representative unit cube can be defined from the sectioned void area distribution and the void volume distribution. The mean sectioned void area and the sectioned void area distribution are required to determine the distribution of the two phases on the six faces of the unit cube. The mean void volume and void volume distribution are required so that the number of voids in the unit cube can be calculated and distributed in such a manner that the porosity of the unit cube is equal to the bulk porosity of the granular material. The size of the unit cube will be determined from the particle size distribution. As a result, each cubicle in the unit cube will be occupied either by the continuous or the discontinuous phase.

The next step is to define the resistance between nodes. This can be done first in terms of the conductivity of the two phases. Then, to account for contact resistance between particles, a number of resistances equal to the contact resistance replaces an equal number

of already determined resistances between solid cubicles. These resistances are randomly distributed and oriented, and their number is given by the unit cube size and the coordination number. It is important to note at this point that the geometric parameters such as coordination number, etc. published in the literature have been determined for packed beds constructed of equally sized particles. Consequently a mean particle size must be determined from the particle size distribution of the granular material in question. However, as indicated in Appendix F, no such procedure has been found up to now for packed beds containing broad particle size distribution.

Once the geometry of the unit cube and the resistance between nodes have thus been defined, it is possible to determine the temperature distribution in a manner similar to the nodular model. Then, the conduction heat flux in the mean heat flow direction can be determined from the summation of individual heat fluxes between cubicles.

As indicated in the Introduction, the concept of an effective thermal conductivity consistent with the Fourier-Biot Law necessitates that the granular materials be considered as pseudo-homogeneous systems, in which case the volume of the granular material is assumed large with respect to the volume of individual grains. For such granular systems the photon mean free path is expected to be small compared to a linear dimension of the system, and consequently only thermal radiation in the optically thick limit need to be considered. In this case, according to the analysis presented in Appendix B, first the conduction heat transfer and radiation heat transfer processes can be

separated, and second the radiative heat flux can be related to the effective extinction coefficient by a simple equation. Finally, the total heat flux in granular materials is the sum of the conduction heat flux and radiation heat flux, and the effective thermal conductivity of the system can be determined from the Fourier-Biot Law.

An approximate method, similar to the one described in Figure 10-1, is presented in Figure 10-2. The only difference between the two methods is the inclusion of the radiation heat transfer process. That is, recognizing that the determination of the extinction coefficient of granular materials is an extensive and difficult task, in the method of Figure 10-2 only radiation heat transfer between particle surfaces and radiation heat transfer in solid particles are considered.

Summarizing, it has been shown that any future attempt to develop more refined models for the calculation of the effective thermal conductivity of granular materials should be based on a realistic approximation of the geometry and radiation heat transfer. In particular, it is suggested that the following experimental program be undertaken.

1. Determination of the void volume distribution and the sectioned void area distribution in terms of the particle size distribution, particle shape and porosity. The work of Debbas and Rumpf [51] is a step in the right direction, but the number of cases examined is not sufficient to justify any generalized conclusions. It is therefore suggested that experimental work, similar to the one described in Reference [51] be undertaken and extended to granular systems composed

of equal sized particles, narrow particle size distribution and broad particle size distribution.

2. Experimental work to determine the extinction coefficient of specific granular systems similar to the one described by Bastin et al [85], or experimental work to determine the radiation heat transfer in solid particles of various sizes similar to the one described by Merrill [118].

3. It is evident from Figure E-1 that the range of porosities for which the coordination number of spherical particles has been experimentally determined is too narrow to justify any of the correlations suggested in the literature. Consequently, further experimental work is required for the determination of the coordination number over a wider range of porosities. Also the coordination number of irregularly shaped particles should be determined and compared to that of spheres, so that more accurate expressions can be found for the number and distribution of contact areas in granular materials.

Experimental work on the areas mentioned above is not only essential for the analysis of the thermal conductivity of stagnant packed beds, but will also be a tremendous contribution to analytical work on fluid flow through packed beds and heat transfer in packed beds with fluid flow.

A problem that has been identified in this study is the selection of a mean particle diameter for packed beds consisting of a broad

particle size distribution. As indicated in Chapter 8 and Appendix F, the solution of this problem is solely based on experimental evidence. However, due to this problem, the majority of the models of this study have been applied to random packings of equal size spheres, and to granular materials composed of narrow particle distribution only.

Finally, it should be noted that no anisotropy of thermal conductivity has been considered in this study. However, it is possible to include the variation of the thermal conductivity in granular materials in the horizontal and vertical directions by considering the change of the contact pressure between particles in the horizontal and vertical directions. As indicated in Reference [86] the pressure tensor in a granular material can be written as

$$p_{ij} = p_o \delta_{ij} + p_1 z_i z_j \tag{10-1}$$

where p_o, p_1 are constants and z_i are the components of a unit vector in the direction of the applied load. It follows that the pressure in the direction of the applied load is

$$p_v = p_o + p_1 \tag{10-2}$$

while in the horizontal direction it is

$$p_n = p_o \tag{10-3}$$

When the granular material is loaded under its own weight

$$p_\nu = g\int_0^D \rho(z)\, dz \tag{10-4}$$

Assuming that the expansion of the granular material is constrained in the horizontal direction it follows that

$$p_n = \frac{\nu}{1-\nu}\ p_\nu \tag{10-5}$$

Combination of Equations (10-2) through (10-5) determines p_ν and p_n in terms of density and depth. Then, p_ν can be used in the determination of the contact resistance in the direction of the applied load and p_n in the determination of the contact resistance in the horizontal direction. As a result, the temperature distribution and consequently the effective thermal conductivity will be different when the mean heat flow direction is the direction of the applied load and when the mean heat flow direction is the horizontal.

It is evident that the variation of the thermal conductivity in the two directions will be significant only in the case of granular materials at low pressures because only in this case variation of the contact resistance will affect detectably the calculated effective thermal conductivity of the granular system.

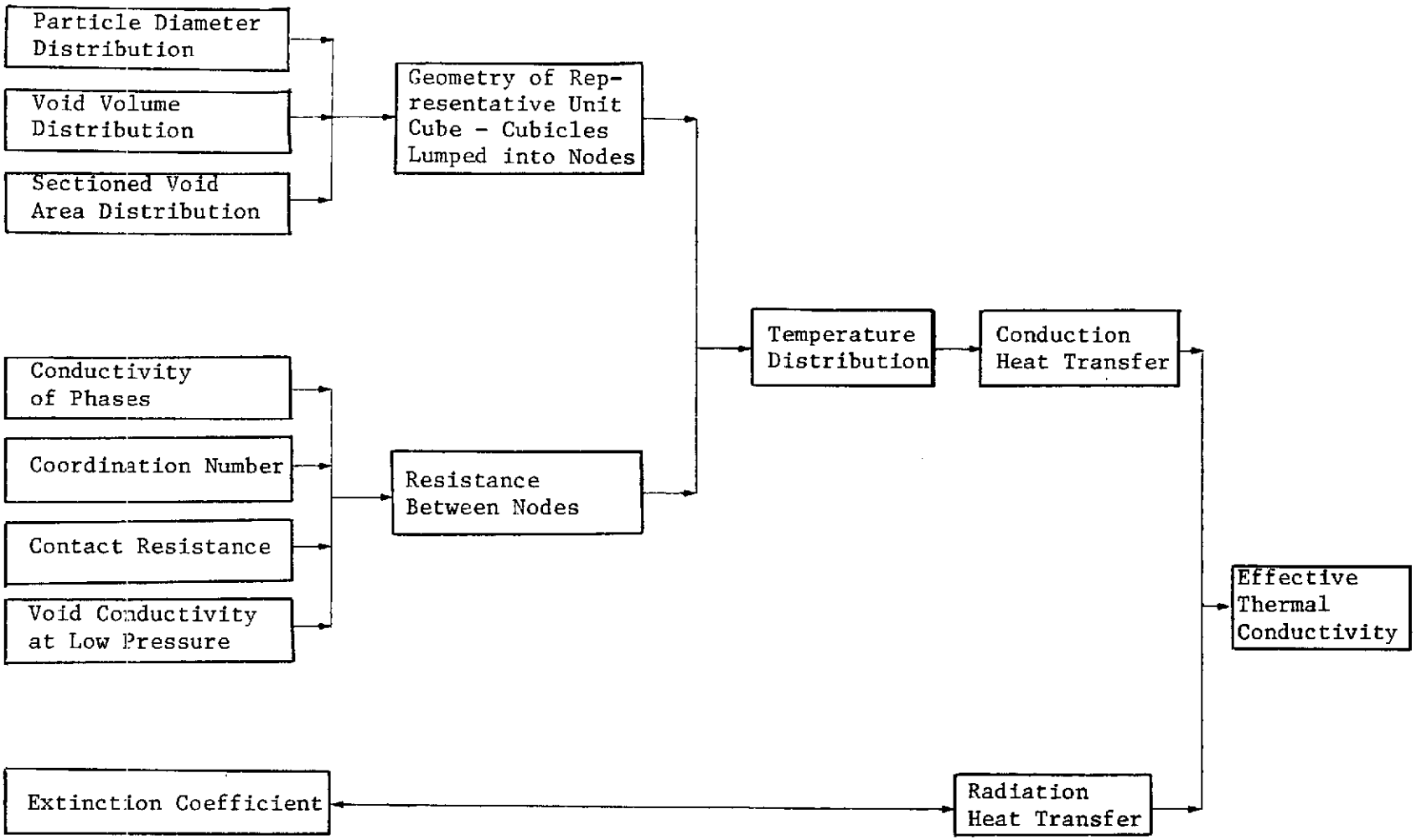

FIGURE 10-1. FLOW CHART FOR THE CALCULATION OF THE EFFECTIVE THERMAL CONDUCTIVITY OF GRANULAR MATERIALS.

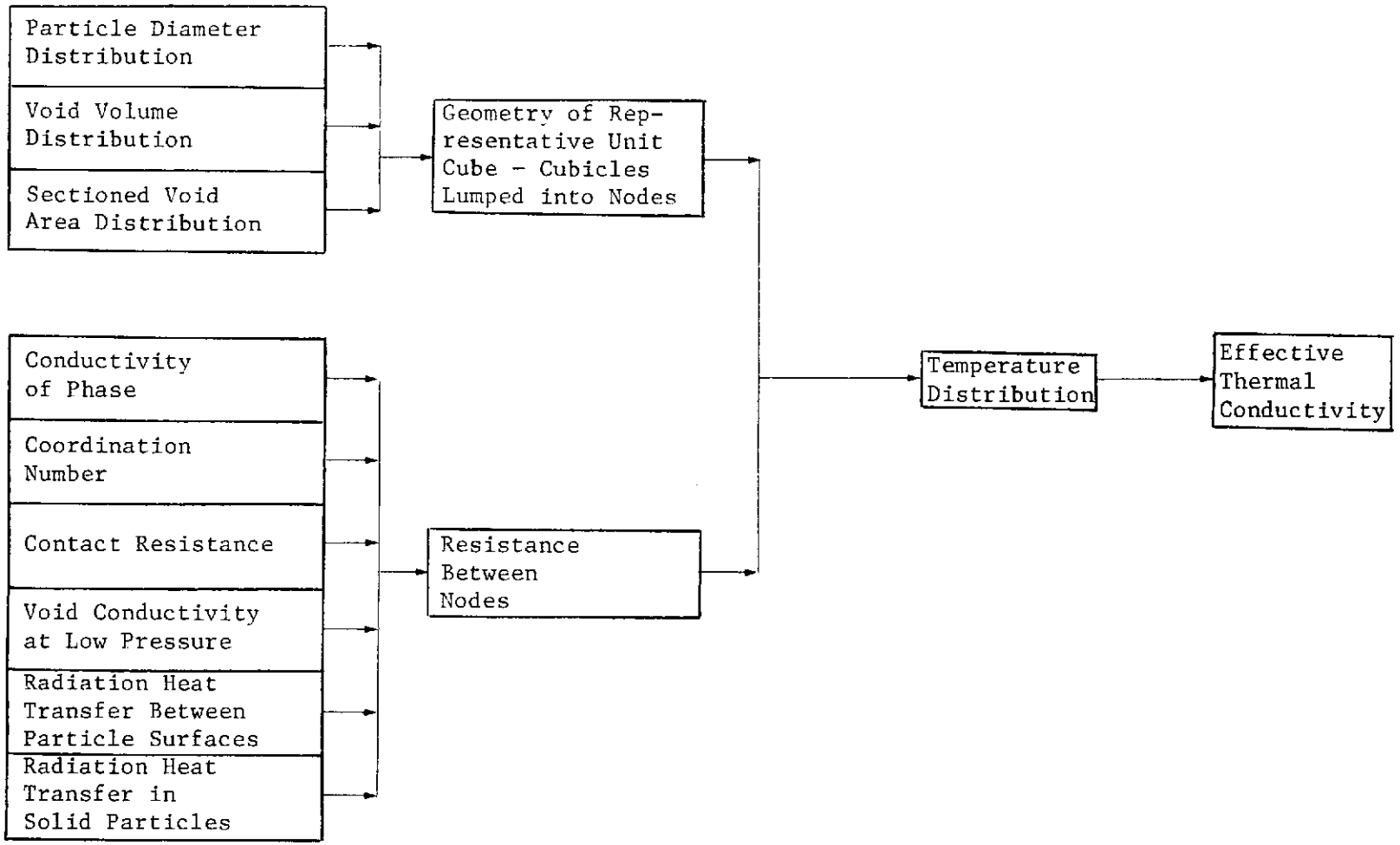

FIGURE 10-2. FLOW CHART FOR AN APPROXIMATE CALCULATION OF THE EFFECTIVE CONDUCTIVITY OF GRANULAR MATERIALS.

REFERENCES

1. Wesselink, A. F., "Heat Conductivity and Nature of the Lunar Surface Material," Bulletin of the Astronomical Institutes of the Netherlands, Vol. 10, No. 390, 351, (1948).

2. Clegg, P. E., Bastin, J. A. and Gear, A. E., "Heat Transfer in Lunar Rock," Monthly Notices of the Royal Astronomical Society, Vol. 133, 63, (1966).

3. Fountain, J. A. and West, E. A., "Thermal Conductivity of Particulate Basalt as a Function of Density in Simulated Lunar and Martian Environments," Journal of Geophysical Research, Vol. 75, No. 20, 4063, (1970).

4. Gorring, R. L. and Churchill, S. W., "Thermal Conductivity of Heterogeneous Materials," Chemical Engineering Progress, Vol 57, No. 7, 53, (1961).

5. Haughey, D. P. and Beveridge, G. S. G. "Local Voidage Variation in a Randomly Packed Bed of Equal Sized Spheres," Journal of Engineering Science, Vol 21, 905, (1966).

6. Waddams, A., "The Flow of Heat Through Granular Materials," Journal of the Society of Chemical Industry, Vol 63, 337, (1944).

7. Wiener, O., "The Theory of Mixtures for Fields with Constant Currents," Akademie der Wissenschaften. Leipsiz, Math-Phys. Kl. Abhandlungen, Vol. 32, 507, (1912).

8. Tsao, G. T., "Thermal Conductivity of Two-Phase Materials," Industrial and Engineering Chemistry, Vol. 53, No. 5, 395, (1961).

9. Maxwell, J. C., A Treatise on Electricity and Magnetism, Vol. 1, 3rd ed., Oxford University Press, London, 1892, p. 440.

10. Burgers, H. C., "The Conductivity of Diluted Air Crystal Mixtures," Physikalische Zeitschrift, Vol. 20, 73, (1919).

11. Fricke, H., "The Electrical Conductivity of a Suspension of Homogeneous Spheroids," Physical Review, Vol. 24, 515, (1924).

12. DeVries, D. A., Physics of Plant Environment, 2nd ed., North Holland Publishing Co., Amsterdam, 1966, p. 210.

13. Hamilton, R. L. and Crosser, O. K., "Thermal Conductivity of Heterogeneous Two-Component Systems," Industrial and Engineering Chemistry Fundamentals, Vol. 2, 187, (1962).

14. Rayleigh, Lord, "On the Influence of Obstacles Arranged in Rectangular Order Upon the Properties of a Medium," Philosophical Magazine and Journal of Science, Vol. 34, 481, (1892).

15. Runge, I., "On the Electrical Conductivity of Metallic Aggregates," Zeitschrift fur Technische Physik-Leipzig, Vol. 6, 61, (1925).

16. Meredith, R. E. and Tobias, C. W., "Resistance to Potential Flow Through a Cubical Array of Spheres," Journal of Applied Physics, Vol. 31, 1270, (1960).

17. Laubitz, M. J., "Thermal Conductivity of Powders," Canadian Journal of Physics, Vol. 37, 798, (1959).

18. Bruggeman, D. A. G., "Dielectric Constant and Conductivity of Mixtures of Isotropic Materials," Annalen Physik, Vol. 24, 636, (1935).

19. Meredith, R. E. and Tobias, C. W., "Conductivities in Emulsions," Electrochemical Society Journal, Vol. 108, 286, (1961).

20. Baxley, A. L. and Cooper, J. R., "Thermal Conductivity of Two Phase Systems-Part IV; Thermal Conductivity of Suspensions," University of Arkansas Experimental Station, Fayetteville, Arkansas, (1966).

21. Deissler, R. G. and Boegli, J. S., "An Investigation of Effective Thermal Conductivities of Powders in Various Gases," Transactions of the ASME, Vol. 80, 1417, (1958).

22. Lichteneker, K., "The Electrical Conductivity of Periodic and Random Aggregates," Physikalische Zeitschrift, Vol. 27, 115, (1926).

23. Woodside, W. and Messmer, J. H., "Thermal Conductivity of Porous Media in Unconsolidated Sands," Journal of Applied Physics, Vol. 32, 1688, (1961).

24. Lichteneker, K., "The Electrical Conductivity of Periodic and Random Aggregates," Physikalische Zeitschrift, Vol. 25, 169, (1924).

25. Son Frey, G. S., "The Electrical Conductivity of Binary Aggregates," Zeitschrift fur Electrochemie, Vol. 38, 260, (1932).

26. Schotte, W., "Thermal Conductivity of Packed Beds," American Institute of Chemical Engineers Journal, Vol. 6, 63, (1960).

27. Smith, W. O., "The Thermal Conductivity of Dry Soil," Soil Science, Vol. 53, 435, (1942).

28. Sauer, M. C., Southwick, P. F., Spiegler, K. S., and Wyllie, M. R. J., "Electrical Conductance of Porous Plugs," Industrial and Engineering Chemistry, Vol. 47, No. 10, 2187, (1955).

29. Yagi, S. and Kunii, D., "Studies on Effective Thermal Conductivities in Packed Beds," American Institute of Chemical Engineers Journal, Vol. 3, 373, (1957).

30. Kunii, D. and Smith, J. M., "Heat Transfer Characteristics of Porous Rocks," American Institute of Chemical Engineers Journal, Vol. 6, 71, (1960).

31. Willhite, G. P., Kunii, D., and Smith, J. M., "Heat Transfer in Beds of Fine Particles," American Institute of Chemical Engineers Journal, Vol. 8, No. 3, 340, (1962).

32. Masamune, S. and Smith, J. M. "Thermal Conductivity of Beds of Spherical Particles," Industrial and Engineering Chemistry, Vol. 2, No. 2, 136, (1963).

33. Dul'nev, G. N., "Heat Transfer Through Solid Disperse Systems," Journal of Engineering Physics, Vol. 9, No. 3, 399, (1965).

34. Luikov, A. V., Shashkov, A. G., Vasiliev, L. L. and Fraiman, Yu.E., "Thermal Conductivity of Porous Systems," International Journal of Heat and Mass Transfer, Vol. 11, 117, (1968).

35. Schumann, T. E. W. and Voss, V., "Heat Flow Through Granulated Material," Fuel in Science and Practice, Vol. 13, 249, (1934).

36. Preston, F. W., "Mechanism of Heat Transfer in Unconsolidated Porous Media at Low Flow Rates," Ph.D. Dissertation, Pennsylvania State University, (1957).

37. Wilhelm, R. H., Johnson, W. C., Wynkoop, R., and Collier, D. W., "Reaction Rate, Heat Transfer and Temperature Distribution in Fixed-Bed Catalytic Converters," Chemical Engineering Progress, Vol. 44, No. 2, p. 105, (1948).

38. Hengst, G., "The Thermal Conductivity of Powdered Thermal Insulators at High Pressure," Ph.D. Dissertation, Technische Hochschule Munchen, (1934).

39. Lyalikov, A. S., "Thermal Conductivity of Granular Materials," Ph.D. Dissertation, Tomsk Polytechnic Institute, U.S.S.R., (1956).

40. Kaganer, M. G., "Thermal Insulation in Low Temperature Engineering," Izd. Mashinostroenie, (1966).

41. Deissler, R. G. and Eian, C. S., "Investigation of Effective Thermal Conductivities of Powders," National Advisory Committee for Aeronautics Research Memorandum, E52C05, (1952).

42. Krupiczka, R., "Analysis of Thermal Conductivity in Granular Materials," CHEMIA STOSOWANA, Vol. 2B, 183, (1966).

43. Russell, H. W., "Principles of Heat Flow in Porous Insulators," Journal of the American Ceramic Society, Vol. 18, 1, (1935).

44. Bernstein, R. S., "Investigation of Natural Fuel Combustion Processes," Gesenergoizdat, (1948).

45. Godbee, H. W., and Ziegler, W. T., "Thermal Conductivity of MgO, Al_2O_3, and ZrO_2 Powders to 850°C," Journal of Applied Physics, Vol. 37, No. 1, 56, (1965).

46. Topper, L., "Analysis of Porous Thermal Insulating Materials," Industrial and Engineering Chemistry, Vol. 47, No. 7, (1955).

47. Webb, J., "Thermal Conductivity of Soil," Nature, No. 4517, 989, (1956).

48. Woodside, W., "Calculation of the Thermal Conductivity of Porous Media," Canadian Journal of Physics, Vol. 36, 815, (1958).

49. Haughey, D. P. and Beveridge, G. S. G., "Structural Properties of Packed Beds - A Review," Canadian Journal of Chemical Engineering, Vol. 47, 130, (1969).

50. Stange, K., "The Mixing of Random Systems as a Basis for Estimating Mixing Data," Chemic Ing. Tech. Vol. 6, 331, (1954).

51. Debbas, S. and Rumpf, H., "On the Randomness of Beds Packed with Spheres or Irregular Shaped Particles," Chemical Engineering Science Vol. 21, 583, (1966).

52. Warren, J. E. and Messmer, J. H., "Correspondence-Thermal Conductivity of Two Phase Materials," Industrial and Engineering Chemistry, Vol. 1, No. 3, 222, (1962).

53. Crane, R. A. and Vachon, R. I., "Effective Thermal Conductivity of Granular Materials," XII International Conference on Thermal Conductivity, Birmingham, Alabama, p. 99, (1972).

54. Somerton, W. H., University of California, Berkeley, California, Personal Communication.

55. Miller, I. and Freund, J. E., Probability and Statistics for Engineers, 1st ed., Prentice Hall, Englewood Cliffs, New Jersey, 1965, p. 245.

56. Gorring, R. L. and Churchill, S. W., "Thermal Conductivity of Heterogeneous Materials," Document 6754, American Documentation Institute, Library of Congress, Washington, D. C.

57. Verschoor, H. and Schuit, G. C. A., "Heat Transfer to Fluids Flowing Through a Bed of Granular Solids," Applied Scientific Research, Vol. 42, 97, (1950).

58. Kling, G., "The Heat Conduction of Spherical Aggragates in Still Gases," Forschung, Vol. 9, 28, (1938).

59. Kannuluik, W. G. and Martin, L. H., "Conduction of Heat in Powders," Proceedings of the Royal Society of London, A141, 144, (1933).

60. DeNee, P. B., "Thermal Conductivity of Granular Materials at Low Temperatures," Ph.D. Dissertation, Lehigh University, (1964).

61. Dul'nev, G. N., Platunov, E. S., Muratova, B. L., Sigalova, Z. V., "A Method of Determing the Thermal Conductivity of Powdered and Fibrous Insulation as a Function of Filler Gas Pressure, "Inzhenerno-Fizicheskii Zhurnal, Vol. 9, No. 6, 751, (1965).

62. Prins, J. A., Schenk, J., and Schram, A. J. G. L., "Heat Conduction by Powdero in Various Gaseous Atmospheres at Low Pressure," Physica, XVI, 4, 379, (1950).

63. Wechsler, A. E., "Thermal and Mechanical Properties of Evacuated Powders," Powder Technology, 3, 163, (1969-1970).

64. Wechsler, A. E. and Glaser, P. E., "Pressure Effects on Postulated Lunar Materials, " Icarus, 4, 335, (1965).

65. Bernett, E. C., Wood, H. L., Jaffe, L. D., Martens, H. E., "Thermal Properties of a Simulated Lunar Material in Air and in Vacuum," AIAA Journal, Vol. 1, No. 6, 1402, (1963).

66. Dallavalle, J. M., "Micromeritics", 2nd ed., Pitman Publishing Corporation, New York, (1948).

67. Hilsenrath, J. et. al., "Tables of Thermodynamic and Transport Properties of Air, Argon, Carbon Dioxide, Carbon Monoxide, Hydrogen, Nitrogen, Oxygen and Steam", Pergamon Press, New York, (1960).

68. Crane, R. A., "Thermal Conductivity of Randomly Packed Granular Materials," Ph.D. Dissertation, Auburn University, (1973).

69. Loeb, A. L., "Thermal Conductivity: VIII, A Theory of Thermal Conductivity of Porous Materials," Journal of The American Ceramic Society, Vol. 37, No. 2, 96, (1954).

70. Cheng, S. C. and Vachon, R. I., "The Prediction of the Thermal Conductivity of Two and Three Phase Solid Heterogeneous Mixtures," Int. J. Heat Mass Transfer, Vol. 12, 249, (1969).

71. Neville, A. M. and Kennedy, J. B., "Basic Statistical Methods for Engineers and Scientists," International Textbook Company, Scranton, Pennsylvania, (1964).

72. Trezek, G. J. and Witwer, J. G., "Finite-Difference Methods for Inhomogeneous Regions," Trans. of the ASME, Vol. 94, Series C, No 3, 321, (1972).

73. Kanager, M. G., "Contact Heat Transfer Heat Transfer in Granular Material Under Vacuum," Inzhenerno-Fizicheskii Zhurnal, Vol. 11, No. 1, 30, (1966).

74. Westlake, J. R., "A Handbook of Numerical Matrix Inversion and Solution of Linear Equations," John Wiley and Sons, Inc., (1968).

75. Argo, W. B. and J. M. Smith, "Heat Transfer in Packed Beds," Chemical Engineering Progress, Vol. 49, No. 8, 443, (1953).

76. Dul'nev, G. N. and Sigalova, Z. V., "Effective Thermal Conductivity of Granular Materials", Inzhenerno-Fizicheskii Zhurnal, Vol. 13, No. 5, (1967).

77. Jacob, Max. "Heat Transfer," Vol. I, p.85, Eighth Printing, John Wiley and Sons, Inc., (1962).

78. Jefferson, T. B. et al, "Thermal Conductivity of Graphite-Silicone Oil and Graphite-Water Suspensions," Ind. Eng. Chem., 50, 1589, (1958).

79. Kennard, E. H., "Kinetic Theory of Gases," McGraw - Hill Book Company, Inc., (1938).

80. Wachman, H. Y., "The Thermal Axxommodation Coefficient: A Critical Survey," ARS Journal, Vol. 32, No. 1, 2, (1962).

81. Chen, J. C. and Churchill, S. W., "Radiant Heat Transfer in Packed Beds," A.I.Ch.E. Journal, Vol. 9, No. 1, 35, (1963).

82. Rosseland, S., "Theoretical Astrophysics," Oxford University Press, Clarendon, England, (1936).

83. Van der Held, E. F. M., "The Contribution of Radiation to the Conduction of Heat," Appl. Sci. Research, Section A, Vol. 3, 237, (1952) ; Section A, Vol. 4, 77, (1953).

84. Troitsky, V. S., "Thermal Conductivity of Lunite as Dependent on Temperature," Nature, February 18, page 688, (1967).

85. Bastin, J. A., Clegg, P. E. and Fiedler, G., "Infrared and Thermal Properties of Lunar Rock," Science, Vol. 167, No. 3918, 728, (1970).

86. Sexl, R. U. et al "Radiative Aspects of Lunar Materials,", NAS8-25585.

87. Cooper M. G., Mikic, B. B. and Yovanovich, M. M., "Thermal Contact Conductance," Int. J. Heat Mass Transfer, Vol. 12, 279, (1969).

88. Carslaw, H. S. and Jaeger, J. C., "Conduction of Heat in Solids," Clarendon Press, Oxford, (1948).

89. Shlykov, Y. P. and Ganin, Y. A., "Thermal Resistance of Metallic Contacts," Int. J. Heat Mass Transfer, Vol. 7, 921, (1964).

90. Smith, W. O., Foote, P. D. and Busang, P. F., Phys. Rev., 34, 1271, (1929).

91. Scott, G. D., Nature, 188, 908, (1960).

92. Bernal, J. D. and Mason, J., Nature, 188, 910, (1960).

93. Fountain, J. A. and Scott, R. W., "Thermal Conductivity of a Particulate Sample in an Environment that Simulates the Planet Mars," NASA Internal Note IN-SSL-T-68 - 15, (1968).

94. Jaffe, L. D., "Lunar Surface Strength," Icarus, Vol. 6, 75, (1967).

95. Jaffe, L. D., "Lunar Surface Exploration by Surveyor Spacecraft," Journal of Geophysical Research, Vol. 72, No. 2, 773, (1967).

96. Verbalovich, T., and Jaffe, L. D., "Surveyor 3, A Preliminary Report - Summary of Result," NASA sp-146, 1967.

97. Christensen, E. M., "Surveyor 5, A Preliminary Report - Lunar Surface Mechanical Properties," NASA sp-163, 1967.

98. Christensen, E. M. et al., "Surveyor 6, A Preliminary Report - Lunar Surface Mechanical Properties," NASA sp-166, 1968.

99. Hapke, B. W., "Lunar Surface Composition Inferred from Optical Properties," Science, Vol. 159, No. 3810, 76, (1968).

100. Matveev, Y. G., Suchkin, G. L., and Troitskii, V. S., "Change of Lunite Density with Depth in the Surface Layer," Soviet Astronomy - AJ, Vol. 9, No. 4, 626, (1966).

101. Jones, B. P., "Density - Depth Model for the Lunar Outermost Layer," Journal of Geophysical Research, Vol. 73, No. 3, 7631, (1968).

102. Hapke, B. W., "On the Particle Size Distribution of Lunar Soil," Planetary Space Science, Vol. 16, 101, (1968).

103. Gorz, H. et al., "Particle Size and Shape Distributions of Lunar Fines By CESEMI," Proceedings of the Second Lunar Science Conference, Houston, Vol. 3, 2021, (1971).

104. Sparrow, E. M., and Cess, R. D.,"Radiation Heat Transfer," Brooks/ Cole Publishing Company, Belmont, California, 254, (1966).

105. Cremers, C. J., and Birkebak, R. C., "Thermal Conductivity of Fines from Apollo 12," Proceedings of the Second Lunar Science Conference, Houston, Vol. 3, 2311, (1971).

106. Cheng, S. C., and Vachon, R. I., "Thermal Conductivity of Packed Beds and Powder Beds," International Journal of Heat and Mass Transfer, Vol. 33, 1201, (1969).

107. Beveridge, G. S. G., and Haughely, D. P., "Axial Heat Transfer in Packed Beds," International Journal of Heat and Mass Transfer, Vol. 14, No. 8, 1093, (1971).

108. Holm, R., "Electric Contacts Handbook," Cambridge University Press, 1911.

109. Jean, J. H., "Electricity and Magnetism," Cambridge University Press, 1911.

110. See e.g. Lamb, H., "Treatise on the Mathematical Theory of Elasticity," Dover, 1957.

111. Hill, F. B., and Wilhelm, R. H., "Radiative and Conductive Heat Transfer in Quiescent Gas Solid Bed of Particles," AICHE Journal, Vol. 5, 1959.

112. Snoddy, W. E., and et al., "Infrared Emission During Simulated Lunar Eclipses," AIAA Progress in Astronautics and Aeronautics, 5469, (1967).

113. Turkevich, A. L., Franzgrote, E. J., and Paterson, J. H., "Chemical Analysis of the Moon at Surveyor 6 Landing Site," NASA sp-166, 1968.

114. Cuttitta, F. and et al., "Elemental Composition of Some Apollo 12 Lunar Rocks and Soils," Proceedings of the Second Lunar Science Conference, Houston, Vol. 2, 1217, (1971).

115. Tittmann, B. R., Housley, R. M., "Surface Elastic Wave Propagation Studies in Lunar Rocks," Proceedings of the Second Lunar Science Conference, Vol. 3, 2337, (1971).

116. Kanamori, H. et al., "Elastic Wave Velocities of Apollo 12 Rocks at High Pressures," Proceedings of the Second Lunar Science Conference, Vol. 3, 2323, (1971).

117. Chandrasekhar, S., "Radiative Transfer," Dover Publications, Inc., (1960).

118. Merrill, R. B., "Thermal Conduction Through an Evacuated Idealized Powder Over the Temperature Range of 100 to 500 K," Ph.D. Dissertation, Brigham Young University, (1968).

119. Gold, T. et al., "Some Physical Properties of Lunar Samples," Proceedings of the Second Lunar Science Conference, Houston, Vol. 3, 2173, (1971).

120. Yagi, S., and Kunii, D., "Studies of Heat Transfer Near Wall Surface in Packed Beds," AICHE Journal, Vol. 6, No. 1, 97, (1960).

121. Cremers, C. J. et al., "Thermal Characteristics of the Lunar Surface Layer," International Journal of Heat and Mass Transfer, Vol. 15, 1045, (1972).

122. Campbell, K. J., Ulrichs, J., and Gold, T., "Density of Lunar Surface," Science, Vol. 189, 973, (1968).

123. Fountain, J. A., West, E. A., "Thermal Conductivity of Particulate Basalt as a Function of Density in Simulated Lunar and Martian Environments," Journal of Geophysical Research, Vol. 75, No. 20, 4063, (1970).

124. Heywood, H., "Particle Size and Shape Distribution for Lunar Fines Sample 12057,72," Proceedings of the Second Lunar Science Conference, Houston, Vol. 3, 1989, (1971).

125. Sellers, G. A. et al., "Composition and Grain-Size Characteristics of Fines from the Apollo 12 Double-Core Tube," Proceedings of the Second Lunar Science Conference, Vol. 1, 665, (1971).

126. Quaide, W. et al., "Investigations of the Natural History of the Regolith at the Apollo 12 Site," Proceedings of the Second Lunar Science Conference, Vol. 1, 701, (1971).

127. Cremers, C. J., Birkebak, R. C., and Dawson, J. P., "Thermal Conductivity of Fines from Apollo 11," Proceedings of Apollo 11 Lunar Science Conference, Vol. 3, 2045, (1970).

128. Watson, K., "The Thermal Conductivity Measurements of Selected Silicate Powders in Vacuum from 150-350 K," Ph.D. Thesis, California Inst. of Technology, Pasadena, Calif., 1964.

BIBLIOGRAPHY

1. Staple, W. J., "Boundary Conditions and Conductivities Used in the Isothermal Model of Evaporation from Soil," Soil Science Society of America Proceedings, Vol. 35, No. 6, (1971).

2. Wierenga, P. G. and DeWit, C. T., "Simulation of Heat Transfer in Soils," Soil Science Society of America Proceedings, Vol. 34, (1970).

3. Hisakado, Terumasa, "On the Mechanism of Contact Between Solid Surfaces, (1st Report)," Bulletin of JSME, Vol. 12, No. 54, (1969).

4. Hisakado, Terumasa, "On the Mechanism of Contact Between Solid Surfaces, (2nd Report)," Bulletin of JSME, Vol. 12, No. 54, (1969).

5. Hisakado, Terumasa, "On the Mechanism of Contact Between Solid Surfaces, (3rd Report)," Bulletin of JSMA, Vol. 12, No. 54, (1969).

6. Clausing, A. M. and Chao, B. T., "Thermal Contact Resistance in a Vacuum Environment," Journal of Heat Transfer, (1965).

7. Aberdeen, J., and Laby, T. H., "Conduction of Heat through Powders and its Dependence on the Pressure and Conductivity of the Gaseous Phase," Proceedings of Royal Society of London, Vol. 113, (1927).

8. Agrawal, M. P., and Bhandari, R. C., "Effect of Particle Shape on the Formation Resistivity Factor of Unconsolidated Porous Media," Indian J. Pure Appl. Phys., Vol. 7, (1969).

9. Aksel'rud, G. A., "Solution of a Generalized Problem of Heat or Mass Transfer in a Bed," Inzhenerno-Fizicheskii Zhurnal, Vol. 11, No. 1, (1966).

10. Archie, G. E., "The Electrical Resistivity Log as an Aid in Determining Some Reservoir Characteristics," Petroleum Technology Proceedings, T.P. 1422, (1941).

11. Ben-Amoz, M. "The Effective Thermal Properties of two Phase Solids," Int. J. Engng. Sci., Vol. 8, (1970).

12. Fritz, W., and Kuster, W., "A Contribution to the Knowledge of Heat Conductivity of Porous Materials," Warme-Und Stoffubertragung, Bd. 3, (1970).

13. Kumar, I. J., "An Extended Variational Formulation of the Non-Linear Heat and Mass Transfer in a Porous Medium," International Journal of Heat and Mass Transfer, Vol. 14, (1971).

14. Wyllie, M. R. J., and Southwick, P. F., "An Experimental Investigation of the S. P. and Resistivity Phenomena in Dirty Sands," Journal of Petroleum Technology, Vol. 44, (1954).

15. Berg, T. G., Owe, Medonald, R. L., and Trainer, R. J., Jr., "The Packing of Spheres," Power Technology, Vol. 3, (1969/70).

16. Blum, E. H., and Wilhelm, R. H., "A Statistical Geometrical Approach to Random-Packed Beds," A.I.Ch.E. - I Chem. E. Symposium Series, No. 4, (1965).

17. Bridgwater, J., Bagster, D. F. Chen, and Hallam, J. H., "Geometric and Dynamic Similarity in Particle Mixing," Powder Technology, Vol. 2, (1968/69).

18. Cahn, D. S., and D. W. Fuerstenav, "Simulation of Diffusional Mixing of Particulate Solids by Monte Carlo Techniques," Powder Technology, Vol. 1, (1967).

19. Cahn, David S., and Fuerstenav, Douglas W., "A Probabilistic Model of the Diffusional Mixing of Particulate Solids," Powder Technology, Vol. 2, (1968/69).

20. Dullien, F. A. L., Rhodes, E., and Schroeter, S. R., "Comparative Testing of Some Statistical Methods for Obtaining Particle Size Distributions," Powder Technology, Vol. 3, (1969/70).

21. McAdams, H. T., "Probability Foundations of Particle Statistics," Powder Technology, Vol. 2, (1968/69).

22. Prager, S., "Interphase Transfer in Stationary Two-Phase Media," Chemical Engineering Science, Vol. 18, (1963).

23. Roblee, L. H. S., Baird, R. M. and Tierney, J. W., "Radial Porosity Variations in Packed Beds," A.I. Ch.E. Journal, Vol. 4, No. 4, (1958).

24. Thadani, Mohan C., and Peebles, Fred N., "Variation of Local Void Fraction in Randomly Packed Beds of Equal Spheres," I & E.C. Process Design and Development, Vol. 5, No. 3, (1966).

25. Williams, J. C., "The Properties of Non-Random Mixtures of Solid Particles," Powder Technology, Vol. 3, (1969/70).

26. Horia, Ki-iti and Simmons, G., "Thermal Conductivity of Rock-Forming Minerals," Earth and Planetary Science Letters 6, (1969).

27. Kinger, W. D., Francl, J., Coble, R. L., and T. Vasilos, "Thermal Conductivity: X, Data for Several Pure Oxide Materials Corrected to Zero Porosity," Journal of American Ceramic Society, Vol. 37, No. 2, (1954).

APPENDIX A

LOW PRESSURE EFFECTS

Figure (A-1) shows a typical pressure dependence curve of the effective thermal conductivity of a gas-powder mixture. For higher pressures (10 atm or higher depending on the nature of the gas and the particle size [37]) a large rise in the effective conductivity is noted, due to convection. When the mean free path of the gas molecules approaches the characteristic length of the gas space, the effective conductivity becomes pressure dependent, as indicated by the portion between A and B of Figure (A-1). Further reduction of the pressure does not result in any appreciable changes

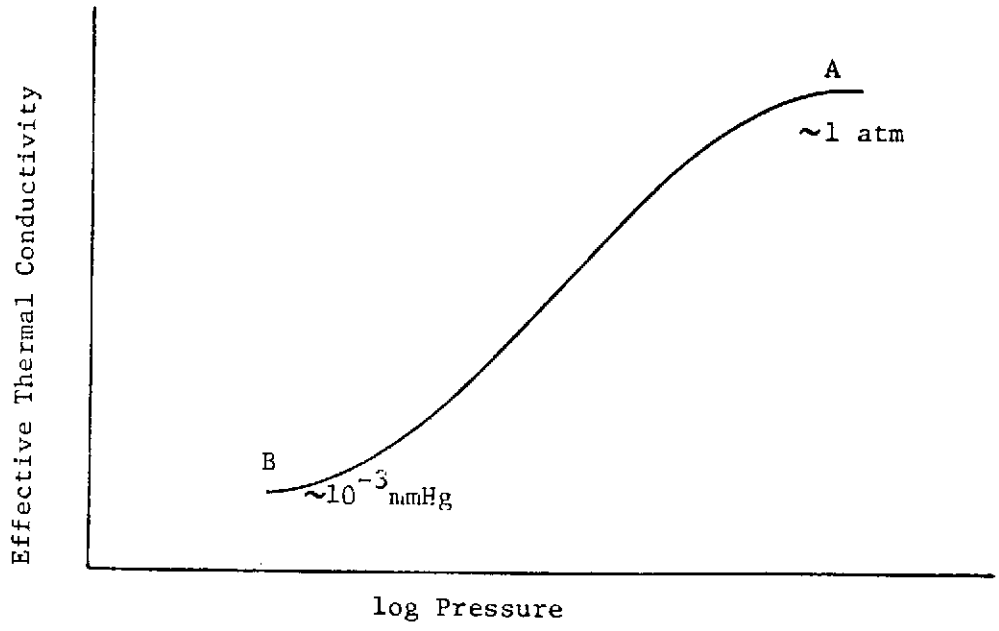

Fig. A-1. Pressure Dependence of Effective Thermal Conductivity

in the effective conductivity, since at this region the dominant modes of heat transfer are conduction through the contact areas between particles and radiation.

Thermal conduction in rarefied gases was first analyzed in the pioneer works of Smoluchowski and Knudsen, as indicated by Kennard [79]. Kennard's equation for the effective conductivity, k_g^*, of a gas between two parallel plates of the same material, separated by a relative small distance, D_p, is:

$$k_g^* = \frac{k_g}{1 + 2\frac{g^*}{D_p}} \tag{A-1a}$$

where g^* is the temperature jump distance at one of the plates, given by:

$$g^* = \frac{2-\alpha}{\alpha}\ \frac{2\gamma}{\gamma+1}\ \frac{1}{Pr}\ \lambda \tag{A-1b}$$

where α is the thermal accommodation coefficient, γ is the ratio of the specific heats of the gas, Pr is the Prandtl number and λ is the mean free path of the gas molecules. Equation (A-1) indicates that k_g^* decreases with respect to k_g when λ/D_p increases.

The principal difficulty in applying this equation lies in evaluating the thermal accommodation coefficient, α, and the effective pore length, D_p. As indicated in [80], several attempts have been made to predict the accommodation coefficient analytically, but they have not proved particularly successful. Furthermore, the

accommodation coefficient is strongly influenced by parameters describing the solid surface (i.e. smoothness, impurities, etc. not reported in experimental work on the conductivity of granular materials), and experimentally determined values of α are not available for solids other than pure metals and alloys [80]. For this reason, most investigators of the effective conductivity of heterogeneous mixtures have either set $\alpha = 1$, effectively assuming that the solid surface is so irregular that most of the molecules struck it a number of times before escaping, or they have included α in an experimentally determined coefficient.

Dulnev and Sigalova [76] and Luikov et al [34] have used Equation (A-1) in the same form given by Kennard. Deissler and Boegli [21] found from their experimental data on magnesium oxide in air that the pressure at which the effective conductivity begins to vary with pressure (breakaway pressure) is 15 psia at 340°F. From this they evaluated the Knudsen number ($Kn = \lambda/d$), based on the mean particle size, to be 0.00072. Finally, arguing that Kn at the breakaway pressure must be independent of the gas, powder, temperature and pressure, they found from Equation (A-1) that the breakaway pressure in the English system of units is given by:

$$p_b = 1770 \times 10^{-24} \frac{T}{s^2 d} \qquad \text{(A-2)}$$

where T is the temperature and s is the molecular diameter of the gas. Equation (A-2) seems to correlate their experimental data with

good accuracy. It is of particular importance that the value of the Knudsen number corresponding to the breakaway pressure is much less than unity, indicating that most of the heat transfer through a powder takes place in the immediate vicinity of the contact areas. Effectively, this means that the dimensions effective in transferring heat in the voids are much less than the effective geometric length of the void.

Schotte [26] and Masamune and Smith [32] found expressions for D_p in terms of the porosity of the system, based on geometric considerations. They then substituted the expressions in Equation (A-1).

Woodside and Messmer [23] arguing that when the normal mean free path, λ, of the gas molecules is much larger than a characteristic pore size, then the effective mean free path, $\bar{\lambda}$, must depend on λ as well as on D_p, have shown that:

$$k_g^* = k_g \cdot \frac{p\, D_p}{p\, D_p + B} \qquad \text{(A-3)}$$

where

$$B = \frac{\sigma_D\, T}{\pi \sqrt{2}\, s^2}$$

σ_b is the Boltzman constant. Equation (A-3) predicts higher values for k_g^* than Equation (A-1) by a factor of roughly 2.5. It is interesting to note that also in this case the characteristic dimension

of the void space, with respect to heat conduction in the gas occupying this space, is amaller than the mean particle diameter by a factor of roughly 100.

Summarizing, it is seen that almost all investigators, with the exception of [23], have used Kennard's equation to predict the effect of pressure on the conductivity of the gaseous phase. The principal difficulty in applying this equation lies in the determination of the thermal accommodation coefficient and D_p. The value of α is assumed by all investigators to be unity. The determination of D_p is postponed until a later section. In Figure (A-2) the dependence of the thermal conductivity of CO_2 on pressure is indicated, according to Equations (A-1) and (A-3).

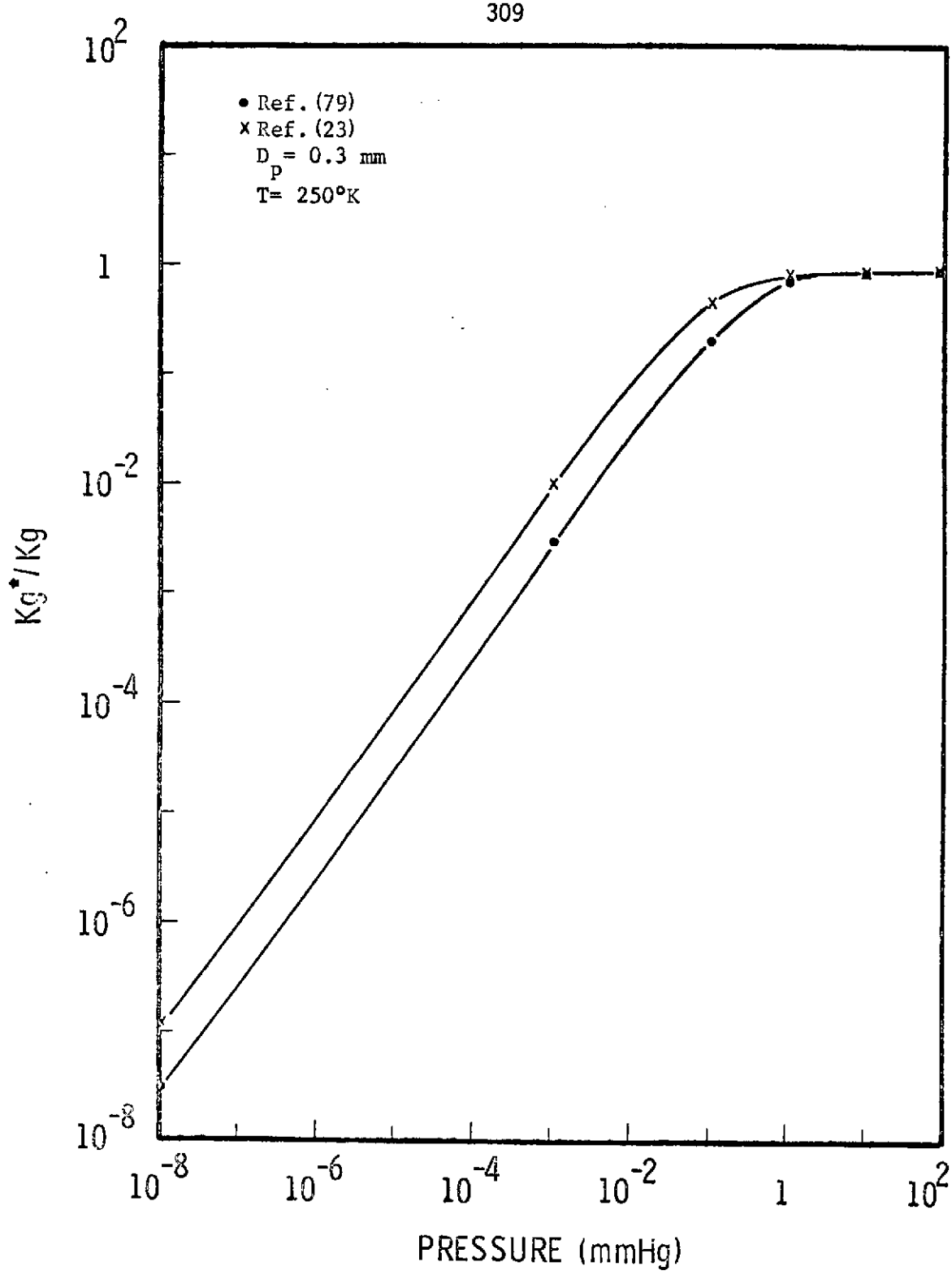

FIGURE A-2. EFFECT OF PRESSURE ON THE THERMAL CONDUCTIVITY OF CO_2.

APPENDIX B

RADIATION HEAT TRANSFER IN GRANULAR MATERIALS

Thermal radiation is known to be a dominant mode of heat transfer in evacuated granular materials, or in powders at elevated temperatures. Consequently it is no wonder that it has received considerable attention in the literature. However, due to the scarcity of information about absorption and scattering of radiation in granular materials, only approximate methods have been developed for the inclusion of radiation as a mode of heat transfer in granular materials.

According to Van der Held [83] the complete equation of Fourier, including radiant heat flux, is

$$C_p \rho \frac{\partial T_o}{\partial t} = \text{div}(k_{e_c} \text{ grad } T_o) + 4 \int_o^\infty n_l^2 \beta_l (J_l - I_{l,T_o}) dl dV_o \quad \text{(B-1)}$$

where $4n_l^2 \beta_l I_{l,T_o} dl dV_o$ is the radiation emitted by a volume element dV_o between the wavelengths l and $l + dl$, having an absorption coefficient at these wavelengths β_λ and a refractive index n_l. Similarly $4n_l^2 \beta_l J_l \, dl \, dV_o$ is the radiation absorbed by dV_o. $I_{l,T} \, dl$ and $J_l \, dl$ are the black body radiation and mean irradiance respectively of a plane surface between the wavelengths l and $l + dl$ at dV_o. In Equation (B-1) k_{e_c} is the effective thermal conductivity of the medium due to conduction heat transfer only.

A second equation is required relating J_1 and $I_{1,T}$. This can be obtained by letting the mean irradiance of dV_o be the sum of the radiation emitted and scattered by all volume elements dV, and reaching dV_o, plus the irradiance of dV_o from the bounding walls. According to Van der Held [83], assuming diffuse radiation, this equation is

$$4J_{1_o} = \int_{(v)} (\beta_1 I_{1,T} + \sigma_1 J_1) \frac{e^{-T_1 r}}{\pi r^2} dV + \int_{(s)} [e_{1,\gamma} I_{1,T} + (1-e_{1,\gamma}) J_1] \frac{e^{-t_1 r}}{\pi r^2} \cos \gamma \, dS \qquad \text{(B-2)}$$

where σ_1 is the monochromatic scattering coefficient, $\varepsilon_1 = \beta_1 + \sigma_1$ is the monochromatic scattering coefficient, r is the distance between dV_o and dV or dS (surface element on bounding walls), $e_{1,\gamma}$ is the monochromatic spectral emissivity of the walls, and γ is the angle the distance between dV_o and dS makes with the normal on dS.

Combination of Equations (B-1) and (B-2) together with the boundary conditions determines the solutions of the heat transfer problem in granular materials. Although this system of equations appears to be quite formidable, it should be noted that the equations are very general in nature. The complexity of these equations has been reduced considerably in a number of specific situations, and these situations will now be discussed. First, however, it should be noted that the integral term in Equation (B-1) represents the net radiation heat transfer to dV_o, or if $\overline{q}_r$ is the radiant heat flux, the integral term is equal to -div $\overline{q}_r$. Consequently, an alternate form of Equation (B-1) is

$$C_p \rho \frac{\partial T_o}{\partial t} = \text{div } (k_{e_c} \text{ grad } T_o) - \text{div } \vec{q}_r \tag{B-3}$$

Also, the total heat flux vector within the medium will consist of the sum of the conduction and radiation contributions, and consequently is given by

$$\overline{q} = - k_{e_c} \text{ grad } T = \overline{q}_r \tag{B-4}$$

Assuming one-dimensional steady-state combined conduction and radiation for a medium bounded by two parallel surfaces, Equations (B-3) and (B-4) reduce to

$$k_{e_c} \frac{d^2T}{dx^2} = \frac{dq_r}{dx} \tag{B-5}$$

$$q = - k_{e_c} \frac{dT}{dx} + q_r = \text{constant} \tag{B-6}$$

where x is the distance normal to one surface. Further assuming that the absorption and scattering coefficients are both independent of the wavelength, and that the distance between the bounding surfaces is large compared to the photon mean free path (optically thick limit), it has been shown in detail by Sparrow and Cess [104, 117] that the radiation flux can be written as

$$q_r = - \frac{16\sigma_b T^3}{3\varepsilon} \frac{dT}{dx} \tag{B-7}$$

Combination of Equations (B-6) and (B-7) yields

$$q = -\left(k_{e_c} + \frac{16\sigma_b T^3}{3\varepsilon}\right) \frac{dT}{dx} = \text{constant} \qquad \text{(B-8)}$$

It is seen that in this specific case the conduction and radiation processes can be separated, and the total heat flux is represented as the sum of heat transfer by pure conduction and heat transfer by pure radiation. Consequently the effective conductivity of the granular material is the sum of an effective conductivity due to pure conduction and a radiant conductivity which is related to the cube of the absolute temperature. Unfortunately, no experimental data have been reported on the extinction coefficient of granular materials and powders, and consequently Equation (B-8) cannot be applied due to lack of experimental information. However, the result that the effective conductivity can be represented as the sum of two terms, one being a constant and the second related to the cube of the absolute temperature, has been extensively used in the correlation of data on evaluated granular materials.

Clegg et al [2] following a similar procedure assumed that scattering of radiation may be neglected, and using the Rosseland equation for the optically thick limit, they obtained the following equation for the radiant conductivity.

$$k_r = \frac{16}{3} \sigma_b \frac{T^3}{\bar{a}(T)} \qquad \text{(B-9)}$$

where $\bar{a}(T)$ is the Roselland mean absorption coefficient.

Chen and Churchill [81] on the other hand represented the radiant intensity in packed beds by forward and backward fluxes, and derived the following expression for the radiant conductivity:

$$k_r = \frac{8\,\sigma_b\,T^3}{a + 2b} \tag{B-10}$$

where a is the absorption volumetric coefficient and b is the back scattering volumetric coefficient. They also determined experimentally the values of a and b for borosilicate glass, aluminum oxide, carbon steel, and silicon carbide beds.

Another approximation is to assume one-dimensional steady-state combined conduction and radiation for a medium bounded by two parallel diffuse surfaces, where the distance between the bounding surfaces is small compared to the photon mean free path (optically thin limit). In this case, it has been shown by both Van der Held [83] and Sparrow and Cess [117] that the radiation heat flux is

$$q_r = \frac{\sigma_b(T_1^4 - T_2^4)}{(1/e_1) + (1/e_2) - 1} \tag{B-11}$$

where T_1 and T_2 are the absolute temperatures of the bounding surfaces, and e_1 and e_2 are the emissivities of the bounding surfaces. If $e_1 = e_2$ and $T_1 - T_2 = \Delta T$ is small, one can write

$$T_1^4 - T_2^4 = (T_1^2 + T_2^2)\,(T_1 + T_2)\,(T_1 - T_2) \simeq 4T^3\,\Delta T$$

Combination of Equations (B-6) and (B-11) yields

$$q = - \left(k_{e_c} + \frac{4\sigma_b \, e \, T^3 \, dx}{2 - e}\right) \frac{dT}{dx} \qquad \text{(B-12)}$$

Again it is seen that the conduction and radiation processes are separable. Further, this is the result for radiation transfer through a nonparticipating medium.

Equation (B-12) has been used extensively by investigators that have utilized models based on regular geometric arrangements which permit an algebraic formulation of the heat transfer processes. Russell [43], Wesselink [1], Jacob [77] and Argo and Smith [75] assumed that with respect to radiation a mixture can be treated as alternating solid and gas layers perpendicular to the heat flow. In this case, the radiant conductivity of the gas phase is given by

$$k_r = \frac{4\sigma_b \, e \, D_p \, T^3}{2 - e} \qquad \text{(B-13)}$$

Some investigators have assumed that D_p is equal to the particle diameter d. Others have set $D_p = d/(1-P)$.

Schotte [26] assumed spherical particles and considered that the radiation from a plane located on one side of a particle to a plane located on the far side of the particle consists of two parts. First, the radiation across the void space surrounding the particle. Second,

there is radiation from the particle surface in series with conduction through the particle. Combining these two modes, he derived the following equation for the radiant conductivity

$$k_r = \frac{1 - P}{\frac{1}{k_s} + \frac{1}{k_{r_0}}} + P\, k_{r_0} \qquad \text{(B-14a)}$$

where k_{r_0} is the radiant conductivity between particle surfaces which Schotte expressed as

$$k_{r_0} = 4\sigma_b\, e\, d\, T^3 \qquad \text{(B-14b)}$$

It should be noted that when k_s is much larger than k_{r_0}, Equation (B-14a) reduces to

$$k_r \simeq 4\sigma_b\, e\, d\, T^3 \qquad \text{(B-14c)}$$

Laubitz, on the other hand, assumed the granular material to be cubic obstacles randomly distributed in cubical volumes, and considering the probability that radiation will pass a cube without hitting an obstacle, he developed the following expression for the radiant conductivity

$$k_r = 4\sigma_b\, e\, d\, T^3\, [1 - (1-P)^{2/3} + (1-P)^{4/3}]/(1-P) \qquad \text{(B-15)}$$

It should be noted that in all the above developments for which specific geometric configurations have been considered, it has been assumed that the particles are opaque to thermal radiation. The validity of this assumption depends on both the material of the solid phase and the size of the particles compared to the wavelength of radiation. It has been shown by Merrill [118] that glass beads less than 100μ in diameter cannot be assumed opaque to thermal radiation even at relatively low temperatures. For the case of transparent particles Merrill assumed that the radiant conductivity is equal to the conductivity of the photon gas transmitted through the particles given be

$$k_r = \frac{1}{3} C \nu \lambda_p \tag{B-16}$$

where C is the specific heat capacity of the photon gas, is the average velocity and λ_p is the photon mean free path. The energy density of a photon gas is given by

$$V = \frac{4}{c} \sigma_b T^4 \tag{B-17}$$

Consequently

$$C = \frac{\partial V}{\partial T} = \frac{16}{c} \sigma_b T^3 \quad \text{and}$$

$$k_r = \frac{16}{3} \sigma_b T^3 \lambda_p \tag{B-18}$$

It is easily seen that Equation (B-18) is the same as the radiative component of Equation (B-8), with the exception that for the development of Equation (B-8) the heterogeneous mixture has been assumed to be a pseudo-homogeneous material whereas in Equation (B-18) only the solid phase is considered.

Rosseland [82] treated the radiation heat transfer as a diffusion of photons, and considering a random walk process, he obtained the following expression for the radiant conductivity

$$k_r = \frac{4}{3} \sigma_b \, d \, T^3 \tag{B-19}$$

Troitsky [84] and Bastin et al [85] have suggested that the conduction radiation in the voids and pure radiation processes should be considered acting in parallel, and consequently the effective radiant conductivity should be expressed as

$$k_r = \frac{4\sigma_b \, P \, D_p \, e \, T^3}{2 - e} + \frac{16}{3} \sigma_b \frac{T^3}{\bar{a}(T)} \tag{B-20}$$

Loeb [69] considered the case of the radiant conductivity of pores in consolidated porous media. Assuming that linear heat flow is not distrubed in the solid surrounding the pores, he derived the following expression for pores having perfect geometric shapes

$$k_r = 4\gamma \, D_p \, e \, \sigma_b \, T^3 \tag{B-21}$$

where γ is a shape factor that depends on the geometry of the pore.

Summarizing the equations for radiant conductivity, it is seen that they can be classified into three groups.

1. Those assuming the heterogeneous mixture to be a pseudohomogeneous material;
2. Those based on regular geometric arrangements that permit an algebraic formulation of the radiative heat transfer processes;
3. Those based on random walk processes.

Although the first class provides the best approximation to the interaction between pure conduction heat transfer and pure radiation heat transfer, lack of experimental work on the radiative properties of heterogeneous mixtures necessitates the application of the second class of equations. Moreover, the experimentally determined values of a and b by Chen and Churchill [81], indicate on one hand that both a and b depend on the type of bed, the solid material and the temperature, and on the other hand that is is perhaps easier to determine the effective thermal conductivity of granular materials experimentally than to determine a and b. For these reasons, at this point it is only possible to include quantitatively the conduction-radiation process in the voids in models of heterogeneous mixtures, while the pure radiation process can only be discussed qualitatively.

In Figure B-1 the values of k_r predicted by various models are plotted verous temperature. In Figure B-2 models of the second and third classifications are compared to Chen and Churchill's model for an aluminum oxide bed at high temperatures.

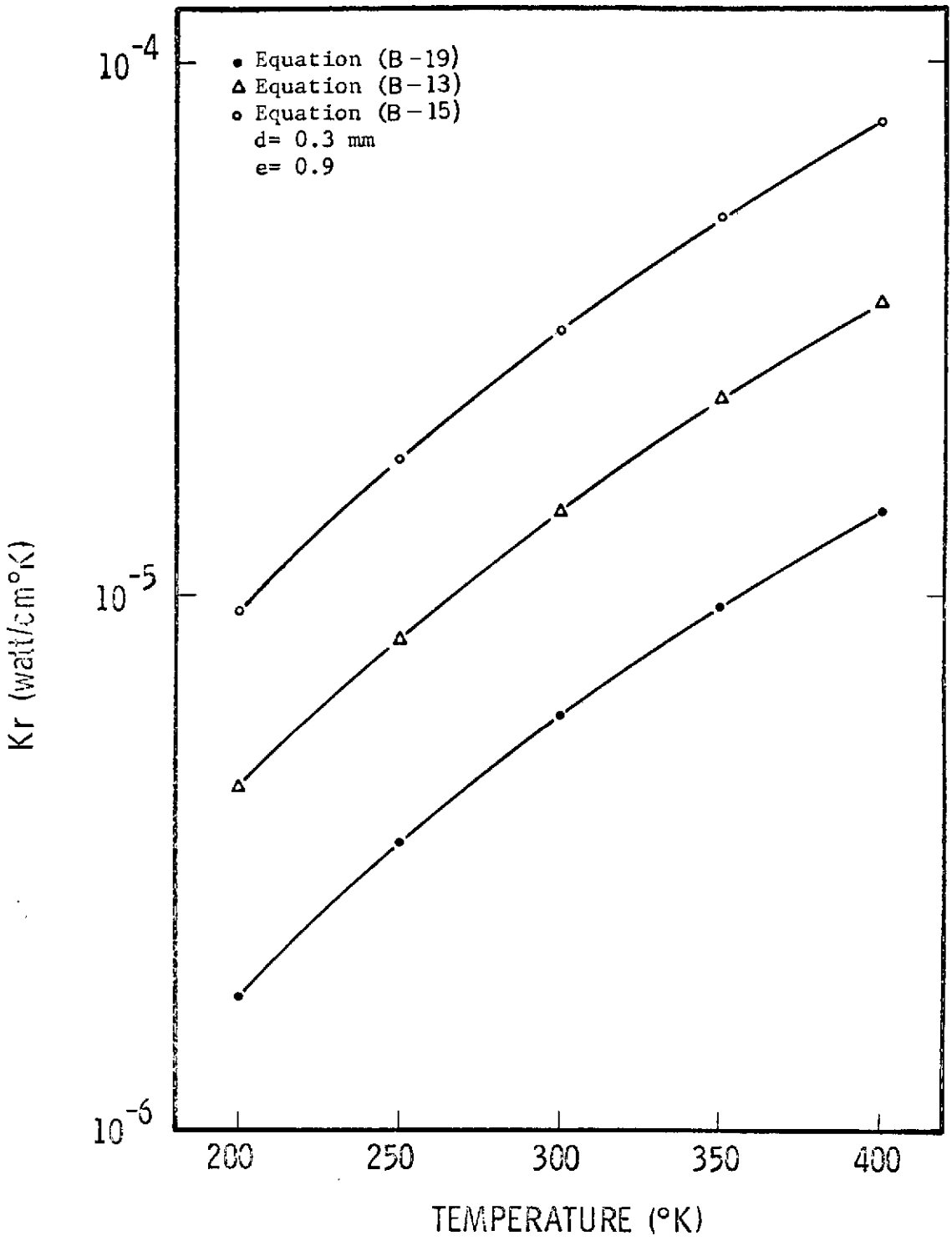

FIGURE B-1. COMPARATIVE VALUES OF Kr.

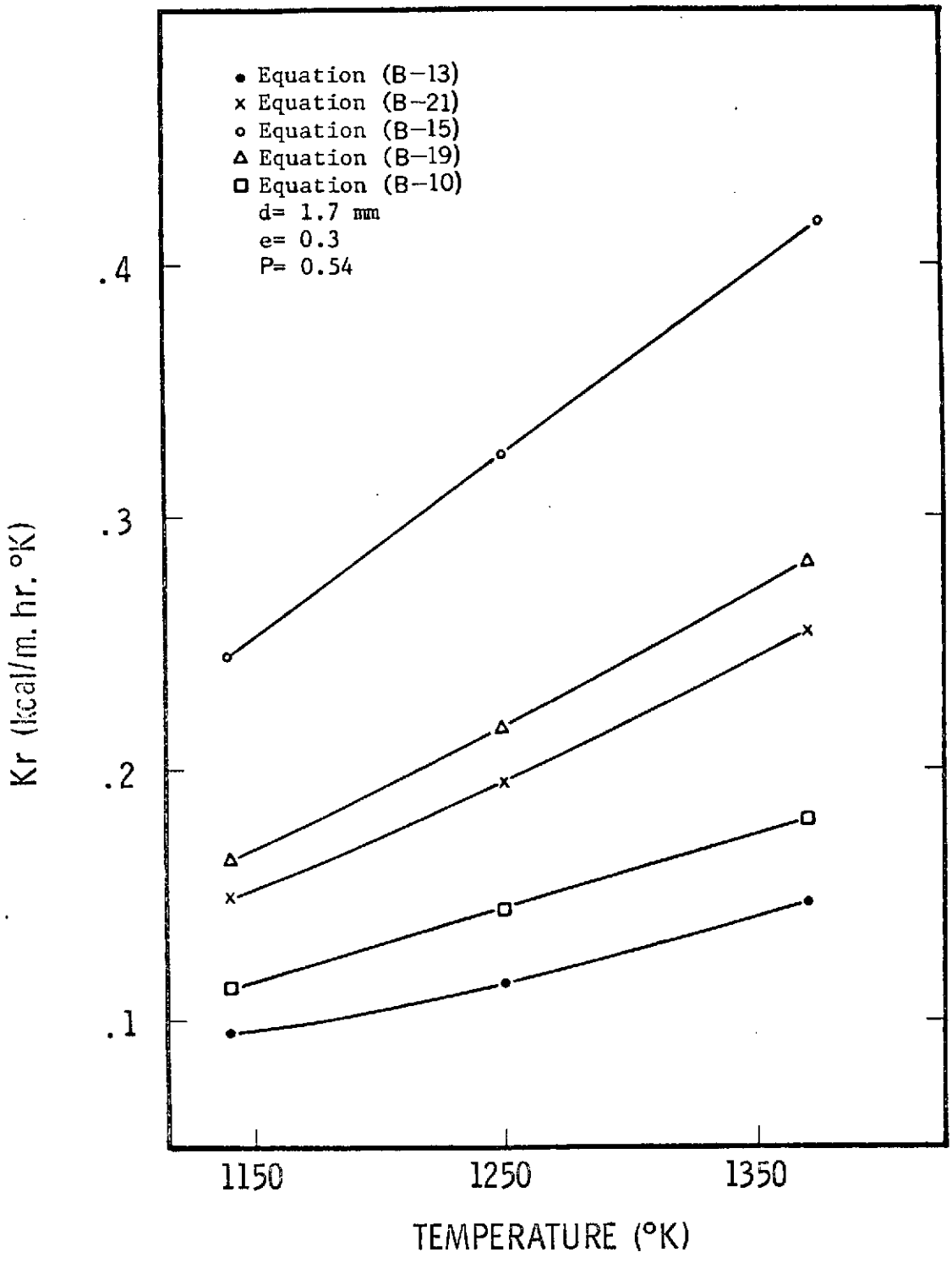

FIGURE B-2. COMPARATIVE VALUES OF Kr FOR AN ALUMINUM OXIDE BED.

APPENDIX C

CONTACT RESISTANCE

In accordance with [34] the heat flow from one particle to another contracts in the neighborhood of the contact area between two particles. This contraction of the heat flow lines is amplified in the case of powders under vacuum or in the case of granular materials with a high ratio of constituent conductivities, in which cases the heat flow through contact areas is a major mode of heat transfer. The importance of the contact resistance in the flow of heat in granular materials can be illustrated by the fact that it offers the only explanation as to why the heat flow through perlite at high vacuum at boundary temperatures 76 - 20°K is greater than at temperatures 70 - 4°K, as indicated in [34].

The general procedure followed in the literature is to express the action of the contact areas as a resistance to the heat flow acting between the particle temperatures. Evidently, the heat flow through the contact points depends on the contact area between particles. The expression used by almost all investigators for the radius of this area is Hertz's relation:

$$r_c = \left[\frac{3}{4} \cdot \frac{1-\nu^2}{E} F_1 \cdot \frac{d}{2}\right]^{1/3} \qquad (C\text{-}1)$$

where d, ν and E are the diameter, Poisson's ratio and elastic constant respectively of the solid particles, and F_1 is the force acting on the contact area. In the case of packed beds in which pressures between particles are due to the layers above the layer under consideration, an expression has been derived for the pressure tensor in [86], the corrected form of which is:

$$p_{ij} = \frac{g}{1-\nu}\left(\int_0^D \rho(x)\, dx\right)\left[\nu\, \delta_{ij} + (1-2\nu)\, z_i z_j\right] \qquad \text{(C-2)}$$

Multiplication of Equation (C-2) with the unit normal vector to the contact area gives the average pressure.

As indicated in [87] contact resistance in general depends on the following parameters: apparent contact pressure, solid thermal conductivities, surface roughness, surface waviness, interstitial fluid thermal conductivity, solid hardness, solid modulus of elasticity and mean contact temperature level. However, due to the complexity at which these parameters interact, and the difficulty to express a number of these parameters analytically, the procedure taken by many investigators is to examine the contact resistance in the case of smooth spheres, and correlate the derived expressions by experimentally determined coefficients.

Carslaw and Jaeger [88] examined the thermal resistance of a circular contact area on a semi-infinite body, and found it to be:

$$R_{\infty}^{T} = 1/4\ r_c\ k_s \tag{C-3}$$

under the condition of constant temperature on the area having radius r_c, and:

$$R_{\infty}^{q} = 8/3\ \pi^2\ r_c\ k_s \tag{C-4}$$

under the condition of constant heat flux at the area. The values of R_{∞}^{T} and R_{∞}^{q} differ by 8 percent.

Kanager [73], considered the case of a smooth sphere, thermally insulated everywhere except at two diametrically opposite contact areas. He solved Laplace's equation for this problem, and under the assumption that the temperature of the contact area is equal to the arithetic mean of the temperatures at the center and at the periphery, he found an expression for the equivalent thermal resistance of the sphere, R_s. Then comparing the ratio $R_s/2\ R_{\infty}^{q}$, he found that it increases almost linearly from 1 to 1.05 for values of r_c/r from 0 to 0.1, where r is the radius of the sphere. His

conclusion was that Equations (C-3) and (C-4) provide a sufficiently accurate approximation for the contact resistance.

Luikov [34] states that in addition to the contraction of the heat flow lines, the effect of the microroughness of real particles should be included in the estimation of the contact resistance, together with the effect of any oxidizing film covering the particles. Thus, the contact resistance of granular systems can be represented as the sum of three components:

$$R_c = R_L + R_o + R_{sp} \tag{C-5}$$

where R_L is twice the expression given in Equation (C-3), R_o is the resistance due to any oxidizing film, and R_{sp} is given by:

$$R_{sp} = \frac{h_r k_k}{\pi r_c^2 k_s} \tag{C-6}$$

where h_r and k_k are experimentally determined coefficients depending on the height of the microroughnesses and on the thermal conductivity of the micrographs respectively. Luikov lists the recommended values for h_r and k_k for a number of granular material classes. Finally, he indicates that the thermal conductivity at the contact areas can be represented by:

$$k_{cr} = \frac{1}{R_c d} \tag{C-7}$$

In the case of granular materials under externally applied loads, and in cases when particle deformations cannot be assumed elastic, the contact resistance is given in terms of the applied load, the porosity and the solid conductivity by experimentally derived correlations [34, 61, 89]. Wilhelm et al [37], have developed the following empirical equation for the effect of contact areas:

$$\log_{10} (k_{cr} \times 10^5) = 0.859 + 3.12 \left(\frac{k_s}{p}\right) \qquad \text{(C-8)}$$

where k_{cr} and k_s are in cal/cm sec. °C. In general the values predicted by Equation (C-8) are much higher than those predicted by Equation (C-7).

APPENDIX D

EFFECTIVE PORE SIZE

The equation for k_g^* and k_r have been expressed in terms of an effective distance between particle surfaces D_p, called the effective pore size. In the case of k_g^*, this is the mean distance gas molecules travel from the surface of one particle to that of another, when the molecular mean free path is large. It follows that this parameter is significant both for the geometric characterization of the granular material, as well as for the heat transfer process.

The initial investigations on the characteristics of packings were concerned with systematic arrangements of spheres [66]. By this method, in order to determine the effective pore size for a range of porosities, it was assumed that the spacing of spheres in rhombohedral array is increased by assuming a halo of thickness δ around each sphere, and δ is adjusted to the observed porosity. Dul'nev et al [61] considered this case, and found that the effective pore size is given by:

$$D_p = 4.2\ d\ (A - 2/3) \qquad (D\text{-}1)$$

where: $A = [0.74/(1-P)]^{1/3}$

Haughey and Beveridge [5] investigated both analytically and experimentally the case of randomly packed beds of equal-sized spheres for loose packed (P = 0.3812 - 0.4), poured packed (P = 0.364) and close packed (P = 0.3587) beds. Then, they generalized their results for a wide range of porosities. The reported expressions for the mean void hydraulic diameter and for the mean void equivalent hole volume are respectively as follows:

$$(D_p)_h = \frac{2}{3} \; d \; P/(1-P) \qquad (D\text{-}2)$$

$$V_h = \frac{\pi}{6} \; d^3 \; P/(1-P) \qquad (D\text{-}3)$$

Debbas and Rumpf [51] studied the randomness of beds packed with spheres or irregular shaped particles by means of a statistical approach. Their results are similar to those of Haughey and Beveridge, however the range of porosities examined is not wide enough to allow extrapolation to a wider range of porosities. Nevertheless, an important conclusion that can be reached by the results of both papers is that the local mean voidage is normally distributed, and that beds packed with spheres or irregular particles are in general subject to a statistical analysis. Effectively, it has been shown that in such beds all particles of the same size and shape have the same probability to occupy each unit volume of the mixture. The approach taken by Debbas and Rumpf appears to be very promising with respect to the geometric characterization of

granular materials, but the limited number of experimental data prohibits any generalized conclusions.

The equations presented up to this point have been obtained from geometric considerations. However, as indicated in a previous section, for powders under reduced pressures, most of the heat transfer through the voids takes place in the vicinity of the contact areas. This means that the dimensions effective in conducting heat through the voids are much less than the effective geometric length of the void. To account for this phenomenon, Masamune and Smith [32] considered the volume occupied by pendular rings around the contact points between particles, and derived the following expression for the conduction effective pore size:

$$(D_p)_c = n\, d\, [(\sec\theta - 1)^2\, (1 - (\tfrac{\pi}{2} - \theta)\tan\theta)] \qquad \text{(D-4)}$$

$$n = 6.93 - 5.51\ \frac{P - 0.260}{0.476 - 0.260}$$

$$\theta = \cos^{-1}\,(1 - \tfrac{1}{n}\,)$$

Dul'nev et al [61] have reported the following equation for $(D_p)_c$ based on the kinetic theory of gases:

$$(D_p)_c = d\ \frac{1.14\ P - 0.14}{6(1 - P)} \qquad \text{(D-5)}$$

Another approach is to correlate the experimentally determined values for the breakaway pressure to Equation (A-1). Effectively, the pressure at which the effective thermal conductivity of a granular material is reduced by 5 percent was determined from a number of experimental data in the region A of Figure A-1. Subsequently, the value of k_g^*/k_g required to attain this decrease in k_e was calculated, and from Equation (A-1) the corresponding value of $(D_p)_c$ was determined. The experimental data were taken from References [21, 32, 58, 59, 61, 62, 63]. The least squares fit of $(D_p)_c/d$ as a function of P is:

$$\frac{(D_p)_c}{d} = \frac{0.2177\ P - 0.051}{1 - P} \qquad \text{(D-6)}$$

for

$$0.3 < P < 0.7$$

The values of D_p/d predicted by the equations discussed in this section are plotted in Figure D-1 as a function of P.

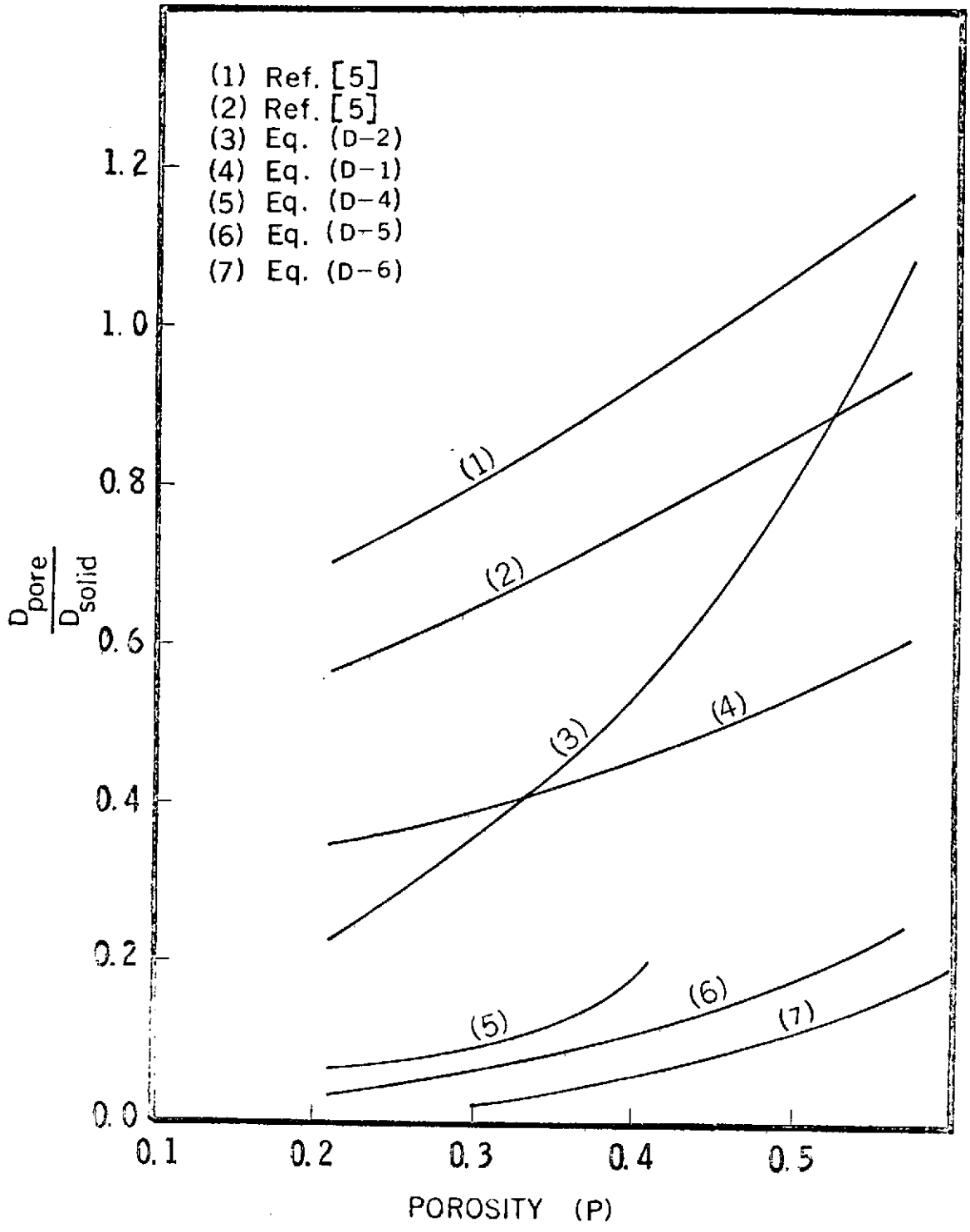

FIGURE D-1. EQUIVALENT PORE SIZE OF GRANULAR MATERIALS.

APPENDIX E

COORDINATION NUMBER

It is evident that the heat flux through contact areas depends on the number of contacts each particle has with its neighbors, or the coordination number n [5]. This number is known for regular packings of spheres and is 6 for cubic packing (P = 0.476), 8 for orthorhombic packing (P = 0.3954), 10 for tetragonal-sphenoidal packing (P = 0.3019), and 12 for rhombohedral packing (P = 0.2595). In addition to these fixed values, extensive experimental work has been done [49, 90, 91, 92] to find the coordination number for random packed beds of spheres, as indicated in Figure E-1. However, almost all of the experimental work has been carried out for loose random and close random beds, and consequently in order to find a relation between n and P extrapolation beyond the experimental data is required.

Dul'nev et al [61] have proposed the following equation:

$$n = 11.6 \, (1 - P) \qquad \text{(E-1)}$$

represented by curve 5 in Figure E-1. However it is seen that the predicted values of n are too high at large porosities.

Willhite et al [31] used the results of Smith et al [90] and proposed the following equation:

$$n = 6 \cdot \frac{5.01 - 8.42 \, P}{1.91 - 1.91 \, P} \qquad \text{(E-2)}$$

However, as noted in [49], this equation is in good agreement with the experimental results of Smith et al, but not with recent experimental data.

Kunii and Smith [30] considered the packed bed to be composed of spheres in the most open packed state and in the closest packed state, and taking into account the frequency and orientation of each cell, they derived the following semi-empirical relationship for the coordination number:

$$n = 13.86 - 51.0\ (P - 0.26) \tag{E-3}$$

This equation is represented by curve 2 in Figure E-1, and it is seen that it overpredicts n for low values of P.

Haughey and Beveridge [5, 49] examined the distribution of the number of sphere centers found in spherical shells at varying distances from a given sphere, and for a random bed of spheres they developed the following expression for the coordination number:

$$n = 22.47 - 39.39\ P \tag{E-4}$$

This equation is represented by curve 3 in Figure E-1, and it is seen that it provides the best fit to experimental data.

It should be noted that all equations and experimental data presented in Figure 8 are based on randomly or regularly packed

beds of spheres. However, all heat transfer models, in which contact resistance has been included, have utilized one of these equations for the coordination number. In this study Equation (E-4) has been used, with the reservation that although its application has been extended to mixtures of non-uniform particles, no better expression has been found for real physical systems.

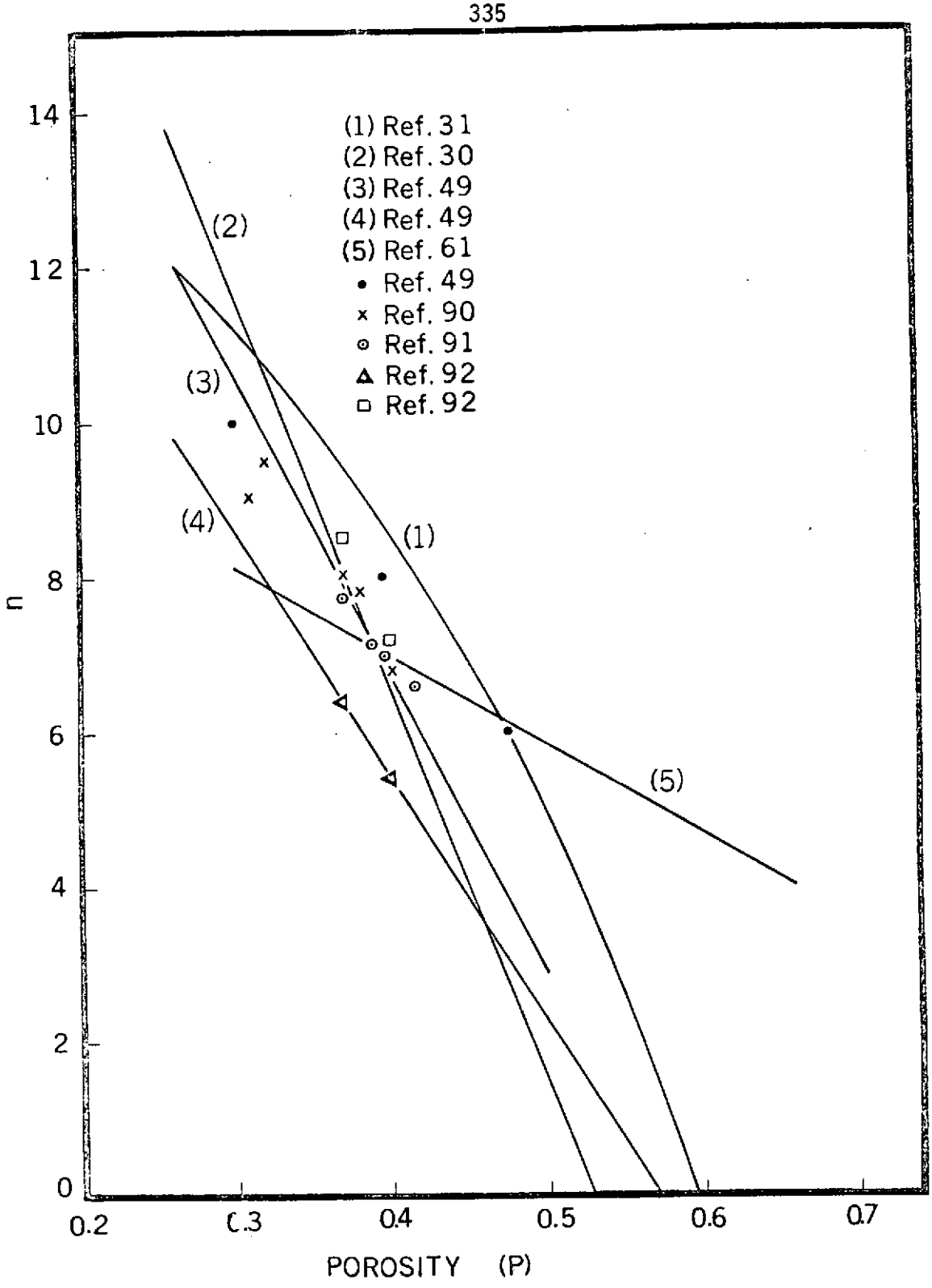

FIGURE E-1. CO-ORDINATION NUMBER.

APPENDIX F

PACKING THEORY

One of the most significant complications in the development of a model that predicts reasonably well the effective thermal conductivity of heterogeneous materials is the construction of the geometry of such a model. This complication arises from the large number of parameters associated with the structural properties of packed beds, as indicated in an excellent review of the subject by Haughey and Beveridge [49].

In general, the structural properties of packed beds are characterized either by a single representative dimension, or through a distribution described by mean, variance, skewness, etc. In this study the first approach has been utilized. Moreover, the equations presented for the effective pore size and coordination number are based on random packings of equal sized spheres. This approach has been necessitated by the fact that most experimental and statistical work in the literature is referred to this type of packings. Even for this simplified case, it can be seen from Figures D-1 and E-1 that the effective pore size and coordination number suggested by various investigators differ greatly.

Most practical applications involve a particle size variation between 2 and 100 fold. The mixing of smaller particles into a bed

of larger particles produces two opposing effects. On one hand, the smaller particles tend to increase the voidage by forcing the larger particles apart thus increasing the size of voids between particles, on the other hand the smaller particles tend to decrease the voidage by filling the voids between larger particles. The characteristics of such packed beds do not depend only on the particle shape, and size ratio but also on the amount of each size fraction present. Consequently, from the same particle size distributions, packed beds having a wide range of voidages can be obtained. As indicated in [49, 50, 51, 66] very little information exists about the characteristics of packed beds involving large particle size variations. Consequently, a great degree of ambiguity exists whether a volume mean particle size together with the associated effective pore size calculated from the expressions given in Appendix D provide a sufficiently accurate description of the packed bed. This is especially important in the case of evacuated powders, in which case both particle size and effective pore size are primary parameters in the calculation of the effective thermal conductivity. In particular, for lunar fines the particle size range is from 0.1μm to approximately 800μm [119], with most of the particles in the lower size range, and the porosity is assumed to be approximately 0.5. At present, the selection of a particular mean volumetric particle size for the calculation of the effective conductivity is highly speaclative, since no experimental data exist on the local voidage variation for similar packings to compare calculated values.

Evidently, description of packed beds utilizing the local property variations provides a much better approximation to the geometry than characterization of the beds by a single representative dimension. At present, the mean and variance of local properties has been determined in the literature with a satisfactory degree of confidence only for loose packed, poured packed, and close packed random beds of equal sized spheres [5]. Utilization of these data in any future model will probably provide a further refinement to the predicted effective thermal conductivity values of heterogeneous mixtures.

APPENDIX G

FORTRAN IV COMPUTER

PROGRAMS

```
C      THERMAL CONDUCTIVITIES PREDICTED BY FOLLOWING MODELSO
C      1. RUSSELL  2. BERNSTIEN  3. WOODSIDE  4. CRANE AND VACHON
C      (EQUATION 5-2)
       IMPLICIT REAL*4(A-Z)
       INTEGER*4 I,INDEX
       COMMON KC, KD, L, MU, PD, SIGMA, T  ,KE,Q ,CK
       DIMENSION SUM(10),PLOT1(173),PLOT2(173),PLOT3(173),PLOT4(173),
      *Y(173),XLAB(5),YLAB(5),GLAB(5),DATLAB(5)
        DATA SUM,INDEX/10*0.0,0/
       EXTERNAL F
       SUM1BI=0.
       SUM2BI=0.
       SUM3BI=0.
       SUM4BI=0.
       SUMSQ1=0.
       SUMSQ2=0.
       SUMSQ3=0.
       SUMSQ4=0.
       SUMK1E=0.
       SUMK2E=0.
       SUMK3E=0.
       SUMK4E=0.
        PI=3.14159
       READ(5,5)XLAB,YLAB,GLAB,DATLAB
     5 FORMAT(20A4)
   1   WRITE(6,100)
   100 FORMAT(1H1,////////////////,25X,'DATA',17X,'EFFECTIVE THERMAL CONDU
      $CTIVITY (KCAL/M-HR-K) X 100 ',//,25X,'CASE',1X ,
      $'  EXPERIMENTAL  ',' RUSSELL  ',' BERNSTEIN  ',
      $'   WOODSIDE   ',' CRANE &  ',/,30X,
      $'              ',' ','                ',
      $'              ',' VACHON  ',/)
    2  READ(5,3,END=6) KC,KD,PD,EXKE,CASE,CASE1,CASE2,MV,MR
    3  FORMAT(4F10.5,3A4,2(F5.0))
       INDEX=INDEX+1
       Y(INDEX)=ALOG10(EXKE/KC)
       E=1.0-PD
       MU=1.0-PD
       IF (MV.GE.1) CALL VACUUM
       SIGMA=0.32248*PD-0.092543*PD**2
       CALL QG10(0.,1.,F,INTF)
       KE=1./INTF
       IF (MR.GE.1) CALL RAD
       CE=KE/KC
       CXKE=EXKE/KC
       DIF=(CE-CXKE)/CXKE
       K4=KE
       PLOT4(INDEX)=ALOG10(K4/KC)
```

```
C       BERNSTEIN
        EP=E
        IF(PD.GE.0.5) GO TO 44
        K2=KC*(4.0*PD/(1.0+KC/KD)+KD/KC*(1.0-2.0*PD))
        GO TO 46
   44   K2=KC*(4.0*EP/(1.0+KC/KD)+(2.0*PD-1.0))
   46   CONTINUE
        PLOT2(INDEX)=ALOG10(K2/KC)
C       WOODSIDE
        RATIO=PI/6.0
        IF(EP.GE.RATIO) EP=RATIO
        A=SQRT(1.0+4.0/(PI*(KD/KC-1.0)*(6.0*EP/PI)**(2./3.)))
        IF(A.LE.1.00001)A=1.00001
        K3=KC/(1.0-(6.0*EP/PI)**(1./3.)*(1.0-(A-1.0/A)*ALOG((A+1.)/(A-1.))
       *    ))
        K3=K3*2.0
        PLOT3(INDEX)=ALOG10(K3/KC)
C       RUSSELL
        R1=2.0/3.0
         K1=KC*(E**R1+KC/KD*(1.0-E**R1))/(E**R1-E+KC/KD*(1.0-E**R1+E))
        PLOT1(INDEX)=ALOG10(K1/KC)
        WRITE(6,200)INDEX,EXKE,K1,K2,K3,K4
  200   FORMAT(/,25X,I4,4X,5(F10.5,6X))
        BK1=((K1-EXKE)/EXKE)*100.
        BK2=((K2-EXKE)/EXKE)*100.
        BK3=((K3-EXKE)/EXKE)*100.
        BK4=((K4-EXKE)/EXKE)*100.
        K1OFF=ABS(BK1)
        K2OFF=ABS(BK2)
        K3OFF=ABS(BK3)
        K4OFF=ABS(BK4)
        SUM1BI=SUM1BI+BK1
        SUM2BI=SUM2BI+BK2
        SUM3BI=SUM3BI+BK3
        SUM4BI=SUM4BI+BK4
        SQK1ER=K1OFF**2
        SQK2ER=K2OFF**2
        SQK3ER=K3OFF**2
        SQK4ER=K4OFF**2
        SUMSQ1=SUMSQ1+SQK1ER
        SUMSQ2=SUMSQ2+SQK2ER
        SUMSQ3=SUMSQ3+SQK3ER
        SUMSQ4=SUMSQ4+SQK4ER
        SUMK1E=SUMK1E+K1OFF
        SUMK2E=SUMK2E+K2OFF
        SUMK3E=SUMK3E+K3OFF
        SUMK4E=SUMK4E+K4OFF
        GO TO 2
```

```
  6 BOCASE=FLOAT(INDEX)
    AVBI1=SUM1BI/BOCASE
    AVBI2=SUM2BI/BOCASE
    AVBI3=SUM3BI/BOCASE
    AVBI4=SUM4BI/BOCASE
    T1ERAV=SUMK1E/BOCASE
    T2ERAV=SUMK2E/BOCASE
    T3ERAV=SUMK3E/BOCASE
    T4ERAV=SUMK4E/BOCASE
    T1ERVA=((SUMSQ1/BOCASE)-T1ERAV**2)/10000.
    T2ERVA=((SUMSQ2/BOCASE)-T2ERAV**2)/10000.
    T3ERVA=((SUMSQ3/BOCASE)-T3ERAV**2)/10000.
    T4ERVA=((SUMSQ4/BOCASE)-T4ERAV**2)/10000.
    WRITE(6,573)AVBI1,AVBI2,AVBI3,AVBI4,T1ERAV,T2ERAV,T3ERAV,T4ERAV,T1
   *ERVA,T2ERVA,T3ERVA,T4ERVA
573 FORMAT(3X,8F8.2,4F12.4)
    GO TO 621
    CALL ORIGIN(2.5,3.5,1)
     CALL GRAPH(173,Y,PLOT1,3,-7,-5.,-5.,2.,0.,2.,0.,XLAB,YLAB,GLAB,
   *DATLAB)
    CALL ORIGIN(8.5,0.,1)
     CALL GRAPH(173,Y,PLOT2,3,-7,-5.,-5.,2.,0.,2.,0.,XLAB,YLAB,GLAB,
   *DATLAB)
    CALL ORIGIN(8.5,0.,1)
     CALL GRAPH(173,Y,PLOT3,3,-7,-5.,-5.,2.,0.,2.,0.,XLAB,YLAB,GLAB,
   *DATLAB)
    CALL ORIGIN(8.5,0.,1)
     CALL GRAPH(173,Y,PLOT4,3,-7,-5.,-5.,2.,0.,2.,0.,XLAB,YLAB,GLAB,
   *DATLAB)
    CALL ORIGIN(8.5,0.,1)
621 CONTINUE
    STOP
    END
    FUNCTION F(P)
    REAL MU,KC,KD,INTF,KE,LAMMA,KBOLTZ,K,KNUDSN,L,KR
    COMMON KC, KD, L, MU, PD, SIGMA, T  ,KE,Q  ,CK
    X=SIGMA*SQRT(2.0)
    FNORM=ERF((1.0-MU)/X)-ERF((0.-MU)/X)
    P2=(ERF((1.0-MU)/X)-ERF((P-MU)/X))/FNORM
    F=1.0/(KC+(KD-KC)*P2)
    RETURN
    END
```

```
      SUBROUTINE VACCUM
      REAL MU,KC,KD,INTF,KE,LAMMA,KBOLTZ,K,KNUDSN,L,KK
      COMMON KC, KD, L, MU, PD, SIGMA, T  ,KE,Q  ,CK
      READ(5,4)T,PRESS,DIAG,K,PR,L,A
4     FORMAT(7E10.0)
      KBOLTZ=1.3804E-23
      PI=3.14159
      C1=.495
      CH=PRESS*1.333224E+7
      CH=PRESS
      WRITE(6,100) CH,DIAG, A, PR, K, L
100   FORMAT(6E11.4)
      LAMMA=KBOLTZ*T/(SQRT(2.)*CH*PI*DIAG**2)*10.0**5
      G=((2.-A)/A)*4.*C1*K/(K+1.)*LAMMA/PR
      KNUDSN=LAMMA/L
      PORE=L*(0.74/MU)**2/43.
      KC=CK/(1.+2.*G/PORE)
      WRITE(6,101) LAMMA,G,KNUDSN,KC
101   FORMAT(4E11.4)
      RETURN
      END
```

```
      SUBROUTINE RAD
      REAL MU,KC,KD,INTF,KE,LAMMA,KBOLTZ,K,KNUDSN,L,KR
      COMMON KC, KD, L, MU, PD, SIGMA, T  ,KE,Q ,CK
      READ(5,1)T,EP
    1 FORMAT (2F10.5)
      EP=0.95
      SIGMAR=5.668E-8
      D=L
      KR=4.0*EP*SIGMAR*D*T**3/((2.0-EP))
      KE=KE+KR
      RETURN
      END
```

```
C     COMPUER PROGRAM FOR THE NODULAR MODEL
      INTEGER CASE
      REAL KS,KG,KE,KC,KD
      DIMENSION N(N1+2,N1+2,N1+2),R(N1+2,N1+2,N1+2),T(N1+2,N1+2,N1+2),TK
     *(6,N1+2,N1+2,N1+2)
      DIMENSION D(3),C(6)
      N1
      N2=N1+2
      N3=N1+1
      N4=N1-1
      IY=3
      YFL=0.0
      ITEST=0
    1 READ(5,3,END=1000)KS,KG,P,EXKE,CASE
    3 FORMAT(4F10.5,A5)
      READ(5,159)DIAM,POISON,YOUNG,DENS,DEPTH,COEF1,COEF2
  159 FORMAT(E8.3,F4.3,2E8.3,F4.3,F5.4,F4.2)
      WRITE(6,4)
    4 FORMAT(///)
      ITEST=ITEST+1
      M1=N1**3
      M2=N2**3
      M=0
      PORES=P*FLOAT(M2)
      LPORES=PORES
      DO 2 I=1,N2
      DO 2 J=1,N2
      DO 2 K=1,N2
      N(I,J,K)=0
    2 CONTINUE
   20 IA=0
   21 IA=IA+1
      IX=IY
      CALL RANDU(IX,IY,YFL)
      D(IA)=YFL*FLOAT(N2)
      IF(IA-3)21,22,22
   22 CONTINUE
      I1=D(1)
      I2=D(2)
      I3=D(3)
      I=I1+1
      J=I2+1
      K=I3+1
      LA=N(I,J,K)
      IF(LA-1)23,20,20
   23 N(I,J,K)=1
      M=M+1
      IF(M-LPORES)20,24,24
```

```
 24 CONTINUE
    WRITE(6,340)M
340 FORMAT(3X,'M=',I4)
    A=0.5
    DO 5 K=2,N3
    DO 6 I=1,N2
    DO 6 J=1,N2
  6 T(I,J,K)=A
    A=A+1.
  5 CONTINUE
    DO 38 K=2,N3
    DO 38 I=2,N3
    DO 38 J=2,N3
    IF(N(I,J,K))7,7,8
  7 B=1.
    GO TO 9
  8 B=0.
  9 IF(I-2)202,202,160
160 IF(N(I-1,J,K))202,11,12
 11 C(1)=1.0
    GO TO 203
 12 C(1)=0.
203 TK(1,I,J,K)=((B*KS+(1.-B)*KG)*(C(1)*KS+(1.-C(1))*KG))/(0.5*(B*KS+(
   *1.-B)*KG)+0.5*(C(1)*KS+(1.-C(1))*KG))
    GO TO 13
202 TK(1,I,J,K)=0.
 13 IF(I-N3)161,204,204
161 IF(N(I+1,J,K))204,14,15
 14 C(2)=1.0
    GO TO 205
 15 C(2)=0.
205 TK(2,I,J,K)=((B*KS+(1.-B)*KG)*(C(2)*KS+(1.-C(2))*KG))/(0.5*(B*KS+(
   *1.-B)*KG)+0.5*(C(2)*KS+(1.-C(2))*KG))
    GO TO 16
204 TK(2,I,J,K)=0.
 16 IF(J-2)206,206,162
162 IF(N(I,J-1,K))206,17,18
 17 C(3)=1.0
    GO TO 207
 18 C(3)=0.
207 TK(3,I,J,K)=((B*KS+(1.-B)*KG)*(C(3)*KS+(1.-C(3))*KG))/(0.5*(B*KS+(
   *1.-B)*KG)+0.5*(C(3)*KS+(1.-C(3))*KG))
    GO TO 19
206 TK(3,I,J,K)=0.
 19 IF(J-N3)163,208,208
163 IF(N(I,J+1,K))208,30,31
 30 C(4)=1.0
    GO TO 209
```

```
 31 C(4)=0.
209 TK(4,I,J,K)=((B*KS+(1.-B)*KG)*(C(4)*KS+(1.-C(4))*KG))/(0.5*(B*KS+(
   *1.-B)*KG)+0.5*(C(4)*KS+(1.-C(4))*KG))
    GO TO 32
208 TK(4,I,J,K)=0.
 32 IF(K-2)210,210,350
350 IF(N(I,J,K-1))210,33,34
 33 C(5)=1.0
    GO TO 211
 34 C(5)=0.
211 TK(5,I,J,K)=((B*KS+(1.-B)*KG)*(C(5)*KS+(1.-C(5))*KG))/(0.5*(B*KS+(
   *1.-B)*KG)+0.5*(C(5)*KS+(1.-C(5))*KG))
    GO TO 35
210 TK(5,I,J,K)=0.
 35 IF(K-N3)351,212,212
351 IF(N(I,J,K+1))212,36,37
 36 C(6)=1.0
    GO TO 213
 37 C(6)=0.
213 TK(6,I,J,K)=((B*KS+(1.-B)*KG)*(C(6)*KS+(1.-C(6))*KG))/(0.5*(B*KS+(
   *1.-B)*KG)+0.5*(C(6)*KS+(1.-C(6))*KG))
    GO TO 38
212 TK(6,I,J,K)=0.
 38 CONTINUE
    PRES=DEPTH*(1.-P)*DENS
    RSP=0.93*(DIAM/2.)*((((1.-(POISUN**2))*PRES)/(YOUNG*((1.-P)**2)))*
   **0.3333)
    HR=COEF1*DIAM
    KC=RSP/((0.5+((HR*COEF2)/(3.14*RSP)))*DIAM)
    CONTR=KC*KS
185 IF(ITEST-1)186,186,187
186 CONTAC=95.*(22.47-(39.39*P))
    GO TO 191
187 IF(ITEST-3)188,188,189
188 CONTAC=100.*(22.47-(39.39*P))
    GO TO 191
189 IF(ITEST-6)190,190,191
190 CONTAC=110.*(22.47-(39.39*P))
191 CONTINUE
    IF(CONTAC)158,157,157
158 CONTAC=0.
157 CONTINUE
    LCONT=CONTAC
    WRITE(6,325)LCONT,CONTR
325 FORMAT(3X,'LCONT=',I4,' CONTR=',E10.5)
    NUM=0
    NTEST=0
302 IA=0
```

```
      NTEST=NTEST+1
  300 IA=IA+1
      IX=IY
      CALL RANDU(IX,IY,YFL)
      D(IA)=YFL*FLOAT(N1)
      IF(IA-3)300,301,301
  301 CONTINUE
      I1=D(1)
      I2=D(2)
      I3=D(3)
      I=I1+2
      J=I2+2
      K=I3+2
      IF(N(I,J,K))302,303,302
  303 IF(N(I-1,J,K))304,305,304
  305 IF(TK(1,I,J,K)-CONTR)306,304,306
  306 IF(I-2)330,330,70
  330 TK(1,I,J,K)=CONTR
      GO TO 71
   70 TK(2,I-1,J,K)=CONTR
      TK(1,I,J,K)=CONTR
   71 NUM=NUM+1
  304 IF(N(I+1,J,K))307,309,307
  309 IF(TK(2,I,J,K)-CONTR)331,307,331
  331 IF(I-N3)72,308,308
  308 TK(2,I,J,K)=CONTR
      GO TO 73
   72 TK(1,I+1,J,K)=CONTR
      TK(2,I,J,K)=CONTR
   73 NUM=NUM+1
  307 IF(N(I,J-1,K))310,311,310
  311 IF(TK(3,I,J,K)-CONTR)332,310,332
  332 IF(J-2)80,80,74
   80 TK(3,I,J,K)=CONTR
      GO TO 75
   74 TK(4,I,J-1,K)=CONTR
      TK(3,I,J,K)=CONTR
   75 NUM=NUM+1
  310 IF(N(I,J+1,K))313,314,313
  314 IF(TK(4,I,J,K)-CONTR)315,313,315
  315 IF(J-N3)76,81,81
   81 TK(4,I,J,K)=CONTR
      GO TO 77
   76 TK(3,I,J+1,K)=CONTR
      TK(4,I,J,K)=CONTR
   77 NUM=NUM+1
  313 IF(N(I,J,K-1))316,318,316
  318 IF(TK(5,I,J,K)-CONTR)319,316,319
```

```
319 IF(K-2)82,82,83
 82 TK(5,I,J,K)=CONTR
    GO TO 84
 83 TK(5,I,J,K)=CONTR
    TK(6,I,J,K-1)=CONTR
 84 NUM=NUM+1
316 IF(N(I,J,K+1))321,322,321
322 IF(TK(6,I,J,K)-CONTR)86,321,86
 86 IF(K-N3)323,87,87
 87 TK(6,I,J,K)=CONTR
    GO TO 85
323 TK(6,I,J,K)=CONTR
    TK(5,I,J,K+1)=CONTR
 85 NUM=NUM+1
    IF(NTEST-15000)321,321,100
321 IF(NUM-LCONT)302,324,324
324 CONTINUE
    DO 88 J=2,N3
    DO 88 K=2,N3
    TK(1,2,J,K)=0.
    TK(2,N3,J,K)=0.
 88 CONTINUE
    DO 89 I=2,N3
    DO 89 K=2,N3
    TK(3,I,2,K)=0.
    TK(4,I,N3,K)=0.
 89 CONTINUE
    DO 90 I=2,N3
    DO 90 J=2,N3
    TK(5,I,J,2)=0.
    TK(6,I,J,N3)=0.
 90 CONTINUE
    WRITE(6,500)NUM
500 FORMAT(3X,'NUM=',I4)
502 WRITE(6,501)NTEST
501 FORMAT(3X,'NTEST=',I5)
    L1=0.
101 L1=L1+1
    SR=0.
    DO 10 K=3,N1
    DO 10 I=2,N3
    DO 10 J=2,N3
    R(I,J,K)=TK(1,I,J,K)*(T(I-1,J,K)-T(I,J,K))+TK(2,I,J,K)*(T(I+1,J,K)
   *-T(I,J,K))+TK(3,I,J,K)*(T(I,J-1,K)-T(I,J,K))+TK(4,I,J,K)*(T(I,J+1,
   *K)-T(I,J,K))+TK(5,I,J,K)*(T(I,J,K-1)-T(I,J,K))+TK(6,I,J,K)*(T(I,J,
   *K+1)-T(I,J,K))
    STK=0.
    DO 40 L=1,6
```

```
      TTK=TK(L,I,J,K)
      STK=STK+TTK
   40 CONTINUE
      T(I,J,K)=T(I,J,K)+1.2*(R(I,J,K)/STK)
      SR=SR+ABS(R(I,J,K)/STK)
   10 CONTINUE
      WRITE(6,103)SR
  103 FORMAT(3X,'SR=',E10.4)
      IF(L1-50)150,150,100
  150 IF(SR-5.)102,102,101
  102 CONTINUE
      WRITE(6,104)L1
  104 FORMAT(3X,'L1=',I4)
      AVHEAT=0.
      DO 44 K=2,N1
      THEAT=0.
      DO 45 I=2,N3
      DO 45 J=2,N3
   51 HEAT=(TK(6,I,J,K))*(T(I,J,K+1)-T(I,J,K))
      THEAT=THEAT+HEAT
   45 CONTINUE
      WRITE(6,52)K,THEAT
   52 FORMAT(3X,'K=',I2,'    THEAT=',E10.4)
      AVHEAT=AVHEAT+THEAT
   44 CONTINUE
      KE=AVHEAT/900.
      RATIO=KS/KG
      OFF=((KE-EXKE)/EXKE)*100.
      WRITE(6,105)CASE,KS,KG,P,RATIO,KE,EXKE,OFF
  105 FORMAT(3X,'CASE=',A5,'  KS=',F10.5,'  KG=',F10.5,'  P=',F5.3,'  RA
     *TIO=',F8.2,'  KE=',F10.5,'  EXKE=',F10.5,'  OFF=',F7.2)
  100 CONTINUE
      GO TO 1
 1000 STOP
      END
```

```
C       CALCULATION OF EFFECTIVE THERMAL CONDUCTIVITY OF GRANULAR MATER-
C       IALS AT ATMOSPHERIC PRESSURES EXK=EXPERIMENTAL COND., KC=COND. OF
C       CONTINUOUS(GAS OR LIQUID) PHASE, KD=COND. OF DISCONTINUOUS (SOLID)
C       PHASE, P=POROSITY, F=VOLUME FRACTION OF SOLID PHASE, K1=EFF. COND.
C       BY MODEL, K2=BY KRUPICZKA, K3=BY RUSSELL, K4=BY LICHTENECKER AND
C       SON FREY, K5=BY JEFFERSON, K6=BY MAXWELL, K7=BY RAYLEIGH, K8= BY
C       WOODSIDE AND MESSMER, K9=BY MEREDITH AND TOBIAS.
        INTEGER CASE
        REAL K1,K2,K3,K4,K5,K6,K7,K8,K9,KC,KD,KS,KG,K1P,K1BIAS,K2BIAS,K3BI
       *AS,K4BIAS,K5BIAS,K6BIAS,K7BIAS,K8BIAS,K9BIAS
        DIMENSION BK1(100),BK2(100),BK3(100),BK4(100),BK5(100),BK6(100),BK
       *7(100),BK8(100),BK9(100),VOLF(100),KC(100),KD(100),EXK(100),RK(100
       *),RK1(100),RK2(100),RK3(100),RK4(100),RK5(100),RK6(100),RK7(100),R
       *K8(100),RK9(100),POR(100),K1BIAS(100),K2BIAS(100),K3BIAS(100),K4BI
       *AS(100),K5BIAS(100),K6BIAS(100),K7BIAS(100),K8BIAS(100),K9BIAS(100
       *),K1(100),K2(100),K3(100),K4(100),K5(100),K6(100),K7(100),K8(100),
       *K9(100)
        NOCASE=92
        SUM1BI=0.
        SUM2BI=0.
        SUM3BI=0.
        SUM4BI=0.
        SUM5BI=0.
        SUM6BI=0.
        SUM7BI=0.
        SUM8BI=0.
        SUM9BI=0.
        SUMSQ1=0.
        SUMSQ2=0.
        SUMSQ3=0.
        SUMSQ4=0.
        SUMSQ5=0.
        SUMSQ6=0.
        SUMSQ7=0.
        SUMSQ8=0.
        SUMSQ9=0.
        SUMK1E=0.
        SUMK2E=0.
        SUMK3E=0.
        SUMK4E=0.
        SUMK5E=0.
        SUMK6E=0.
        SUMK7E=0.
        SUMK8E=0.
        SUMK9E=0.
        DO 35 I=1,NOCASE
        READ(5,4)KS,KG,P,EXKE,CASE,K1P
    4   FORMAT(4F10.5,A5,F10.5)
```

```
      READ(5,159)DIAM,POISON,YOUNG,DENS,DEPTH,COEF1,COEF2
  159 FORMAT(E8.3,F4.3,2E8.3,F4.3,F5.4,F4.2)
      K1(I)=K1P/100.
      EXK(I)=EXKE
      VOLF(I)=1.-P
      POR(I)=P
      F=1.-P
      C=KG
      D=KS
      KC(I)=KG
      KD(I)=KS
      K2(I)=KG*((KS/KG)**(.280-(.757*ALOG10(P))-(.057*ALOG10(KS/KG))))
      FP=(1.-P)**.6667
      FQ=(1.-P)**.33333
      R=KG/KS
      K3(I)=KG*(FP+R*(1.-FP))/(FP-1.+P+R*(2.-P-FP))
      K4(I)=KG*(1.-FQ+FP+R*(1.-FQ))/(1.-FQ+R)
      W=2.*KG+KS-2.*(1.-P)*(KG-KS)
      Z=2.*KG+KS+F*(KG-KS)
      K6(I)=C*W/Z
      B=F**3.3333*1.569*(C-D)/(4.*C+3.*D)
      K7(I)=C*(W-B)/(Z-B)
      K8(I)=C*(((F+0.03)**2*D)/(0.03*D+F*C))+0.97-F)
    6 X=(D/C-1.)/(D/C+2.)
      K9(I)=(2.+2.*F*X)*(2.+F*(2.*X-1.))/((2.-X*F)*(2.-F*(X+1.)))*C
      XN=.403/FQ-.5
      XK=C*D*(2.*D/(D-C)**2*ALOG(D/C)-2./(D-C))
      XP=.7854/(1.+2.*XN)**2
      K5(I)=C*(1.-XP)+XP*(.5+XN)*XK*C/(.5*C+XN*XK)
      K1BIAS(I)=(((K1(I)-EXKE)/EXKE)*100.)
      K2BIAS(I)=(((K2(I)-EXKE)/EXKE)*100.)
      K3BIAS(I)=(((K3(I)-EXKE)/EXKE)*100.)
      K4BIAS(I)=(((K4(I)-EXKE)/EXKE)*100.)
      K5BIAS(I)=(((K5(I)-EXKE)/EXKE)*100.)
      K6BIAS(I)=(((K6(I)-EXKE)/EXKE)*100.)
      K7BIAS(I)=(((K7(I)-EXKE)/EXKE)*100.)
      K8BIAS(I)=(((K8(I)-EXKE)/EXKE)*100.)
      K9BIAS(I)=(((K9(I)-EXKE)/EXKE)*100.)
      BK1(I)=ABS(K1BIAS(I))
      BK2(I)=ABS(K2BIAS(I))
      BK3(I)=ABS(K3BIAS(I))
      BK4(I)=ABS(K4BIAS(I))
      BK5(I)=ABS(K5BIAS(I))
      BK6(I)=ABS(K6BIAS(I))
      BK7(I)=ABS(K7BIAS(I))
      BK8(I)=ABS(K8BIAS(I))
      BK9(I)=ABS(K9BIAS(I))
      RK1(I)=K1(I)/C
```

```
      RK2(I)=K2(I)/C
      RK3(I)=K3(I)/C
      RK4(I)=K4(I)/C
      RK5(I)=K5(I)/C
      RK6(I)=K6(I)/C
      RK7(I)=K7(I)/C
      RK8(I)=K8(I)/C
      RK9(I)=K9(I)/C
      RK(I)=D/C
      SUM1BI=SUM1BI+K1BIAS(I)
      SUM2BI=SUM2BI+K2BIAS(I)
      SUM3BI=SUM3BI+K3BIAS(I)
      SUM4BI=SUM4BI+K4BIAS(I)
      SUM5BI=SUM5BI+K5BIAS(I)
      SUM6BI=SUM6BI+K6BIAS(I)
      SUM7BI=SUM7BI+K7BIAS(I)
      SUM8BI=SUM8BI+K8BIAS(I)
      SUM9BI=SUM9BI+K9BIAS(I)
      SQK1ER=BK1(I)**2
      SQK2ER=BK2(I)**2
      SQK3ER=BK3(I)**2
      SQK4ER=BK4(I)**2
      SQK5ER=BK5(I)**2
      SQK6ER=BK6(I)**2
      SQK7ER=BK7(I)**2
      SQK8ER=BK8(I)**2
      SQK9ER=BK9(I)**2
      SUMSQ1=SUMSQ1+SQK1ER
      SUMSQ2=SUMSQ2+SQK2ER
      SUMSQ3=SUMSQ3+SQK3ER
      SUMSQ4=SUMSQ4+SQK4ER
      SUMSQ5=SUMSQ5+SQK5ER
      SUMSQ6=SUMSQ6+SQK6ER
      SUMSQ7=SUMSQ7+SQK7ER
      SUMSQ8=SUMSQ8+SQK8ER
      SUMSQ9=SUMSQ9+SQK9ER
      SUMK1E=SUMK1E+BK1(I)
      SUMK2E=SUMK2E+BK2(I)
      SUMK3E=SUMK3E+BK3(I)
      SUMK4E=SUMK4E+BK4(I)
      SUMK5E=SUMK5E+BK5(I)
      SUMK6E=SUMK6E+BK6(I)
      SUMK7E=SUMK7E+BK7(I)
      SUMK8E=SUMK8E+BK8(I)
      SUMK9E=SUMK9E+BK9(I)
   35 CONTINUE
      WRITE(6,1)
    1 FORMAT('1',/////15X,'TABLE II. EXPERIMENTAL AND PREDICTED THERMAL
```

```
  *CONDUCTIVITIES')
   WRITE(6,60)
60 FORMAT(35X,'FOR VARIOUS MODELS')
   WRITE(6,3)
 3 FORMAT(//15X,'CASE',4X,'EXKE',4X,'MODEL',3X,'KRUPIC.',2X,'RUSSELL'
  *,3X,'LICHT.',1X,'JEFFERSON')
   DO 36 I=1,48
   WRITE(6,7)I,EXK(I),K1(I),K2(I),K3(I),K4(I),K5(I)
 7 FORMAT(16X,I2,1X,6F9.4)
36 CONTINUE
   WRITE(6,1)
   WRITE(6,60)
   WRITE(6,3)
   DO 37 I=49,92
   WRITE(6,2)I,EXK(I),K1(I),K2(I),K3(I),K4(I),K5(I)
 2 FORMAT(16X,I2,1X,6F9.4)
37 CONTINUE
   WRITE(6,61)
61 FORMAT('1',/////14X,'TABLE III. EXPERIMENTAL AND PREDICTED THERMAL
  * CONDUCTIVITIES')
   WRITE(6,60)
   WRITE(6,33)
33 FORMAT(//15X,'CASE',5X,'EXKE',4X,'MAXWELL',2X,'RAYLEIGH',3X,'W AND
  * M',3X,'M AND T')
   DO 38 I=1,48
   WRITE(6,30)I,EXK(I),K6(I),K7(I),K8(I),K9(I)
30 FORMAT(16X,I2,1X,5F10.4)
38 CONTINUE
   WRITE(6,61)
   WRITE(6,60)
   WRITE(6,33)
   DO 39 I=49,92
   WRITE(6,31)I,EXK(I),K6(I),K7(I),K8(I),K9(I)
31 FORMAT(16X,I2,1X,5F10.4)
39 CONTINUE
   WRITE(6,40)
40 FORMAT('1',/////15X,'TABLE IV. PERCENTAGE ERROR BETWEEN PREDICTED
  *AND EXPERIMENTAL')
   WRITE(6,41)
41 FORMAT(31X,'THERMAL CONDUCTIVITIES')
   WRITE(6,42)
42 FORMAT(//15X,'CASE',5X,'MODEL',5X,'KRUPIC.',4X,'RUSSELL',4X,'LICHT
  *.',3X,'JEFFERSON')
   DO 43 I=1,48
   WRITE(6,44)I,K1BIAS(I),K2BIAS(I),K3BIAS(I),K4BIAS(I),K5BIAS(I)
44 FORMAT(16X,I2,1X,5F11.3)
43 CONTINUE
   WRITE(6,40)
```

```
      WRITE(6,41)
      WRITE(6,42)
      DO 45 I=49,92
      WRITE(6,46)I,K1BIAS(I),K2BIAS(I),K3BIAS(I),K4BIAS(I),K5BIAS(I)
   46 FORMAT(16X,I2,1X,5F11.3)
   45 CONTINUE
      WRITE(6,62)
   62 FORMAT('1',/////15X,'TABLE V. PERCENTAGE ERROR BETWEEN PREDICTED A
     *ND EXPERIMENTAL')
      WRITE(6,41)
      WRITE(6,47)
   47 FORMAT(//19X,'CASE',5X,'MAXWELL',4X,'RAYLEIGH',5X,'W AND M',5X,'M
     *AND T')
      DO 48 I=1,48
      WRITE(6,49)I,K6BIAS(I),K7BIAS(I),K8BIAS(I),K9BIAS(I)
   49 FORMAT(20X,I2,1X,4F12.3)
   48 CONTINUE
      WRITE(6,62)
      WRITE(6,41)
      WRITE(6,47)
      DO 50 I=49,92
      WRITE(6,51)I,K6BIAS(I),K7BIAS(I),K8BIAS(I),K9BIAS(I)
   51 FORMAT(20X,I2,1X,4F12.3)
   50 CONTINUE
      WRITE(6,12)
   12 FORMAT('1',2X,115H                    MEAN AND VARIANCE OF PERCENTAGE
     *ERROR BETWEEN MODEL PREDICTED AND EXPERIMENTAL THERMAL CONDUCTIVIT
     *Y)
      WRITE(6,13)
   13 FORMAT(24X,5HMODEL,5X,7HKRUPIC.,5X,7HRUSSELL,6X,6HLIGHT.,3X,9HJEFF
     *ERSON,6X,7HMAXWELL,4X,8HRAYLEIGH,3X,9HW AND MS,5X,7HM AND T)
      BCCASE=NOCASE
      AVBI1=SUM1BI/BCCASE
      AVBI2=SUM2BI/BCCASE
      AVBI3=SUM3BI/BCCASE
      AVBI4=SUM4BI/BCCASE
      AVBI5=SUM5BI/BCCASE
      AVBI6=SUM6BI/BCCASE
      AVBI7=SUM7BI/BCCASE
      AVBI8=SUM8BI/BCCASE
      AVBI9=SUM9BI/BCCASE
      T1ERAV=SUMK1E/BCCASE
      T2ERAV=SUMK2E/BCCASE
      T3ERAV=SUMK3E/BCCASE
      T4ERAV=SUMK4E/BCCASE
      T5ERAV=SUMK5E/BCCASE
      T6ERAV=SUMK6E/BCCASE
      T7ERAV=SUMK7E/BCCASE
```

```
      T8ERAV=SUMK8E/BOCASE
      T9ERAV=SUMK9E/BOCASE
      T1ERVA=((SUMSQ1/BOCASE)-T1ERAV**2)/10000.
      T2ERVA=((SUMSQ2/BOCASE)-T2ERAV**2)/10000.
      T3ERVA=((SUMSQ3/BOCASE)-T3ERAV**2)/10000.
      T4ERVA=((SUMSQ4/BOCASE)-T4ERAV**2)/10000.
      T5ERVA=((SUMSQ5/BOCASE)-T5ERAV**2)/10000.
      T6ERVA=((SUMSQ6/BOCASE)-T6ERAV**2)/10000.
      T7ERVA=((SUMSQ7/BOCASE)-T7ERAV**2)/10000.
      T8ERVA=((SUMSQ8/BOCASE)-T8ERAV**2)/10000.
      T9ERVA=((SUMSQ9/BOCASE)-T9ERAV**2)/10000.
      WRITE(6,16)AVBI1,AVBI2,AVBI3,AVBI4,AVBI5,AVBI6,AVBI7,AVBI8,AVBI9
   16 FORMAT(6X,6HAVGERR,6X,9F12.5)
      WRITE(6,14)T1ERAV,T2ERAV,T3ERAV,T4ERAV,T5ERAV,T6ERAV,T7ERAV,T8ERAV
     *,T9ERAV
   14 FORMAT(6X,6HAVBIAS,6X,9F12.5)
      WRITE(6,15)T1ERVA,T2ERVA,T3ERVA,T4ERVA,T5ERVA,T6ERVA,T7ERVA,T8ERVA
     *,T9ERVA
   15 FORMAT(6X,6HVARERR,7X,9F12.5)
      WRITE(6,17)
   17 FORMAT(///45X,34H DIMENSIONLESS CONDUCTIVITY RATIOS)
      WRITE(6,18)
   18 FORMAT(//131H       KC          KD          P       KD/KC      MODEL
     *KRUPIC.   RUSSELL    LICHT.  JEFFERSON  MAXWELL   RAYLEIGH WO AND
     *MS  M AND T                )
      DO 20 I=1,NOCASE
   19 FORMAT(13F10.4)
   20 WRITE(6,19)KC(I),KD(I),POR(I),RK(I),RK1(I),RK2(I),RK3(I),RK4(I),RK
     *5(I),RK6(I),RK7(I),RK8(I),RK9(I)
      STOP
      END
```

```
C       THERMAL CONDUCTIVITIES PREDICTED BY FOLLOWING
C       MODELSO  1. SON FREY  2. WOODSIDE AND MESSMER
C       3. HENGST  4. GORRING AND CHURCHILL
        IMPLICIT REAL*4(A-Z)
        INTEGER*4 I,INDEX,IERO,IERR1,IER
        DIMENSION SUM(10),PLOT1(173),PLOT2(173),PLOT3(173),PLOT4(173),
       *Y(173),XLAB(5),YLAB(5),GLAB(5),DATLAB(5)
         DATA SUM,INDEX/10*0.0,0/
        SUM1BI=0.
        SUM2BI=0.
        SUM3BI=0.
        SUM4BI=0.
        SUMSQ1=0.
        SUMSQ2=0.
        SUMSQ3=0.
        SUMSQ4=0.
        SUMK1E=0.
        SUMK2E=0.
        SUMK3E=0.
        SUMK4E=0.
         PI=3.14159
        READ(5,5)XLAB,YLAB,GLAB,DATLAB
      5 FORMAT(20A4)
    1   WRITE(6,100)
  100 FORMAT(1H1,////////////////,25X,'DATA',17X,'EFFECTIVE THERMAL CONDU
       $CTIVITY (KCAL/M-HR-K) X 100 ',//,25X,'CASE',1X ,
       $'  EXPERIMENTAL  ','    SON FREY    ','   WOODSIDE     ',
       $'     HENGST     ','    GORRING &   ',/,30X,
       $'                ','                ','  & MESSMER     ',
       $'                ','    CHURCHILL   ',/)
     2  READ(5,3,END=6) KC,KD,PD,EXKE,CASE,CASE1,CASE2
     3  FORMAT(4F10.5,3A4)
        INDEX=INDEX+1
        Y(INDEX)=ALOG10(EXKE/KC)
        E=1.0-PD
C       SONFREY  EQ
        R7=1.0/3.0
         R8=KC/KD
        K1=KC*(1.0-E**R7+E+R8*(E**R7-E))/(1.0-E**R7+R8*E**R7)
        PLOT1(INDEX)=ALOG10(K1/KC)
C       WOODSIDE & MESSMER  EQ
        K2=KC*((E+0.03)**2*KD/(0.03*KD+E*KC)+0.97-E)
        PLOT2(INDEX)=ALOG10(K2/KC)
C       HENGST
        N=11.6*E
        K3=KC*(N*E*KD/(2.0*(KD-KC))*(KD/(KD-KC)*ALOG(KD/KC)-1.0))
        PLOT3(INDEX)=ALOG10(K3/KC)
C       GORRING & CHURCHILL
```

```
      X=1.0
      C=10.*PD/PI
      IF(PD.LE.0.314159) GO TO 4
      C=(3.0*PI/(5.0*PI-20.0*PD))**1.5
      X=1.0/C**(1.0/3.0)
    4 B=(KC/(C*(KD-KC)))**(1.0/3.0)
      K4=KC*(PI/(6.0*(1.0-KC/KD)*C*B)*(ALOG(SQRT(B**2-B*X+X**2)/(B+X))
     *      +SQRT(3.0)*ATAN((2.0*X-B)/(SQRT(3.0)*B))-SQRT(3.)*ATAN
     *(-1.0/SQRT(3.0))                )+1.0-PI*X**2/4.)
      KH=EXKE
      IF(K4.GT.EXKE) KH=K4
      SUM(4) = SUM(4) + ((K4-EXKE)/KH)**2
      PLOT4(INDEX)=ALOG10(K4/KC)
      WRITE(6,200)INDEX,EXKE,K1,K2,K3,K4
  200 FORMAT(/,25X,I4,4X,5(F10.5,6X))
      BK1=((K1-EXKE)/EXKE)*100.
      BK2=((K2-EXKE)/EXKE)*100.
      BK3=((K3-EXKE)/EXKE)*100.
      BK4=((K4-EXKE)/EXKE)*100.
      K1OFF=ABS(BK1)
      K2OFF=ABS(BK2)
      K3OFF=ABS(BK3)
      K4OFF=ABS(BK4)
      SUM1BI=SUM1BI+BK1
      SUM2BI=SUM2BI+BK2
      SUM3BI=SUM3BI+BK3
      SUM4BI=SUM4BI+BK4
      SQK1ER=K1OFF**2
      SQK2ER=K2OFF**2
      SQK3ER=K3OFF**2
      SQK4ER=K4OFF**2
      SUMSQ1=SUMSQ1+SQK1ER
      SUMSQ2=SUMSQ2+SQK2FR
      SUMSQ3=SUMSQ3+SQK3ER
      SUMSQ4=SUMSQ4+SQK4ER
      SUMK1E=SUMK1E+K1OFF
      SUMK2E=SUMK2E+K2OFF
      SUMK3E=SUMK3E+K3OFF
      SUMK4E=SUMK4E+K4OFF
      IF(INDEX.EQ.14) GO TO 1
      IF(INDEX.EQ.28) GO TO 1
      IF(INDEX.EQ.42) GO TO 1
      IF(INDEX.EQ.56) GO TO 1
      IF(INDEX.EQ.70) GO TO 1
      IF(INDEX.EQ.84) GO TO 1
      IF(INDEX.EQ.98) GO TO 1
      IF(INDEX.EQ.112) GO TO 1
      IF(INDEX.EQ.126) GO TO 1
```

```
      IF(INDEX.EQ.140) GO TO 1
      IF(INDEX.EQ.154) GO TO 1
      GO TO 2
    6 BOCASE=FLOAT(INDEX)
      AVBI1=SUM1BI/BOCASE
      AVBI2=SUM2BI/BOCASE
      AVBI3=SUM3BI/BOCASE
      AVBI4=SUM4BI/BOCASE
      T1ERAV=SUMK1E/BOCASE
      T2ERAV=SUMK2E/BOCASE
      T3ERAV=SUMK3E/BOCASE
      T4ERAV=SUMK4E/BOCASE
      T1ERVA=((SUMSQ1/BOCASE)-T1ERAV**2)/10000.
      T2ERVA=((SUMSQ2/BOCASE)-T2ERAV**2)/10000.
      T3ERVA=((SUMSQ3/BOCASE)-T3ERAV**2)/10000.
      T4ERVA=((SUMSQ4/BOCASE)-T4ERAV**2)/10000.
      WRITE(6,573)AVBI1,AVBI2,AVBI3,AVBI4,T1ERAV,T2ERAV,T3ERAV,T4ERAV,T1
     *ERVA,T2ERVA,T3ERVA,T4ERVA
  573 FORMAT(3X,8F8.2,4F12.4)
      GO TO 621
      CALL ORIGIN(2.5,3.5,1)
       CALL GRAPH(173,Y,PLOT1,3,-7,-5.,-5.,2.,0.,2.,0.,XLAB,YLAB,GLAB,
     *DATLAB)
      CALL ORIGIN(8.5,0.,1)
       CALL GRAPH(173,Y,PLOT2,3,-7,-5.,-5.,2.,0.,2.,0.,XLAB,YLAB,GLAB,
     *DATLAB)
      CALL ORIGIN(8.5,.1,1)
       CALL GRAPH(173,Y,PLOT3,3,-7,-5.,-5.,2.,0.,2.,0.,XLAB,YLAB,GLAB,
     *DATLAB)
      CALL ORIGIN(8.5,.1,1)
       CALL GRAPH(173,Y,PLOT4,3,-7,-5.,-5.,2.,0.,2.,0.,XLAB,YLAB,GLAB,
     *DATLAB)
      CALL ORIGIN(8.5,.1,1)
  621 CONTINUE
      STOP
      END
```

```
C      THERMAL CONDUCTIVITY PREDICTED BY FOLLOWING
C      MODELSO  1. WILLHITE, KUNII AND SMITH  2. SCHUMANN
C      AND VOSS  3. PRESTON  4  KRUPICZKA
       IMPLICIT REAL*4(A-Z)
       INTEGER*4 I,INDEX
       DIMENSION SUM(10),PLOT1(173),PLOT2(173),PLOT3(173),PLOT4(173),
      *Y(173),XLAB(5),YLAB(5),GLAB(5),DATLAB(5)
        DATA SUM,INDEX/10*0.0,0/
       SUM1BI=0.
       SUM2BI=0.
       SUM3BI=0.
       SUM4BI=0.
       SUMSQ1=0.
       SUMSQ2=0.
       SUMSQ3=0.
       SUMSQ4=0.
       SUMK1E=0.
       SUMK2E=0.
       SUMK3E=0.
       SUMK4E=0.
        PI=3.14159
       READ(5,5)XLAB,YLAB,GLAB,DATLAB
     5 FORMAT(20A4)
     1 WRITE(6,100)
   100 FORMAT(1H1,////////////////,25X,'DATA',17X,'EFFECTIVE THERMAL CONDU
      $CTIVITY (KCAL/M-HR-K) X 100 ',//,25X,'CASE',1X ,
      $'  EXPERIMENTAL  ',','    WILLHITE,   ',','    SCHUMANN    ',
      $'    PRESTON     ',','    KRUPICZKA   ',/,30X,
      $'                ',',' KUNII & SMITH ',','     & VOSS     ',
      $'                ',','                ',/)
     2 READ(5,3,END=6) KC,KD,PD,EXKE,CASE,CASE1,CASE2
     3 FORMAT(4F10.5,3A4)
       INDEX=INDEX+1
       Y(INDEX)=ALOG10(EXKE/KC)
       E=1.0-PD
C      WILLHITE, KUNII,& SMITH
       N=3.0*(5.01-8.42*PD)/(1.91-1.91*PD)
       IF(N.LE.1.0) N=1.0
       THETA=ARSIN(SQRT(1.0/N))
       GAMMA=0.5
       ALPHA=1.0/(2.0*N)*(1.0-KC/KD)**2/(ALOG(KD/KC-
      *  (KD/KC-1.0)*COS(THETA))-(1.0-KC/KD)*(1.0-COS(THETA)))
       K1=KC*(1.0+E*(1.0-KC/KD)+GAMMA/ALPHA*(1.0-KC/KD)**2*E)
       KH=EXKE
       IF(K1.GT.EXKE) KH=K1
       SUM(1) = SUM(1) + ((K1-EXKE)/KH)**2
       PLOT1(INDEX)=ALOG10(K1/KC)
C   SHUMANN
```

```
      IF(PD.GE.0.5) GO TO 31
      KE=KEXP
      M=.2
   30 Y1=M*(M+1.)*ALOG((1.+M)/M)-M-PD
      IF(ABS(Y1).LT..0005)GO TO 40
      YP=(2.0*M+1.0)*ALOG((1.0+M)/M)-2.0
      M=M-Y1/YP
      GO TO 30
   31 M=10000.
   40 K2=KC*PD**3+KC*(1.-PD**3)*KD/(KC+M*(KC-KD))*(1.0+M*(1.0+M)*(KC-KD)
     */(KC+M*(KC-KD))*ALOG(KC*(1.0+M)/(M*KD)))
      PLOT2(INDEX)=ALOG10(K2/KC)
C     PRESTON
      K3=1.88574*K2**0.959
      PLOT3(INDEX)=ALOG10(K3/KC)
C     KRUPICZKA
      K4=KC*(KD/KC)**(0.280-0.757*ALOG10(PD)-0.057*ALOG10(KD/KC))
      PLOT4(INDEX)=ALOG10(K4/KC)
      WRITE(6,200)INDEX,EXKE,K1,K2,K3,K4
  200 FORMAT(/,25X,I4,4X,5(F10.5,6X))
      BK1=((K1-EXKE)/EXKE)*100.
      BK2=((K2-EXKE)/EXKE)*100.
      BK3=((K3-EXKE)/EXKE)*100.
      BK4=((K4-EXKE)/EXKE)*100.
      K1OFF=ABS(BK1)
      K2OFF=ABS(BK2)
      K3OFF=ABS(BK3)
      K4OFF=ABS(BK4)
      SUM1BI=SUM1BI+BK1
      SUM2BI=SUM2BI+BK2
      SUM3BI=SUM3BI+BK3
      SUM4BI=SUM4BI+BK4
      SQK1ER=K1OFF**2
      SQK2ER=K2OFF**2
      SQK3ER=K3OFF**2
      SQK4ER=K4OFF**2
      SUMSQ1=SUMSQ1+SQK1ER
      SUMSQ2=SUMSQ2+SQK2ER
      SUMSQ3=SUMSQ3+SQK3ER
      SUMSQ4=SUMSQ4+SQK4ER
      SUMK1E=SUMK1E+K1OFF
      SUMK2E=SUMK2E+K2OFF
      SUMK3E=SUMK3E+K3OFF
      SUMK4E=SUMK4E+K4OFF
      IF(INDEX.EQ.14) GO TO 1
      IF(INDEX.EQ.28) GO TO 1
      IF(INDEX.EQ.42) GO TO 1
      IF(INDEX.EQ.56) GO TO 1
```

```
      IF(INDEX.EQ.70) GO TO 1
      IF(INDEX.EQ.84) GO TO 1
      IF(INDEX.EQ.98) GO TO 1
      IF(INDEX.EQ.112) GO TO 1
      IF(INDEX.EQ.126) GO TO 1
      IF(INDEX.EQ.140) GO TO 1
      IF(INDEX.EQ.154) GO TO 1
      IF(INDEX.EQ.168) GO TO 1
      GO TO 2
    6 BOCASE=FLOAT(INDEX)
      AVBI1=SUM1BI/BOCASE
      AVBI2=SUM2BI/BOCASE
      AVBI3=SUM3BI/BOCASE
      AVBI4=SUM4BI/BOCASE
      T1ERAV=SUMK1E/BOCASE
      T2ERAV=SUMK2E/BOCASE
      T3ERAV=SUMK3E/BOCASE
      T4ERAV=SUMK4E/BOCASE
      T1ERVA=((SUMSQ1/BOCASE)-T1ERAV**2)/10000.
      T2ERVA=((SUMSQ2/BOCASE)-T2ERAV**2)/10000.
      T3ERVA=((SUMSQ3/BOCASE)-T3ERAV**2)/10000.
      T4ERVA=((SUMSQ4/BOCASE)-T4ERAV**2)/10000.
      WRITE(6,573)AVBI1,AVBI2,AVBI3,AVBI4,T1ERAV,T2ERAV,T3ERAV,T4ERAV,T1
     *ERVA,T2ERVA,T3ERVA,T4ERVA
  573 FORMAT(3X,8F8.2,4F12.4)
      GO TO 621
      CALL ORIGIN(2.5,3.5,1)
       CALL GRAPH(173,Y,PLOT1,3,-7,-5.,-5.,2.,0.,2.,0.,XLAB,YLAB,GLAB,
     *DATLAB)
      CALL ORIGIN(8.5,0.,1)
       CALL GRAPH(173,Y,PLOT2,3,-7,-5.,-5.,2.,0.,2.,0.,XLAB,YLAB,GLAB,
     *DATLAB)
      CALL ORIGIN(8.5,0.,1)
       CALL GRAPH(173,Y,PLOT3,3,-7,-5.,-5.,2.,0.,2.,0.,XLAB,YLAB,GLAB,
     *DATLAB)
      CALL ORIGIN(8.5,0.,1)
       CALL GRAPH(173,Y,PLOT4,3,-7,-5.,-5.,2.,0.,2.,0.,XLAB,YLAB,GLAB,
     *DATLAB)
      CALL ORIGIN(8.5,0.,1)
  621 CONTINUE
      STOP
      END
```

```
C      THERMAL CONDUCTIVITIES PREDICTED BY FOLLOWING
C      MODELS 0  1. EQUATION 6-16  2. EQUATION 6-17
C      3. EQUATION 6-18  4. LICHTENECKER 3-D
       IMPLICIT REAL*8 (A-Z)
       INTEGER*4 I,INDEX
          COMMON MU,SIGMA,KC,KD
       DIMENSION SUM(10),PLOT1(173),PLOT2(173),PLOT3(173),PLOT4(173),
      *Y(173),XLAB(5),YLAB(5),GLAB(5),DATLAB(5),PLOT5(173),PLOT6(173)
        DATA SUM,INDEX/10*0.0,0/
       MU=0.499
          PI=3.141592653589793
       SIGMA=10.0D0
       SUM4BI=0.
       SUMSQ4=0.
       SUMK4E=0.
       READ(5,190)XLAB,YLAB,GLAB,DATLAB
 190   FORMAT(20A4)
  1    WRITE(6,100)
  100  FORMAT(1H1,////////////////,25X,'DATA',17X,'EFFECTIVE THERMAL CONDU
     $CTIVITY (KCAL/M-HR-K) X 100 ',//,25X,'CASE',1X ,
     $'  EXPERIMENTAL  ','  EQUATION 6-16 ','  EQUATION 6-17 ',
     $'  EQUATION 6-18 ','   LICHTENKER   ',/)
    5 READ(5,3,END=6) KC,KD,PD,EXKE,CASE,CASE1,CASE2
    3  FORMAT(4F10.5,3A4)
       INDEX=INDEX+1
       Y(INDEX)=DLOG10(EXKE/KC)
       E=1.0-PD
       IF(PD.GE.0.5) MU=0.51
       EPSI=1.0D0-PD
          X=SIGMA*DSQRT(2.0D0)
       FN1=X*DSQRT(PI)/2.0D0
          IF(PD.LT.0.5)GO TO 12
          IF(PD.GT.0.5)GO TO 21
       X1=(1.0D0-MU)/X
       X2=(0.0D0-MU)/X
       FN=FN1*(DERF(X1)-DERF(X2))
       CALL DQG32(0.0D0,1.0D0,F,INTF)
          KE1=INTF/FN
       CALL DQG32(0.0D0,1.0D0,F2,REMN)
   12  DO 11 I=1,6
   50  CALL DQG32(0.0D0,1.0D0,F1,ANSW)
       X1=(1.0D0-MU)/X
       X2=(0.0D0-MU)/X
       FN=FN1*(DERF(X1)-DERF(X2))
          BNSW=1.00-ANSW/FN
       IF(BNSW.LE.PD) GO TO 11
       MU=MU+10.0D0**(-I)
       GO TO 50
```

```
   11 MU=MU-10.0D0**(-I)
      GO TO 7
   21 DO22 I=1,6
    9 CALL DQG32(0.0D0,1.0D0,F1,ANSW)
      X1=(1.0D0-MU)/X
      X2=(0.0D0-MU)/X
      FN=FNI*(DERF(X1)-DERF(X2))
         BNSW=1.D0-ANSW/FN
      IF(BNSW.GE.PD) GO TO 22
      MU=MU-10.0D0**(-I)
      GO TO 9
   22 MU=MU+10.0D0**(-I)
      GO TO 7
         KE2=FN/REMN
      PLOT5(INDEX)=DLOG10(KE1/KC)
      PLOT6(INDEX)=DLOG10(KE2/KC)
      RK = KD/KC
      FO=DEXP(-2.4006+0.83611*DLOG(RK)-0.0036959*DLOG(RK)**2+12.426*PD
     *        -16.278*PD**2-3.0926*DLOG(RK)*PD+0.0019151*DLOG(RK)**3
     *        -0.034069*DLOG(RK)**2*PD+3.3197*DLOG(RK)*PD**2
     *        +2.5768*PD**3)
      FINF=DEXP(6.038+0.28697*DLOG(RK)-0.0796930*DLOG(RK)**2-42.035*PD
     *        +94.701*PD**2-0.91135*DLOG(RK)*PD+0.0029629*DLOG(RK)**3
     *        +0.0040281*DLOG(RK)**2*PD+0.80897*DLOG(RK)*PD**2
     *        -69.049*PD**3)
      FW=1.5287+0.064259*DLOG(RK)-0.0064623*DLOG(RK)**2-6.1759*EPSI
     *        +11.059*EPSI**2+0.22176*DLOG(RK)*EPSI+0.00015041*DLOG(RK)
     *    **3-0.0042453*DLOG(RK)**2*EPSI-0.10971*DLOG(RK)*EPSI**2
     *        -7.2252*EPSI**3
      IF(FW.GE.1.0)FW=1.0
      IF(FW.LE.0.0)FW=0.0
       K3=KE2-FW*(KE2-KE1)
      PLOT3(INDEX)=DLOG10(K3/KC)
       K2=KE1*FO
      PLOT2(INDEX)=DLOG10(K2/KC)
         K1=KE2*FINF
      PLOT1(INDEX)=DLOG10(K1/KC)
C     LICHTENKER  EQ
       K=1.5*(KD-KC)/((2.0*DSQRT(KD)+DSQRT(KC))*(2.0*DSQRT(KC)+
     *    DSQRT(KD)))
      K4=(KC**(PD*(1.0-K*E)))*(KD**(E*(1.0+K*PD)))
      PLOT4(INDEX)=DLOG10(K4/KC)
      BK4=((K4-EXKE)/EXKE)*100.
      K4OFF=DABS(BK4)
      SUM4BI=SUM4BI+BK4
      SQK4ER=K4OFF**2
      SUMSQ4=SUMSQ4+SQK4ER
      SUMK4E=SUMK4E+K4OFF
```

```
      GO TO 5
    6 BOCASE=FLOAT(INDEX)
      AVBI4=SUM4BI/BOCASE
      T4ERAV=SUMK4E/BOCASE
      T4ERVA=((SUMSQ4/BOCASE)-T4ERAV**2)/10000.
      WRITE(6,576)AVBI4,T4ERAV,T4ERVA
  576 FORMAT(3X,3F20.5)
      WRITE(6,200)INDEX,EXKE,K1,K2,K3,K4
  200 FORMAT(/,25X,I4,4X,5(F10.5,6X))
      WRITE(6,572)BK1,BK2,BK3
  572 FORMAT(3X,'BK1=',F7.2,'    BK2=',F7.2,'    BK3=',F7.2)
      WRITE(6,573)AVBI1,AVBI2,AVBI3,T1ERAV,T2ERAV,T3ERAV,T1ERVA,T2ERVA,T
     *3ERVA
  573 FORMAT(3X,9F12.4)
      CALL ORIGIN(2.5,3.5,1)
       CALL GRAPH(-173,Y,PLOT1,3,-7,-5.,-5.,2.,0.,2.,0.,XLAB,YLAB,GLAB,
     *DATLAB)
      CALL ORIGIN(8.5,0.,1)
       CALL GRAPH(-173,Y,PLOT2,3,-7,-5.,-5.,2.,0.,2.,0.,XLAB,YLAB,GLAB,
     *DATLAB)
      CALL ORIGIN(8.5,.1,1)
       CALL GRAPH(-173,Y,PLOT3,3,-7,-5.,-5.,2.,0.,2.,0.,XLAB,YLAB,GLAB,
     *DATLAB)
      CALL ORIGIN(8.5,.1,1)
       CALL GRAPH(-173,Y,PLOT4,3,-7,-5.,-5.,2.,0.,2.,0.,XLAB,YLAB,GLAB,
     *DATLAB)
      CALL ORIGIN(8.5,.1,1)
      STOP
      END
      DOUBLE PRECISION FUNCTION F(P)
      IMPLICIT REAL*8 (A-Z)
         COMMON MU,SIGMA,KC,KD
         F=DEXP(-0.5D0*((P-MU)/SIGMA)**2)*KD*KC/(P*(KC-KD)+KD)
         RETURN
         END
      DOUBLE PRECISION FUNCTION F1(P)
      IMPLICIT REAL*8 (A-Z)
         COMMON MU,SIGMA,KC,KD
         F1=P*DEXP(-0.5D0*((P-MU)/SIGMA)**2)
         RETURN
         END
      DOUBLE PRECISION FUNCTION F2(P)
      IMPLICIT REAL*8 (A-Z)
         COMMON MU,SIGMA,KC,KD
         F2=DEXP(-0.5*((P-MU)/SIGMA)**2)/(KC+(KD-KC)*P)
         RETURN
         END
```

```
C       THERMAL CONDUCTIVITY PREDICTED BY THE FOLLOWING
C       MODELSO  1. MAXWELL  2. RAYLEIGH  3. MEREDITH
C       AND TOBIAS  4. BRUGGEMAN
        IMPLICIT REAL*4(A-Z)
        INTEGER*4 I,INDEX
        DIMENSION SUM(10),PLOT1(173),PLOT2(173),PLOT3(173),PLOT4(173),
       *Y(173),XLAB(5),YLAB(5),GLAB(5),DATLAB(5)
         DATA SUM,INDEX/10*0.0,0/
        SUM1BI=0.
        SUM2BI=0.
        SUM3BI=0.
        SUM4BI=0.
        SUMSQ1=0.
        SUMSQ2=0.
        SUMSQ3=0.
        SUMSQ4=0.
        SUMK1E=0.
        SUMK2E=0.
        SUMK3E=0.
        SUMK4E=0.
         PI=3.14159
        READ(5,5)XLAB,YLAB,GLAB,DATLAB
      5 FORMAT(20A4)
    1   WRITE(6,100)
    100 FORMAT(1H1,////////////////,25X,'DATA',17X,'EFFECTIVE THERMAL CONDU
       $CTIVITY (KCAL/M-HR-K) X 100 ',//,25X,'CASE',1X ,
       $'  EXPERIMENTAL  ','     MAXWELL    ','    RAYLEIGH    ',
       $'    MEREDITH    ','    BRUGGEMAN   ',/,30X,
       $'                ','                ','                ',
       $'    & TOBIAS    ','                ',/)
      2  READ(5,3,END=6) KC,KD,PD,EXKE,CASE,CASE1,CASE2
      3  FORMAT(4F10.5,3A4)
         INDEX=INDEX+1
         Y(INDEX)=ALOG10(EXKE/KC)
         E=1.0-PD
C        MAXWELL  EQ
         K1=KC*(KD+2.0*KC-2.0*E*(KC-KD))/(KD+2.0*KC+E*(KC-KD))
         PLOT1(INDEX)=ALOG10(K1/KC)
C        RAYLEIGH  EQ
         R1=(2.0*KC+KD)/(KC-KD)
         R2=(3.0*KC-3.0*KD)/(4.0*KC+3.0*KD)
         R3=10.0/3.0
         K2=KC*(R1-2.0*E-0.525*R2*E**R3)/(R1+E-0.525*R2*E**R3)
         PLOT2(INDEX)=ALOG10(K2/KC)
C        MEREDITH & TOBIAS
         K3=KC*(4.0*KC+2.0*KD-2.0*E*(KC-KD))/(4.0*KC+2.0*KD+E*(KC-KD))
        *   *(4.0*KC+2.0*KD-E*(4.0*KC-KD))/(4.0*KC+2.0*KD-E*(KC+2.0*KD))
         PLOT3(INDEX)=ALOG10(K3/KC)
```

```
C     BRUGGEMAN
      KEFF=EXKE
   10 Y1=(KEFF-KD)/(KC-KD)*(KC/KEFF)**(1./3.)-PD
      IF(ABS(Y1).LT..0005)GO TO 20
      YP=1./(KC-KD)*(KC/KEFF)**(1./3.)-(1./3.)*(KEFF-KD)/(KC-KD)*(KC**(1
     *./3.))/(KEFF**(4./3.))
      KEFF=KEFF-(Y1/YP)
      IF(KEFF.LE.0.0) KEFF=1.0E-8
      GO TO 10
   20 K4=KEFF
      PLOT4(INDEX)=ALOG10(K4/KC)
      WRITE(6,200)INDEX,EXKE,K1,K2,K3,K4
  200 FORMAT(/,25X,I4,4X,5(F10.5,6X))
      BK1=((K1-EXKE)/EXKE)*100.
      BK2=((K2-EXKE)/EXKE)*100.
      BK3=((K3-EXKE)/EXKE)*100.
      BK4=((K4-EXKE)/EXKE)*100.
      K1OFF=ABS(BK1)
      K2OFF=ABS(BK2)
      K3OFF=ABS(BK3)
      K4OFF=ABS(BK4)
      SUM1BI=SUM1BI+BK1
      SUM2BI=SUM2BI+BK2
      SUM3BI=SUM3BI+BK3
      SUM4BI=SUM4BI+BK4
      SQK1ER=K1OFF**2
      SQK2ER=K2OFF**2
      SQK3ER=K3OFF**2
      SQK4ER=K4OFF**2
      SUMSQ1=SUMSQ1+SQK1ER
      SUMSQ2=SUMSQ2+SQK2ER
      SUMSQ3=SUMSQ3+SQK3ER
      SUMSQ4=SUMSQ4+SQK4ER
      SUMK1E=SUMK1E+K1OFF
      SUMK2E=SUMK2E+K2OFF
      SUMK3E=SUMK3E+K3OFF
      SUMK4E=SUMK4E+K4OFF
      GO TO 2
    6 BOCASE=FLOAT(INDEX)
      AVBI1=SUM1BI/BOCASE
      AVBI2=SUM2BI/BOCASE
      AVBI3=SUM3BI/BOCASE
      AVBI4=SUM4BI/BOCASE
      T1ERAV=SUMK1E/BOCASE
      T2ERAV=SUMK2E/BOCASE
      T3ERAV=SUMK3E/BOCASE
      T4ERAV=SUMK4E/BOCASE
      T1ERVA=((SUMSQ1/BOCASE)-T1ERAV**2)/10000.
```

```
      T2ERVA=((SUMSQ2/BOCASE)-T2ERAV**2)/10000.
      T3ERVA=((SUMSQ3/BOCASE)-T3ERAV**2)/10000.
      T4ERVA=((SUMSQ4/BOCASE)-T4ERAV**2)/10000.
      WRITE(6,573)AVBI1,AVBI2,AVBI3,AVBI4,T1ERAV,T2ERAV,T3ERAV,T4ERAV,T1
     *ERVA,T2ERVA,T3ERVA,T4ERVA
  573 FORMAT(3X,8F8.2,4F12.4)
      GO TO 621
      CALL ORIGIN(2.5,3.5,1)
       CALL GRAPH(173,Y,PLOT1,3,-7,-5.,-5.,2.,0.,2.,0.,XLAB,YLAB,GLAB,
     *DATLAB)
      CALL ORIGIN(8.5,0.,1)
       CALL GRAPH(173,Y,PLOT2,3,-7,-5.,-5.,2.,0.,2.,0.,XLAB,YLAB,GLAB,
     *DATLAB)
      CALL ORIGIN(8.5,0.,1)
       CALL GRAPH(173,Y,PLOT3,3,-7,-5.,-5.,2.,0.,2.,0.,XLAB,YLAB,GLAB,
     *DATLAB)
      CALL ORIGIN(8.5,0.,1)
       CALL GRAPH(173,Y,PLOT4,3,-7,-5.,-5.,2.,0.,2.,0.,XLAB,YLAB,GLAB,
     *DATLAB)
      CALL ORIGIN(8.5,0.,1)
  621 CONTINUE
      STOP
      END
```

```
C     THERMAL CONDUCTIVITIES CALCULATED BY THE
C     FOLLOWING MODELS 1. WILHELM ET AL  2. LICH-
C     TENECKER 2-D  3. KANAGER
      IMPLICIT REAL*4(A-Z)
      INTEGER*4 I,INDEX
      DIMENSION SUM(10),PLOT(172),Y(172),XLAB(5),YLAB(5),GLAB(5),DATLAB(
     *5),PLOT1(172),PLOT2(172),PLOT3(172)
      DATA SUM,INDEX/10*0.0,0/
      SUMB11=0.
      SUMB12=0.
      SUMB13=0.
      SUMSQ1=0.
      SUMSQ2=0.
      SUMSQ3=0.
      SUMK1E=0.
      SUMK2E=0.
      SUMK3E=0.
      PI=3.14159
      READ(5,5)XLAB,YLAB,GLAB,DATLAB
    5 FORMAT(20A4)
    2 READ(5,3,END=5) KC,KD,PD,EKKE,CASE,CASE1,CASE2
    3 FORMAT(4F10.5,3A4)
      INDEX=INDEX+1
      Y(INDEX)=ALOG10(EXKE/KC)
      E=1.0-PD
C     WILHELM ET AL
      IF(PD.GE.0.5) GO TO 31
      M=.2
   30 Y1=M*(M+1.)*ALOG((1.+M)/M)-M-PD
      IF(ABS(Y1).LT..0005)GO TO 40
      YP=(2.0*M+1.0)*ALOG((1.0+M)/M)-2.0
      M=M-Y1/YP
      GO TO 30
   31 M=10000.
   40 K7=(KC*PD)**3+KC*(1.-PD)**3)*KD/((KC+M*(KC-KD))*(1.0+M*(1.0+M)*(KC-KD)
     */(KC+M*(KC-KD)))*ALOG((KC*(1.0+M)/(M*KD)))
      K8=(10.**.859)*(10.**(3.12*(KD/(100.*360.*PD))))*.0036
      K1=100.*K8+K7
      PLOT1(INDEX)=ALOG10(K1/KC)
C     LICHTENECKER
      K2=(KC**PD)*(KD**E)
      PLOT2(INDEX)=ALOG10(K2/KC)
C     KANAGER
      N=11.5*E
      A=KD-KC
      K3=((N*E*KC*KD)/(2.*A))*(((KD/A)*ALOG(KD/KC))-1.)
      PLOT3(INDEX)=ALOG10(K3/KC)
      EK1=((1-EXKE)/EXKE)*100.
```

C-5


```
      B(2=(((2-EX(E)/EX(E)*100.
      B(3=(((3-EXKE)/EX(E)*100.
      (1DFF=ABS(BK1)
      (2DFF=ABS(BK2)
      (3DFF=ABS(B(3)
      SJM1BI=SJM1BI+B(1
      SJM2BI=SJM2BI+B(2
      SJM3BI=SJM3BI+B(3
      SQ(1ER=(1DFF**2
      SQ(2ER=(2DFF**2
      SQ(3ER=(3DFF**2
      SJMSQ1=SJMSQ1+SQ(1ER
      SJMSQ2=SJMSQ2+SQ(2ER
      SJMSQ3=SJMSQ3+SQ(3ER
      SJM(1E=SJMK1E+(1DFF
      SJM(2E=SJMK2E+(2DFF
      SJM(3E=SJMK3E+(3DFF
      WRITE(5,203)INDEX,EX(E,B(1,B(2,B(3
  203 FORMAT(3X,'CASE=',I3,'    EK(E=',F10.5,'    DIF1=',F7.2,'    DIF2=',F
     *7.2,'    DIF3=',F7.2)
      GO TO 2
    5 BDCASE=FLOAT(INDEX)
      AVBI1=SJM1BI/BDCASE
      AVBI2=SJM2BI/BDCASE
      AVBI3=SJM3BI/BDCASE
      T1ERAV=SJMK1E/BDCASE
      T2ERAV=SJMK2E/BDCASE
      T3ERAV=SJMK3E/BDCASE
      T1ERVA=T1ERVA
      T1ERVA=((SJMSQ1/BDCASE)-T1ERAV**2)/10000.
      T2ERVA=((SJMSQ2/BDCASE)-T2ERAV**2)/10000.
      T3ERVA=((SUMSQ3/BDCASE)-T3ERAV**2)/10000.
      WRITE(6,573)AVBI1,AVBI2,AVBI3,T1ERAV,T2ERAV,T3ERAV,T1ERVA,T2ERVA,T
     *3ERVA
  573 FORMAT(3X,6F10.2,3F14.4)
      STOP
      END
```